

**Organic ligand complexation reactions on
aluminium-bearing mineral surfaces studied *via*
in-situ Multiple Internal Reflection Infrared
Spectroscopy, adsorption experiments, and
surface complexation modelling**

A thesis submitted to the University of Manchester for the degree of
Doctor of Philosophy
in the Faculty of Engineering and Physical Sciences

2010

Charalambos Assos

School of Earth, Atmospheric and Environmental Sciences

Table of Contents

LIST OF FIGURES	4
LIST OF TABLES	8
ABSTRACT	10
DECLARATION.....	11
COPYRIGHT STATEMENT	12
CHAPTER 1 INTRODUCTION	13
AIMS AND OBJECTIVES	38
CHAPTER 2 THE USE OF IR SPECTROSCOPY IN THE STUDY OF ORGANIC LIGAND SURFACE COMPLEXATION	40
INTRODUCTION.....	40
METHODOLOGY	44
<i>Materials</i>	44
<i>MIR-FTIR spectroscopy</i>	45
<i>Sample preparation and coating procedure</i>	45
<i>MIR-FTIR Measurements</i>	46
THEORETICAL BACKGROUND	47
THE USE OF IR TECHNIQUES FOR THE STUDY OF MINERAL-ORGANIC LIGAND INTERACTIONS AT THE MOLECULAR SCALE	60
CASE STUDY: THE COMPLEXATION OF OXALIC ACID ON KAOLINITE STUDIED VIA FLOW THROUGH IN SITU MIR-FTIR SPECTROSCOPY	72
<i>Results and discussion</i>	72
SUMMARY AND CONCLUSIONS	82
CHAPTER 3 COMPLEXATION OF PHTHALIC AND SALICYLIC ACID ON THE SURFACE OF KAOLINITE.....	83
INTRODUCTION.....	83
METHODOLOGY	87
<i>Materials</i>	87
<i>Multiple Internal Reflection (MIR) - FTIR Spectroscopy</i>	88
<i>Adsorption Experiments</i>	89
<i>Surface Complexation Modelling</i>	94
RESULTS AND DISCUSSION.....	95
<i>IR spectroscopic measurements</i>	95
<i>Macroscopic adsorption properties</i>	128
<i>Surface complexation modelling</i>	136
SUMMARY AND CONCLUSIONS.....	173

CHAPTER 4 THE ADSORPTION OF HUMIC ACID ON KAOLINITE AND GIBBSITE.....	175
INTRODUCTION.....	175
METHODOLOGY	177
<i>Materials</i>	177
<i>Humic acid titrations</i>	178
<i>Modelling</i>	179
<i>Adsorption experiments</i>	181
<i>IR spectroscopy</i>	184
RESULTS AND DISCUSSION.....	185
<i>Acid-base properties of humic acid</i>	185
<i>Adsorption experiments</i>	194
<i>IR measurements</i>	223
<i>Proposed binding mechanisms from the combined study of spectroscopic and macroscopic adsorption data</i>	234
CONCLUSIONS	235
CHAPTER 5 GENERAL DISCUSSION AND CONCLUSIONS.....	237
REFERENCES.....	246
APPENDIX.....	260

List of Figures

Chapter 1

Figure 1-1 Schematic representation of surface complex formation.....	15
Figure 1-2 The distribution diagram of the three surface species ($X-OH$, $X-OH_2^+$ and $X-O^-$) assumed by the 2-pK model for a hypothetical mineral surface on which protons are the only adsorbing ions.	17
Figure 1-3 Schematic representation of the electric double layer according to the Stern-Grahame model.	22
Figure 1-4 Rates of silicate dissolution as a function of pH, at far from equilibrium conditions.	32

Chapter 2

Figure 2-1 Coordination modes of the carboxylate functional group.	41
Figure 2-2 Schematic representation of the experimental set-up used for the acquisition of <i>in situ</i> MIR-FTIR spectra of organic ligand surface complexes.....	45
Figure 2-3 Vibrational modes of the carboxyl group in its protonated and anionic state.....	49
Figure 2-4 The IR spectra of aqueous phthalate collected at pH 7, aqueous strontium-phthalate complex collected at pH 7, and aqueous iron-phthalate complex collected at pH 3.	55
Figure 2-5 The propagation of the IR beam through the internal reflection element.	62
Figure 2-6 Steps required to isolate the spectrum of a surface species.	65
Figure 2-7 (a) The infrared spectrum of adsorbed salicylic acid onto gibbsite, from a 7.5×10^{-4} M solution at pH 5, obtained after 56 minutes of reaction time. (b) The infrared spectrum of the surface complex in (a) obtained after 2 hours reaction time (c) the difference spectrum obtained by subtracting (b) from (a).	70
Figure 2-8 The negative peaks appearing on the spectrum of adsorbed phthalic acid following the dissolution of the magnesite coating from the ZnSe crystal.	71
Figure 2-9 Oxalate species distribution as a function of pH.	73
Figure 2-10 IR spectra of aqueous oxalic acid as a function of pH.	74
Figure 2-11 IR spectra of adsorbed oxalic acid on kaolinite, from a 5×10^{-3} M and 5×10^{-4} M oxalic acid solution, at pH 3.5.	75
Figure 2-12 IR spectra of adsorbed oxalic acid on kaolinite, from a 5×10^{-3} M oxalic acid solution, obtained at pH 3.5 and three different background electrolyte concentrations....	79
Figure 2-13 The spectra of adsorbed oxalic acid on kaolinite, at pH 6, from a 5×10^{-3} M and 5×10^{-4} M oxalic acid solution.....	80

Chapter 3

Figure 3-1 IR spectra of aqueous phthalic acid as a function of pH.	96
Figure 3-2 Species distribution of a 0.02 M phthalic acid solution as a function of pH	97
Figure 3-3 Representative IR spectra of aqueous phthalic acid (H_2Phth), hydrogen phthalate ($HPhth^{1-}$), and phthalate ($Phth^{2-}$).....	98
Figure 3-4 Species distribution of a 0.02 M salicylic acid solution over the pH range 1 to 14.	101
Figure 3-5 Representative IR spectrum of the aqueous salicylate monoion ($HSal^{1-}$), collected at pH 5.95.....	101
Figure 3-6 IR spectra of adsorbed phthalate on kaolinite as a function of pH, from a 1×10^{-3} M phthalic acid solution.....	103

Figure 3-7 Comparison of the carboxylate stretching region for the spectra of adsorbed phthalic acid displayed in figure 6.....	106
Figure 3-8 IR spectra of adsorbed phthalic acid on kaolinite at pH 5, as function of ionic strength, from a 1×10^{-3} M phthalic acid solution.	107
Figure 3-9 Possible coordination modes for inner sphere complexed phthalic acid with a surficial aluminium cation.	108
Figure 3-10 IR spectra of adsorbed phthalic on kaolinite, at pH 4, from three different initial phthalate concentrations.	110
Figure 3-11 IR spectra of adsorbed phthalic acid on kaolinite, at $I = 0$ and 0.01 M NaCl, from a 1×10^{-3} M phthalic acid solution at pH 3.....	112
Figure 3-12 IR spectra of salicylic acid adsorbed on kaolinite from a 5×10^{-4} M salicylic acid solution as a function of pH.....	115
Figure 3-13 IR spectra of salicylic acid adsorbed on kaolinite at pH 3 and 6.....	116
Figure 3-14 IR spectra of adsorbed salicylic acid from a 5×10^{-4} M salicylic acid solution on kaolinite, at pH 3 and 5.....	117
Figure 3-15 IR spectra of adsorbed salicylic acid on kaolinite from a 5×10^{-3} M salicylic acid solution at 0, 0.01 and 0.03 M NaCl, at pH 5.	118
Figure 3-16 IR spectra of adsorbed salicylic acid on kaolinite at pH 4 as a function of total salicylate concentration in solution.....	119
Figure 3-17 Time dependent IR spectra of adsorbed salicylic acid from a 5×10^{-4} M salicylic acid solution on kaolinite obtained at pH 4.....	120
Figure 3-18 Differences in the spectroscopic features of aqueous salicylic (recorded at pH 6) and adsorbed salicylic acid on kaolinite.	121
Figure 3-19 Possible coordination modes for adsorbed salicylic acid on a mineral surface.	123
Figure 3-20 IR spectra of complexed salicylate with iron (III) and aluminium ions in solution, and on the surface of kaolinite (pH 6)..	124
Figure 3-21 IR spectra of adsorbed salicylic acid from a 5×10^{-4} M salicylic acid solution on kaolinite, at pH 6 and 10.....	127
Figure 3-22 Adsorption of phthalic acid on kaolinite as a function of pH at an ionic strength of 0.01 M NaCl expressed.	130
Figure 3-23 Adsorption of salicylic acid on kaolinite as a function of pH at an ionic strength of 0.01 M NaCl.....	131
Figure 3-24 The dependence of surface charge and ligand charge on pH and how these parameters are related to the adsorption behaviour of phthalic acid on kaolinite.....	132
Figure 3-25 Fractional adsorption of phthalic acid (open circles) and salicylic acid (closed circles) as a function of ionic strength at pH 4.....	135
Figure 3-26 Schematic representation of the position of surface species at the surface-solution interface and of the relationship between surface charge and surface potential according to the constant capacitance model; the triple layer model and the extended constant capacitance model	141
Figure 3-27 Idealised structural representation of kaolinite. Adopted from Warne et al. (2000).	150
Figure 3-28 Proton surface density on kaolinite at 0.1 M, 0.01 M, and 0.001M	153
Figure 3-29 Potentiometric titration data for a kaolinite suspension, at $I = 0.01$ M, shown as net hydrogen ions added.....	157
Figure 3-30 Phthalate adsorption on kaolinite as a function of pH, at $I = 0.01$ M NaCl and three systems with different initial phthalate concentration to surface area ratios (Phth : S.A).	160
Figure 3-31 Predicted phthalate speciation in a kaolinite-phthalate system as a function of pH using the parameters listed in Table 7.....	162
Figure 3-32 Predicted phthalate speciation in a kaolinite-phthalate system as a function of pH using the parameters listed in Table 7.....	162
Figure 3-33 The distribution of surface functional groups and phthalate surface complexes according to the proposed model.....	164
Figure 3-34 The effect of varying C1 and C2 values on the predicted relative ratios of the inner and outer sphere complexes.....	166

Figure 3-35 Salicylate adsorption on kaolinite as a function of pH, at I = 0.01 M NaCl and three systems with different initial salicylate concentration to surface area ratios (Sal : S.A).....	169
Figure 3-36 Predicted salicylate speciation in a kaolinite-salicylate system as a function of pH using the parameters listed in Table 9.....	170
Figure 3-37 Predicted salicylate speciation in a kaolinite-salicylate system as a function of pH using the parameters listed in Table 9.....	171

Chapter 4

Figure 4-1 Acid-base titration curves for the humic acid sample used in the present study.....	188
Figure 4-2 Acid-base titration data for humic acid at I = 0.001, 0.01 and 0.1 M NaCl, shown as total hydrogen (T_H) in mM added in the solution.	191
Figure 4-3 Fractional concentration of the three proton binding sites according to the non electrostatic model.....	192
Figure 4-4 Adsorption of humic acid on gibbsite as a function of pH.....	195
Figure 4-5 Adsorption of humic acid on kaolinite as a function of pH.....	195
Figure 4-6 Humic acid adsorption density on kaolinite (circles) and gibbsite (squares).....	198
Figure 4-7 Adsorption isotherms of humic acid onto gibbsite at pH 5, 7, 9 and a background electrolyte of 0.01 M NaCl.	199
Figure 4-8 Adsorption isotherms of humic acid onto kaolinite at pH 4, 5, 7, 9 and a background electrolyte of 0.01 M NaCl.	200
Figure 4-9 Adsorption isotherms of humic acid on gibbsite at pH 5 in 0.01, 0.05 and 0.1 M NaCl.	201
Figure 4-10 Adsorption isotherms of humic acid on kaolinite at pH 5 in 0.01, 0.05 and 0.1 M NaCl.	201
Figure 4-11 Humic acid adsorption on gibbsite as a function of background electrolyte (NaCl) concentration at pH 5, 7 and 9.....	206
Figure 4-12 Humic acid adsorption on kaolinite as a function of background electrolyte (NaCl) concentration at pH 5, 7 and 9.....	206
Figure 4-13 Effect of cation type on the extent of humic acid adsorption on kaolinite (Kao) and gibbsite (Gib).....	208
Figure 4-14 The change in solution pH during successive 1 mL additions of humic acid (1 g/L) in a 20 g/L gibbsite suspension, at 0.001 M NaCl	219
Figure 4-15 Effect of sulphate ions on the adsorption of humic acid onto gibbsite and kaolinite	222
Figure 4-16 Comparison of humic acid adsorption densities on gibbsite obtained in sodium sulphate solutions and sodium chloride solutions, at pH 5 and pH 9	222
Figure 4-17 IR spectra of aqueous humic acid in aqueous solution at pH 3.5, 5 and 7.....	224
Figure 4-18 IR spectra of adsorbed humic acid, from a 0.1 g/L humic acid solution, on kaolinite.....	226
Figure 4-19 The difference in relative intensity of the bands arising from C=O and COO ⁻ stretching vibrations observed in aqueous and adsorbed humic acid.	227
Figure 4-20 Comparison of adsorbed humic acid spectra on kaolinite and gibbsite at pH 3.5.....	229
Figure 4-21 IR spectra of aqueous Fluka humic acid (FHA) and ACROS humic acid (AHA).....	231
Figure 4-22 pH-dependent absorption features for AHA and FHA obtained from the subtraction of the aqueous humic acid spectra collected at pH 3.5 from the aqueous spectra collected at pH 7.....	232
Figure 4-23 Adsorbed humic acid spectra on kaolinite at 0.001 M NaCl, obtained from 0.1 g/L solutions of ACROS humic acid (AHA) and Fluka humic acid (FHA).	233

Appendix

- Figure A- 1** Differences in the spectroscopic features of salicylic acid observed following adsorption on gibbsite at pH 5 from a 5×10^{-4} M salicylic acid solution. Peak positions and assignments correspond to the adsorbed species.....261
- Figure A- 2** IR spectra obtained for adsorbed salicylic acid onto gibbsite at three different pH values, from a 5×10^{-4} M salicylic acid solution. The spectra have been offset for clarity.262
- Figure A- 3** IR spectra obtained for adsorbed salicylic acid onto gibbsite from a 5×10^{-4} M salicylic acid solution, in the presence of 0.01 M NaCl and with no added electrolyte, at pH 3 and pH 5.262
- Figure A- 4** IR Spectra of adsorbed salicylic acid onto gibbsite at pH 3 and 5 as a function of salicylic acid concentration. Spectra have been offset for clarity.263
- Figure A- 5** The development of surface species during the adsorption of salicylic over time from a 5×10^{-4} M salicylic acid solution at pH 3.264

List of Tables

Chapter 2

Table 2-1 Peak frequency positions exhibited by the vibrational modes of the carboxyl group found in some common LMW organic acids.....	51
Table 2-2 Peak frequency positions of the aqueous oxalate and hydrogen oxalate species obtained in this study	74
Table 2-3 Literature assignment of the IR absorption bands arising from the vibrational modes of inner sphere complexed oxalate species.....	76
Table 2-4 Peak frequency positions and assignment for the IR spectra of adsorbed oxalic acid at the kaolinite-water interface	81

Chapter 3

Table 3-1 The chemical structure and some physicochemical properties of the organic acids used in the study.	87
Table 3-2 Literature absorption band maxima (cm^{-1}) and assignments for the aqueous phthalate ion (Phth^{2-}), in the frequency region of the carboxylate stretching vibrations.....	99
Table 3-3 Absorption band peak positions for the three aqueous phthalic acid species, in the frequency region between 1200 to 1800cm^{-1} obtained in the present study	100
Table 3-4 Tableau format of the stoichiometric coefficients for the surface reactions relevant to the adsorption of an anionic species.....	148
Table 3-5 Examples of varying modelling approaches employed for the description of the acid-base properties of kaolinite.	155
Table 3-6 Best-fit model parameters for the acid-base titration data of kaolinite according to the CCM.	158
Table 3-7 Model parameters used for the description of phthalate adsorption data on kaolinite according to the extended constant capacitance model.....	160
Table 3-8 The effect of varying C_1 and C_2 values on the optimised surface complexation constants ($\log K_{is}$ and $\log K_{os}$) and on the overall model fits (VY).	165
Table 3-9 Model parameters used for the description of phthalate adsorption data on kaolinite according to the extended constant capacitance model.....	168

Chapter 4

Table 4-1 Summary of the acid-base properties of humic acid reported in the literature	186
Table 4-2 Carboxylic and phenolic group concentrations for the humic acid used in the present study, estimated from the titration curves shown in Figure 1.	187
Table 4-3 Optimised model parameters describing the acid-base behaviour of humic acid, at three ionic strengths, according to the three site nonelectrostatic model proposed.	190

Table 4-4 Comparison of the optimised model parameters obtained using the Diffuse Layer Model (DLM) and the non electrostatic model (NEM).....	194
Table 4-5 Langmuir model parameters obtained from the adsorption isotherm data. .	203
Table 4-6 Humic acid maximum adsorption densities on kaolinite reported in the literature.	205
Table 4-7 Peak frequencies positions of the absorption bands originating from carboxyl vibrational modes of aqueous and adsorbed humic acid at 0.01 M NaCl.....	229

Abstract

Organic ligand complexation reactions at the mineral-water interface play an important role in several environmental and geochemical processes such as adsorption, dissolution, precipitation, pollutant transport, nutrient cycling, and colloidal stability. Although organic ligand surface complexation reactions have been extensively studied, a molecular level understanding regarding the mechanisms underlying the adsorption of such compounds is still limited. The purpose of the current study was to investigate the interactions between some common naturally occurring organic ligands and a common aluminosilicate clay mineral, kaolinite, using a combination of macroscopic and microscopic experimental methods. Molecular level information regarding the structure and binding mode of adsorbed species was obtained using *in situ* MIR-FTIR spectroscopy. Other experimental techniques including adsorption experiments, surface titrations, and surface complexation modelling were also employed in order to quantify and describe the macroscopic adsorption properties of the organic ligands examined. Three low molecular weight organic acids (oxalic, salicylic, and phthalic acid) and humic acid were chosen as representative organic ligands.

Spectroscopic evidence revealed that low molecular weight organic acids are able to form both inner and outer sphere complexes on kaolinite, and the relative concentrations of these surface complexes varies with solution chemistry. Inner sphere coordination modes inferred are a mononuclear bidentate for oxalate (five-membered chelate ring) and phthalate (seven-membered chelate ring); and a mononuclear monodentate (six-membered pseudochelate ring) for salicylic acid. Similar coordination modes were shown to form on simpler mineral (hydr)oxides. Elucidation of the coordination chemistry of these ligands can provide insights into the dissolution mechanisms of silicate minerals

In contrast to low molecular weight organic acids, there was no evidence of inner sphere complexation by humic acid acids on kaolinite or gibbsite. The combined spectroscopic and macroscopic adsorption results suggest that cation bridging and van der Waals interactions are the two most probable mechanisms for the adsorption of humic acid by these mineral substrates. This finding casts doubts over the use of low molecular weight organic acids as humic acid analogs.

Declaration

No portion of the work referred to in the thesis has been submitted in support of an application for another degree or qualification of this or any other university or other institute of learning.

Copyright Statement

The author of this thesis (including any appendices and/or schedules to this thesis) owns certain copyright or related rights in it (the “Copyright”) and he has given The University of Manchester certain rights to use such Copyright, including for administrative purposes.

Copies of this thesis, either in full or in extracts and whether in hard or electronic copy, may be made **only** in accordance with the Copyright, Designs and Patents Act 1988 (as amended) and regulations issued under it or, where appropriate, in accordance with licensing agreements which the University has from time to time. This page must form part of any such copies made.

The ownership of certain Copyright, patents, designs, trade marks and other intellectual property (the “Intellectual Property”) and any reproductions of copyright works in the thesis, for example graphs and tables (“Reproductions”), which may be described in this thesis, may not be owned by the author and may be owned by third parties. Such Intellectual Property and Reproductions cannot and must not be made available for use without the prior written permission of the owner(s) of the relevant Intellectual Property and/or Reproductions.

Further information on the conditions under which disclosure, publication and commercialisation of this thesis, the Copyright and any Intellectual Property and/or Reproductions described in it may take place is available in the University IP Policy (see <http://www.campus.manchester.ac.uk/medialibrary/policies/intellectual-property.pdf>), in any relevant Thesis restriction declarations deposited in the University Library, The University Library’s regulations (see <http://www.manchester.ac.uk/library/aboutus/regulations>) and in The University’s policy on presentation of Theses.

Chapter 1 Introduction

The interactions taking place between solute species and mineral surfaces have been the subject of extensive research for several decades. Adsorption, the process by which chemical species accumulate at the mineral-water interface, is a key reaction which influences the distribution of species between the aqueous and the solid phase; the electrostatic properties of mineral surfaces; and mineral surface reactivity (Stumm, 1992). The effects brought about by adsorption can in turn affect several environmental and geochemical processes, including the transport of trace elements and pollutants, colloidal stability, mineral weathering and precipitation. However, there is still a need to better understand fundamental aspects of adsorption, especially at the molecular scale, in order to gain insights into the underlying mechanisms involved in adsorption processes. As a result, the adsorption of chemical species onto mineral surfaces is still a topic of significant scientific interest. Given the importance of adsorption as a subject of research, the present study aims to investigate the adsorption of naturally occurring organic acids, an important class of organic ligands, on mineral surfaces.

Prior to the description of the chemical reactions occurring at the mineral-water interface it is necessary to clarify the relevant terminology often used in the literature, and introduce some important concepts that will be referred to throughout this study. The chemical reactions involving the coordination of chemical species from the overlying solution (termed adsorbates) to the mineral surface (termed adsorbent) are known as adsorption reactions. The stable molecular entity formed following the binding of a solute species to an ion located on the surface of a mineral (typically a metal cation) is referred to as a surface complex and the reaction as surface complexation (Sparks, 2003). The resulting surface complex can either be a neutral or a charged species. Chemical species that bind to surface cations and aqueous cations to form surface and aqueous complexes respectively, are generally referred to as ligands. Moreover, if a ligand is able to form two or more coordinative bonds with the central metal cation (surface or aqueous), then the resulting complex is termed a chelate complex.

The uptake of a wide range of organic (e.g. humic substances, citrate, oxalate, EDTA) and inorganic ions (e.g. sulphate, phosphate, arsenate) by different mineral substrates has been demonstrated in many studies (e.g. Bhattacharyya and Gupta, 2008; Bradl, 2004; Dzombak and Morel, 1990; Evanko and Dzombak, 1998; Filius et al.,

1997; Geelhoed et al., 1997; Goldberg and Johnston, 2001; Lackovic et al., 2003b; Schlautman and Morgan, 1994; Tombacz et al., 2000). The resulting surface complexes formed can be distinguished into two main types according to the binding mechanism involved, namely inner sphere and outer sphere complexes (Figure 1-1). Species coordinating through electrostatic forces of attraction to surface groups of opposite charge are termed outer sphere complexes and the adsorption process is referred to as non specific adsorption or physisorption. Conversely species which form direct chemical bonds with surface sites are termed inner sphere complexes and the adsorption processes is referred to as specific adsorption or chemisorption. Inner sphere complexation occurs through a ligand exchange mechanism where a surface hydroxyl group exchanges with other ligands from the overlying solution (Stumm, 1995).

In general, inner sphere complexes are more strongly bound to the surface due to the strong covalent bonds involved in surface complex formation as opposed to the relatively longer-range and weaker coulombic forces associated with outer sphere complexation (Brown et al., 1995; Parks, 1990). Moreover, outer sphere complexed species typically retain their hydration sphere whereas during inner sphere adsorption one or more water molecules are displaced from the hydration sphere of the adsorbed species (Brown et al., 1995; Cotter-Howells and Paterson, 2000).

Depending on their molecular geometry, ligands may bind to the surface via different coordination modes. Coordination modes of adsorbed oxygenated ligands can be classified into two main categories according to the structure of the surface complex formed; namely monodentate and bidentate modes. A monodentate surface complex forms when a single oxygen from the adsorbed ligand binds to the surface (structure A; Figure 1-1) and a bidentate surface complex when two ligand oxygen atoms bind to the surface (structures B and C; Figure 1-1). If both oxygen atoms of the bidentate complex bind to the same metal centre, the resulting surface complex is termed mononuclear bidentate complex (or chelate complex; structure C) and if each oxygen is coordinated to two different surface centres it is termed binuclear bidentate complex (or bridging structure; B).

In the literature, the terms binding mode and coordination mode are often used interchangeably and may refer to either the type of surface complex formed and/or the structural geometry of the surface complex. In this study the term binding mode will be used to refer to the nature of the bond formed between adsorbed species and surface sites (i.e. inner sphere or outer sphere complexation). Conversely the term coordination mode will only refer to the structural geometry of surface bound ligands (i.e. monodentate or multidentate; mononuclear or binuclear).

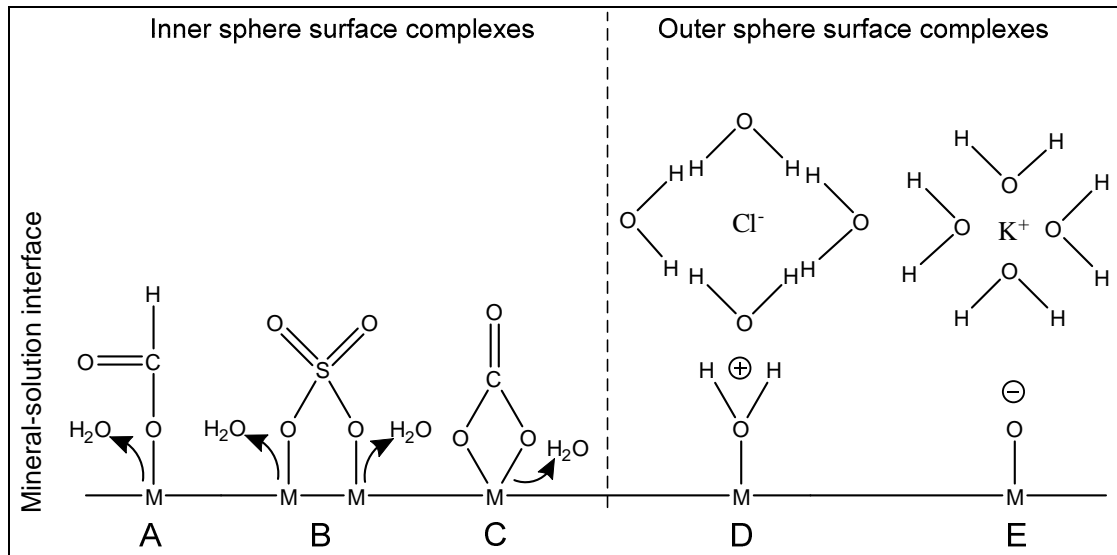


Figure 1-1 Schematic representation of surface complex formation. Ions displacing a surface functional group to form a direct chemical bond with a surface cation, through ligand exchange reactions, are termed inner sphere surface complexes (A-C). Surface cations act as a Lewis acid, and oxygen atoms in surface hydroxyl groups or in adsorbing species act as a Lewis base. A Lewis acid site is a site that accepts electron pairs from the adsorbing species and a Lewis base site is a site that donates free electron pairs (Stumm, 1992). Conversely ions bound to surface functional groups through electrostatic forces of attractions are termed outer sphere surface complexes and retain their hydration sphere (D and E).

The mineral water interface

The mineral-water interface is the location where the interactions between mineral surface sites and solutes from the overlying solution take place. Because adsorption reactions, as well as many of their associated geochemical processes are surface dependent phenomena, their study requires a prior understanding of the physicochemical properties of the mineral-water interface. In order to demonstrate the importance of the mineral-water interface in surface adsorption processes, an overview of its physical and chemical nature will be provided.

The electric double layer (EDL) theory and the surface complexation theory (SCT) have been instrumental in improving our understanding of the mineral-water interface. Briefly, the EDL theory describes the distribution of charges (i.e. ions) along the mineral water interface, and the SCT describes the chemical equilibria governing surface complex formation by assuming that adsorption occurs through the interactions between discrete surface sites and solute species. The combination of these two complementary theories provides a comprehensive conceptual model for the atomistic level description of the chemical reactions occurring at the mineral water interface. This in turn enables the interpretation, modelling and prediction of adsorption data.

Depending on the structural composition of the mineral phase, various different surface terminal functional groups are exposed on mineral surfaces. However for most silicate and oxide minerals the most important surface functional groups are hydroxyl groups (Stumm and Wollast, 1990). Surface functional groups have coordinative properties similar to those of their corresponding counterparts found in aqueous species and can thus bind to a variety of chemical species through surface coordination (or complexation) reactions (Stumm, 1986). Accordingly, adsorption can be described in terms of surface complexation reactions between discrete surface binding sites (e.g. surface hydroxyl groups) and dissolved species in a manner analogous to aqueous complex formation (Langmuir, 1997). The chemical reactivity of these surface hydroxyl groups is responsible for the charge development on the surface and for the coordinative interactions occurring between solute species and mineral surfaces.

The formation of a layer of surface hydroxyl groups on mineral surfaces can be explained by the reactive nature of atoms located on mineral surfaces. Such surficial atoms are under-coordinated with respect to the atoms located in the bulk crystal lattice, and therefore surface atoms tend to have a higher reactivity than their bulk phase counterparts. When in contact with water, these coordinatively unsaturated surface atoms will readily react with water molecules in order to complete the vacancies in their outer shell. Upon adsorption of water molecules, surface hydroxyl groups may form following the hydroxylation of surface cations and the protonation of surface anions (Koretsky, 2000).

Surface hydroxyl groups are often represented by the general $>X-OH$ species, where $>X$ denotes a surface metal centre. Because surface hydroxyl groups exhibit an amphoteric character they can either protonate or deprotonate, depending on the solution conditions. This acid-base behaviour of surface hydroxyl groups is commonly represented by the 2-pK formalism where surface groups undergo two protonation steps as shown below



and hence all surface sites can be envisaged as being occupied by $-OH$, $-OH_2^+$ and $-O^-$ groups. For the hypothetical single-site mineral surface shown in Figure 1-2, the majority of surface species are positively charged at low pH and deprotonate with increasing pH to form first neutral species and then negatively charged species. The acid-base reactions of these amphoteric hydroxylated surface sites, therefore, give rise

to a pH-dependent surface charge with high pH resulting in a net negative surface charge (i.e. predominance of $>X-O^-$ groups on the surface), and with low pH resulting in a net positive surface charge (i.e. predominance of $>X-OH_2^+$ groups on the surface).

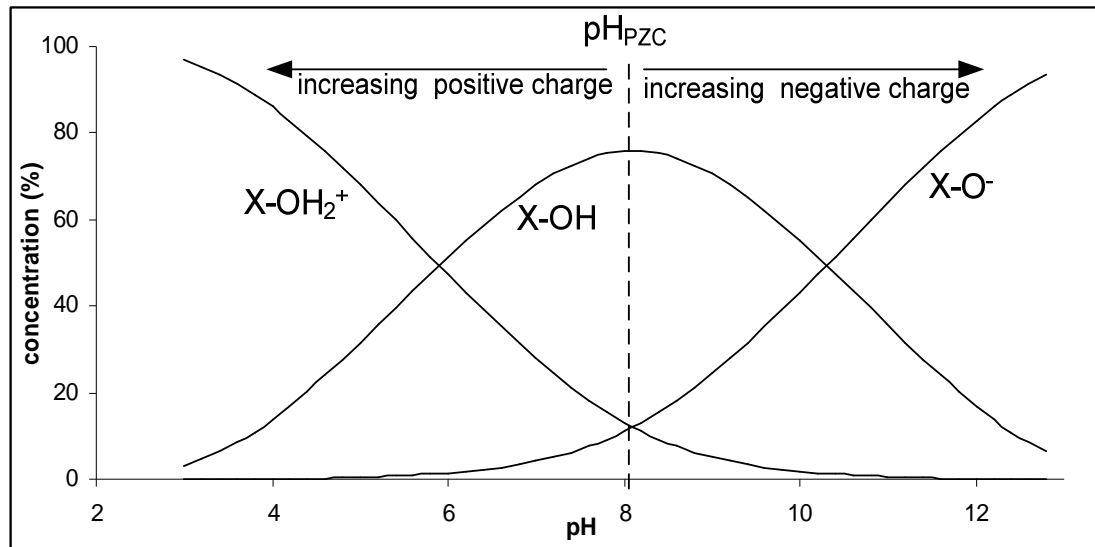


Figure 1-2 The distribution diagram of the three surface species ($X-OH$, $X-OH_2^+$ and $X-O^-$) assumed by the 2-pK model for a hypothetical mineral surface on which protons are the only adsorbing ions. At pH values lower than the pH_{PZC} the concentration of positively charged surface species, and thus the net positive surface charge increases; whereas above the pH_{PZC} the concentration of negatively charged surface species, and thus the net negative surface charge, increases.

Surface charge acquired by the ionisation of surface hydroxyl groups, as described above, is therefore variable because it is strongly pH-dependent. At a particular pH value where the sum of positively charged sites is equal to the sum of negatively charged sites, the net surface charge will be zero and the particular pH value is referred to as the pH of point of zero charge (pH_{PZC}), or sometimes as the pH of zero point charge (pH_{ZPC}). As will be discussed below, the assumption that the pH_{PZC} is equivalent to the pH value where the sum of protonated sites is equal to the sum of deprotonated sites is only valid for minerals with no permanent surface charge and in solutions where OH^- and H^+ are the only charge determining ions.

To describe surface speciation and thus the charging behaviour of a mineral surface according to the 2-pK approach, two equilibrium constants are required and these can be derived from the mass law equations relevant to each protonation step (i.e. reactions 1-1 and 1-2). Corresponding mass law equations and equilibrium constants for reactions 1-1 and 1-2 are given by

$$K_1^{app} = \frac{(>XOH)}{(>XO^-)(H^+)} \quad \mathbf{1-3}$$

$$K_2^{app} = \frac{(>XOH_2^+)}{(>XOH)(H^+)} \quad \mathbf{1-4}$$

The equilibrium constants, K_1^{app} and K_2^{app} , are apparent equilibrium constants, also known as conditional constants, because they are dependent on surface charge and thus vary with pH. The equilibrium constants describing surface protonation are also referred to as proton affinity constants or proton binding constants in the literature.

The adsorption of other ions can be described and formulated in terms of surface species formed in a similar manner to that used for the protonation/deprotonation reactions of surface functional groups. For example the binding a divalent ligand (L^{2-}) to a surface site can be represented by



and the respective mass law equation by

$$K^{app} = \frac{(>XL^{1-})}{(>XOH)(L^{2-})(H^+)} \quad \mathbf{1-6}$$

The equilibrium constant for the mass law equation given above, K^{app} , is also a conditional constant since the adsorption reaction is influenced by surface charge. Equilibrium constants independent of surface charge effects, termed intrinsic equilibrium constants, can only be obtained by introducing an electrostatic correction term to mass law equations. Further information regarding equilibrium constants will be given in chapter 3.

In the examples of surface reactions given above (reactions 1-1,1-2, and 1-5), solute species are assumed to interact with a single-type of surface functional groups, that is a general $>X-OH$ group. In surface complexation theory, the representation of all surface functional groups by a common surface group provides a simple conceptual framework for describing surface chemical reactions and surface charge development. It must be noted however that various hydroxyl groups exposed to the surface may not be structurally and chemically equivalent. Even for simple (hydr)oxides, containing a single cation type, surface hydroxyl groups may be singly, doubly or triply coordinated if they are coordinated with one, two or three surface cations respectively. Therefore the

properties of the various surface groups are represented by an average surface hydroxyl group, since different sites will have distinctly different acid-base properties and reactivities (Casey, 1995). Structural heterogeneity can be addressed by the use of multi-site models which allow for surface reactions to occur in two or more different structurally different surface binding sites.

The pH_{PZC} , along with surface site density (concentration of surface hydroxyl groups per unit surface area of the mineral; typically given in sites/ m^2) and the surface area of the mineral (surface area per unit mass of mineral; typically in m^2/g), are important surface parameters required for the description of surface adsorption reactions. The pH_{PZC} relates to the charging behaviour of the surface and thus to the nature of the electrostatic interactions between the surface and solute species. Site density and surface area, on the other hand, will govern the number of available surface sites for adsorption and hence the adsorptive capacity of the mineral surface.

Surface charge and the electric double layer (EDL)

The pH-dependent surface charge arising from the proton donor-acceptor reactions of surface functional groups is also referred to as the net proton charge. Because this type of charge originates from the adsorption of protons (or hydroxyl groups), the proton charge density is correlated to the surface concentration of protons and hydroxyl groups. The proton charge density (σ_{H}), expressed in coulombs per square meter (C/m^2) is given by

$$\sigma_{\text{H}} = F(\Gamma_{\text{H}} - \Gamma_{\text{OH}}) \quad \mathbf{1-7}$$

where Γ_{H} and Γ_{OH} represent the adsorption densities of hydrogen and hydroxyl ions (mol/m^2) respectively, and F is the Faraday constant ($96485 \text{ C}/\text{mol}$). Therefore, the proton charge density of a mineral surface can be experimentally determined from the amount of hydrogen and hydroxyl ions adsorbed on the surface. Although metal (hydr)oxides primarily exhibit a variable pH-dependent surface charge, surface charge may also develop from two other main factors.

(1) Mineral surfaces may develop a permanent surface charge due to lattice imperfections and due to isomorphous substitution of cations in the crystal lattice. As the name suggests this type of charge is permanent and thus independent of pH. Isomorphous substitution is particularly important for clay minerals which typically have a predominant permanent negative charge owing to the substitution of metal

cations with different valence in the crystal structure. For example, the substitution of a silicon atom for an aluminium atom in the siloxane layer (Si-O-Si) of kaolinite will lead to an increased negative charge on the silicon basal plane due to the formation of the negative (Si-O-Al)⁻¹ group (Wieland and Stumm, 1992).

In addition to the permanent negative charge, clay minerals also possess a pH-dependent surface charge analogous to that of metal (hydr)oxide surfaces originating from the acid-base reactions of surface hydroxyl groups located at edge sites. The net surface charge on clay minerals, however, is typically found to be negative over the entire pH range due to the small edge surface area relative to the rest planar surface area.

(2) The adsorption of solute species, other than protons, can also impart a surface charge on mineral particles. Species that can influence the charge of the surface are typically charged ions and are collectively termed potential or charge determining species. In general, adsorbed cations tend to increase the net positive charge (or decrease the net negative charge) of the surface, and adsorbed anions tend to increase the net negative charge when compared to systems where acid-base reactions are the only contributors to surface charge (Stumm, 1993). Hence the amount of variable charge that can be developed on a mineral surface will not only be influenced by the acid-base equilibria of surface functional groups, but also by the adsorption of other solute species.

The net total surface charge developed on the surface of minerals can be determined by the sum of the individual permanent and variable charge contributions as follows (Stumm, 1993)

$$\sigma_o = \sigma_p + \sigma_H + \sigma_{is} + \sigma_{os} \quad \mathbf{1-8}$$

where σ_o is the net total surface charge, σ_p is the permanent structural charge, σ_H is the net proton charge and σ_{is} and σ_{os} denote the charge from other potential determining species adsorbed as inner sphere and outer sphere complexes respectively.

The development of surface charge will in turn affect the distribution of solution ions in the vicinity of the mineral surface. More specifically, the electrostatic charge on the surface attracts a diffuse layer of oppositely charged ions (counterions) in the solution adjacent to the surface, and the concentration of these ions will be determined by the magnitude of the surface charge. As a result there is an increased concentration of counterions relative to the bulk aqueous phase near the surface. Furthermore, the concentration of counterions is highest in the region adjacent to the surface and

decreases progressively with distance until it reaches a minimum steady value that corresponds to the bulk solution concentrations. At the same time ions possessing the same charge as that of the surface (co-ions) will be repelled from the surface region, leading to a near-surface solution which is depleted of such ions when compared to the bulk solution phase.

These changes occurring near and on the surface result in the creation of the mineral water interface which has different physical and chemical properties from those of the bulk mineral and of the bulk solution phases. The redistribution of solute ions near the surface leads to a charge separation at the mineral-water interface which is idealised as an electric double layer (EDL). The EDL theory assumes that the electrostatic charge developed at the mineral-water interface is separated into two layers: one layer of fixed charge on the surface of the mineral, and a diffuse layer of electrostatically bound counterions in the solution adjacent to the surface which balances the excess surface charge. The separation of charges in turn leads to the establishment of an electrical potential across the EDL of the interfacial region. The electrical potential generated at the interface is at a maximum value on the surface of the mineral and declines with distance towards the bulk solution phase (conventionally assumed to be zero).

Different theoretical models have been developed to describe the distribution of electrical potential and charge (i.e ions) at the mineral water interface. For example the distribution of surface charge and potential within the electric double layer can be represented according to the Stern-Grahame EDL model (Figure 1-3) and the charge balance is given by (Davis and Kent, 1990)

$$\sigma_o + \sigma_\beta + \sigma_d = 0 \qquad \mathbf{1-9}$$

where σ_o is the surface charge density, σ_β is the charge of the β -plane (Stern layer) and σ_d represents the charge of the diffuse layer. The Stern-Grahame model is an improved version of the Gouy-Chapman model which also describes the distribution of counterions in an electrolyte solution adjacent to a charged surface. Importantly, the Stern-Grahame model takes into account the finite size of ions and hence assumes that there is a minimum distance of approach between counterions and the surface (Davis and Kent, 1990).

According to the Stern-Grahame model, ions located in the Stern layer are specifically adsorbed to the surface whereas ions in the diffuse layer are nonspecifically adsorbed and retain their hydration shells. In the diffuse layer ion distribution follows

the Gouy-Chapman distribution and the potential decreases in an almost exponential manner with distance away from the Stern layer.

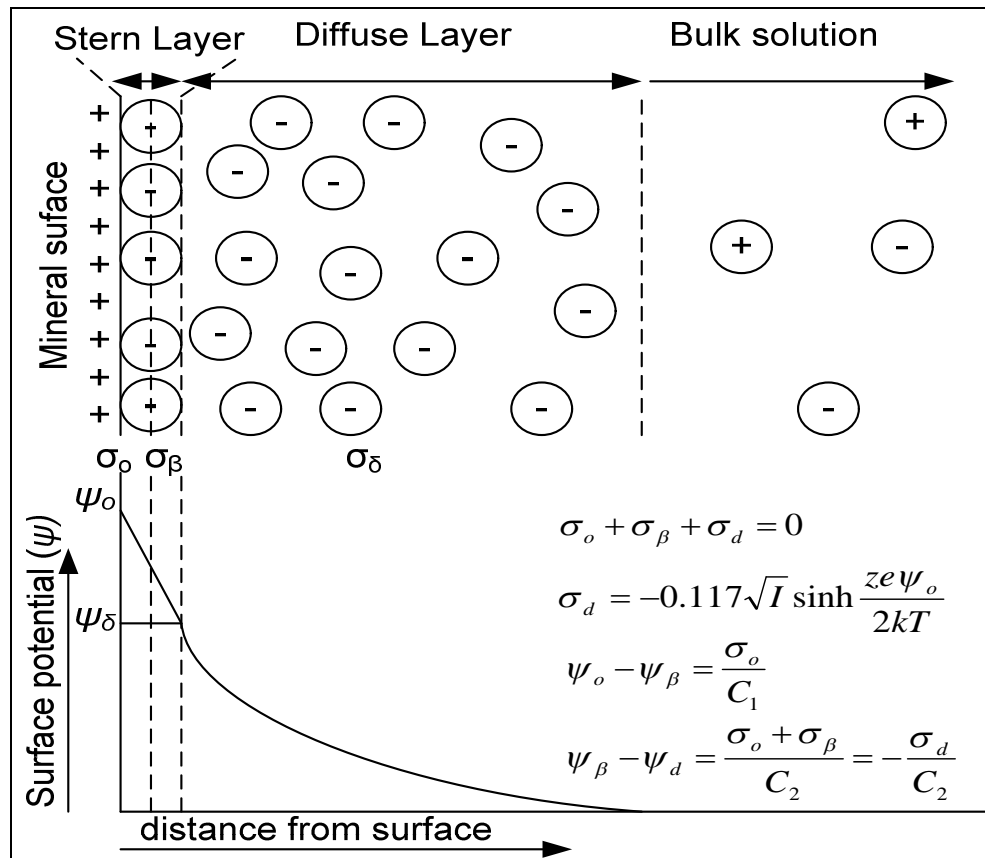


Figure 1-3 Schematic representation of the electric double layer according to the Stern-Grahame model. The surface charge-potential relationship is also included. The Stern layer (β - plane) is the closest distance of approach between counterions and the surface. The surface potential in the Stern layer falls linearly whereas in the diffuse layer the surface potential declines near exponentially according to the Gouy-Chapman charge-potential relationship. For the equations given, I is the ionic strength (mol/L), z is the valence of the electrolyte ions, ψ_o is the potential at the surface (volts), k is the Boltzmann constant, T is the absolute temperature (K), C_1 and C_2 the inner layer (between the α -plane and β -plane) and outer layer (between the β -plane and d -plane) capacitance (F/m^2) respectively. Adopted by Davis and Kent (1990).

Ions attracted to the diffuse layer by coulombic forces do not affect the magnitude of the surface charge and hence they are referred to as indifferent electrolyte ions (Tombacz, 2002). However the concentration and valence of the indifferent ions influence the thickness of the diffuse layer and as a result the potential profile at the interface. Higher concentrations and/or higher valency ions decrease the thickness of the diffuse layer and as a result the distance from the surface in which the potential of the double layer falls to zero (i.e. a more rapid decrease in potential).

The electric double layer theory can therefore be used to describe the distribution of charge (i.e. ions) at the mineral-water interface, the change in electrical

potential away from the surface, and the effects of electrostatic forces on surface related phenomena. However, in the EDL theory the surface of a mineral is treated as a structure-less continuum and its interactions with the solution are only governed by electrostatic effects that can be described in terms of bulk properties (Stumm, 1997). The surface complexation theory addresses this limitation by providing an atomistic approach for the description of surface reaction occurring at the mineral water interface.

Surface complexation modelling

Adsorption is a competitive process with ions competing for available surface binding sites and with different ions having different affinities for surface binding sites. Therefore, the extent of adsorption for any particular species is influenced by a variety of factors including solution chemistry (e.g. pH, ionic strength), surface properties (e.g. surface area, site density) the chemical affinity of the solute species for surface sites, and the charging behaviour of both the surface species and of the solute species.

The ability to predict the macroscopic adsorption behaviour of solute species on mineral surfaces under a wide range of solution conditions is one of the main goals of surface science. Predictive adsorption models have been extensively used in the literature for the quantitative description of experimental adsorption data. Early modelling attempts were based on empirical models such as adsorption isotherm equations and partitioning equations. Such models typically employ simple mathematical equations which relate the concentration of adsorbed species to the concentration of free species in solution. However, these models are often of limited use because they fail to take into account the electrostatic interactions between solute species and mineral surfaces.

In contrast to these empirical models, surface complexation models (SCMs) are semi-empirical chemical models that provide an atomistic description of the coordinative interactions occurring at the mineral-water interface. SCMs (also referred to as electrostatic adsorption models) can quantify the adsorption data over a wide range of experimental conditions by incorporating the basic principles of the surface complexation theory and of the EDL theory.

In surface complexation modelling charge distribution at the mineral-water interface is conceptualised using the EDL theory, with a layer of fixed charge on the surface and a diffuse layer of counterions in the solution adjacent to the surface. The use of the EDL theory in surface complexation modelling is of great importance because the

effects of surface charge on adsorption can be accounted for by applying an electrostatic correction factor to the mass law equations describing surface reactions.

Although different surface complexation models (SCMs) have been developed, all these models are based on the same fundamental principles. Importantly, SCMs assume that the adsorption capacity and surface charge arise from the chemical reactions of surface binding sites (i.e. surface functional groups) and therefore the adsorption density and surface charge density are both restricted by the concentration of surface binding sites. In addition all SCMs use an equilibrium approach to define the chemical reactions between surface groups and solute species and hence adsorption is modelled via mass law equations.

The difference between various surface complexation models is based on the structural representation of the electric double layer (Davis and Kent, 1990; Kraepiel et al., 1998; Sahai and Sverjensky, 1997). Common surface complexation models that have been used for the description ion adsorption on mineral surfaces include the constant capacitance model (CCM), the diffuse layer model (DLM), and the triple layer model (TLM). Although in all SCMs the surface charge is assumed to be balanced by the charge of the diffuse layer ($\sigma_o + \sigma_d = 0$), each model considers a different charge distribution, and thus a different electrostatic potential profile, across the charged interface.

Depending on the specific surface complexation model employed, adsorbed ions can be located in one or more adsorption planes located between the charged surface and the bulk solution phase. According to the DLM, charge on the surface plane (σ_o) develops by the adsorption of protons and hydroxyls, as well as by the specific adsorption of other ions, on surface binding sites. Non specifically adsorbed ions located in the diffuse layer neutralise the charge on the surface and comprise the second plane of the EDL. Unlike specifically adsorbed ions on the surface plane, counterions in the diffuse layer are not associated with specific surface functional groups.

The TLM has three interfacial planes (i.e. three adsorption planes) and allows for both specific and non specific interactions with surface functional groups. The three interfacial planes are: (1) a surface plane in which H^+ , OH^- and other specifically adsorbed ions are located. This plane is also referred to as the α -plane or the inner Helmholtz plane and defines the distance of closest approach of specifically adsorbed ions. (2) a near surface plane in which adsorbed ions are weakly bound to surface sites with at least one water molecule existing between these adsorbed ions and surface sites. This plane is also referred to as the β -plane or the outer Helmholtz plane and defines the distance of closest approach for ions retaining their hydration shells. Typically the

boundary of the inner Helmholtz plane is assumed to pass through the centre of specifically adsorbed ions and the boundary of the outer Helmholtz plane passes through the centre of non specifically hydrated adsorbed ions, in their position of closest approach. (3) A diffuse layer of non specifically adsorbed counterions. Although hydrated ions in the β -plane and in the diffuse layer of the TLM are non specifically adsorbed (i.e. held by coulombic attractions) their main difference lies in the type of association with surface functional groups. The ions in the diffuse layer do not bind to specific surface sites and remain free in solution whereas the ions in the β -plane are coordinated to surface functional groups.

Surface coordination and mineral dissolution mechanisms

The coordinative interactions occurring at the mineral water interface can have a strong effect on the rates of surface-controlled processes such as mineral precipitation and dissolution, the formation of secondary minerals and corrosion of metals (Stumm and Wollast, 1990). The dependence of mineral dissolution and precipitation reactions on the surface coordination environment of adsorbed species has perhaps received the greatest attention in the literature. According to the coordination chemical theory proposed by Stumm and coworkers (e.g. Biber et al., 1994; Furrer and Stumm, 1986; Stumm, 1997; Stumm and Wollast, 1990; Wieland et al., 1988; Zinder et al., 1986), the dissolution rates of mineral oxides depend on the specific interactions between solute species and mineral surfaces. Central to this theory is the recognition that these interactions cause a change in the coordinative environment of metal centres exposed at mineral surfaces.

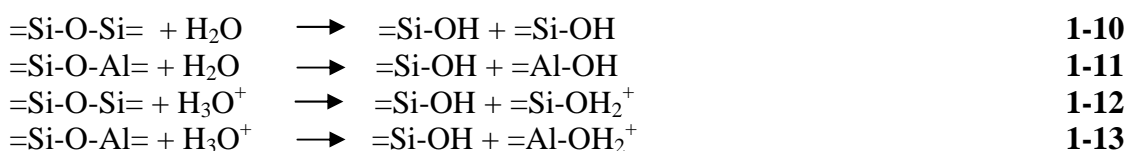
It has been shown that dissolution rates primarily dependent on (a) the nature of bonds formed between solute ions and surface adsorption centres and (b) on the coordination geometry of adsorbed species on surface sites (Stumm, 1995). As a result the establishment of a relationship between surface speciation and mineral dissolution rates has become a primary goal of numerous studies. Principal solute ions involved in mineral dissolution reactions are H^+ , OH^- , H_2O and ligands.

In far from equilibrium conditions a mineral dissolution reaction consists of three principle steps: (a) the attachment of solute species to surface cations which polarises; (b) the detachment of surficial cations; and (c) the transport of these cations to the bulk solution and the renewal of a surface site by protonation (Furrer and Stumm, 1986). Two reaction mechanisms are thought to be involved in the dissolution of metal

(hydr)oxides and silicate minerals, a proton-promoted dissolution and a ligand-promoted dissolution reaction mechanism. These two main dissolution pathways are generally treated as independent parallel reaction mechanisms and are thus additive.

Proton-promoted dissolution

The acid-base reactions of oxygen atoms that bridge surficial metal cations can have a significant effect on the rates of dissolution rates by increasing the reactivity of surface sites. Under acidic conditions surface protonation enhances the dissolution rates because adsorbed protons polarise and weaken critical surface metal-oxygen bonds and thus facilitating the detachment of metal cations from the mineral surface (Furrer and Stumm, 1986). It is generally accepted that the key step in the dissolution of most silicate and aluminosilicate minerals is the hydrolysis of bridging oxygen bonds following the adsorption of hydrogen ions. Such hydrolysis reactions include (Stumm, 1997; Xiao and Lasaga, 1994)



Ligand-promoted dissolution

Ligands adsorbing on surface sites through a ligand exchange reaction enhance dissolution by enabling the detachment of surface cations (Furrer and Stumm, 1986). Similar to the effect of adsorbed protons, adsorbed ligands destabilise important metal-oxygen framework bonds by shifting the electron density distribution towards the coordination sphere of surface metal centres (Stumm, 1992). As a result adsorbed ligands can decrease the activation energy for hydrolysis and thus increase the release of metal cations from the surface.

The ligand promoted dissolution mechanism of metal (hydr)oxides and aluminosilicates is assumed to occur independently from the protolytic dissolution mechanism (e.g. Blake and Walter, 1999; Furrer and Stumm, 1986; Wieland and Stumm, 1992; Wogelius and Walther, 1991). Furthermore, the greatest effect exerted by organic ligands on dissolution rates is in the near neutral pH region where the effect of proton promoted dissolution is at minimum (Blake and Walter, 1999; Welch and Ullman, 1993). Moreover, the structures and binding modes of the cation-ligand surface complexes formed were shown to have a significant effect on dissolution rates. Whether

a ligand forms an inner sphere or an outer sphere complex is important due to the influence of the surface complex on the reactivity of the mineral surface.

The weak interactions between outer sphere complexed ligands and surface sites cause minimal changes in the electron density distribution of the mineral surface, and therefore are not expected to have a major influence, if any, on the dissolution rates (Furrer and Stumm, 1986; Koretsky, 2000). It is important to note, however, that recent studies have demonstrated that outer sphere complexed organic ligands can in fact inhibit mineral dissolution rates. This effect was attributed to the ability of outer sphere complexed species to prevent protons from attacking dissolution-active surface sites and thus resulting in the reduction of the protolytic dissolution rate (Johnson et al., 2005; Johnson et al., 2004a; Yoon et al., 2005).

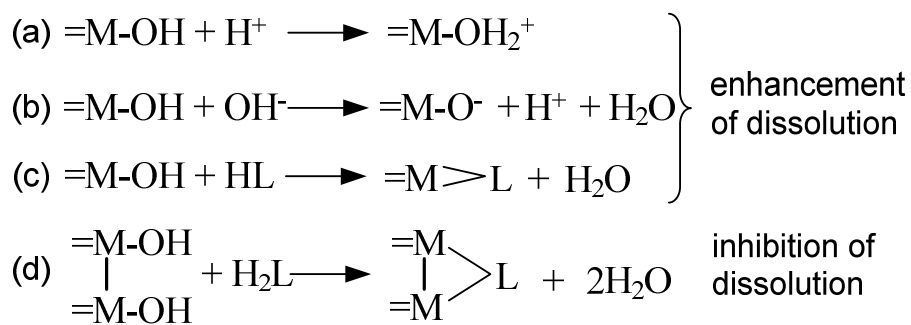
Although inner sphere complexes have a more profound effect on dissolution rates in comparison to outer sphere complexes, the dissolution rates are also related to the structure (i.e. coordination mode) of the inner sphere complex formed. Mononuclear, bidentate surface complexes (chelate structures) are known to be more effective in enhancing mineral dissolution rates than monodentate structures. Conversely, binuclear bidentate surface complexes (bridging structures) inhibit dissolution because of the much higher energy needed to simultaneously remove two metal cations from the surface (Furrer and Stumm, 1986). In addition to forming surface structures that inhibit or prevent dissolution, such inhibitor species can also decrease the proton and/or ligand promoted dissolution rates by competing with other dissolution enhancing species for available surface sites (Biber et al., 1994).

Other species can inhibit dissolution rates solely due to a surface blocking effect rather than by the type of surface complex formed. For example free Al^{3+} can inhibit kaolinite dissolution due to the competition of aluminium and hydrogen ions for available surface sites (Ganor et al., 1995). Similarly inhibitor species can also affect the ligand promoted dissolution mechanism by competing with dissolution enhancing ligands. For example chromate and arsenate were found to decrease the ability of oxalate to promote the dissolution rates of goethite by decreasing the extent of oxalate adsorption due to the competition between these oxyanions and oxalate ions for surface sites (Eick et al., 1999).

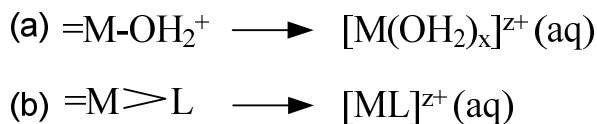
Dissolution rates

The dissolution reactions of oxides and aluminosilicate minerals are usually treated as surface controlled reactions for which the rate limiting step is the release of ions from the surface and into the solution. Surface controlled dissolution rates for simple oxide minerals can be generalised into two reaction steps, a fast reaction step involving the coordination of solute species on dissolution active surface sites and a slow (i.e. rate limiting) step involving the detachment of a metal cation from the surface (Stumm, 1986)

(1) Fast surface coordination step: surface site + solute species (H^+ , OH^- , ligand) \rightarrow surface species



(2) Slow surface detachment step (rate-limiting step): surface species $\rightarrow M(aq)$



This reaction scheme is a simplified model which explains the mechanism by which ligands and protons can affect mineral dissolution rates. Other smaller reactions steps may also be involved in the dissolution reaction. Typically prior to the detachment of a surficial metal centre, a number of protonation steps equivalent to the valency of the metal cation is required. Hence for the dissolution of a divalent metal oxide, two adjacent hydroxyl groups which are coordinated to the same metal centre need to be protonated. This relatively fast stepwise protonation is then followed by a slow (rate-limiting) step which involves the detachment of the metal cation from the surface (Stumm, 1986). For silicate minerals similar dissolution reaction schemes have been proposed which, however, involve a larger number of reaction steps.

Mineral dissolution rates will thus be determined by the particular effect of surface bound species in weakening the critical metal-oxygen bonds at the mineral surface (i.e. their effect on the rate limiting step of dissolution). As a result the binding

and coordination modes of the surface complexes formed have an important effect on surface reactivity, that is, its tendency to dissolve. As discussed earlier, protons and some types of ligands can facilitate the detachment of surface cations and thus enhance the dissolution rate by increasing the rate of the rate-limiting step. Conversely, other ligands may inhibit the detachment of surface cations and thus decrease the rate-limiting step of the dissolution reactions.

According to the surface controlled dissolution model proposed by Furrer and Stumm (1986), dissolution rates are proportional to the surface concentrations of the various species that can influence the surface reactivity of the mineral. These surface species are termed the precursor complexes and are the final species formed in the series of reaction steps occurring during dissolution prior to the rate limiting step of the reaction. For the two-step reaction sequence shown above, the dissolution reaction is limited by the second reaction step and hence the dissolution rate law will be dependent on the concentration of surface species formed in the first step so that (Stumm and Wollast, 1990)

$$R = k (C_j) \quad \mathbf{1-14}$$

where R is the dissolution rate in $\text{mol/m}^2\cdot\text{s}$ and C_j is the surface concentration of the precursor species (e.g. protonated surface site; $>X\text{-OH}_2^+$ and/or a specifically adsorbed ligand; $>X\text{-L}$). Furthermore, C_j is proportional to the surface site density (S), the mole fraction of dissolution active surface sites (γ_a), and the probability of finding a specific surface site in the coordinative arrangement of the precursor complex (p_j).

In the acid region, the overall dissolution rate can be represented as the sum of the proton promoted dissolution rate and of the ligand promoted dissolution rate. In a system including a single rate enhancing ligand and at pH values below the pH_{PZC} the total dissolution rate, R_T ($\text{mol/m}^2\cdot\text{s}$), corresponds to the net proton promoted (R_H) and net ligand promoted dissolution rates (R_L) as expressed as by the following rate law (Furrer and Stumm, 1986)

$$R_T = R_H + R_L = k_H (C_H^s)^n + k_L (C_L^s) \quad \mathbf{1-15}$$

where C_H^s and C_L^s are the concentrations of surface bound protons and surface bound ligands respectively (mol/m^2); k_H and k_L are dissolution rate constants ($1/\text{s}$); and n is the rate order for proton promoted dissolution. For ideal cases the exponent n corresponds to the oxidation state of the surficial metal centre and hence for aluminium

and iron (III) n is equal to 3 (Stumm and Wollast, 1990). Additional individual dissolution rates can be included to the dissolution rate equation if different dissolution enhancing ligands are present in the system. Provided that the various ligand-promoted rates are additive, then the dissolution rate can be given by

$$R_T = R_H + R_{L1} + R_{L2} + R_{L3} + R_{L3} + \dots = R_H + \sum_i R_{Li} \quad \mathbf{1-16}$$

According to equations 1-15 and 1-16 the concentration of positively charged surface sites ($>X-OH_2^+$) has a strong influence on the dissolution rate by increasing the term relating to the proton promoted dissolution (R_H). However, dissolution rates are also proportional to the concentration of negatively charged sites ($>X-O^-$), and thus to the extent of deprotonation. The deprotonation of surface sites is comparable to the binding of OH^- ions on surface sites and the hydroxyl promoted dissolution can be expressed in a similar manner as that for proton promoted dissolution (Stumm, 1992)

$$R_{OH} = k_{OH} (C_{OH}^s)^m \quad \mathbf{1-17}$$

where R_{OH} is the dissolution rate due to surface deprotonation; C_{OH}^s is the surface concentration of hydroxyl ions; k_{OH} is the reaction constant; and m the rate order of the reaction. By combining the individual dissolution rates then the total dissolution rate can be represented in terms of surface species concentrations

$$R_T = k_H (C_H^s)^n + k_{OH} (C_{OH}^s)^m + \sum_i k_{Li} (C_{Li}^s) \quad \mathbf{1-18}$$

where the first term corresponds to the proton promoted dissolution rate, the second term to the hydroxyl promoted dissolution rate and the third term to the sum of ligand promoted dissolution rates. Reductive dissolution where a reducing ligand transfers electrons to the surface is considered as a special type of ligand promoted dissolution (Biber et al., 1994).

Because the surface concentration of hydrogen and hydroxyl ions, the surface charge, and the pH are interrelated, dissolution rates can also be related to surface charge and the pH of the solution. As already mentioned surface charge, particularly for metal (hydr)oxides, is primarily governed by the relative concentrations of $>X-OH_2^+$ and $>X-O^-$ surface species. Hence the general rate law (reaction 1-18) predicts minimal proton and hydroxyl promoted dissolution rates near the pH of zero net proton charge (pH_{ZNPC}) where the concentration of positively and negatively charged sites is minimal.

The pH_{ZNPC} is the pH value where the net proton charge is equal to zero ($\sigma_{\text{H}} = 0$). Increasing dissolution rates are expected either with increasing positive charge as the pH of the solution decreases below the pH_{ZNPC} or with increasing negative charge as the pH of the solution increases above the pH_{ZNPC} (Stumm and Wollast, 1990).

Therefore mineral dissolution rates can also be related to the pH of the solution and hence dissolution rate laws relating to the concentration of proton and hydroxyl ions in solution can also be derived. At far from equilibrium conditions, the dissolution rates of most silicate minerals exhibit a similar pH dependence as the one shown in Figure 1-4. At acidic conditions, dissolution rates increase exponentially with increasing hydrogen ion concentration in solution according to the empirical rate law

$$R_{\text{H}} = k_{\text{H}}[\text{H}^+]^p \quad \mathbf{1-19}$$

where k_{H} is a rate constant and p is an exponent that varies with the type of mineral and is typically between 0.3-1 (Drever, 1994). Note that the value for p is not the same as the value for n used in reaction 15 since the concentration of hydrogen ions in solution is not necessarily linearly related to the concentration of adsorbed hydrogen ions (Drever and Stillings, 1997; Stumm, 1992). At near neutral conditions and above some transition pH, typically above 4-5, the dissolution rate becomes independent of pH so that

$$R_{\text{neutral}} = k_{\text{N}} \quad \mathbf{1-20}$$

At even higher pH values and above a pH transition point in the alkaline region at about 8, dissolution rates increase exponentially with increasing pH

$$R_{\text{OH}} = k_{\text{OH}}[\text{OH}^-]^q \quad \mathbf{1-21}$$

where q is typically between 0.3-0.5 (Drever, 1994; Drever and Stillings, 1997).

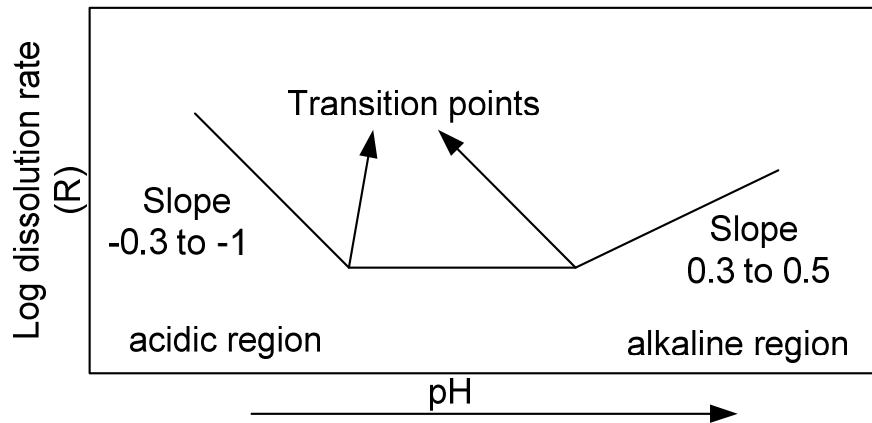


Figure 1-4 Rates of silicate dissolution as a function of pH, at far from equilibrium conditions. Increased hydrogen concentrations in the acidic region and increased hydroxyl concentrations in the alkaline region result in increased dissolution rates. Note that the dissolution rate is plotted in a logarithmic scale meaning that in the acidic region an increase of one pH unit will result in a decreased dissolution rate by a factor of about 3 (assuming a slope of 0.5). Adopted by Drever (1994).

The role of organic ligands on mineral dissolution

The effect of organic ligands on mineral dissolution rates has been the subject of considerable interest for many years. Typically the dissolution rates measured in the presence of low molecular weight organic ligands (such as oxalate, citrate, salicylate) are faster than those measured in the presence of inorganic acids under the same pH (e.g. Bennett et al., 1988; Blake and Walter, 1999; Cama and Ganor, 2006; Chin and Mills, 1991; Drever and Stillings, 1997; Franklin et al., 1994; Stillings et al., 1996; Welch and Ullman, 1993; Wogelius and Walther, 1991). However, the mechanisms by which organic ligands can catalyse the dissolution reaction are still a matter of controversy (Cama and Ganor, 2006). Two competing theories exist that may explain the influence of organic ligands on dissolution rates: either by an indirect proton promoted dissolution mechanism or by a direct ligand promoted dissolution mechanism.

In the presence of organic ligands increased proton-promoted dissolution rates can be achieved in three principle ways. (1) Organic ligands can form strong aqueous cation-ligand complexes with metal cations removed from the surface by dissolution. These complexation reactions can decrease the chemical activity of aqueous cations and hence the saturation state of the solution with respect to the dissolving mineral. As a result organic ligands have the potential to enhance the proton promoted dissolution rate by reducing the Gibbs free energy (ΔG_r) of the dissolution reaction by forming aqueous cation-ligand complexes (Drever and Stillings, 1997).

The Gibbs free energy evaluates the degree of saturation (i.e. deviation from equilibrium) of the solution and is calculated by (Cama and Ganor, 2006)

$$\Delta G_r = RT \ln \left(\frac{IAP}{K_{eq}} \right) \quad 1-22$$

where IAP is the ion activity product of the solution, K_{eq} is the solubility constant, R is the gas constant, and T is the absolute temperature. The further away from chemical equilibrium (i.e. solution at higher undersaturation) ΔG_r values become increasingly negative. At $\Delta G_r = 0$ the dissolution reaction is at equilibrium and therefore the dissolution reaction rate is equal to the precipitation reaction rate.

(2) It has been shown that under acidic conditions the far from equilibrium dissolution rates of aluminosilicates can be inhibited by free aluminium species which are the dominant species in solution (Ganor et al., 1995). By complexing aluminium ions in solution, organic ligands can significantly reduce the activity of aqueous Al^{3+} species and consequently their possible inhibition effects on dissolution rates.

(3) At acidic conditions, adsorbed organic ligands can reduce the positive charge of mineral surfaces induced by the protonation of surface functional groups. As a result more protons can accumulate at the mineral-water interface due to the reduced electrostatic repulsions and this can in turn increase the proton promoted dissolution rates.

Although all of the above mechanisms have the potential to contribute indirectly to the proton promoted dissolution, adsorbed organic ligands can also increase dissolution rates through a direct ligand promoted mechanism. As discussed earlier, direct ligand coordination to surface metal centres can destabilise important metal-oxygen framework bonds and therefore increase the rates of dissolution by facilitating the detachment of surface cations.

Organic ligands in the environment

Natural organic matter (NOM), the dominant source of organic ligands, is a ubiquitous, reactive component in the environment and can be found in both soluble and insoluble forms. Non-dissolved NOM occurs as the main organic constituent of soils and sediments, and is generally termed soil organic matter (SOM). In its soluble form NOM is referred to as dissolved organic matter (DOM) and can be a prevalent constituent of both surface and ground waters.

Origin and structure of NOM

NOM is formed in both terrestrial and aquatic environments by the chemical and physical degradation of plant and animal matter and through microbial biosynthesis and metabolism (Schnitzer, 1989). Due to the diverse nature of parent material and decomposition processes, NOM consists of a heterogeneous mixture of organic compounds with varying chemical and structural compositions. NOM constituents can be distinguished into two major components, namely non humic substances (non-HS) and humic substances (HS). Non humic substances comprise the well characterised fraction of organic matter with major components including compounds of known structures and properties such as low molecular weight (LMW) organic acids, amino acids, amino sugars, nucleic acids, carbohydrates, and lipids (Piccolo, 2001; Van Hees et al., 2005).

Typical concentrations of the non-humic substances in soil solutions range from 0.1-5 μM for amino acids and amino sugars; 0.1-50 μM for dicarboxylic and tricarboxylic LMW organic acids (such as oxalic and citric acid); and up to 1mM for monocarboxylic LMW organic acids (such as formic and acetic acid) and sugars (such as glucose) (Strobel, 2001; Van Hees et al., 2005). Overall the concentrations of these organic compounds are relatively low in soil solutions with, for example, the fraction of carbon in LMW weight carboxylic acids accounting for a maximum of up to 10% of the total DOC in soil solutions (Strobel, 2001; Van Hees et al., 2000).

In contrast to non-humic substances, humic substances consist of complex high molecular weight organic macromolecules which lack specific chemical and physical characteristics and hence comprise the ill-defined fraction of natural organic matter. It has to be noted however that some authors have challenged the polymeric view in which humic molecules are considered as a unique class of high molecular weight organic molecules. Instead they suggested that the apparent high molecular values observed for these macromolecules originate from the association of smaller organic molecules, via intramolecular interactions, in a supramolecular structure (Burdon, 2001; Piccolo, 2001; Sutton and Sposito, 2005)

Humic substances constitute the major class of organic compounds in aquatic environments and represent between 50-75% of the total dissolved organic carbon (DOC) in natural waters (Robards et al., 1994). Humic substances can be further subdivided into three fractions, namely humin, humic acids, and fulvic acids. These

three broad categories are operationally defined according to their solubility in aqueous solutions and each category covers a wide range of structurally different compounds. Fulvic acids are defined as the fraction of humic substances that is soluble in water under all pH conditions whereas humic acids comprise the fraction which is insoluble in water under pH 2. The third category, humin, is defined as the fraction of humic substances which remains insoluble in water at all pH values (Drever, 1988).

Despite the fact that humic substances comprise the major fraction of NOM, there is still limited knowledge about various aspects of their chemical and physical properties. The chemical properties of humic and fulvic acids are believed to resemble the properties of other LMW organic acids because both types of compounds contain similar types of acidic functional groups. Carboxylic and phenolic functionalities are considered to be the two most important functional groups in organic compounds as they are responsible for the charging behaviour and binding properties of both low molecular organic acids and humic acids. Therefore the use of simple well defined organic acids has provided valuable information regarding the chemical behaviour of humic acids in the environment.

The importance of organic matter

Owing to its widespread occurrence and reactivity, organic matter has the ability to participate in various important chemical reactions in soils, sediments and aqueous solutions. It is therefore not surprising that the properties and role of natural organic matter in the environment have attracted much scientific interest over the years. Particular attention has been and is still given to the environmental behaviour of humic acids and of LMW organic acids because they are believed to be the most reactive phases of NOM and thus key components for determining the properties and behaviour of NOM.

The ability of various NOM constituents (mainly organic acids) to act as ligands enables the formation of aqueous complexes with ions in solution as well as surface complexes with mineral surfaces. Such complexation reactions can affect several important environmental processes including the environmental behaviour (e.g. speciation, solubility, sorption, transportation, bioavailability) of both organic and inorganic pollutants and trace elements (e.g. Fairhurst and Warwick, 1998; Jones, 1998; Koopal et al., 2001; Murphy et al., 1994; Spark et al., 1997; Van Hees et al., 2000); mineral weathering and precipitation (e.g. Drever and Stillings, 1997; Stumm, 1997);

soil formation (Van Hees et al., 2000); nutrient cycling (Harley and Gilkes, 2000; Johnson and Loeppert, 2006); colloidal stability of mineral particles and thus the transport, coagulation and sedimentation rates of colloids (O'Melia, 1989); the carbon biogeochemical cycle (Van Hees et al., 2005); and the preservation of organic matter in sediments and soils (Kaiser and Guggenberger, 2000).

The diverse array of processes in which organic matter participates in, is primarily related to the influence of adsorbed organic matter on modifying the properties of mineral surfaces. However, the underlying mechanisms by which organic ligands affect various surface dependent processes are still not fully understood. The study of organic ligand surface complexation reactions is, therefore, essential for extending our understanding of the mechanisms and kinetics of several chemical reactions occurring in nature.

This study is mainly motivated by the controversy concerning the mechanisms by which organic ligands enhance mineral dissolution rates. Mineral dissolution plays an important role in a wide variety of geochemical processes such as pH regulation and composition of natural waters; elemental geochemical cycling; global carbon cycling and long term climate effects; and soil formation. Knowledge about the interactions of organic matter constituents with mineral surfaces is key to understanding and ultimately predicting the effects of organic ligands on the dissolution mechanisms. Particularly, information regarding surface speciation, binding mode and structural coordination of adsorbed organic ligands can provide insights into how organic ligands affect mineral surface reactivity. It is therefore of major importance to determine whether a particular species forms an outer sphere or an inner sphere complex and for the case of inner sphere complexation whether the adsorbed species forms a mononuclear, binuclear or multinuclear surface complex.

Although the adsorption properties of organic ligands on metal (hydr)oxides and clay minerals have been extensively studied, the adsorption mechanisms are not yet fully understood and the binding modes proposed in the literature are often contradictory. Additionally, the poor understanding of the nature of humic substances has led many authors to use other simpler organic compounds as analogues to these complex molecules in the study of the role of humic acids in soils and waters (e.g. Biber and Stumm, 1994; Evanko and Dzombak, 1998; Filius et al., 1997). Furthermore for many mineral-organic ligand systems the adsorption mechanisms have been primarily determined indirectly from macroscopic adsorption properties.

During the last years there has been a growing body of studies investigating mineral surface-organic ligand interactions using a wide variety of spectroscopic

methods such as Infrared (IR) spectroscopy, Raman spectroscopy, X-ray Diffraction (XRD) spectroscopy, atomic force microscopy (AFM), X-ray absorption fine structure (XAFS) spectroscopy, and nuclear magnetic resonance (NMR) spectroscopy. IR spectroscopy is the most commonly used spectroscopic method for the study of coordinative interactions between organic ligands and mineral surfaces (e.g. Axe and Persson, 2001; Boily et al., 2000b; Dobson and McQuillan, 2000; Johnson et al., 2004a; Kubicki et al., 1999). The successful application of IR spectroscopy to the analysis of surface complexation reactions is attributed to the fact that various functional groups present in NOM constituents absorb characteristic frequencies of IR radiation. Importantly, the two main functional groups (carboxylic and phenolic groups) responsible for the binding of organic compounds are IR active and their IR absorption features are influenced by their coordinative and binding environment. Therefore, IR spectroscopy can be a very useful tool in the study of the interactions between surface functional groups and organic ligand functional groups by providing direct experimental observations for the binding and coordination mode of adsorbed ligands.

Early IR spectroscopic investigations were conducted under *ex situ* conditions (i.e. dry conditions) and it is only recently that novel IR spectroscopic techniques have been developed which are able to probe surface speciation in the presence of an aqueous phase. These *in situ* methods, such as attenuated total internal reflection (ATR) - IR spectroscopy, enable the study of adsorbed species in environmentally relevant experimental conditions since most reactions in nature occur in the presence of water. To date, however, such *in situ* spectroscopic studies investigating organic ligand complexation have focused on simple metal (hydr)oxides such as those of aluminium and iron (e.g. Axe and Persson, 2001; Biber and Stumm, 1994; Dobson and McQuillan, 1999; Dobson and McQuillan, 2000; Drelich et al., 1988; Duckworth and Martin, 2001; Hwang et al., 2007; Johnson et al., 2004a; Johnson et al., 2004b; Kubicki et al., 1999; Nordin et al., 1998; Persson and Axe, 2005; Rosenqvist et al., 2003). Furthermore most previous experimental studies have used low molecular weight organic acids and therefore there is little spectroscopic data on humic and fulvic acid adsorption.

The molecular level interactions between organic ligands and clay minerals, at the mineral water interface, have received only limited attention thus far (e.g. Angove et al., 2006; Ikhsan et al., 2004b; Kubicki et al., 1999; Specht and Frimmel, 2001). This is somewhat surprising considering that clay minerals are important constituents in many geologic settings and they comprise, along with metal (hydr)oxides, the major adsorbent phases in soils. Therefore there is a requirement to further investigate the coordinative interactions between organic ligands and clay minerals.

In order to make progress in the understanding of organic ligand complexation reactions at the mineral-water interface, the present study has used kaolinite as the mineral substrate for most of the experiments conducted. Kaolinite has been chosen for the following reasons. (1) It is a common clay mineral with a relatively simple structure (2) The surface properties of kaolinite and its dissolution rates in both inorganic and organic acid solutions have been widely investigated (Cama and Ganor, 2006; Carroll-Webb and Walther, 1988; Chin and Mills, 1991; Ganor et al., 2003; Ganor et al., 1995; Huertas et al., 1998; Schroth and Sposito, 1997; Wieland and Stumm, 1992; Xie and Walther, 1992). (3) Kaolinite can represent the adsorption properties of non-expandable two-layer silicate minerals and thus can provide insights into how organic ligands adsorb on layer silicates. (4) The binding mechanisms to simple metal (hydr)oxides and coordination modes of the organic ligands used in this study have been reported in the literature. It is therefore interesting to compare whether organic ligands coordinate to the surfaces of clay minerals and of metal (hydr)oxides through similar adsorption mechanisms.

Aims and objectives

The main aim of the present study is to investigate the interactions between some common naturally occurring organic ligands and kaolinite in order to gain a better understanding of the binding and coordination modes of these ligands on clay minerals. The adsorption behaviour is examined *via* a series of macroscopic adsorption experiments including surface titrations, adsorption edge experiments and adsorption isotherms. Surface complexation modelling is also employed for the description of the adsorption data. Surface speciation at the molecular level is examined using a flow through, *in situ* IR technique that allows the collection of real-time spectroscopic data of adsorbed species. The combined analysis of data obtained from these different experimental methods allows for a more definitive determination of the mechanisms involved in organic ligand adsorption.

The theory and application of IR spectroscopy in the study of surface complexation reactions is given in Chapter 2. In addition, Chapter 2 provides information regarding the particular IR experimental technique used in this thesis, including advantages and limitations over other IR spectroscopic techniques used in the literature. In Chapter 3, surface complexation of salicylic acid and phthalic acid on

kaolinite is investigated for the first time using a combined experimental approach including IR spectroscopic observations, macroscopic adsorption properties, and surface complexation modelling. Chapter 4 examines the adsorption mechanisms of humic acid on kaolinite and gibbsite using both direct and indirect observations from IR spectroscopy and macroscopic adsorption experiments respectively. Finally some concluding remarks are given in Chapter 5 including the implications of the results obtained for important geochemical processes and areas for future research.

Chapter 2 The use of IR spectroscopy in the study of organic ligand surface complexation

Introduction

Organic ligand surface complexation reactions have received considerable attention for many years. Due to their reactive nature and widespread occurrence, organic acids, an important class of organic ligands, are often associated with mineral surfaces and with aqueous species in solution. In aqueous solutions these organics can form aqueous complexes with a wide range of metal cations, anions, and organic compounds and the resulting changes to the chemical speciation can have a significant effect on the solubility, transport and bioavailability of the individual components in these complexed species (Jones, 1998). Upon adsorption onto mineral particles organic acids can induce changes in the chemical and physical properties of mineral surfaces and therefore can play a key role in several surface dependent processes such as pollutant transport, adsorption, precipitation, and mineral dissolution reactions (Cama and Ganor, 2006; Lee et al., 1989; Murphy et al., 1992; Redman et al., 2002; Schroth and Sposito, 1998; Stumm, 1997).

The term “organic acid” refers to a wide range of acid group-containing organic compounds which constitute the reactive phase of natural organic matter (NOM). These organic compounds range from simple low molecular weight (LMW) organic acids to the complex, ill defined fractions of NOM such as humic and fulvic acids, which are collectively termed humic substances. The carboxylic group, and the hydroxyl group to a lesser extent, are believed to be the most important functional groups present in organic acids because they govern several of NOM’s properties (e.g charge, solubility, adsorption affinity) and therefore its environmental behaviour (Drever, 1988; Saada et al., 2003b).

Carboxylic acids and carboxylate-bearing organic compounds adsorb on the surface of minerals through electrostatic and/or chemical interactions between the carboxylate moiety and surface binding sites. According to the binding mechanism involved in the adsorption process, the surface complexes formed can be classified into two main types; namely inner sphere and outer sphere surface complexes. Ions binding through electrostatic forces of attraction and/or hydrogen bonding to surface groups of

opposite charge are termed outer sphere surface complexes. Conversely, ions exchanging for surface hydroxyl groups to form direct chemical bond with surface sites are termed inner sphere surface complexes.

In addition to the binding mechanisms involved in the uptake of organic compounds, the coordination mode of the surface bound ion is another important parameter in the study of surface complexation reactions. Depending on its molecular geometry and functionality, a chemisorbed ligand may bind to the surface *via* different coordination modes. Surface bound carboxylate groups can yield three possible surface structures: a mononuclear monodentate, a mononuclear bidentate, or a binuclear bidentate structure (Figure 2-1). A monodentate (or unidentate) structure forms when a single oxygen from the carboxylate group binds to the surface and a bidentate structure forms when both oxygens bind to the surface. If both oxygen atoms in the bidentate structure coordinate to the same surface metal centre, the structure is referred to as a mononuclear bidentate complex (chelate structure) whereas if each oxygen is coordinated to a different metal centre the surface complex is termed a binuclear bidentate complex (bridging structure). For dicarboxylic acids, bidentate structures, may also form *via* two formal monodentate structures, with respect to the two carboxylate groups.

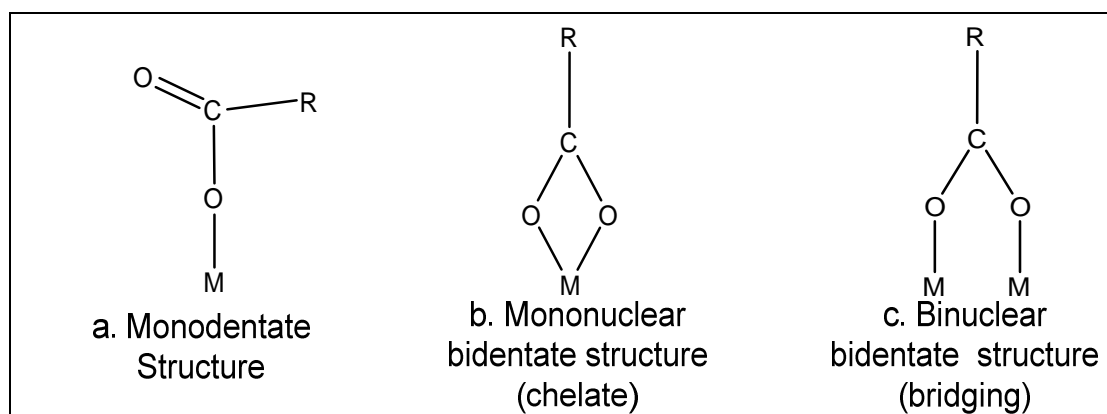


Figure 2-1 Coordination modes of the carboxylate functional group. Monodentate structures bind to a surface metal *via* a single C-O bond whereas bidentate structures bind *via* two C-O bonds. Mononuclear structures involve a single surface metal and binuclear structures involve two different surface metals. R represents a C_n-CH_3 group and M represents a surface metal cation.

The study of the reactions taking place between the functional groups of organic acids and mineral surfaces can provide a better understanding of the mechanisms involved in the sorption of both simple and complex organic acids on mineral surfaces. This in turn will help understand the role of organic acids in the environment and

ultimately model the geochemical processes in which organic acids are involved. Because the coordination mode of the adsorbed ions relates to surface reactivity and hence mineral dissolution rates, detailed molecular level information on the binding and coordination modes can provide further evidence regarding the mineral dissolution mechanisms in the presence of organic ligands. In particular the structure of the surface complex formed is critical to the dissolution enhancing properties of the adsorbed organic ligand. Ligands forming mononuclear bidentate (chelate) surface complexes can promote dissolution whereas binuclear bidentate (bridging) complexes can inhibit dissolution (Eick et al., 1999; Furrer and Stumm, 1986; Stillings et al., 1998; Stumm, 1997). For example Furrer and Stumm (1986) observed that bidentate ring complexes have a significant effect on the dissolution rate of Al_2O_3 , while monodentate complexes show little or no effect. The inhibiting effect of binuclear complexes was attributed to the much higher energy needed to simultaneously remove two metal centres from the surface of the solid.

Over the last decades considerable effort has been devoted to understand the underlying mechanisms for the adsorption of organic ligands on mineral surfaces, and to infer the structure of the resulting surface complex (Dobson and McQuillan, 2000; Duckworth and Martin, 2001; Evanko and Dzombak, 1998; Filius et al., 1997; Kubicki et al., 1999; Kummert and Stumm, 1980; Tipping, 1981). The adsorption mechanisms of LMW acids on various metal (hydr)oxides and clay minerals have been widely studied using batch adsorption experiments and several different spectroscopic techniques.

The use of IR spectroscopy is by far the most widely used method for the study of organic ligand complexation on the surface of minerals at the molecular-level. Such studies can provide direct evidence for the binding and coordination mode of adsorbed species. Different IR techniques have been used to investigate the adsorption reactions of organic ions at the surface of minerals. Early IR spectroscopic techniques were limited to the analysis of samples in the absence of an aqueous phase (*ex situ* experiments). More recently, however, the development of attenuated total reflection (ATR) FTIR spectroscopy allowed IR measurements to be made in the presence of an aqueous phase (*in situ* experiments). This technique is sometimes also referred to as multiple internal reflection (MIR) FTIR spectroscopy.

Since then, *in situ* ATR-FTIR spectroscopy has been employed in numerous studies for the investigation of surface bound organic ligands at the mineral water interface. Such investigations have revealed important information regarding the nature of bonds and structural geometry of adsorbed organic ligands. Low molecular weight

organic acids were shown to exhibit a large variety of binding modes and structural types, which depend on the chemical structure of the organic ligand. The coexistence of two or more surface complexes has also been demonstrated in many mineral-organic acid systems. For example acetic and benzoic acids were found to form two different types of outer sphere complexes on goethite (Noren and Persson, 2007) whereas oxalic (Axe and Persson, 2001) and phthalic acid (Boily et al., 2000b) were both found to form one outer and one inner sphere complex on goethite.

It is also well documented now that the coordination mode of adsorbed ligands may also be influenced by the structural characteristics of mineral surfaces. For example the coordination mode of salicylic acid was found to be influenced by the chemical composition of the oxide, with a mononuclear five-membered chelate structure forming on the surface of goethite, and a six-membered pseudochelate structure forming on the surface of aluminium oxide. Conversely the morphology of the mineral oxide did not influence the structure of the surface complex since adsorbed salicylic acid has the same coordination mode on α -, γ -, and δ -Al₂O₃ (Biber and Stumm, 1994). However, surface morphology may affect the relative distribution of the surface complexes forming upon adsorption. The adsorption of phthalic acid on gibbsite with high surface roughness showed an increase in the relative importance of inner sphere complexes when compared to the adsorption on gibbsite with lower surface roughness and a regular morphology (Rosenqvist et al., 2003).

Although progress has been made during the last years in the study of organic surface complexation reactions there are still contradicting results in the literature. Furthermore there is limited data on the structural environment of adsorbed organic ligands on clay minerals. In light of the importance of organic acid complexation reactions and the increasingly widespread use of IR spectroscopy in the study of interfacial reactions, the aims of this study are to: (1) provide an overview on how organic-mineral interactions can be studied at the molecular scale using IR spectroscopy; (2) present the *in situ* flow through MIR-FTIR technique used for the collection of IR data in this thesis; (3) outline the advantages of the present experimental technique over other IR spectroscopic techniques used in the literature; (4) discuss the problems and limitations identified for the IR method used; (5) examine the surface complexation reactions of a low molecular weight organic acid (oxalic acid) using the *in situ* MIR-FTIR flow through experimental approach presented.

A common well-studied aluminosilicate mineral, kaolinite, was chosen as the mineral substrate. The effect of oxalic acid on kaolinite dissolution rates has been widely investigated (e.g. Cama and Ganor, 2006; Chin and Mills, 1991; Sutheimer et

al., 1999; Wang et al., 2005; Wieland and Stumm, 1992) and thus knowledge about the coordination mode of oxalic acid will provide further insights for the dissolution mechanism of kaolinite. Although the coordination mode of oxalic acid onto kaolinite has been considered elsewhere, the IR spectroscopic results obtained are contradictory (Kubicki et al., 1999; Specht and Frimmel, 2001).

Methodology

The methodology section refers to the experimental procedure employed for the study of adsorbed oxalate species on kaolinite. Because a similar experimental procedure was used throughout this thesis, the purpose of the methodology section is to introduce the reader to the experimental set up and procedure used to obtain the IR spectra of adsorbed species. Further details regarding the application of this experimental technique to the study of surface complexation reactions will be given later on.

Materials

Kaolinite (KGa-2) was purchased from the Clay Minerals Society, Source Clays Minerals Repository. X-ray diffraction (XRD) analysis was performed in order to verify the crystal structure and identify potential impurities. No other crystalline phases or impurities were observed in these mineral samples. Note that XRD detection limit is about 5% for crystalline phases.

Analar grade oxalic acid, purchased by Sigma-Aldrich, and 15 M Ω - deionised water were used for the preparation of the ligand solutions used in the IR experiments. The pH of the solutions was adjusted to the required value by the addition of either 0.1 M HCl or 0.1 M NaOH. All the glassware used in the experiments was cleaned by first rinsing with acetone, then ethanol and finally thoroughly rinsing with de-ionised water.

MIR-FTIR spectroscopy

The IR spectra of adsorbed organic species were recorded by means of Multiple Internal Reflection Fourier Transform Infra-Red (MIR-FTIR) spectroscopy using an *in situ* flow-through experimental method developed at the University of Manchester for the study of surface complexation reactions at the mineral-water interface (Morris and Wogelius, 2008). A schematic diagram of the experimental set up used for the collection of *in situ* MIR-FTIR spectra is shown in Figure 2-2.

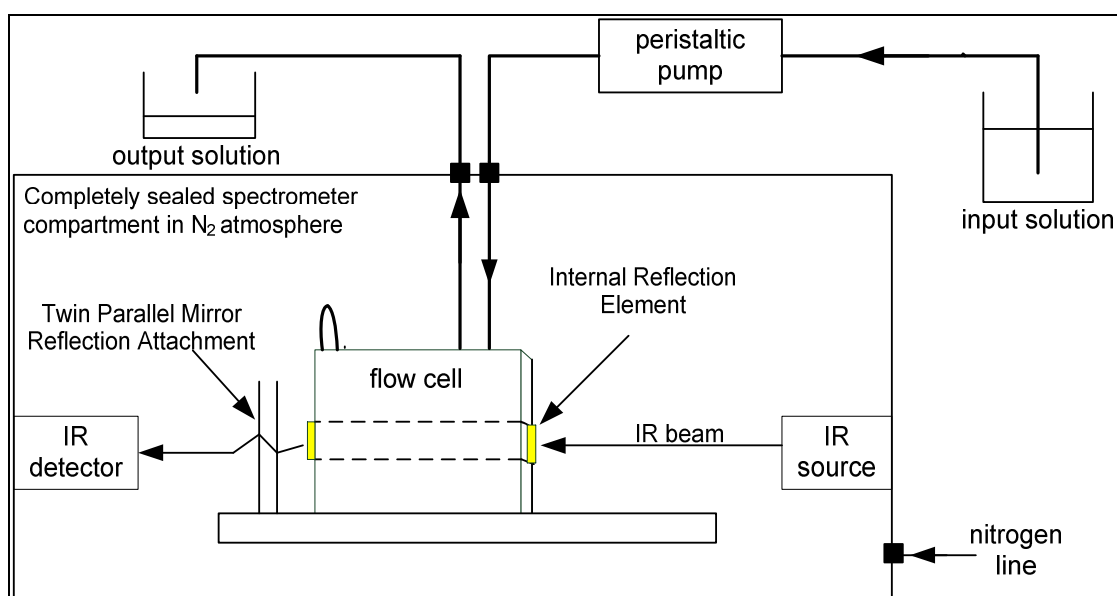


Figure 2-2 Schematic representation of the experimental set-up used for the acquisition of *in situ* MIR-FTIR spectra of organic ligand surface complexes.

Sample preparation and coating procedure

The following crude particle size fractionation procedure was employed in order to remove the larger particle size fraction of the minerals used in IR measurements. About 0.5 g of kaolinite was mixed with 50 mL of de-ionised water in a glass beaker and kept shaken with a magnetic stirrer for 30 minutes. The mineral suspension was then sonicated for 10 minutes using an ultrasonic water bath, and then allowed to stand for 3 minutes. Following sonication, the overlying solution was decanted and transferred to another beaker. Another 40 mL of water were added to the sedimented particles remaining and the new mineral suspension was sonicated for a further 20 minutes and then allowed to stand for 3 minutes. The overlying solution was removed,

mixed with the decanted solution obtained in the first step and then centrifuged for 20 minutes. The supernatant was pipetted out and the remaining solid particles were dried at 40°C. Only the fraction of the particles obtained by this method was subsequently used for the coating of the internal reflection element (IRE).

The mineral substrate was deposited on the surface of the IRE (ZnSe crystal) using a similar procedure to that described by Peak et al. (1999). Briefly, the coating procedure involved the application, using a pipette, of 1 mL of the mineral suspension (0.45 g/L) across the surface of one side of the ZnSe crystal and then allowed to dry at room temperature. This simple procedure was found to result in a stable thin film of evenly distributed mineral particles on the surface of the crystal. Following deposition, the crystal was kept at an angle and the mineral film was rinsed by allowing a few droplets of water to gently flow across the crystal in order to remove any loose particles from the surface. The film was then dried under a low pressure nitrogen stream and immediately positioned within the flow cell used in the IR experiments. A new mineral coating was used for each experimental condition examined (pH and ionic strength).

MIR-FTIR Measurements

Adsorbed species

The IR spectra at the mineral-solution interface were obtained during the course of the reaction in a flow through cell in which the reacting solution was allowed to come into contact with the mineral coated ZnSe. Details about the home-build cell and the ZnSe crystal used can be found in Morris and Wogelius (2008). IR measurements were made using a Bio-rad FTS 6000 spectrometer equipped with a deuterated triglycine sulphate (DTGS) detector. The spectrometer chamber and the cell were purged with nitrogen for at least 16 hours before data collection in order to remove atmospheric CO₂ and water vapour. Each spectrum recorded consisted of 256 co-added scans, collected at a spectral resolution of 4 cm⁻¹.

IR spectra of adsorbed species, at the different pH values and ionic strengths, were collected in separate experiments according to the following procedure. After the initial nitrogen purging phase of the spectrometer chamber, the dry background spectrum of the mineral coated ZnSe crystal was recorded. All subsequent spectra collected were ratioed against this background spectrum to remove spectral contributions associated with the ZnSe crystal and the bulk mineral phase. Following

the collection of the dry background spectrum and prior to the addition of the organic ligand solution into the flow cell, de-ionized water was pumped, using a peristaltic pump, through the cell for the collection of the water baseline spectrum. When the water baseline was stable (no changes observed in the intensity of the absorption bands of water during successive scans), the flow was switched from water to the organic ligand solution. While the ligand solution was constantly pumped into the flow cell, IR spectra were recorded at regular intervals for at least 2 hours. The water baseline spectrum was subtracted from each spectrum obtained, in order to eliminate the spectral interference due to the strong IR absorption of water. This subtraction procedure (subtraction of the background spectrum and water baseline) allows the collection of an IR spectrum containing absorption bands that arise from the surface species alone by excluding the absorption bands arising from water, the ZnSe crystal and the bulk mineral phase that would otherwise dominate the IR spectrum.

Replicate experiments for different solution conditions were performed in order to check the reproducibility of the IR spectra obtained and identify possible spectral artefacts which may lead to incorrect interpretation. Inaccurate subtraction procedure and contamination during sample treatment, handling and analysis are potential sources of spectral artefacts. Baseline corrections or other spectral transformations were not used. The highest organic concentrations used for the IR experiments were below the detection limit for the aqueous species, measured with the uncoated IRE.

Solution species

The IR spectra of the aqueous organic solutions, at different pH values, were obtained with the uncoated ZnSe crystal being in contact with a 0.1 M oxalic acid aqueous solution within the flow cell. The same experimental setup and subtraction procedure was used as that described for the collection of the IR spectra of adsorbed species.

Theoretical background

This section provides an overview on the application of IR spectroscopy to the study of the interactions taking place between organic ligands and mineral surfaces. The following discussion will focus on carboxylic acids because the carboxyl group is

considered as the key functional group involved in surface complexation reactions. Moreover, the carboxylic group is one of the most common functional groups found in both LMW organic acids and natural organic matter. The spectroscopic features that can be used to obtain molecular level information about the surface complex formed will be first examined. Then different IR experimental techniques employed in the study of interfacial reactions will be introduced.

The carboxyl frequency region

Depending on their molecular structure, organic compounds will yield different IR absorption bands with frequency positions corresponding to the vibrational motions of their structural moieties. IR spectroscopy is well suited for the study of carboxyl groups, in particular, because several carboxyl vibrational modes are IR active and thus give rise to characteristic absorption bands.

Vibrational mode frequencies are generally reported in wavenumbers and the values given correspond to the peak frequency/wavenumber positions of the absorption bands (i.e. frequency at maximum intensity). The wavenumber ($\tilde{\nu}$) defines the number of waves per unit length (cm^{-1}) and is given by

$$\tilde{\nu} = \frac{1}{\lambda} \quad \text{2-1}$$

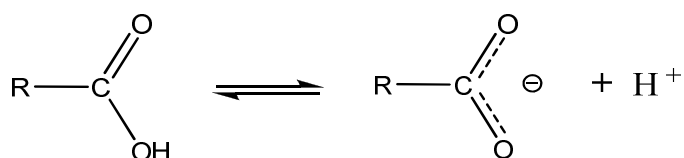
where λ is the wavelength (cm). The wavelength is related to the energy and the frequency of the IR radiation by

$$E = h\nu = \frac{hc}{\lambda} = hc\tilde{\nu} \quad \text{2-2}$$

where E is the energy (J), ν is the frequency (Hz), h is the Planck's constant (6.6×10^{-34} J/s) and c is the speed of light (3×10^{10} cm/s). Therefore according to the above equation energy is proportional to wavenumber and inversely proportional to wavelength. The infrared radiation is conventionally divided into three spectral regions; the near-, mid-, and far-IR regions. The far-IR region covers the wavenumber range from 400 to 10 cm^{-1} , the mid-IR region from 4000 to 400 cm^{-1} , and the near-IR region from 14000 to 4000 cm^{-1} . In general, IR studies of organic molecules are restricted to the mid-IR region.

Vibrational modes of the carboxyl group

A protonated carboxyl group gives rise to two vibrational modes, one stretching mode of a C=O bond ($\nu_{\text{C=O}}$) and one stretching mode of a C-OH bond ($\nu_{\text{C-OH}}$). Upon deprotonation, the electron density distribution within the carboxyl group is equally shared between the two C-O bonds of the carboxylate group. Consequently the C=O bond character of the carboxylic group is lost resulting into two equivalent C-O bonds with an intermediate character between the C=O and C-O bond (Colthup et al., 1990). This effect is illustrated in the following acid-base equilibrium reaction of a carboxyl group.



The deprotonated carboxylate group also gives rise to two different vibrational modes, one symmetric stretching mode ($\nu^{\text{s}}_{\text{COO}^-}$) where the two equivalent C-O bonds move in cooperation, and one asymmetric stretching mode ($\nu^{\text{as}}_{\text{COO}^-}$) where the two C-O bonds move in opposition. Figure 2-3 shows a schematic representation of the four possible vibrational modes exhibited by the carboxyl group.

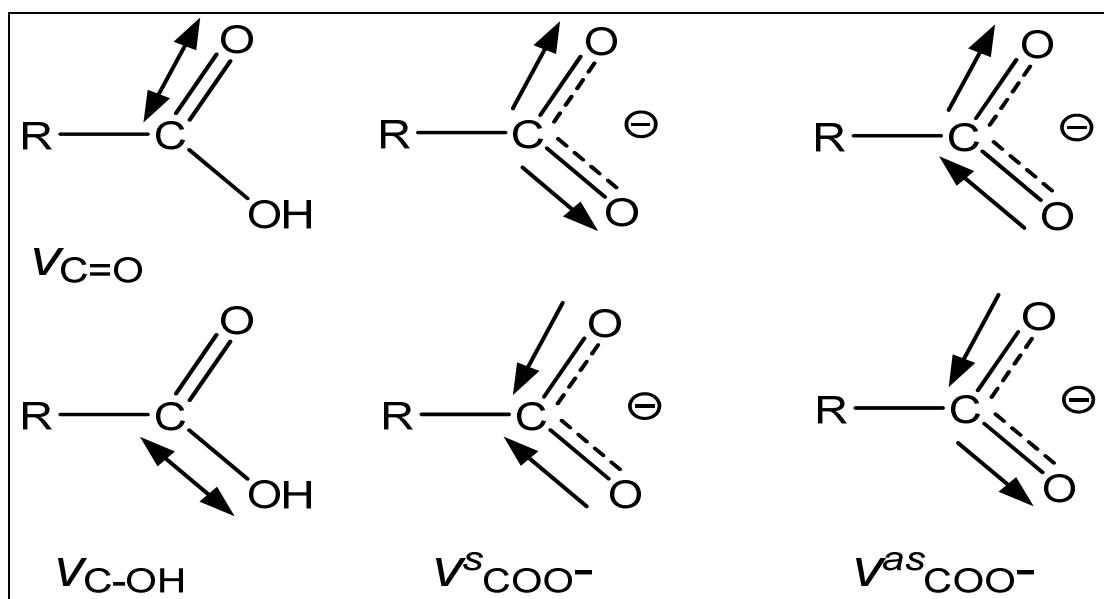


Figure 2-3 Vibrational modes of the carboxyl group in its protonated and anionic state. The protonated carboxyl group gives rise to two stretching vibrational modes, one C=O stretching mode ($\nu_{\text{C=O}}$) and one C-OH stretching mode ($\nu_{\text{C-OH}}$). The two equivalent C-O bonds in the carboxylate group can either move in cooperation giving rise to the symmetric stretching vibration ($\nu^{\text{s}}_{\text{COO}^-}$) or in opposition giving rise to the asymmetric stretching vibration ($\nu^{\text{as}}_{\text{COO}^-}$).

Because the pH of the solution governs the protonation state of carboxylic groups (as well as of other acidic functional groups), the IR spectra of all carboxylic acids change significantly, but also systematically, as a function of pH. At low pH values, and below the protonation constant (pKa) of the carboxyl group, the IR spectrum will consist of two bands originating from the C=O and C-OH stretching modes of the protonated carboxyl group. Following deprotonation of the carboxyl group (pH > pKa), the absorption bands arising from the C=O and C-OH stretching modes are replaced by two new absorption bands which originate from the symmetric and asymmetric stretching vibrational modes of the deprotonated carboxyl group. This sensitivity of the IR spectra to the structural changes induced by protonation/deprotonation reactions makes IR spectroscopy an excellent diagnostic tool for determining the protonation state of organic acids, in both the aqueous and the adsorbed state. Absorption bands corresponding to C=O and C-OH stretching vibrations are a distinctive feature of a protonated carboxyl group.

Factors affecting vibrational mode frequencies

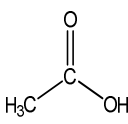
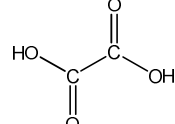
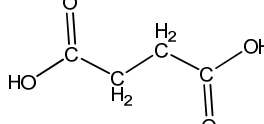
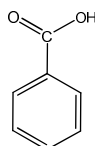
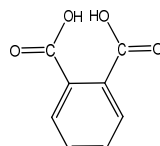
The vibrational frequencies for any particular carboxyl vibrational mode lie in the same frequency region, and hence are characteristic of that mode. Stretching frequencies of the C=O moiety in a carboxyl group typically range between 1690 and 1750 cm^{-1} and of the C-OH moiety between 1200 and 1300 cm^{-1} . The typical range of asymmetric COO^- stretching frequencies is from 1540 to 1650 cm^{-1} , and for symmetric COO^- stretching vibrations from 1300 to 1420 cm^{-1} (Hay and Myneni, 2007). Therefore, the absorption bands in the IR spectra of carboxylic bearing organic molecules can be assigned to specific vibrational modes according to their frequency position.

The exact peak frequency positions of carboxyl vibrational modes found in different organic compounds are influenced by the structural and coordination environment of the carboxyl group. As seen in Table 2-1, the local structural environment of the carboxyl group within an organic molecule has a significant effect on the frequency positions of carboxyl vibrational modes. This is because the surrounding environment influences the electron distribution density of the carboxyl group (especially if other electron withdrawing groups are adjacent to the carboxyl group); vibrational coupling with other vibrational modes of the molecule; and intermolecular or intramolecular interactions (such as hydrogen bonding) of the carboxylic group (Hay and Myneni, 2007).

Moreover, for molecules containing two or more carboxylic groups the frequency of specific vibrations can also be influenced by the protonation state of

neighbouring groups. For example the stretching mode of the C-OH moiety found in the doubly protonated oxalic acid yields an absorption maximum at 1233 cm^{-1} . Upon deprotonation of the first carboxylic group ($\text{pKa}_1 < \text{pH} < \text{pKa}_2$), the C-OH stretching vibration of the second group shifts to 1242 cm^{-1} . A small shift is also observed for the C=O vibration once the first carboxylic acid group deprotonates. The asymmetric stretching vibration of the carboxylate group (COO^-) is even more influenced by the deprotonation state, with an absorption maximum at 1609 cm^{-1} for the singly protonated oxalate molecule and 1569 cm^{-1} for the fully deprotonated oxalate molecule (Persson and Axe, 2005).

Table 2-1 Peak frequency positions exhibited by the vibrational modes of the carboxyl group found in some common LMW organic acids.

Organic Acid	acetic	oxalic	succinic	benzoic	phthalic
Structure					
Vibrational mode	Peak frequency positions (cm^{-1})*				
$\nu_{\text{C=O}}$	1711	1735	1717	1705	1705
$\nu_{\text{C-OH}}$	1279	1233	1238	1319/1279	1290
$\nu^{\text{as}}_{\text{COO}^-}$	1552	1569	1549	1542	1556
$\nu^{\text{s}}_{\text{COO}^-}$	1415	1308	1395	1388	1383

* Peak frequency positions were obtained from Rotzinger et al. (2004) for acetic acid; Persson and Axe (2005) for oxalic acid; Cabaniss et al. (1998) for succinic acid; Tunesi and Anderson (1992) for benzoic acid; and Nilsson et al. (1996) for phthalic acid. For molecules containing more than one carboxylic group the reported values of the $\nu^{\text{as}}_{\text{COO}^-}$ and $\nu^{\text{s}}_{\text{COO}^-}$ vibrations correspond to the fully deprotonated species and of the $\nu_{\text{C=O}}$ and $\nu_{\text{C-OH}}$ vibrations to the fully protonated molecule.

In addition to the local structural environment, the IR absorption frequencies exhibited by the carboxyl group are very sensitive to the group's coordination environment. Coordination of the carboxyl group to other chemical species, such as metal ions and surface sites, can bring about significant changes to the electron distribution and therefore to the frequency of vibrations. The strong influence of the coordination environment on the vibrational frequencies exhibited by a functional group forms the basic principle behind the use of IR spectroscopy in the study of adsorption reactions. The analysis of the IR spectra, prior and after adsorption, enables the

detection of any changes occurring in the local coordination environment of the adsorbed species. A brief discussion reviewing some general ideas on how IR spectroscopic data can be used to obtain molecular level information about the surface complexes formed will follow.

The study of ligand surface complexation reactions using IR spectroscopy is based on the comparisons between the IR spectra of the uncomplexed aqueous species and of the adsorbed species, obtained under the same experimental conditions (such as pH and ionic strength). Due to the fact that carboxyl-containing organic ligands coordinate to surface sites primarily through the carboxyl group, the study of the interactions taking place between mineral surfaces and such ligands is mainly based on the differences occurring in the IR bands of the carboxyl group upon adsorption.

An initial step requires the interpretation of the IR spectra obtained for the aqueous organic ligand. Although carboxyl vibrational modes exhibit characteristic IR “fingerprints” that enable their identification, other molecular vibrational modes not associated with the carboxyl group may also be positioned in the same frequency region and thus making the interpretation of the IR spectra more difficult. The response of the IR spectra of aqueous species to pH variations can guide the assignment of specific IR spectroscopic features to corresponding vibrational modes. Absorption bands affected by the degree of protonation can be assigned to the vibrations of the carboxyl group since the molecular skeletal vibrations are less susceptible to the degree of protonation. Bands decreasing in intensity as the pH rises will typically correspond to the motions of the protonated carboxylic group (C-OH and C=O bonds) whereas bands increasing in intensity as the pH rises typically correspond to the motions of the deprotonated group (C-O bonds of the COO⁻ group). Interestingly, carboxyl functional groups found in complex organic macromolecules, such as humic acids, show similar IR patterns as a function of pH to those seen in simple LMW organic acids (Lumsdon and Fraser, 2005; Yoon et al., 2004a).

In principle the analysis of the IR spectra of adsorbed species can give insights into the number of structurally different surface species coordinating to the surface; as well as the binding and coordination modes of these surface species. Spectroscopic differences between the IR spectra of free and adsorbed species which can be used for the structural characterisation of the surface complexes formed include the emergence or absence of absorption bands; frequency shifts of absorption bands; and variations in the relative intensity of individual absorption bands.

Based on the differences found between the adsorbed and aqueous IR spectra, it is possible to identify the number of structurally different surface species involved in

adsorption. If an organic ligand forms different types of surface complexes, then each surface complex is expected to yield absorption bands with different peak frequency positions. Therefore the presence of additional bands in the carboxylate stretching frequency region (either well resolved bands, or appearing as shoulders to the main absorption band) may be indicative of the existence of structurally different surface complexes.

Resolving the spectral contributions of individual types of surface complexes from the IR spectra can be a relatively simple procedure. The response of individual absorption bands as a result of changing solution conditions can be used to distinguish between different surface complexes. Changes in relative band intensities or the emergence of new peaks in the IR spectra of adsorbed species as a function of pH, and/or ligand concentration, and/or ionic strength indicate the presence of structurally different surface complexes (Axe and Persson, 2001; Boily et al., 2000a; Johnson et al., 2004b; Klug and Forsling, 1999; Nordin et al., 1997; Nordin et al., 1998; Persson and Axe, 2005; Persson et al., 1998; Rosenqvist et al., 2003; Yoon et al., 2004b). Conversely bands showing the same variation in intensity as a response to changing experimental conditions can be assigned to the same type of surface complex. Changes in relative band intensities occur because different solution conditions influence the relative surface concentration of adsorbed species and this in turn will influence the respective spectral contributions of each surface species in the IR spectrum obtained.

Once the number of surface complexes is determined, the spectroscopic features associated with each surface complex can be analysed for their structural characterisation. The effect of surface coordination on the carboxyl vibrational frequencies provides valuable information regarding the binding and coordination mode of the surface complex formed. The most straightforward analysis that can be carried out is to determine the binding mode of the surface complex.

Binding mode: The comparison of the IR spectrum arising from an adsorbed complex with the IR spectrum of the aqueous free species provides direct experimental evidence on the type of surface complex formed. Inner sphere complexed species typically result in significant changes in the IR spectrum of the adsorbed molecule as compared to the spectrum of the aqueous molecule. This is because direct chemical bonding to the surface can cause significant chemical, electronic, and symmetrical changes to occur on the adsorbed species. In contrast, outer sphere complexation involves weak electrostatic interactions between the surface and the adsorbed species and therefore causes minimal effects on the structural and chemical properties of surface

bound species. As a result outer sphere complexed species give rise to absorption bands positioned in similar frequencies positions to those obtained for their respective uncomplexed aqueous species. In general absorption bands appearing at similar frequencies to those observed in the free aqueous species can be assigned to outer sphere complexes and the emergence of new bands or shifts to different frequencies are indicative of inner sphere complexes (Rotzinger et al., 2004).

The effects of inner and outer sphere complexation on the spectral features of the carboxylic group have been previously demonstrated by the differences observed between the IR spectra of aqueous carboxylic species and that of their respective aqueous complexes formed with metal cations. For example the IR spectra of the aqueous complexes formed between phthalate and large divalent cations have been previously used as model spectra for outer sphere adsorbed phthalic acid. Conversely the IR spectra of aqueous aluminium- and iron-phthalate complexes have been used as model spectra of inner sphere complexation (Hwang et al., 2007; Nordin et al., 1997).

In order to illustrate the effects of complexation on the resulting IR absorption spectra obtained, the spectra of aqueous phthalic acid, aqueous strontium-phthalate and aqueous iron-phthalate complexes, all collected as part of this study, are shown in Figure 2-4. The carboxylate stretching region in the IR spectrum of the aqueous Fe(III)-phthalate species shows distinct changes from the spectrum of the aqueous phthalate species, indicating direct coordination of the carboxylate group to the metal ion. The aqueous Fe(III)-phthalate complex yields a characteristic band centred at about 1420 cm^{-1} (see inset) which is absent in the aqueous uncomplexed species and is therefore ascribed to an inner sphere complex. Absorption bands positioned at about 1420 cm^{-1} in the IR spectra of surface bound phthalate species have also been previously attributed to inner sphere complexed phthalic acid (e.g. Boily et al., 2000b; Klug and Forsling, 1999; Rosenqvist et al., 2003).

In contrast to the IR spectrum of Fe(III)-phthalate species, the IR spectrum of the strontium-phthalate species is identical to that of the aqueous phthalate species, indicating at most a weak association between the carboxylic group and strontium (i.e. outer sphere complexation). Adsorption-induced changes in the carboxylate region which are consistent with the changes occurring in the spectra obtained for such aqueous metal-carboxylate species can therefore provide additional evidence for the type of surface complex formed when the metal ion centre is exposed at a solid surface.

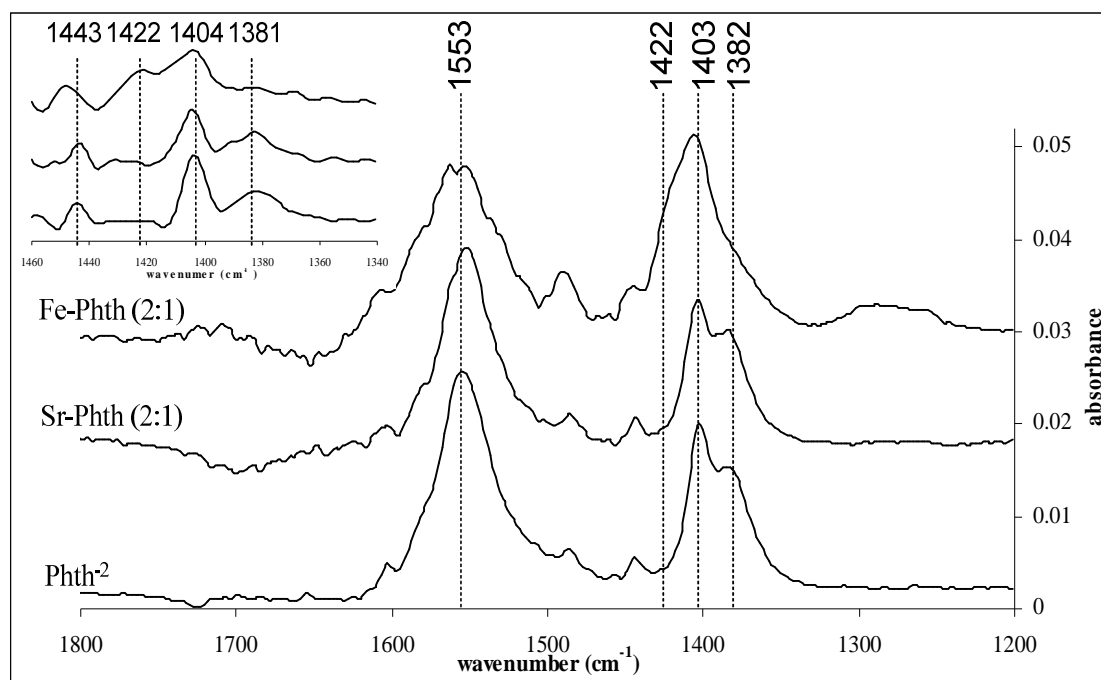


Figure 2-4 The IR spectra of aqueous phthalate collected at pH 7, aqueous strontium-phthalate complex collected at pH 7, and aqueous iron-phthalate complex collected at pH 3. The metal-phthalate complexes were prepared at a molar ratio of 2:1. Inset: Spectral deconvolution in the symmetric stretching region for the three spectra. The band in the carboxylate symmetric stretch region of the Fe(III)-Phth complex can be resolved into two bands with peak positions at 1422 and 1404 cm^{-1} . The band at 1422 cm^{-1} corresponds to the $\nu_{\text{C-O}}^{\text{s}}$ mode of the carboxylate group bonded to iron whereas the band at 1404 cm^{-1} originates from the $\nu_{\text{C-O}}^{\text{s}}$ mode originating from the uncomplexed phthalate ion. The IR spectrum of Sr-Phth complex is identical to that of aqueous phthalate suggesting a weak interaction (i.e. outer sphere complexation)

It has to be noted, however, that the IR spectra of outer sphere complexed species may also show some characteristic features when contrasted to the IR spectra of the aqueous species. Following the adsorption of various LMW carboxylic acids small shifts to higher frequencies of the carboxylate asymmetric stretching vibration (typically up to 10 cm^{-1}) and band broadening of certain peaks are generally consistent with outer sphere complexation (Axe and Persson, 2001; Boily et al., 2000a; Johnson et al., 2005; Johnson et al., 2004a; Rosenqvist et al., 2003). As proposed by Boily et al. (2000a), these effects originate from surface species which are hydrogen bonded to heterogeneous surface sites. Hydrogen bonded carboxyl groups have some water molecules from their hydration shell being replaced by surface bound water molecules or surface hydroxyl groups resulting in hydrogen bond asymmetry and therefore to an overall solvation asymmetry. This solvation asymmetry of the hydrogen bonded surface species is responsible for the small shifts of the asymmetric stretching vibration to higher frequencies (Boily et al., 2000a; Johnson et al., 2005).

Band broadening is caused by the wide distribution of hydrogen bond strengths forming between the adsorbed species and protons located in different surface hydroxyl

groups of varying acidities, as well as protons located in surface bound water molecules (Axe and Persson, 2001; Boily et al., 2000b; Rosenqvist et al., 2003). Similar functional groups coordinated to the surface via different hydrogen bond strengths exhibit absorption bands with slightly different peak frequency positions, thus explaining the band broadening. Band broadening is also observed for inner sphere complexed species and is also indicative of surface species with different coordination environments (Boily et al., 2000b; Roddick-Lanzilotta and McQuillan, 2000). For example a ligand may be adsorbed to surface sites of different metal coordination number or even to different types of metal centres.

Therefore, inner and outer sphere complexed surface species can be distinguished according to their band frequency positions relative to those found for the corresponding aqueous, uncomplexed species. In addition, the effect of ionic strength on the IR spectra of adsorbed organic acids has also been used to differentiate between outer sphere and inner sphere adsorption (e.g. Klug and Forsling, 1999; Nordin et al., 1997). The presence of a background electrolyte can suppress the formation of outer sphere complexed species because the electrolyte ions can compete with outer sphere adsorbed ions for available sites on the surface. Conversely, the formation of inner sphere complexes is relatively unaffected by the background electrolyte. Hence absorption band intensities showing a dependence on the ionic strength of the solution are often assigned to outer sphere complexes.

Coordination mode: Information regarding the coordination mode of surface complexes formed can be inferred from the relative positions and shapes of characteristic absorption bands found in the spectra of adsorbed species when compared to those of aqueous species. Therefore knowledge about the effects of the coordination environment on the resulting IR spectra is essential for determining the structural geometries of the surface species.

Adsorbed carboxyl groups are expected to yield IR spectra which are characteristic of their coordination mode. This is because the carboxyl coordination environment in each of the three coordination modes (Figure 2-1) can have a significant effect on the vibrational frequencies exhibited by the surface bound carboxyl group. In contrast, there are relatively small differences in the IR spectra of surface bound carboxyl groups which adopt the same coordination mode on different mineral substrates (Dobson and McQuillan, 2000; Yoon et al., 2004b). As a result, infrared band positions arising from an adsorbed carboxylic group will primarily depend on the coordination mode of the adsorbed ligand and to a lesser extent on the nature of the

surface site. It therefore follows that similar IR absorption profiles obtained for a particular species adsorbed on different mineral substrates are indicative of a similar coordination mode. Inferring the coordination modes of inner sphere complexed species, however, can be a challenging task.

Because the IR spectra exhibited by surface bound carboxyl groups depend on their particular coordination mode, it is possible for the different coordination modes to be correlated to particular IR absorption patterns. For example, following adsorption, the emergence of absorption bands to specific frequency positions, or characteristic band shifts may provide evidence about the coordination mode of the carboxyl group. The findings of previous studies can be therefore utilised in order to allow for generalisations regarding the coordination mode of surface coordinated carboxyl groups. For simple LMW organic acids, typical band shifts expected for different types of carboxylic coordination modes, following binding to metal ions (surficial or aqueous), have been derived from theoretical and empirical evidence. It must be emphasized however that any generalisations made relating specific spectral IR features to specific coordination modes will only be applicable for similar types of organic ligands.

The difference in separation between the symmetric ($\nu^s_{\text{COO}^-}$) and asymmetric ($\nu^{\text{as}}_{\text{COO}^-}$) stretching frequency of a surface bound COO^- group ($\Delta\nu = \nu^s_{\text{COO}^-} - \nu^{\text{as}}_{\text{COO}^-}$) when compared to the $\Delta\nu$ value of the corresponding aqueous ion, has been commonly used as a diagnostic tool for deducing the coordination mode of surface bound carboxylic groups (e.g. Dobson and McQuillan, 1999; Dobson and McQuillan, 2000; Duckworth and Martin, 2001; Kirwan et al., 2003; Rotzinger et al., 2004; Van den Brand et al., 2004; Zelenak et al., 2007). For carboxylic acids, monodentate surface structures tend to have higher band separations ($\Delta\nu = 350\text{-}500\text{ cm}^{-1}$) when compared to the free carboxylate ion, whereas chelate structures (mononuclear bidentate) exhibit smaller separations ($\Delta\nu = 60\text{-}100\text{ cm}^{-1}$). Bridging complexes (binuclear bidentate) typically have a similar frequency difference as the one found in the free ionic form ($\Delta\nu = 150\text{-}180\text{ cm}^{-1}$) (Dobson and McQuillan, 1999; Kirwan et al., 2003). Nara et al. (1996) demonstrated that a similar correlation also exists between the stretching frequencies of a carboxylate group and its coordination type to aqueous metal cations.

The abovementioned general set of guidelines is based on empirical observations where the coordination geometry of adsorbed carboxylate groups was found to be correlated to the splitting between the symmetric and asymmetric stretching vibrational modes (Deacon and Phillips, 1980; Nilsson et al., 1996). The differences in the relative change between the $\nu^{\text{as}}_{\text{C-OO}^-}$ and $\nu^s_{\text{C-OO}^-}$ stretching modes observed can be

explained by the differences in the molecular symmetry of the carboxylate group. Carboxylate groups bonded in a monodentate mode possess a lower molecular symmetry than bidentate structures because only one C-O bond is coordinated to the surface. This leads to a greater difference between the strength of the two C-O vibrations and therefore the frequencies of the carboxylate stretching vibrations exhibit a higher $\Delta\nu$ (Duckworth and Martin, 2001). The lower $\Delta\nu$ values exhibited by the chelate complexes when compared to those of the aqueous species are attributed to the smaller C-O-C angle found in the chelate structures (Nara et al., 1996).

It must be noted, however, that the applicability of this method for carboxylic ligands, other than acetates, has been questioned by some authors because other more complex factors, than the bond strength and angle, may also influence the $\Delta\nu$ values such as intramolecular vibrational interactions (Deacon and Phillips, 1980; Zelenak et al., 2007). Moreover, in the case where more than one absorption band is present in the carboxylate stretching region, band assignment to different vibrational modes may be difficult. This is particularly true for carboxylic acids with additional functional groups located adjacent to the carboxylate group. Absorption bands may be originating from the coupling of the carboxylate stretching modes with other vibrational modes exhibited by the organic molecule. Consequently, it may not be possible to determine the exact position of the “pure” carboxylate stretching vibrations and hence the $\Delta\nu$ values (Tejedor-Tejedor et al., 1992). Therefore the interpretation of surface structures according to the separation of the carboxylate stretching vibrations should be used with caution, especially for differentiating between mononuclear bidentate and binuclear bidentate modes (Deacon and Phillips, 1980; Nilsson et al., 1996; Rotzinger et al., 2004; Zelenak et al., 2007). Furthermore, the complications associated with the implementation of these rules signify that these rules should not be used alone for classification purposes of the coordination mode but rather be used as a complementary analysis tool.

The comparison of the IR spectra of aqueous carboxylate-metal complexes to those of surface carboxylate complexes provide additional means for differentiating between different possible surface structures. It has been shown that carboxylate complexes with metal cations in solution and with surface sites will show remarkable spectral resemblance provided the carboxylic group has the same coordination mode in both the aqueous complex and the surface complex. (Persson and Axe, 2005). Comparisons of the IR spectra of surface carboxylate complexes with aqueous metal-carboxylate complexes (Nordin et al., 1997; Persson and Axe, 2005), as well as with solid metal-organic salts (Dobson and McQuillan, 1999; Duckworth and Martin, 2001),

of known coordination modes can therefore be used to infer the coordination mode of surface bound carboxylic acids.

Additional information which can be used to help spectral interpretation can be obtained from molecular orbital frequency calculations. Frequency calculations for model systems have been previously used to obtain the theoretical vibration frequencies of aqueous and adsorbed organic ligands (Axe and Persson, 2001; Kubicki et al., 1997; Kubicki et al., 1999; Rosenqvist et al., 2003; Yoon et al., 2004b). Such theoretical studies can help the interpretation of the IR spectra by providing information on the effects of the coordination environment on the IR absorption band positions. This can be done by comparing the theoretical IR spectra of an adsorbed molecule calculated for different coordination modes (typically on a small cluster of atoms which simulates a mineral surface) with the experimental IR spectra obtained. The calculated spectrum which most closely agrees with the experimental spectrum is inferred to result from a model complex which most closely represents physical reality.

For example the experimental IR spectra obtained for adsorbed oxalic acid on boehmite (Axe and Persson, 2001) included IR features resembling those predicted for the theoretical spectra of both an aqueous oxalate ion and an oxalate ion directly bonded to the surface in a mononuclear bidentate (five-membered chelate structure) coordination mode. Theoretical IR frequencies calculated for other surface coordination modes, and especially monodentate structures, showed significant differences to the experimental frequencies. Therefore the authors suggested that specifically adsorbed oxalate forms a five membered ring chelate structure on the surface. The presence of additional spectroscopic features, similar to aqueous oxalate, were used as evidence for the presence of a second surface complex which is bound on the surface via an outer sphere mechanism. The theoretical vibrational frequencies available in the literature for a particular organic ligand can be applicable for different mineral substrates and therefore can be used for the interpretation of the experimental IR spectra obtained in other studies.

In summary, the IR spectra of adsorbed organic ligands, and particularly the carboxyl stretching frequency region, can provide information about the number of different surface complexes forming on the surface; the binding mode of these surface complexes (i.e. inner sphere vs. outer sphere complexation) and; possibly the coordination mode of surface complexes (i.e. mononuclear vs. binuclear; monodentate vs. bidentate). Such information is primarily based on direct comparisons between the IR spectra of adsorbed species and: (1) the IR spectra of the respective aqueous uncomplexed species obtained under the same solution conditions such as ionic strength

and pH, (2) the IR spectra of model compounds with known structures such as aqueous metal-ligand complexes and solid metal-ligand salts, and (3) theoretical IR spectra of model surface species calculated by molecular orbital calculations.

The use of IR techniques for the study of mineral-organic ligand interactions at the molecular scale

The ability of IR spectroscopy to detect any changes in the local coordination environment of organic compounds has led to the development of several different IR experimental methods for the structural characterisation of surface bound organic ligands. Amongst the various *in situ* and *ex situ* IR techniques employed for the investigation of organic ligand interfacial interactions are: diffuse reflectance infrared Fourier transform (DRIFT) spectroscopy (e.g. Klug and Forsling, 1999; Molis et al., 2000; Robert et al., 2000); transmission IR spectroscopy (e.g. Das and Mahiuddin, 2007; Groff, 1983); reflection/absorption infrared (RA-IR) spectroscopy (e.g. Nagayasu et al., 2005); and attenuated total reflection-Fourier transform infrared (ATR-FTIR) spectroscopy (e.g. Axe and Persson, 2001; Duckworth and Martin, 2001; Kubicki et al., 1999). Note that in the spectroscopic context the terms *in situ* and *ex situ* measurements refer to the collection of IR data in the presence and absence of an aqueous phase respectively.

This section provides a brief overview of available IR techniques currently used for the analysis of interfacial reactions in the literature. In turn, the experimental procedure and result reliability of such techniques will be contrasted to those of the experimental approach (*in situ* flow through MIR-FTIR) employed in the present study. In addition, the advantages offered by *in situ* flow through MIR-FTIR experiments over other *in situ* IR spectroscopic methods will be given.

Early spectroscopic investigations carried out to study the adsorption of organic ligands have employed IR transmission techniques (e.g. Parfitt et al., 1977a). Although such techniques are still used, probing interfacial species at low surface coverage and in the presence of water presents difficulties. Water is a very strong absorber in the frequency region where specific carboxyl group vibrational modes are IR active and therefore water can cause interference in the obtained IR spectra. As a result such

techniques can only be used for samples that do not contain water. Moreover, the surface concentration of the adsorbed species may be too low to be detected or absorption bands from the bulk mineral may dominate the IR spectrum.

Typical *ex situ* experiments (transmission or DRIFT spectroscopy) involve the IR analysis of dry pellets (or powder) consisting of the reacted sample and an IR transparent medium, such as KBr. IR measurements performed under *ex situ* conditions offer both advantages and disadvantages over *in situ* experiments. The main advantages include a simpler experimental setup and data processing, because of the absence of bands arising by the IR absorption of water. However, IR sampling in the absence of water serves at the same time as the main disadvantage of *ex situ* experiments. IR spectra obtained under *ex situ* conditions may not be representative of the “true” surface complexes formed at the mineral-water interface, since the absence of the surrounding water medium could affect the coordination and/or binding mode of the adsorbed species. For example, Kang and Xing (2007) observed a change in the dominant binding mode of carboxylic acids upon drying of the mineral surface (kaolinite and montmorillonite). Outer sphere complexes formed at the mineral-water interface were found to change to inner sphere complexes when the aqueous phase was removed.

Furthermore, the removal of the aqueous phase may cause segments of adsorbed organic macromolecules, which extend away from the surface and into the solution, to collapse on the surface. These collapsed segments which are not directly bound to the mineral surface can potentially give rise to IR bands that can interfere with the bands originating from the surface bound functional groups (Kirwan et al., 2003). Additional problems which may affect sample analysis include possible reactions of the sample with the KBr medium, as well as spectral interference from water as a result of water moisture being retained within the KBr disc (Hind et al., 2001). Therefore the IR spectrum of a surface complex obtained under *ex situ* conditions may be different than the spectrum of the respective complex obtained in an aqueous solution.

In order to compensate for the limitations of *ex situ* techniques, ATR-IR techniques have been developed to allow *in situ* IR measurements. ATR-IR is a highly surface sensitive technique which enables the collection of the IR spectra of surface species, even at low surface concentrations and in the presence of water.

Attenuated total reflection IR spectroscopy (ATR-IR)

Total internal reflection is the basic principle exploited by ATR-IR spectroscopy. Instead of the IR beam being transmitted through the sample, in ATR spectroscopy the beam is directed towards an internal reflection element (IRE- an element of high reflective index) at an angle of incidence larger than the critical angle. This allows the IR beam to propagate through the IRE, and be guided by internal reflection towards the IR detector (see Figure 2-5). Although the IR beam is internally reflected, at each point of reflection the incident IR beam forms a standing wave, termed evanescent wave, perpendicular to the surface of the IRE. Any sample in contact with the surface of the internal reflection element will therefore interact with this standing wave. Due to the interaction of the evanescent wave with the sample, the IR radiation is attenuated and hence an absorption spectrum for that sample can be obtained. A higher number of internal reflections will increase the sensitivity of this method, with the number of internal reflections within the IRE depending on the size of the crystal and the angle of incidence of the IR beam. When the IR beam is internally reflected more than once, ATR spectroscopy is sometimes referred to as multiple internal reflection (MIR) spectroscopy.

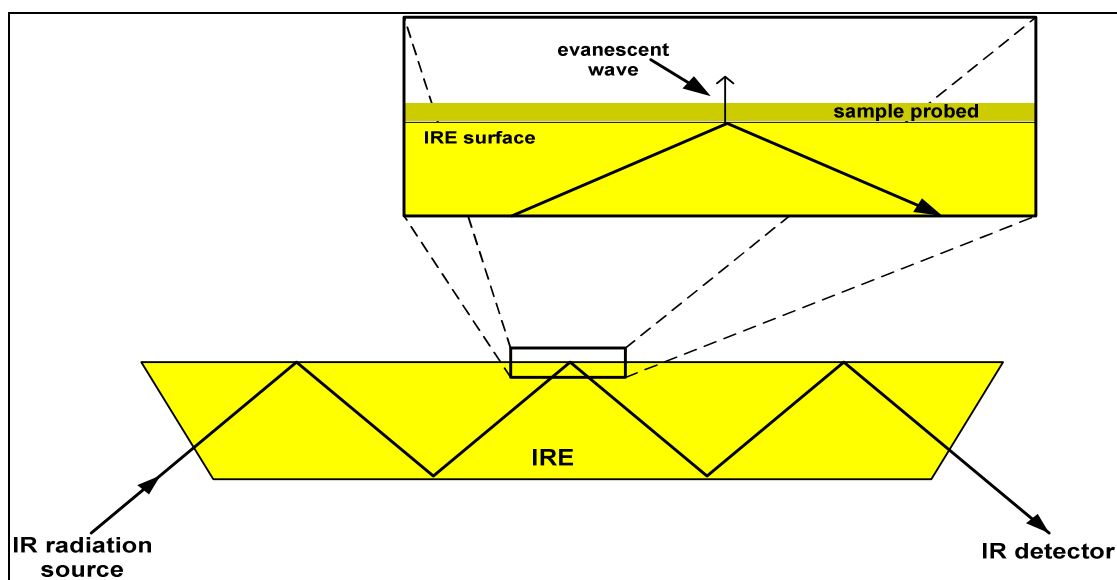


Figure 2-5 The propagation of the IR beam through the internal reflection element. Although the beam is internally reflected, at each point of reflection an evanescent wave forms, which extends beyond the surface of the element and interacts with the sample in contact to the reflection element.

In the literature, ATR-FTIR measurements of interfacial species in the presence of an aqueous phase are carried out using two main experimental approaches. These are

the wet mineral paste approach and the flow through experimental approach. The IR analysis of samples as wet mineral pastes has been the most commonly used *in situ* IR technique. These two experimental procedures will be briefly discussed below.

Analysis of the reacted samples as wet mineral pastes has been widely used for the acquisition of *in situ* IR spectra of adsorbed organic ligands (e.g. Angove et al., 2006; Axe et al., 2006; Bargar et al., 2005; Boily et al., 2000a; Johnson et al., 2005; Johnson et al., 2004a; Lackovic et al., 2003b; Nordin et al., 1998; Persson et al., 1998). In this method, a known mass of the substrate is reacted with a known concentration of the organic ligand and following equilibration the wet paste is separated by centrifugation. The wet paste is directly applied on the surface of the IRE and typically a lid is placed over the sample to prevent drying and enhance contact between the IRE and the sample.

In contrast to the wet paste approach, flow through experiments require the coating of the IRE with the unreacted substrate prior to the addition of the organic ligand. This can be done by applying a suspension of the substrate (typically in water or ethanol) on the surface of the IRE and allowing it to dry, thus forming a thin uniform mineral layer on the surface of the IRE (e.g. Duckworth and Martin, 2001; Hug and Bahnmann, 2006; Rotzinger et al., 2004; Weisz et al., 2002). More sophisticated methods, such as sputtering systems or chemical vapour deposition, have been used for the deposition of thin films on IREs (Drelich et al., 1988). The deposition of sol-gel layers on the surface of the IRE have also been reported (Degenhardt and McQuillan, 1999; Dobson et al., 1997; Dobson and McQuillan, 2000). The mineral coated IRE is then mounted on a flow cell and placed in the IR spectrometer. The reacting solution is pumped in the sample compartment of the flow cell and the mineral substrate is reacted with the aqueous solution.

The main attribute of ATR spectroscopy which permits IR measurements in the presence of water is the short and highly reproducible penetration depth of the evanescent wave (Hind et al., 2001). The penetration depth of the evanescent wave is typically at a depth of few microns and depends on the refractive index of the sample, the frequency of the IR beam, and the angle of incidence of the incoming beam. Penetration depth is defined as ‘the distance required for the amplitude of the electrical field to fall to e^{-1} of its original value at the surface’ and is given by the following equation (Hind et al., 2001)

$$d_p = \frac{\lambda}{2\pi n_1 \sqrt{\sin^2 \theta - (n_2/n_1)^2}} \quad 2-3$$

where d_p is the penetration depth, θ the angle of incidence, n_1 and n_2 the refractive indices of the material and the sample respectively, and λ the wavelength of the incoming radiation.

A short penetration depth is essential for ensuring that a significant fraction of the evanescent wave is absorbed by the interfacial species rather than being completely absorbed by water molecules from the overlying solution. Therefore, although the spectra obtained will be dominated by the strong absorption bands originating from the absorption of IR radiation by water molecules, a fraction of the IR radiation will be absorbed by the adsorbed species. Water absorption bands have to be subtracted from the sample spectrum in order to isolate the absorption bands arising from the surface species alone. The capability of this method to obtain highly reproducible penetration depths during successive scans enables the accurate subtraction of a water background spectrum from the sample IR spectrum.

Subtraction procedure

The subtraction procedure constitutes the most important step in the data collection process of *in situ* IR studies and it involves the removal of the absorption bands not associated with the vibrational modes of the adsorbed species. Such absorption bands dominate the raw IR spectra and originate from the absorption of IR radiation by water molecules, by the bulk mineral phase, by the internal reflection element itself, and by the IR spectrometer. In order to obtain the spectrum of the adsorbed species alone, these additional spectral contributions need to be subtracted from the raw sample spectrum. The subtraction procedure is typically carried out in two steps and, depending on the experimental setup, different spectral contributions are removed in each step.

For flow through experiments, spectral contributions from the IRE and the mineral phase are usually subtracted prior to the addition of the aqueous phase. This is accomplished by first collecting a background spectrum of the flow cell with the dry coated IRE, and this spectrum is ratioed against all the subsequent spectra collected. Following the collection of the background spectrum water is introduced into the cell and a water spectrum (water baseline spectrum) is obtained when the cell is filled with water. After the collection of the water spectrum, the ligand solution is pumped into the cell and allowed to react with the mineral deposited on the IRE element, and sample spectra are recorded during the course of the reaction. The water baseline spectrum is

subtracted from each sample spectrum in order to remove the absorption bands of water. An effective subtraction procedure will result in IR spectra that include absorption bands arising only from the adsorbed organic species (Figure 2-6).

The removal of water contributions can be particularly challenging because the strong IR absorption of water can cause severe interference in the frequency region between 1690-1590 cm^{-1} (peak position of the water absorption band is at 1639 cm^{-1}). If the intensity of the water absorption bands in the water baseline and the sample spectra is not exactly matched, then this will introduce artefacts in the sample spectrum. Over-subtraction and under-subtraction of the water baseline will result in negative and positive bands respectively that can cause strong interference in the frequency region where water is IR active.

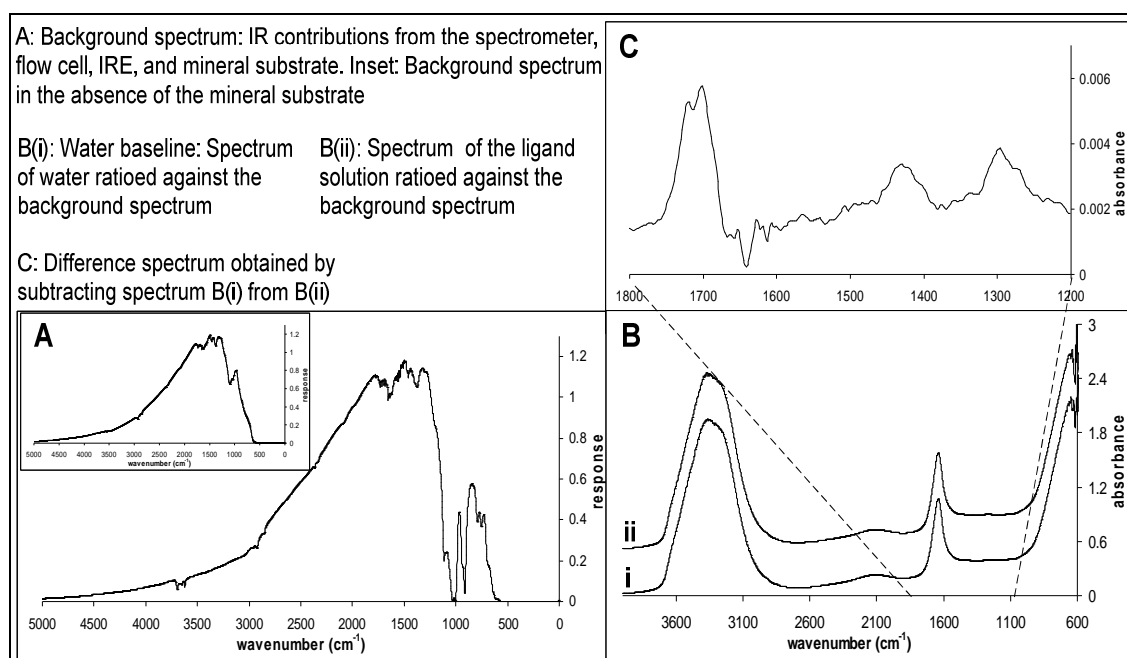


Figure 2-6 Steps required to isolate the spectrum of a surface species. A background spectrum is initially collected (A). The flow cell is then filled with water and a representative spectrum of water, ratioed against the background spectrum is recorded (Bi). Following the collection of the water baseline spectrum the ligand solution is allowed into the flow cell and is allowed to react with the mineral substrate deposited on the IRE. The subsequent IR spectra collected are also ratioed against the background spectrum (Bii). Finally, the water baseline spectrum needs to be subtracted from all the spectra recorded following the reaction of the ligand solution with the mineral substrate in order to remove the strong water absorption bands and obtain the spectra of adsorbed species alone (C).

For samples analysed as wet pastes slightly different subtraction procedures are followed (e.g. Biber and Stumm, 1994; Persson and Axe, 2005). A typical subtraction procedure involves the subtraction of the empty cell spectrum (sample holding region and the IRE) from the spectra acquired for the wet paste sample and for the spectrum of

the supernatant. The subtraction of the background-subtracted supernatant spectrum from the background-subtracted wet paste spectrum yields the IR spectrum of surface species. If the mineral substrate is IR active in the spectral region of interest, a spectrum of the unreacted mineral needs to be subtracted as well. Incomplete subtraction (under-subtraction) of any of these additional spectral contributions can give rise to additional absorption bands in the spectra of the surface species, which can lead to erroneous interpretation. Similarly under-subtraction can lead to spectra exhibiting negative bands which can suppress the “true bands” of the adsorbed species.

The use of flow through experiments offers some advantages over other *in situ* IR spectroscopic techniques. The flow through experimental approach enables the collection of “real time” data from the moment adsorption takes place rather than the collection of spectra after a certain equilibration time (usually more than 24 hours) as in *ex situ* experiments and the wet mineral paste approach. As a result, information on the kinetics of the adsorption process can be obtained and the effects of changing solution conditions can be monitored in real time. In addition, ligand solutions at relevant environmental concentrations can be used (usually concentrations down to 10^{-5} - 10^{-4} M) rather than the unrealistically high concentrations often used in wet paste experiments. At high ligand concentrations specific surface complexes may be forming that would have otherwise been unstable, and thus absent in typical environmental conditions. Furthermore, due to the ability to use ligand concentrations which are below the detection limit for the uncoated IRE, the spectra obtained include contributions only from interfacial species accumulated to the surface due to adsorption. In contrast, in the analysis of wet paste samples aqueous uncomplexed species may also be probed and hence interfere with the spectra of surface species.

Finally a more effective and less complicated subtraction procedure can be used in flow through experiments when compared to the wet paste approach. As previously discussed, specific care must be taken during the subtraction process, in order to isolate the IR spectrum of the interfacial species from the spectral contributions of the bulk mineral phase and from water. For other IR techniques the reference spectrum of the unreacted mineral substrate has to be recorded separately. This may lead to inaccurate subtraction procedure due to variations in the intensities of the absorption bands arising from the bulk mineral phase in these two spectra. For example, this procedure can create a significant problem if the amount of mineral placed in the sample compartment of the spectrometer, when collecting the reference and sample spectra, is not evenly matched. Therefore, if the mineral phase has absorption bands in the spectral region where the

adsorbed organic is IR active, imperfect subtraction will result in negative or positive bands which can interfere with the bands of the surface complex.

Contrary to other IR techniques, in flow through experiments, spectral contributions from the bulk mineral phase are accounted for in the background spectrum. Therefore there is no need to record the IR spectrum of the mineral substrate separately and then subtract this from the measured sample spectra. In addition, because the mineral sample included in the background spectrum is the same sample which is subsequently used for the adsorption experiments, variations arising from the separate analysis of two samples of the same mineral can be eliminated (e.g. differences in the intensity of absorption bands due to small variations in the experimental procedure; effects of sample heterogeneity). Furthermore, the flow cell is kept in place throughout the experiment and thus all the spectra (including the background and water spectra) are recorded at a constant optical alignment and beam path. This ensures a constant IR transmittance which further decreases the imperfections of the subtraction procedure since constant background contributions are expected in the spectra collected. These attributes of the flow through method allow for a more accurate subtraction of the contributions arising from the bulk mineral phase.

Limitations of the *in situ* flow through method

The primary issues identified during the use of the flow through *in situ* method employed here for the study of surface complexation reactions will be addressed in this section. These issues can be grouped into two categories, the problems associated with the data analysis and the problems associated with data collection (i.e. the experimental procedure). A discussion on the data analysis using examples identified both in this study and the literature will be presented first, as it was deemed of greater significance. This will be followed by a discussion of the limitations related to the data collection process.

Data analysis

One of the main issues emerging from the use of the current method concerns the difficulties associated with the interpretation of the IR spectra, a problem which is inherent to all IR methods used in literature. The results obtained can be subject to uncertainties mainly because of the ambiguities in the interpretation of IR spectra.

Spectral interpretation, even for relatively simple systems consisting of simple organic molecules, is not always a straightforward task.

As already mentioned, band assignment to corresponding vibrational modes of aqueous species is primarily based on the effects of pH on the IR spectra. However care must be taken in the assignment of the carboxylic absorption bands because the vibrational modes of the carboxylic group may be coupled to other molecular vibrational modes, adding further complexity to the IR spectra obtained. Furthermore, intramolecular and intermolecular hydrogen bonding interactions of the carboxylic group can potentially generate more complicated IR patterns as a function of pH, or give rise to bands with absorption energies different than those expected for carboxylic groups not involved in hydrogen bonding. This is especially true for polyfunctional molecules in which intramolecular interactions of various vibrational modes within the molecule can yield complex spectra with band overlapping and/or absorption bands which cannot be unambiguously assigned.

Similarly the analysis of the IR spectra of surface complexes may present several difficulties associated with the spectral interpretation of the obtained results. For example, if the adsorbed molecule has the ability to bind to the surface via different coordination and/or binding modes, spectral overlapping may complicate the interpretation of IR spectra since high intensity absorption bands may obscure low intensity absorption bands. This problem is particularly important for IR spectra with a low signal-to-noise ratio where spectral deconvolution methods, often used to resolve overlapping components, may be inadequate.

In addition, it may be impossible to unambiguously assign certain absorption bands exhibited by the surface complex(es) to a specific coordination mode or even to a specific binding mode. For example it has been discussed in a previous section that absorption bands in the IR spectrum of adsorbed species with similar frequencies to those observed in the free aqueous species can be assigned to outer sphere complexes. It has to be noted, however, that it is possible in some cases for outer sphere complexes to exhibit substantial spectral changes, especially when the carboxylic group is hydrogen bonded to the surface. Outer sphere complexes can be categorised into two types which relate to the type of association between the ion and the surface. In the first type the adsorbed ions retain their hydration shell, whereas for the second type the hydration sphere of the adsorbed ion is removed. For the latter case the carboxylic group is hydrogen bonded with surface hydroxyl groups or with surface-coordinated water molecules. This kind of association may lead to spectral changes which can be mistakenly attributed to inner sphere complexation (Noren and Persson, 2007).

Furthermore, from the analysis of the IR spectra alone, it may be impossible to differentiate between two different types of coordination modes. Discriminating between mononuclear and binuclear species is particularly difficult. It is not surprising therefore that in some cases a different number of surface complexes and/or coordination modes have been proposed for the same type of organic acid adsorbed on the same type of mineral substrate. These discrepancies usually arise because similar IR spectra of adsorbed complexes have been interpreted differently by different authors. As suggested by Noren and Persson (2007) this could potentially lead to the erroneous conclusion that individual organic ligands have the ability to bind to the surface via different types of coordination modes. Because of these complexities special caution is needed for the interpretation of the IR spectra and in some cases it may be only possible to propose probable structures.

The problems associated with data analysis are further compounded by the IR data obtained using the current flow through method. Absorption band intensities obtained using the current experimental procedure are relatively low when compared to those obtained using the wet paste approach. As a result for some systems investigated, the interpretation of the IR spectra was particularly challenging as the peak frequency positions of low intensity absorption bands were not well defined.

Data collection process

Water moisture

Although the sample compartment of the spectrometer is continuously purged with nitrogen gas, it was observed that sometimes for long reaction times sharp spiked peaks of increasing intensity were developing over time at the absorption frequency of water. Such peaks originate from small changes in moisture content within the sample compartment, which may be the result of residual moisture or inconstant flow of nitrogen gas during the course of the experiment. Figure 2-7 shows the typical peaks associated with water vapour/moisture which can cause severe spectral interference to the IR measurements. The effects of water vapour interference show the importance of effective nitrogen purging for the complete removal of water vapour prior and during the experiment. For IR spectra consisting of low intensity bands, the effect of water vapour interference was even more pronounced.

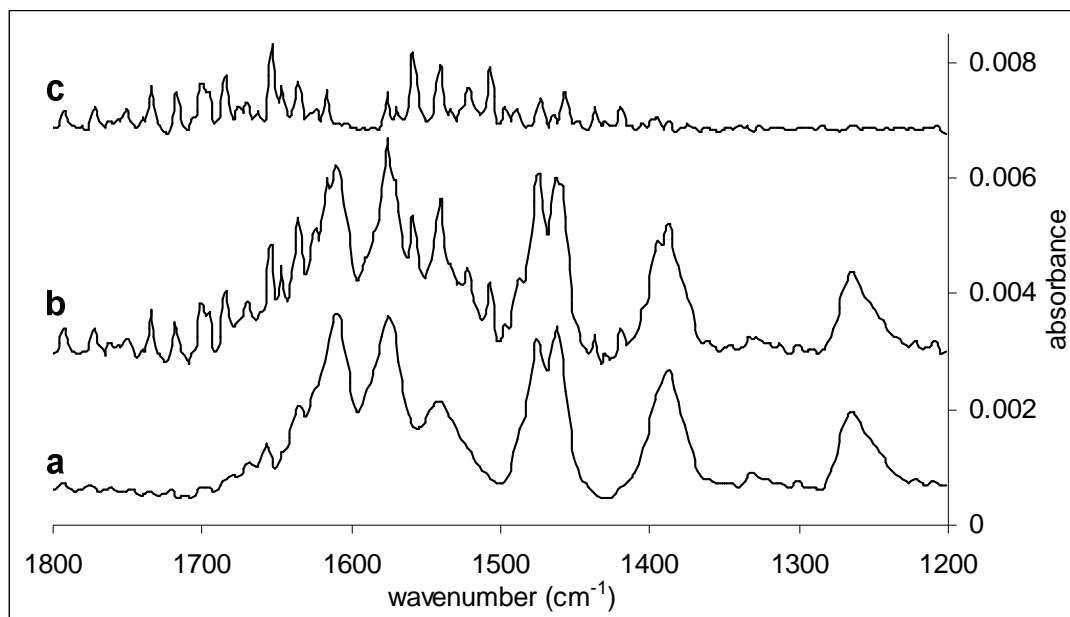


Figure 2-7 (a) The infrared spectrum of adsorbed salicylic acid onto gibbsite, from a 7.5×10^{-4} M solution at pH 5, obtained after 56 minutes of reaction time. (b) The infrared spectrum of the surface complex in (a) obtained after 2 hours reaction time, showing the effects of water vapour interference caused by the change in the nitrogen purge flow. (c) the difference spectrum obtained by subtracting (b) from (a), revealing the characteristic peaks associated with water vapour.

Degradation of the mineral film

Degradation of the mineral coating after long exposure times to water and to the reacting solution can affect the background subtraction procedure. The loss of mineral from the crystal during the experiment gives rise to IR spectra with negative absorption bands in the spectral region where the mineral substrate is IR active. These negative bands can cause severe interference if the absorption bands originating from the surface complex are also present in the same frequency region. In this study the mineral-coated crystal showed some mineral loss over time (typically more than 2 hours) when exposed to the flowing organic solution. By weighing the coated crystal before and after the reaction for a number of different experiments, the resulting mass loss from the film was estimated to be between 10-20%. This problem is further exacerbated if the mineral substrate probed exhibits high dissolution rates. As an example Figure 2-8 shows the spectrum of adsorbed phthalic acid on magnesite after 3 hours of reaction time. A major negative peak develops in the carboxyl IR region (peak frequency at about 1400 cm^{-1}) due to the loss of magnesite from the IRE.

For kaolinite mineral degradation did not present a particular problem as the bands of kaolinite are outside the carboxyl region. Degradation does however affect the quantitative analysis of the IR spectra since the mass of mineral deposited on the IRE

does not remain the same during the course of the experiment. Moreover different mass losses are expected in different experiments as experimental conditions (e.g. pH) can have an effect on the film degradation. As a result absolute band intensities (measure of surface concentration) obtained from different experiments cannot be directly compared and must therefore rely on comparisons between relative band intensities.

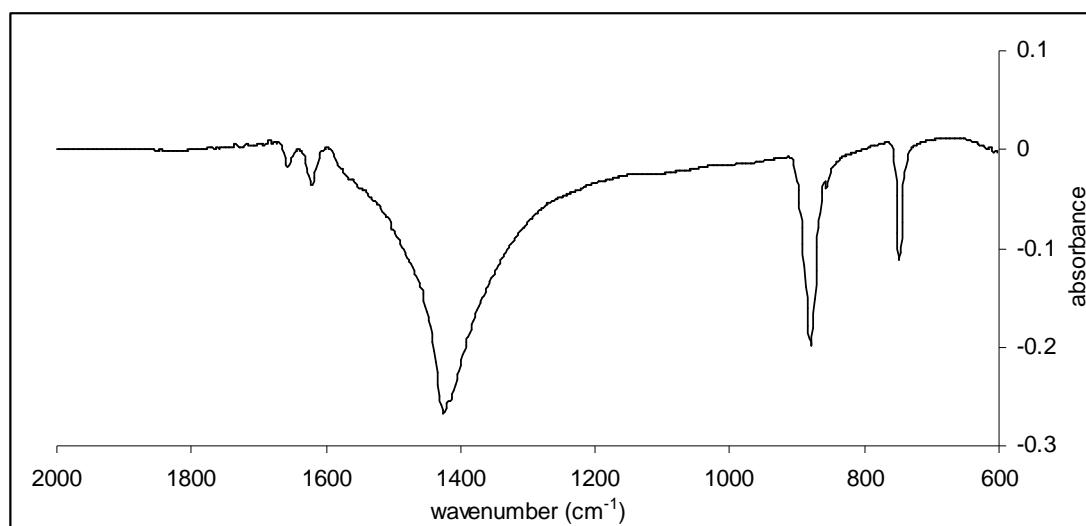


Figure 2-8 The negative peaks appearing on the spectrum of adsorbed phthalic acid following the dissolution of the magnesite coating from the ZnSe crystal.

Mineral Coating

Although the mineral concentration in the suspension which is allowed to dry on the bare crystal is the same for all experiments, the resulting mass of mineral deposited on the crystal will not necessarily be reproducible in separate experiments due to the subsequent water rinsing step (see methodology section). Although care was taken to repeat the rinsing step in a systematic manner it cannot be ensured that the same mass of mineral particles is detached from the film. Moreover the degradation of the film during the course of the experiment, as described above, may also contribute to the differences in mass loss. If the differences in mass are significant then direct comparisons between data taken on different runs should be made with caution as the mineral to ligand ratio will not be matched. Therefore this will limit the quantitative analysis of the results obtained as the band intensities in different experiments will not be directly comparable.

It has to be noted however that mass loss did not present a significant problem in this study as band intensities obtained from repeat experiments were similar. However when a higher mass of the mineral was deliberately deposited on the crystal, significant

differences could be observed in the spectra obtained for two different mineral concentrations at the same solution conditions. For example a tenfold increase in the mass of kaolinite deposited on the crystal resulted in significant differences in the IR spectra of adsorbed oxalic acid.

Bearing in mind the difficulties associated with both spectral acquisition and interpretation, outlined in this section, other techniques are usually used to complement the experimental results obtained for the study of organic adsorption mechanisms to mineral surfaces. Despite these limitations we strongly advocate that *in situ* flow through MIR-FTIR spectroscopy is one of the most promising spectroscopic techniques which can be used for the study of adsorption reactions at the mineral-water interface. The following section will draw upon a case study to demonstrate the application of the present *in situ* flow through MIR-FTIR method for the analysis of adsorbed organic ligands at the molecular level.

Case study: The complexation of oxalic acid on kaolinite studied *via* flow through *in situ* MIR-FTIR spectroscopy

The system chosen for examination involves the adsorption of oxalic acid onto kaolinite. Oxalic acid was chosen because it is a simple organic acid which has been well studied using IR spectroscopy and shown to form stable inner sphere complexes on a variety of metal hydr(oxides). However there is scarce spectroscopic data available for the adsorption of oxalic acid, as well as of other LMW organic acids, on clay minerals. In addition the effect of oxalic acid on the dissolution rates of kaolinite has attracted much scientific interest and hence further insights into the dissolution mechanism can be obtained from the structural information of the surface complex formed.

Results and discussion

Oxalic acid is the simplest aliphatic dicarboxylic acid consisting of only two carboxylic groups joined together via a C-C bond (HOOC-COOH). The species

distribution diagram of aqueous oxalic acid as a function of pH is given in Figure 2-9. In the pH range investigated in the present study (pH 3-6) oxalic acid predominantly exists either as the singly protonated species (HOx^- , hydrogen oxalate) or as the fully deprotonated species (Ox^{2-} , oxalate).

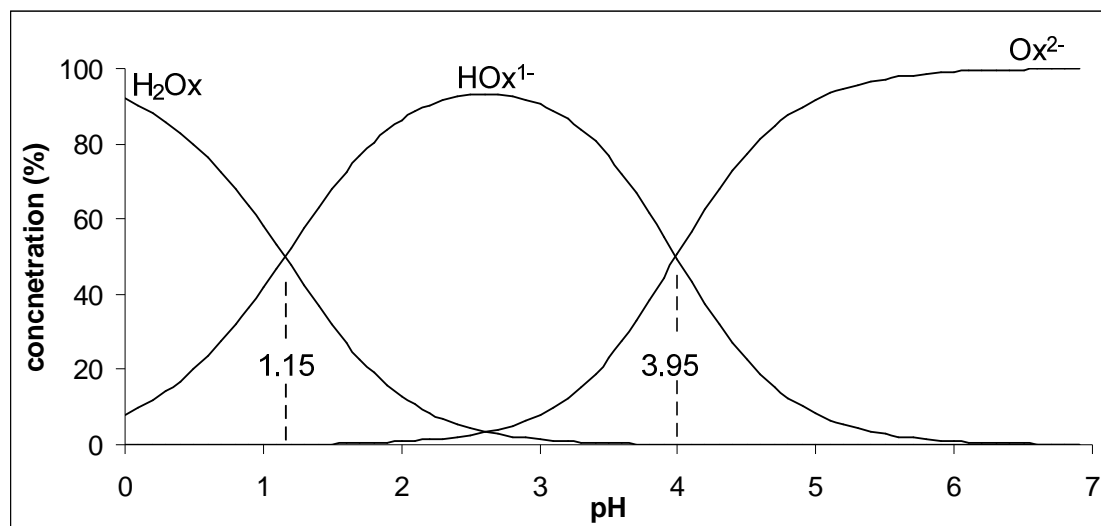


Figure 2-9 Oxalate species distribution as a function of pH. Hydrogen oxalate is the dominant species in solution at pH values higher than about 1.15 ($\text{pK}_{\text{a}1}$). Oxalate becomes the dominant species at pH values above 3.95 ($\text{pK}_{\text{a}2}$). The species distribution diagram was calculated using the Visual MINTEQ ver. 2.60 modelling software.

Aqueous oxalic acid species

The IR spectra of aqueous oxalic acid as a function of pH, displayed in Figure 2-10, reflect the changes occurring to the geometric and electronic structure of oxalic acid as a result of the protonation/deprotonation of the two carboxyl groups. At pH values below the second acid dissociation constant of oxalic acid ($\text{pH} < 4$) hydrogen oxalate (HOOC-COO^-) is the dominant species in solution, while at higher pH oxalate ion ($^-\text{OOC-COO}^-$) predominates. The spectra obtained here are in very good agreement with the IR spectra previously reported for aqueous oxalic acid species (Axe and Persson, 2001; Cabaniss et al., 1998; Degenhardt and McQuillan, 1999; Johnson et al., 2004b; Persson and Axe, 2005; Specht et al., 2000). The origin of the IR absorption bands of aqueous oxalic acid has been discussed in these studies and therefore will only be briefly summarised here.

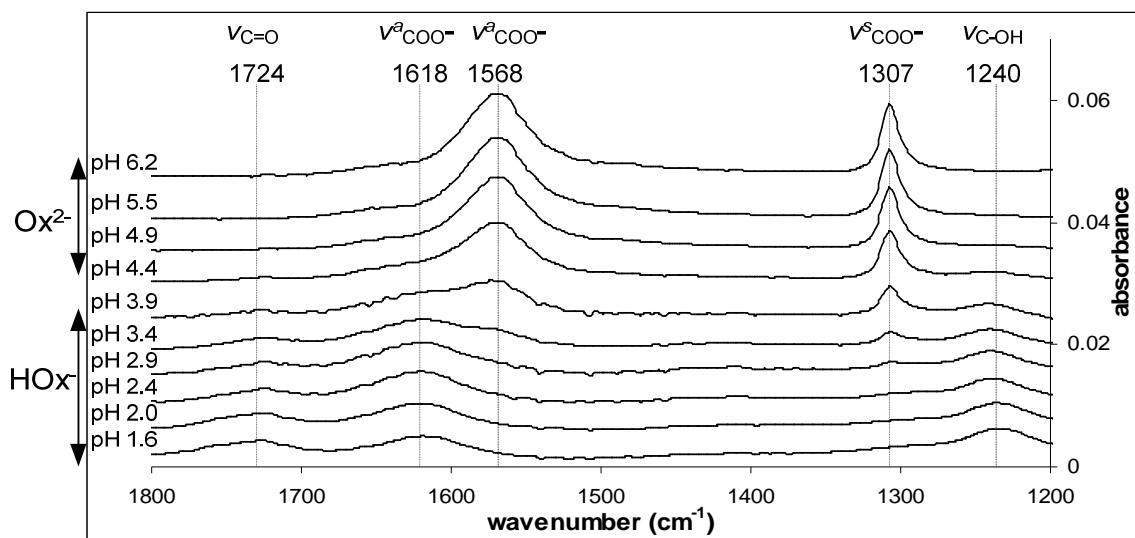


Figure 2-10 IR spectra of aqueous oxalic acid as a function of pH. At pH values below the pKa2 (3.95), HOx⁻ species is the dominant species in solution and the spectra contain IR features arising from both a protonated carboxylic group ($\nu_{C=O}$ and ν_{C-OH}) and a deprotonated carboxylic group (ν_{COO^-}). Above the pKa2 only two absorption bands are present in the IR spectra which arise from the stretching vibrations of deprotonated carboxylate groups. Spectra have been offset for clarity.

The IR spectra of Ox²⁻ species (pH > 4) consist of two prominent absorption bands at 1307 and 1568 cm⁻¹ which are assigned to the symmetric ($\nu^s_{COO^-}$) and asymmetric ($\nu^a_{COO^-}$) stretching modes respectively of the two deprotonated carboxyl groups. The simplicity of the IR spectra is attributable to the highly symmetric structure of the fully deprotonated oxalate ion. The intensities of the aforementioned bands decrease with decreasing pH and, at the same time, two new absorption bands emerge which increase in intensity as the pH of the solution decreases. These two new bands, located at 1240 and 1724 cm⁻¹ originate from the C-OH (ν_{C-OH}) and C=O ($\nu_{C=O}$) stretching modes respectively of the protonated carboxyl group in the HOx⁻ species. The remaining two absorption bands of the HOx⁻ species, located at 1306 cm⁻¹ and 1618 cm⁻¹, are assigned to the symmetric ($\nu^s_{COO^-}$) and asymmetric ($\nu^a_{COO^-}$) stretching modes of the deprotonated carboxylate group. Table 2-2 summarises the peak frequency positions of the aqueous Ox²⁻ and HOx⁻ species.

Table 2-2 Peak frequency positions of the aqueous oxalate and hydrogen oxalate species obtained in this study.

Vibration Mode	Wavenumber (cm ⁻¹)	
	Oxalate (Ox ²⁻)	Hydrogen Oxalate (HOx ⁻)
ν_{C-OH}	-	1240
$\nu^s_{COO^-}$	1307	1306
$\nu^a_{COO^-}$	1568	1618
$\nu_{C=O}$	-	1724

Adsorbed oxalic acid species

IR spectra of adsorbed oxalic acid on kaolinite were collected at two pH values, 3.5 and 6, and at two initial oxalic acid concentrations, 5×10^{-4} and 5×10^{-3} M. Because the pH was found to have a significant effect on the IR spectra obtained, the adsorption of oxalic acid at these two pH values will be discussed separately. The IR spectra of adsorbed oxalate obtained from two different solution concentrations (5×10^{-4} M and 5×10^{-3} M oxalic acid solution) at pH 3.5 are shown in Figure 2-11. The IR spectrum of aqueous oxalic acid recorded at pH 3.6 is also included for comparison. The distinct differences in the IR spectrum of the adsorbed species when compared to the IR spectrum of the aqueous species strongly indicate that oxalic acid is directly coordinated to the surface of kaolinite (i.e. inner sphere complexation). However, additional spectroscopic features in the spectrum obtained at the higher oxalate concentration strongly suggest that at least two structurally different surface complexes coexist on the surface of kaolinite at pH 3.5. The structural identity of these two surface complexes will be discussed in more detail.

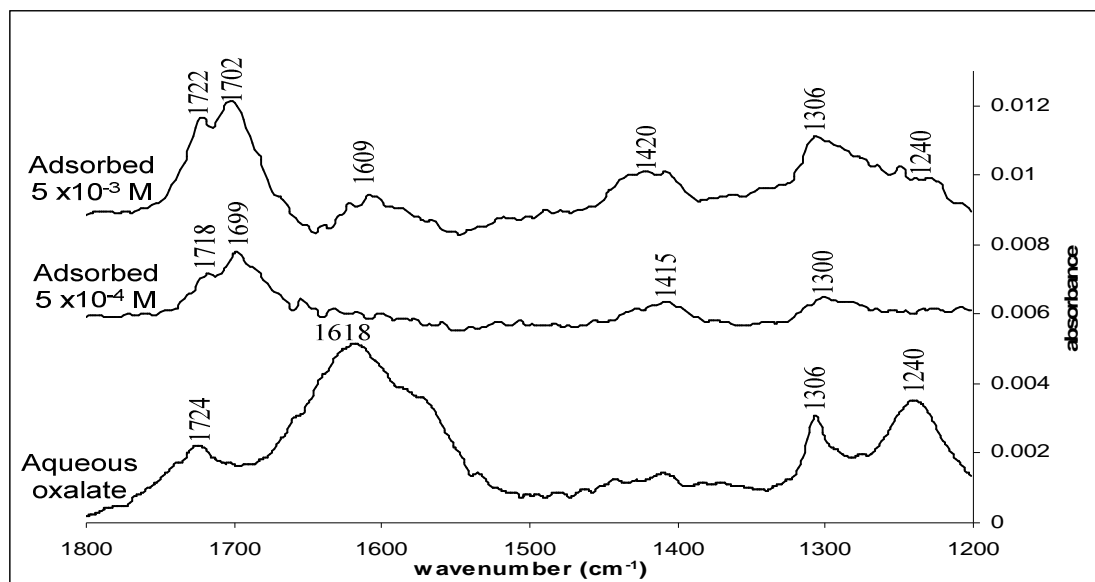


Figure 2-11 IR spectra of adsorbed oxalic acid on kaolinite, from a 5×10^{-3} M and 5×10^{-4} M oxalic acid solution, at pH 3.5. The spectrum of aqueous oxalic acid recorded at pH 3.6 is also included. Spectra have been offset for clarity.

At the lower oxalate concentration examined, adsorbed oxalic acid gives rise to four distinct absorption bands with peak frequency positions at 1718, 1699, 1415, 1300 cm^{-1} . As seen in Figure 2-11, the IR spectrum of adsorbed oxalic acid changes

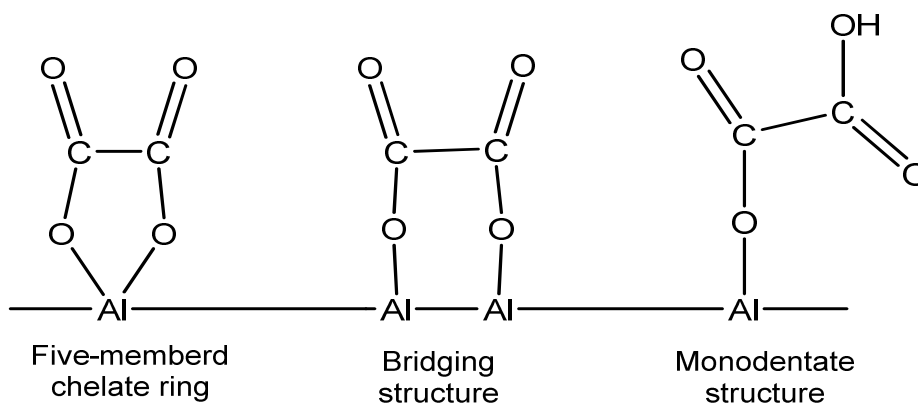
significantly suggesting that oxalate predominantly adsorbs as an inner sphere surface complex. Interestingly, the spectrum of the inner sphere complex identified here shows a strong resemblance to the spectra of inner sphere complexed oxalate species reported in the literature for other mineral substrates (Table 2-3).

Table 2-3 Literature assignment of the IR absorption bands arising from the vibrational modes of inner sphere complexed oxalate species.

Substrate	pH	$\nu_{C=O}$	$\nu_{C-O} + \nu_{C-C}$	$\nu_{C-O} + \delta_{O-C=O}$	References
Titanium Dioxide					
90% Anatase (a)	3.7	1712, 1692	1415	1268	Weisz et. al. (2002)
Anatase (b)	3.7	1717, 1697	1420	1270	Mendive et al. (2006)
Rutile (b)	3.7	1713, 1690	1416	1277	Mendive et al. (2006)
Anatase	3.0	1711,1685	1405	≈1280	Hug and Sulzberger (1994)
Anatase (a or b)	3	1716,1696	1416	1264	Hug and Bahnemann (2006)
Rutile (a or b)	3	1713,1691	1412	1268	Hug and Bahnemann (2006)
TiO ₂ (a or b)	-	1711,1686	1424	1271	Dobson and McQuillan (1999)
Aluminium (hydr)oxides					
Al ₂ O ₃ (a or b)	-	1720,1695	1424	1297	Dobson and McQuillan (1999)
Boehmite (a)	5	1722,1702	1413	1288	(1999)
Boehmite (a)	5.1	1720,1700	1418	1286	Axe and Persson (2001)
Boehmite (a)	2.5	≈1715, 1697	≈1415	≈1285	Yoon et al. (2004)
Corundum (a)	2-6	1721,1700 ^{+/-1}	1423 ^{+/-1}	1291 ^{+/-4}	Yoon et al. (2004)
Gibbsite (a)	5-7	≈1720,1700	≈1415	≈1290	Johnson et al (2004) Rosenqvist et al. (2003)
Iron (oxo) (hydr)oxides					
Goethite (a)	2.7	1713,1692	1404	1255	Persson and Axe (2005)
Goethite (a)	6.8	1713,1692	1427	1255	Persson and Axe (2005)
Hematite (a or b)	5	1720,1701	1423	-	Duckworth and Martin (2001)
Chromium (hydr)oxides					
Cr ₂ O ₃ (a)	3.6	1710, 1680	1410	1260	Garcia Rodenas et al. (1997)
Cr(III) oxide hydroxide(a or b)	3	1708, 1682	1407	1276	Degenhardt and McQuillan(1999)

v denotes a stretching vibration mode and δ a bending vibration mode
 (a) Mononuclear bidentate side-on structure (5-membered chelate ring)
 (b) Binuclear bidentate side-on structure (bridging complex)

In accordance with the studies listed in Table 2-3, the spectrum recorded at pH 3.5 and low oxalate concentration represents the IR spectrum of inner sphere complexed oxalic acid. The band doublet with peak positions at 1718 and 1699 cm⁻¹ arises from the vibrational coupling of two similar carbonyl stretching vibrations ($\nu_{C=O}$) (Degenhardt and McQuillan, 1999; Dobson and McQuillan, 1999; Hug and Bahnemann, 2006; Mendive et al., 2006; Persson and Axe, 2005). The presence of this band doublet indicates that the surface complex possesses two C=O groups and neither of these two moieties is bound to the surface (Axe and Persson, 2001; Clausen et al., 2003). Three possible surface complexes can give rise to this band splitting, a side-on mononuclear bidentate complex (five-membered chelate ring structure), a side-on binuclear bidentate complex (bridging structure) or a monodentate complex, as shown below.



The broad band with a peak position at about 1415 cm^{-1} is characteristic of a chemically bound surface species, it is not present in any of the aqueous oxalate species. This band is assigned to the coupling effect of the motions associated with the stretching vibrations of a C-O ($\nu_{\text{C-O}}$) and a C-C ($\nu_{\text{C-C}}$) bond (Axe and Persson, 2001; Clausen et al., 2003; Dobson and McQuillan, 1999; Hug and Bahnemann, 2006; Persson and Axe, 2005; Weisz et al., 2002). The $\nu_{\text{C-O}}$ mode involves a surface bound oxygen and such a stretching mode typically arises from a side-on surface coordination mode (Degenhardt and McQuillan, 1999). The absorption band with a peak position at about 1300 cm^{-1} arises from the symmetric stretching mode of a C-O bond ($\nu_{\text{C-O}}$) coupled with the bending mode of the O-C=O group ($\delta_{\text{O-C=O}}$).

Although valuable information about the structure of the surface complex is gained from the analysis of the IR spectra, the exact coordination mode of the adsorbed oxalate cannot be inferred. Based on the interpretation of the IR spectra, it can be concluded that the oxalic acid coordinates on kaolinite as either a side-on mononuclear bidentate (chelate structure) or a binuclear bidentate (bridging structure) surface complex. IR spectroscopy cannot differentiate between these two structures and the results must be compared with studies which carried out theoretical frequency calculations for various oxalate coordination modes.

The peaks positioned at 1718, 1699, 1415 and 1300 cm^{-1} are consistent with oxalate forming an inner sphere complex with a side-on, mononuclear, bidentate (five-membered ring chelate) structure (Axe and Persson, 2001; Johnson et al., 2004b; Rosenqvist et al., 2003; Weisz et al., 2002; Yoon et al., 2004b). Other possible coordination modes examined by theoretical frequency calculations, such as end-on mononuclear bidentate (four-membered ring chelate), mononuclear monodentate chelate or bridging structures produced significantly different spectra from the obtained IR

spectra. It can be therefore concluded that the most probable structure of adsorbed oxalate at the kaolinite-water interface is a five-membered chelate ring structure.

The spectra recorded in the higher oxalate concentration experiments (5×10^{-3} M) cannot be accounted for by the presence of only one surface complex. When compared to the spectrum of adsorbed oxalic acid obtained at the lower concentration it can be observed that a new band emerges at around 1609 cm^{-1} and the band positioned at 1301 cm^{-1} shifts to a higher frequency at 1306 cm^{-1} . An additional peak at 1296 cm^{-1} could also be resolved following the deconvolution of the absorption band positioned at 1306 cm^{-1} . The bands located at 1722 , 1702 , 1420 and 1296 cm^{-1} have similar frequency positions to those obtained at lower oxalate concentrations, and therefore are also attributed to a mononuclear bidentate inner sphere surface complex. Small differences in peak positions of the bands assigned to inner sphere adsorbed oxalic acid, obtained at the two different oxalate concentrations, can be related to the precision of the experimental method. Alternatively, Johnson et al. (2004b) have attributed this to small changes in the binding environment of oxalate due to surface crowding effects.

The 1609 cm^{-1} band appearing in the spectrum of adsorbed oxalate, could be originating from a second inner sphere complex which may be forming at these higher oxalate concentrations. Alternatively, this band could be associated with oxalate molecules coordinating to the surface in an outer sphere binding mode. The frequency position of the band at 1609 cm^{-1} lies between the frequency region of the symmetric stretching vibration ($\nu_{\text{C-O}}^{\text{s}}$) exhibited by the singly protonated aqueous HOx^- species (1618 cm^{-1}) and the fully deprotonated aqueous Ox^{2-} species (1569 cm^{-1}). It should be noted however that this band is broad and due to its proximity to the water interference region the exact peak position is less well constrained than other absorption bands.

Due to the close proximity of the 1609 cm^{-1} band to the frequency position of the $\nu_{\text{C-O}}^{\text{a}}$ mode exhibited by the aqueous HOx^- species, it is possible that this band originates from an outer sphere singly protonated oxalate species (HOx^-). Furthermore, the small band observed at about 1240 cm^{-1} , in the adsorbed spectrum, is also consistent to a HOx^- species since it corresponds to the stretching vibration of a hydroxyl group ($\nu_{\text{C-OH}}$) found in the aqueous singly protonated HOx^- species. Conversely, the 1609 cm^{-1} peak may arise from the asymmetric stretching vibration of a fully deprotonated oxalate molecule coordinated to the surface as an outer sphere complex. A shift of the $\nu_{\text{C-O}}^{\text{as}}$ mode to higher frequency values has been previously reported when oxalate is bound to the surface via hydrogen bonding. However the shift observed in the present study (about 40 cm^{-1}) is higher than the typical values reported in the literature (e.g 13 cm^{-1} Persson and Axe, 2004; 20 cm^{-1} Yoon et al., 2004; 8 cm^{-1} Johnson et al., 2004b; 8 cm^{-1}

Axe et al., 2001). The shift of the 1301 cm^{-1} band to 1309 cm^{-1} observed at higher oxalate concentrations is consistent with both singly protonated and fully deprotonated outer sphere complexed oxalate species.

In order to examine whether the band at 1609 cm^{-1} originates from an inner or an outer sphere complex, the spectrum of adsorbed oxalate was collected at different background electrolyte concentrations. The spectra of adsorbed oxalic acid at pH 3.5 and three different background electrolyte concentrations are given in Figure 2-12. The absorption band at 1609 cm^{-1} diminishes with increasing electrolyte concentrations, indicating that this band is associated with an outer sphere complexed species. Oxalic acid involved in this outer sphere complex is most probably a singly protonated species as the band at 1240 cm^{-1} ($\nu_{\text{C-OH}}$) also decreases in intensity along with the peak at 1609 cm^{-1} suggesting that both bands originate from the same surface species.

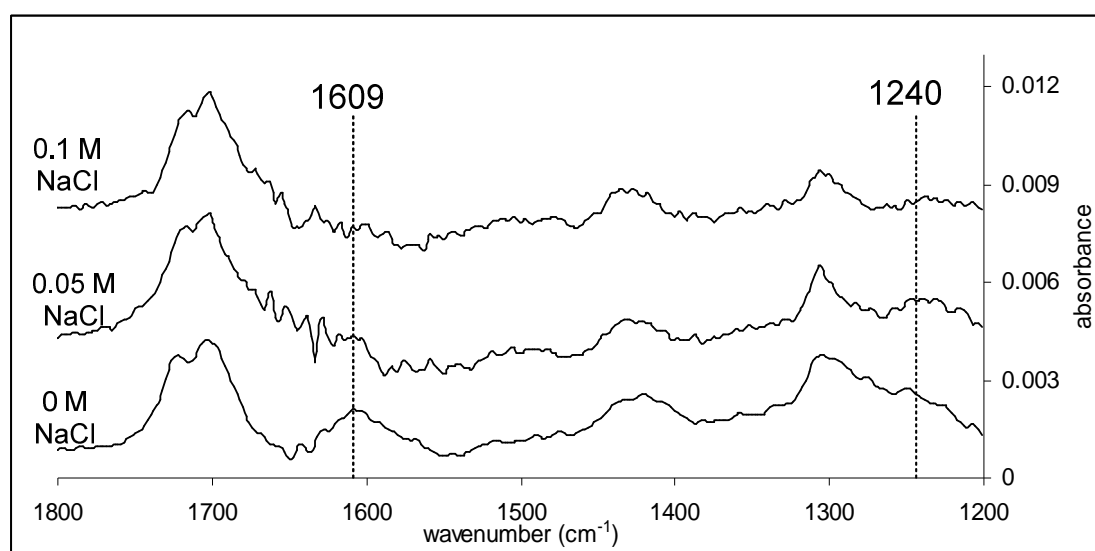


Figure 2-12 IR spectra of adsorbed oxalic acid on kaolinite, from a $5 \times 10^{-3}\text{ M}$ oxalic acid solution, obtained at pH 3.5 and three different background electrolyte concentrations. The band at 1609 shows a dependence on background electrolyte indicating that the band originates from an outer sphere complex.

The spectra of surface bound oxalic acid species adsorbed on kaolinite from two different initial oxalic acid concentrations at pH 6 are shown in Figure 2-13. At the lower concentration examined ($5 \times 10^{-4}\text{ M}$), five absorption peaks were identified at 1723 , 1699 , 1577 , ~ 1430 and 1308 cm^{-1} . Deconvolution of the band at 1308 revealed an additional band with a peak position at 1298 cm^{-1} . In accordance to the interpretation given for the adsorbed species at pH 3.5, the bands at 1723 , 1698 , 1430 and 1298 cm^{-1} are assigned to a side-on mononuclear bidentate structure. The remaining two

absorption bands positioned at 1577 and 1308 cm^{-1} have very similar peak frequencies to the asymmetric and symmetric carboxylate stretching modes of the fully deprotonated aqueous oxalate ion respectively. This similarity in the frequency positions strongly suggests the presence of fully deprotonated, outer sphere complexed oxalate species on the surface. Therefore, at pH 6 two structurally different complexes are formed on the surface of kaolinite, one outer and one inner sphere complex.

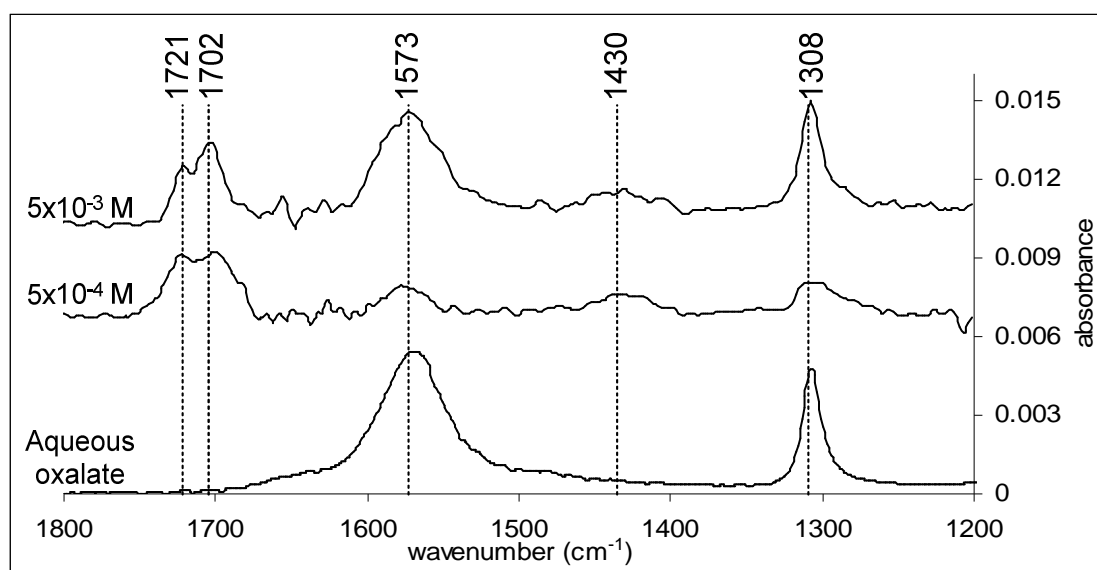


Figure 2-13 The spectra of adsorbed oxalic acid on kaolinite, at pH 6, from a 5×10^{-3} M and 5×10^{-4} M oxalic acid solution. The spectrum of aqueous oxalic acid at pH 5.5 is also included for comparison. The two bands near 1570 and 1308 cm^{-1} have similar positions to the bands observed in the aqueous oxalate complexes and therefore they can be attributed to an outer sphere complex. The relative importance of these two bands is much higher in the higher oxalate concentration indicating an increase in the dominance of outer sphere complexes at higher oxalate concentrations.

At the higher oxalate concentration examined, the importance of the bands at 1573 and 1308 cm^{-1} increases relative to bands associated to inner sphere complexed species, indicating an increase in dominance of outer sphere complexation. The frequency positions of the bands attributed to the inner sphere complex do not show any significant shifts suggesting that these complexes retain the same coordination mode. The band at 1298 cm^{-1} , present as a shoulder in the lower concentration spectrum, is masked by the much higher intensity of the band ascribed to the symmetric stretching vibration of the outer sphere complex at 1307 cm^{-1} .

Although the two absorption bands positioned at 1570 and 1308 cm^{-1} are assigned to an outer sphere surface complex, in a previous study (Specht and Frimmel, 2001) these two bands have been assigned to an inner sphere complex. In order to

investigate this possibility, the spectra of adsorbed oxalate (from a 5×10^{-3} M oxalate solution) were recorded in a 0.05 M NaCl background electrolyte solution, at pH 5.5 (not shown). In the presence of NaCl, the intensities of the bands at 1308 and 1570 cm^{-1} decreased relative to the intensities of the remaining absorption bands in the IR spectrum. The ionic strength dependence of these two bands gives more confidence for the assignment of these two bands to an outer sphere complex.

On the basis of IR data presented here, oxalic acid was found to form two different types of surface complexes at the kaolinite-water interface. At pH 3.5, oxalic acid coordinates to the surface of kaolinite in a mononuclear bidentate side-on mode, forming a five-membered ring chelate structure. At higher concentrations and pH values, the IR spectra revealed the presence of an additional surface complex which coordinates to the surface in an outer sphere mode. At pH 3.5 outer sphere complexed oxalic acid is present as the singly protonated hydrogen oxalate molecule whereas at pH 6 oxalic acid is present as the fully deprotonated oxalate molecule. There is no spectroscopic evidence for a change in the coordination mode of the inner sphere complex at the higher pH values or concentrations examined. Table 2-4 summarises the assignment of the absorption bands found in the IR spectra of adsorbed oxalic acid on kaolinite at different experimental conditions examined.

Table 2-4 Peak frequency positions and assignment for the IR spectra of adsorbed oxalic acid at the kaolinite-water interface.

Aqueous		Adsorbed				Vibrational mode	Assignment
HOx ¹⁻	Ox ²⁻	5 x 10 ⁻⁴ M		5 x 10 ⁻³ M			
		pH 3.5	pH 6	pH 3.5	pH 6		
1724		1718	1723	1722	1721	$\nu_{\text{C=O}}$	ISC
		1699	1699	1702	1702	$\nu_{\text{C=O}}$	ISC
1618	1568			1609		$\nu^{\text{a}}_{\text{COO}^-}$	OSC (HOx ¹⁻)
			1577		1573	$\nu^{\text{a}}_{\text{COO}^-}$	OSC (Ox ²⁻)
		~1415	~1430	~1420	~1430	$\nu_{\text{C-O}^+} \nu_{\text{C-C}}$	ISC
1306	1307			1306		$\nu^{\text{s}}_{\text{COO}^-}$	OSC (HOx ¹⁻)
			1308		1308	$\nu^{\text{s}}_{\text{COO}^-}$	OSC (Ox ²⁻)
		1300	~1298	~1296		$\nu_{\text{C-O}^+} \delta_{\text{O-C=O}}$	ISC
1240				~1240		$\nu_{\text{C-OH}}$	OSC (HOx ¹⁻)

ISC- Inner sphere complex; OSC- Outer sphere complex

Summary and conclusions

IR spectroscopy and particularly multiple internal reflection (MIR) spectroscopy is a widely used experimental technique that allows the study of complexation reactions at the mineral water interface. The sensitivity of the IR spectra to changes in the local coordination environment of the carboxyl group makes IR spectroscopy a very powerful tool for the study of the interactions between carboxyl-bearing compounds and mineral surfaces. Therefore IR spectroscopy can be used to increase the molecular level understanding of the interactions of organic ligands on mineral surfaces. Information which can be obtained includes the number of structurally different surface bound species, as well as their binding and coordination environment.

In this study an *in situ* flow through MIR-IR technique developed at the University of Manchester for the study of organic ligand surface complexation reactions is presented. This IR technique presented offers some significant advantages over the more commonly used *in situ* wet paste method, including (a) the collection of real time spectroscopic data; (b) enables a more robust subtraction procedure and; (c) IR spectra can be obtained at lower, more environmentally relevant organic ligand concentrations. In addition, some of the problems and limitations associated with the use of IR spectroscopy, and in particular of the method presented in this chapter, are discussed.

In the last section of this chapter a case study presenting how the current IR method can be used to obtain structural and binding information of adsorbed oxalic acid on kaolinite. Two different types of oxalate surface complexes were found to coexist on the surface of kaolinite, and their relative concentration was strongly influenced by solution conditions. At pH 3.5 and an initial oxalate concentration of 5×10^{-4} M, oxalate predominately adsorbs in an inner sphere coordination mode (side-on, mononuclear bidentate). At the same pH and an oxalate concentration of 5×10^{-3} M, an additional HOx^- outer sphere complexed species could be identified. At pH 6 one inner and one outer sphere complex were found to coexist at both oxalate concentrations examined. At the higher oxalate concentration however, outer sphere complexed species gained in importance over inner sphere complexed species. The inner sphere complex identified in both pH values has the same coordination mode. In contrast, outer sphere complexed oxalate has a different protonation state at pH 3.5 (HOx^-) and 6 (Ox^{2-}).

Chapter 3 Complexation of phthalic and salicylic acid on the surface of kaolinite

Introduction

Naturally occurring organic acids constitute one of the most important classes of organic ligands found in the environment and due to their widespread occurrence and reactive nature they play a key role in many important environmental, geochemical and biological processes. The adsorption mechanisms and binding modes of organic ligands on mineral surfaces have attracted much attention in the published literature for many decades. However much disagreement persists regarding our understanding of fundamental aspects associated with the adsorption mechanisms by which organic ligands interact with mineral surfaces. As a result the study of ligand surface complexation reactions is still a topic of significant scientific interest.

Because of their reactive nature organic ligands are commonly associated with metal cations on mineral surfaces (e.g. Evanko and Dzombak, 1998; Filius et al., 1997; Tipping, 1981) and in aqueous solutions (e.g. Gustafsson, 2001; Tipping et al., 2002; Zhou et al., 2005). Organic ligand complexation reactions in aqueous solutions can have a significant effect on element speciation, mobility, bioavailability, and adsorption (Angove et al., 1999; Krishnamurti et al., 1997; Onyatta and Huang, 2003; Redman et al., 2002; Schroth and Sposito, 1998; Xu and Ji, 2003).

Furthermore, the adsorption of organic ligands on mineral surfaces has the potential to influence several surface-dependent geochemical processes. Upon adsorption organic ligands can affect the electrostatic properties of mineral surfaces and this in turn will influence the adsorption of both cationic and anionic species. Additionally, adsorbed organics can impart a hydrophobic character to mineral surfaces and therefore can increase the adsorption capacity for non polar hydrophobic organic compounds, the largest group of organic contaminants (Lee et al., 1989; Murphy et al., 1992; Xing et al., 1994). The biodegradation rates of organic ligands, and other organic compounds that may be associated with them, will also be affected by adsorption. Studies have showed that the biodegradation rates of adsorbed organics can decrease significantly and this in turn can impact the fate of organic matter (Arnarson and Keil, 2005; Hedges and Keil, 1999; Mayer, 1994).

Knowledge about the interactions between organic ligands and mineral surfaces can provide insights into the environmental behaviour and effect of these compounds in natural systems. Therefore there is a requirement to obtain detailed information about their adsorption properties and to accurately determine the molecular-level structures and speciation of the surface complexes formed. So far the understanding of the interactions taking place in systems containing considerable amounts of natural organic matter (NOM) is limited. NOM consists of a complex mixture of organic molecules with various structures, molecular weights and properties.

Due to the difficulties arising from the study of systems containing humic substances several LMW acids have been used as natural analogues of the complex components of NOM like humic and fulvic acids. Despite their simpler structural and chemical properties, LMW organic acids have been found to exhibit similar adsorption properties to those of humic substances. Furthermore they are commonly found in nature as a result of microbial and chemical activity. For example, LMW aromatic compounds containing carboxylic and phenolic functionalities such as benzenecarboxylic (mainly between 2-6 COOH groups) and phenolic acids (mainly between 1-3 OH groups and 1-5 COOH groups) were identified as some of the major degradation products of humic substances (Schnitzer, 1991).

One of the most important classes of LMW organic ligands found in the environment are carboxylic acids. The importance of these compounds stems from the fact that they contain carboxylic acid functionalities that act as ligands for surficial metal cations and therefore have the ability to strongly bind to mineral surfaces. Moreover, the carboxylic moiety is the most abundant and reactive functional group found in humic substances (Drever, 1988), and as a result these simple carboxylic acids are expected to exhibit similar adsorption properties to that of humic substances. This has led to the use of such LMW carboxylic acids as NOM-analogues in order to give insights into the interactions of mineral surfaces with naturally occurring organic macromolecules such as humic acids.

The adsorption of organic ligands is influenced by several factors including the chemical and structural characteristics of the mineral substrate and of the adsorbates as well as the pH and ionic strength of the solution. Several different modelling approaches that account for some or all of the aforementioned factors, have been developed and used to describe the adsorption behaviour of ions on mineral surfaces. The simplest models simulate the adsorption of ions as a function of ion concentration (adsorption isotherms) whereas as the more complex take into consideration other sorption-determining factors including solution chemistry and electrostatic effects

(surface complexation models). Surface complexation models (SCMs) are semi-empirical chemical models that describe the formation of surface complexes between aqueous chemical species and surface sites. The ability of SCMs to simulate adsorption data at different experimental conditions (pH, adsorbate concentration, ionic strength) has led to their widespread use for various experimental systems involving different types of adsorbent phases and adsorbates. Such models combine information about the bulk solution properties (composition, pH and ionic strength) with information on the structure and charge of the mineral surface in order to model the competition of solute ions for available surface sites at the mineral-water interface. Although SCMs must be physically and chemically sound, at the same time they must also be as simple as possible. Therefore SCMs provide a simplification of complex systems and the parameters considered in such models do not necessarily provide a representation of the actual chemical environment.

SCMs have been widely used as means to understand and describe the acid-base properties of mineral surfaces and the adsorption behaviour of ionic species at the mineral-water interface. Difficulties arise, however, when attempts are made to apply surface complexation modelling for the description of chemical systems by taking into account only the macroscopic adsorption data. This is because for a given system there might not be a unique model that can simulate the adsorption data. For example, Nordin et al. (1997) reported that the potentiometric and adsorption data of the phthalate-boehmite system could be modelled equally well using either an inner and an outer sphere complex or two outer sphere complexes. Spectroscopic evidence, however, showed that outer and inner sphere phthalate complexes coexist on the boehmite surface and the model could thereby be properly constrained. Similarly, satisfactory model fits for phthalic acid adsorption data on haematite could be obtained by using models that consisted of either one single outer sphere complex or one inner sphere and one outer sphere complex (Hwang and Lenhart, 2009). Therefore incorporating molecular level information in SCMs can significantly improve our ability to model the adsorption behaviour of solute ions over a wide range of solution conditions.

In cases where spectroscopic data is not available the model accepted will be based solely on the subjective judgement of the modeller regarding the appropriateness of a particular model over another. Therefore, the development of a successful surface complexation model requires additional information about the microscopic adsorption properties which can be obtained by molecular-level studies. Such molecular-level data is crucial since it can significantly constrain the model input parameters. Important model parameters that can be obtained from spectroscopy, and thus incorporated in

SCMs, include the number and type of surface species formed, the protonation state of adsorbed species and possibly their exact coordination mode.

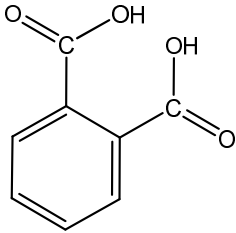
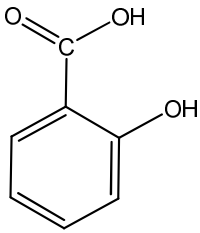
Molecular level information does not only constrain model parameters (e.g. number of surface species) but also the choice of model itself that can be used. For example direct evidence of outer sphere complexed surface species precludes the use of particular SCMs that cannot accommodate species bound in an outer sphere mode. Furthermore, for systems where two or more structurally different surface species have been identified, models can be constrained by spectroscopy to describe the experimental data both qualitatively (i.e. incorporate the number of surface species identified) and quantitatively (i.e. predict the relative importance of surface species as a function of solution conditions).

Information on the nature of the interactions between solute ions and mineral surfaces can be obtained through a variety of experimental techniques. Recent developments in surface-sensitive spectroscopic techniques have enabled the molecular-level study of adsorbed organics at the mineral-water interface. A number of studies have successfully probed the surface complexes forming and provided information on the number of different surface species coexisting on the surface; their coordination and binding modes; protonation states; and how all these parameters vary with solution chemistry. So far, however, there has been little discussion about the adsorption properties of organic ligands on clay minerals. In comparison to oxide minerals, there have been relatively few spectroscopic investigations that have sought to investigate the microscopic adsorption properties of organic ligands on clay minerals.

The aim of this chapter is to investigate the interactions of kaolinite with two LMW carboxylic acids: phthalic and salicylic acid. Both of these ligands have been previously used as natural analogues to humic substances (Evanko and Dzombak, 1998; Filius et al., 1997). Salicylic and phthalic acids (Table 3-1) are structurally similar aromatic compounds which contain carboxylic functionalities. Phthalic acid carries two carboxyl groups in ortho position with respect to each other whereas salicylic acid carries one carboxylic group and one phenolic group in the ortho position. Kaolinite was chosen as the mineral substrate because to date the interactions between organic ligands and clay minerals have received little attention in the literature. However, kaolinite is a common aluminosilicate mineral with well studied physicochemical properties including surface protonation-deprotonation studies and dissolution kinetics (Brady et al., 1996; Cama and Ganor, 2006; Carroll-Webb and Walther, 1988; Huertas et al., 1998; Wieland and Stumm, 1992).

A flow through *in situ* IR spectroscopic technique was employed to obtain molecular level information on the adsorption reactions taking place at the kaolinite-solution interface, such as the number and type of surface complexes formed, as well as the coordination mode(s) and protonation states of surface species. Macroscopic adsorption measurements were also carried out at various solution conditions to determine the adsorption behaviour of phthalic and salicylic acid on kaolinite. Surface complexation models constrained by the IR spectroscopic results were then developed to describe the pH-dependent adsorption behaviour of phthalic and salicylic acid on kaolinite. Model fits to the experimental data and stability constants of the surface species formed on kaolinite were determined according to the extended constant capacitance model (ECCM).

Table 3-1 The chemical structure and some physicochemical properties of the organic acids used in the study.

	Phthalic acid	Salicylic acid
Structure		
Chemical name	1,2-Benzenedicarboxylic acid	2-Hydroxybenzoic acid
Molecular formula	C ₈ H ₆ O ₄	C ₇ H ₆ O ₃
Molar mass	166.1	138.1
Solubility (g/100 ml of water)	0.625 (at 25°C)	0.2 (at 20°C)
pK _{a1} , pK _{a2} *	2.87, 5.23	2.88, 13.56

* pK_a values in 0.01 M NaCl obtained from Evanko and Dzombak (1999).

Methodology

Materials

Kaolinite used in this study is the poorly crystallised reference sample KGa-2, purchased from the Clay Minerals Society Source Clays Repository. X-ray diffraction analysis did not show diffraction peaks other than those corresponding to kaolinite,

hence confirming the identity and relative purity of the sample. The surface area of the sample was $21 \pm 2 \text{ m}^2/\text{g}$, as found by the B.E.T nitrogen gas adsorption method using a Micrometrics Gemini surface area analyser. Kaolinite was washed with deionised water and dried at 40°C prior to the use in any of the experiments. No other pre-treatment methods were applied on kaolinite.

All solutions and mineral suspensions were prepared with $15 \text{ M}\Omega$ deionised water and NaCl was selected as the background electrolyte. Analytical grade salicylic and phthalic acid were obtained from Sigma-Aldrich. Titrants for the acid-base titration experiments were 0.1 M NaOH and 0.1 M HCl volumetric solutions (Sigma-Aldrich), and were used as received.

Multiple Internal Reflection (MIR) - FTIR Spectroscopy

The IR spectra of adsorbed salicylic and phthalic acid on kaolinite were obtained by *in situ* Multiple Internal Reflection-Fourier Transform Infra Red Spectroscopy (MIR-FTIR). A home built flow through cell and a ZnSe crystal (60° face angle, $53 \times 10 \times 2 \text{ mm}$) were employed for the collection of *in situ* IR measurements, using a Bio-rad FTS 6000 spectrometer equipped with a deuterated triglycine sulphate (DTGS) detector. Each spectrum recorded consisted of 256 co-added scans, obtained at a spectral resolution of 4 cm^{-1} . A constant flow of the aqueous solutions through the flow cell and into a waste vessel was achieved by a peristaltic pump.

A similar experimental procedure was used for the collection of interfacial species as the one detailed in chapter 2. Briefly, the kaolinite-coated ZnSe crystal was mounted in the flow cell and this was placed in the sample compartment of the IR spectrometer. The sample compartment, as well as the flow cell itself, were purged with nitrogen for at least 16 hours before the start of the experiments in order to remove atmospheric CO_2 and water vapour. A nitrogen atmosphere was retained in the sample compartment for the duration of the experiments. Prior to the start of the experiments, and while the flow cell was still purging with nitrogen, a background spectrum which consisted of the IR spectrum of the dry kaolinite-coated ZnSe crystal was collected. Following the addition of the aqueous solutions, all the acquired spectra were ratioed against the background spectrum in order to remove spectral contributions arising from the ZnSe and from the mineral substrate.

The strong absorption bands of water dominating the spectra of the adsorbed species were removed by a water subtraction procedure also described in chapter 2. Prior to the addition of the ligand solution, water was pumped through the flow cell until a stable water spectrum could be obtained. The flow was then switch to the ligand solution and the water spectrum obtained was subtracted from all the subsequent spectra recorded.

Following the addition of the ligand solution, IR spectra were recorded at about 5 minute intervals (duration of a full scan) until band intensities reached maximum values. After equilibrium was reached, typically within the first 40-50 minutes of reaction time, spectra were recorded at longer intervals of about 20 minutes for a further 2 hours in order to monitor any changes occurring to the spectra as a function of time. IR spectra of adsorbed species for each specific pH value and ionic strength studied were collected in separate experiments in order to avoid kinetic artefacts from previous conditions carrying over between measurements. Several experiments were repeated to check for the reproducibility of the acquired IR spectra and to ensure that no contamination artefacts were present.

IR spectra of aqueous uncomplexed organic species were collected in a similar manner as that described for the adsorbed species, except that the ZnSe crystal was not coated with kaolinite and much higher ligand concentrations were used. By using an uncoated crystal it was also possible to determine the minimum detection limit of the aqueous species for the experimental setup. Ligand solution concentrations used for the collection of the IR spectra of interfacial species were kept below the detection limit for uncomplexed species. This ensured that all the IR bands in the obtained spectra arise from species accumulating near the surface of the crystal (i.e. adsorbed species) at higher concentrations than the bulk fluid due to interactions with the kaolinite and not from aqueous ligand species.

Adsorption Experiments

Kinetic experiments

Preliminary adsorption experiments performed to determine the kinetics of ligand adsorption indicated a very fast adsorption reaction for both organic acids. Steady state solution concentrations were reached in less than 15 minutes and therefore

for each pH value the mineral-organic suspension was allowed to equilibrate for 45 minutes, allowing enough time for the reaction to reach an equilibrium state.

This finding is consistent with the intensity changes, as a function of time, of the absorption bands in the IR spectra of surface bound phthalic and salicylic acid. Note that the typical equilibration time required for the IR absorption bands to reach steady band intensity values (40-50 minutes; see previous section) includes a time period of about 20-30 minutes during which ligand concentration within the flow cell increases from 0 to a constant value corresponding to the concentration of the input solution.

Adsorption as a function of pH

Adsorption experiments in the pH range between 4 to 10 were carried out in 0.01 M NaCl solutions at 25°C, with the aid of a computer controlled titrator. The concentration of adsorbed ligands was evaluated according to the following experimental procedure. A known mass of kaolinite (between 2-2.5 g) was allowed to equilibrate with 70 ml of the electrolyte solution for about four hours in airtight titration vessels under continuous stirring and continuous flow of water-saturated nitrogen gas above the suspension. Following equilibration, a specific volume of the organic acid stock solution was added to the suspension in order to get the required initial organic acid concentration. The pH of the suspension was then adjusted to the starting pH of the experiment (pH = 4) and left to equilibrate for a further two hours. The pH of the solution was then increased in steps of about 0.5 pH units, by the addition of NaOH, to approximately pH 10. At each pH value, the suspension was allowed to react for a period of 45 minutes and the pH of the solution was continuously monitored and, if needed, was readjusted to the desired pH value. Following equilibration at each pH value, 3 mL of the overlying solution was removed for the analysis of salicylic or phthalic acid concentrations remaining in solution. The sample analysed was then added back to the system before the start of the next step in order to avoid volume changes in solution during the course of the experiment.

Before taking a sample for concentration analysis, stirring of the solution was stopped for 15 minutes and samples were only taken from the top 2-3 cm of the solution in order to ensure a minimum removal of kaolinite from the system. Samples were then filtered through 0.2 µm filter paper, and immediately analysed for organic acid concentration using Ultraviolet-visible (UV-Vis) spectroscopy. UV measurements for phthalic acid were performed at 272 nm and for salicylic acid at 295 nm. Prior to UV analysis, all the samples and standards were acidified by adding 20 µL of 0.1 M HCl

(volume of samples analysed was 2 mL). Sample acidification was required as it was found that at different pH values similar organic acid concentrations yielded different UV absorption maxima. This was particularly evident for phthalic acid because in the pH range examined the three phthalic acid species are present at different ratios, thus affecting the UV absorption maxima.

The amount of organic acid adsorbed on the surface was determined by the difference between the initial and the residual (equilibrium) concentrations in solution. A blank run, carried out for each organic ligand, in which the same experimental procedure was followed but in the absence of the mineral phase showed that adsorptive losses to the container walls and/or to the filter were negligible. Weighing of the filters before and after filtration showed that the mass of kaolinite lost throughout the experiment was less than 1% and therefore mass loss during sampling could be ignored.

To validate the data obtained by the experimental procedure described above, adsorption at specific pH values was examined in a separate series of independent adsorption experiments. Each kaolinite-organic acid system was prepared with ligand to surface area ratios similar to those used in the adsorption experiments described above. A similar experimental setup was also used but for each experiment the adsorption was investigated in only one pH value. Following the addition of the organic ligand, the pH was adjusted and maintained to the target value and the suspension was allowed to equilibrate for three hours. The liquid phase was then separated by centrifugation and filtration and the residual ligand concentration in solution was determined by UV-Vis spectroscopy. The adsorption trend as a function of pH and extent of adsorption was comparable between the two experimental procedures.

These independent experiments were conducted in triplicates to calculate the random error associated with the precision of repeat experiments at the 95% confidence level using the critical t values as follows

$$\bar{x} - t \times \frac{s}{\sqrt{n}} \leq \mu \leq \bar{x} + t \times \frac{s}{\sqrt{n}} \quad \mathbf{3-1}$$

where μ is the estimate for the true value, \bar{x} is the mean value for the three triplicates, t is the critical value at the 95% confidence level (i.e. 4.3 for two degrees of freedom), s is the standard deviation of the measurements, and n is number of samples (i.e. 3). The highest percent error estimated for any data point was about +/-5% of the mean and this error was assumed for all data points.

Adsorption as a function of ionic strength

Salicylic and phthalic acid adsorption on kaolinite as a function of ionic strength was examined in different kaolinite-organic acid systems of varying background electrolyte concentrations (0 - 0.05 M NaCl), at pH 4. The same experimental procedure was followed as the one described for the independent adsorption experiments. For salicylic acid adsorption at a particular ionic strength was examined in 50 mL kaolinite suspensions containing 0.6 g of kaolinite and a salicylic acid starting concentration of 7×10^{-5} M. For phthalic acid adsorption at a particular ionic strength was examined in 50 mL kaolinite suspensions containing 0.7 g of kaolinite and a phthalic acid starting concentration of 1×10^{-4} M.

Potentiometric Titrations

Acid-base titrations were performed on kaolinite suspensions at three different ionic strengths (0.1, 0.01, and 0.001 M NaCl). All titration experiments were carried out using a computer-controlled titrator (Mettler Toledo DL 67) in 100 mL titration vessels. The temperature of the suspensions was kept constant ($25^{\circ}\text{C} \pm 0.05$) by placing the titration vessel into a water jacket connected to a temperature controlled water bath. The main titrator compartment containing the reaction vessel was sealed in an airtight manner. Kaolinite suspensions were continuously stirred by a propeller stirrer that was connected to the automatic titrator in order to achieve a homogeneous mixture. The pH electrode was calibrated using three standard buffer solutions at pH 4, 7 and 10; pH readings were accurate to within 0.01 unit

Kaolinite suspensions were prepared by adding 2 g of dry kaolinite in 50 mL of the background electrolyte solution. Nitrogen gas was directly bubbled through de-ionised water, for about an hour, prior to the addition of kaolinite in order to remove dissolved CO_2 species. By directly pumping nitrogen into the electrolyte solution, a pH value between 6.7-6.9 could be achieved. The addition of kaolinite into nitrogen-purged water resulted in an initial pH reduction to values between 4 - 4.3. The mineral suspension was then sealed in the titrator compartment and allowed to equilibrate for at least four hours before starting the titration experiments. During this equilibration period a gradual increase in the pH of the suspension to values up to 4.4 - 4.6 could be observed. Equilibration times longer than 4 hours did not show any further change in pH. An inert atmosphere in the titration vessel was maintained throughout the duration

of the experiments, including the equilibration period, by a continuous flow of water saturated, CO₂-free nitrogen gas above the suspension.

After this initial equilibration period a known volume of HCl was added to the suspension to lower the pH to approximately 4 and then, by incremental additions of NaOH, the pH was increased to about 10. After each incremental titrant addition (typically 0.03 or 0.04 mL of 0.1 M NaOH) the suspension was allowed to equilibrate and pH readings were recorded. Equilibrium conditions were assumed according to a criterion set for electron potential stability readings. The criterion for electron potential stability was a drift in electrode potential by less than 0.05 mV/min for a minimum equilibration time of 15 minutes. If this criterion was not met equilibrium conditions were assumed after an equilibration time of 35 minutes.

By the incremental addition of known amounts of acid or base in a mineral suspension it is possible to determine the surface concentration of protons. The net adsorption of protons or hydroxyls can be obtained from the concentration of the acid and/or base added and the concentration of the hydrogen and hydroxyl ions measured following equilibration. In an ideal system under a CO₂-free atmosphere, and assuming an inert electrolyte, the proton mass-balance equation is given by (Ganor et al., 2003)

$$\Delta C_s = (C_a - C_b - [H^+] + [OH^-]) \frac{V}{S.A} \quad 3-2$$

where ΔC_s is change in the surface proton concentration (mol m⁻²), C_a and C_b are the concentrations of acid and base added to the suspension respectively (mol l⁻¹), $[H^+]$ and $[OH^-]$ denote the measured concentration of protons and hydroxyl ions in solution after equilibration (mol l⁻¹), V is the volume of the solution (l), and $S.A$ the surface area (m²) of the mineral.

In addition to the proton adsorption reactions, dissolution is another potential proton consuming reaction which has been accounted for in some studies (e.g. Huertas et al., 1998). Dissolution of kaolinite is particularly important in the extreme pH values (pH < 4 and pH > 10) and shows a minimum dissolution rate in near neutral pH region (Cama et al., 2002; Carroll and Walther, 1990; Huertas et al., 1999). No attempt was made to correct for dissolution as no significant dissolution is expected to occur under the experimental conditions of the present study. To ensure minimal dissolution effects, the acid-base titrations were conducted in relatively neutral pH conditions (pH 4-10)

and the equilibration times were relatively short (maximum 35 minutes for each titration point).

Surface Complexation Modelling

Modelling surface protonation

Surface complexation modelling was used to describe the acid-base titration data of kaolinite. The goal of this modelling exercise was to estimate kaolinite's surface parameters by formulating a simple model that can successfully describe the proton adsorption data. The acid-base reactions of kaolinite were modelled according to the Constant Capacitance Model (CCM) using the computer program FITEQL Version 4.0 (Herbelin and Westall, 1999), which is routinely used for the fitting of potentiometric titration data, as well as ion adsorption data on mineral surfaces. FITEQL adjusts the model parameters of a chemical equilibrium problem so that the difference between the experimental data and calculated model values is minimised. Surface parameters obtained included the number of different types of proton binding surface sites, site densities for each proton binding site and surface protonation constants. The interfacial capacitance was also treated as an adjustable parameter and was set to 1.1 F/m^2 as it was found to give the lowest error when all the other parameters were introduced as fixed values. The ability of the model to fit the experimental data was evaluated according to the goodness of fit parameter, $V(Y)$, calculated by FITEQL.

Modelling organic acid adsorption

Macroscopic adsorption data as a function of pH were modelled according to the extended constant capacitance model (ECCM) in a series of model runs which assumed different surface species for each kaolinite-organic acid system. The aim was to identify surface adsorption reactions that link macroscopic adsorption properties with the IR spectroscopic data obtained. Therefore the number of surface species included in each model run was in agreement with the IR spectroscopic results and the set of surface reactions that could best fit the adsorption data was chosen for each kaolinite-ligand system. The ECCM was preferred over the triple layer model (TLM) because all the adsorption experiments were carried out at a single ionic strength value (0.01 M). The ECCM has been previously used in the literature to describe the adsorption of metal

cations (Ikhsan et al., 2004a; Peacock and Sherman, 2005); inorganic anions (Persson and Lövgren, 1996); and organic anions (Ali and Dzombak, 1996; Angove et al., 2002; Johnson et al., 2004a; Lackovic et al., 2003b).

As described by Nilsson et al. (1996), the application of the ECCM in FITEQL requires the use of the TLM and setting the ionic strength of the model to a very high value (e.g. 1×10^9 M) in order for the diffuse layer calculated by the model to become negligible. The optimised surface parameters obtained from the potentiometric titration data of kaolinite (site densities, protonation constants) were used as fixed values when the kaolinite-ligand systems were modelled. Adjustable model parameters for the kaolinite-ligand systems were the equilibrium constants of the adsorption reactions used to fit the adsorption data. Similarly to the titration data, model fits were evaluated according to the goodness of fit parameter calculated by FITEQL.

The distribution of the total capacitance in the two surface planes was systematically varied according to the following equation (Nilsson et al., 1996)

$$\frac{1}{C_{tot}} = \frac{1}{C_1} + \frac{1}{C_2} \quad \mathbf{3-3}$$

where C_{tot} is the total capacitance between the surface and the bulk solution, and C_1 and C_2 are the capacitance values of the inner and outer layer respectively. Total capacitance (1.1 F/m^2) was obtained from model fits of the acid base titration data of kaolinite alone at 0.01 M NaCl. The capacitance values of the inner and outer layer used were those found to give the best description to the adsorption data.

Results and Discussion

IR spectroscopic measurements

The main objective of the spectroscopic part of this study was to identify the number of surface species forming following adsorption, and to determine their binding and coordination modes on the surface of kaolinite. Such information can be derived from the comparison of the IR spectra of aqueous and adsorbed species at different solution conditions. Because organic ligands interact with surface sites primarily through carboxylic and phenolic groups, the spectral region considered is that from

1200 to 1800 cm^{-1} in which the main absorption bands of these functional groups occur. Prior to the spectroscopic analysis of the kaolinite-ligand systems, the spectra of aqueous phthalic and salicylic acid will be examined. The IR spectra of aqueous salicylic and phthalic acid have been previously discussed and spectral interpretation was based on spectral changes occurring as a function of pH and/or on theoretical vibrational frequencies calculated by molecular orbital calculations.

Solution species

(A) Aqueous phthalic acid species

The spectra of aqueous phthalic acid collected at different pH values are shown in Figure 3-1 and are in very good agreement with phthalate IR spectra obtained in previous studies (e.g. Hwang et al., 2007; Loring et al., 2001; Nordin et al., 1997; Rosenqvist et al., 2003). As with all carboxylic acid-containing compounds, the IR spectra of aqueous phthalic acid species exhibit absorption bands in the frequency region 1200 to 1800 cm^{-1} , which originate from the vibrational modes of the carboxylic acid group. In the same frequency region phthalic acid also exhibits vibrational modes related to benzene ring vibrations. The changes observed in the IR spectra as a function of pH reflect the protonation state of the molecule. Phthalic acid carries two carboxyl groups and therefore can exist in three protonation states; the fully protonated, singly protonated, and the fully deprotonated state (see Figure 3-2).

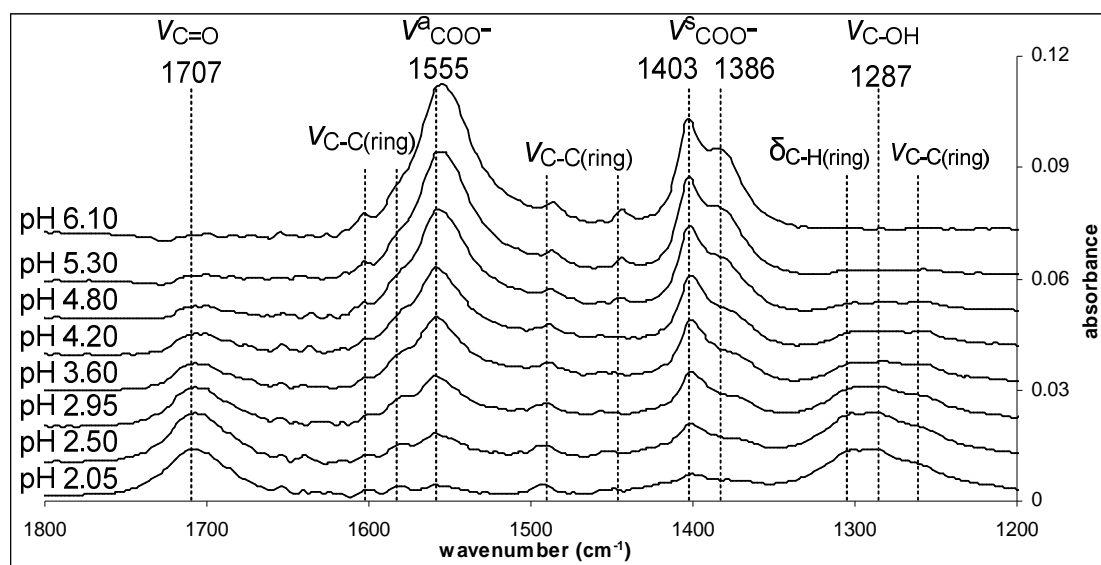


Figure 3-1 IR spectra of aqueous phthalic acid as a function of pH. pH-dependent features in the IR spectra are associated with the stretching vibrations of the carboxylic groups. ν denotes a stretching vibrational mode and δ a bending vibrational mode. The spectra have been offset for clarity.

Absorption bands affected by the degree of protonation can be assigned to the stretching vibrations of the carboxylic group since benzene ring vibrations are less susceptible to changes in the protonation state. The assignment of the absorption bands to specific vibrational modes has been primarily based on the interpretation given by Loring et al. (2001). For clarity, representative IR spectra of the three phthalic acid species are given in Figure 3-3.

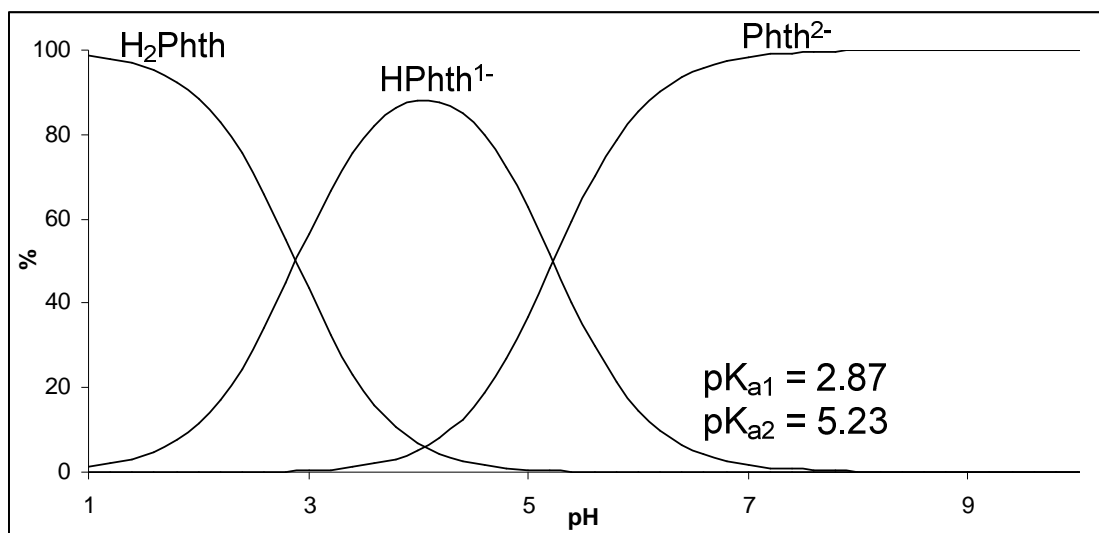


Figure 3-2 Species distribution of a 0.02 M phthalic acid solution as a function of pH . At pH < 2.87 the fully protonated neutral phthalic acid species (H₂Phth) dominates the solution. At pH > 2.87 one carboxyl group dissociates and therefore the singly protonated (and hence singly charged) species (HPhth¹⁻) becomes the dominant species in solution. At pH > 5.23 both carboxyl groups are deprotonated and the fully deprotonated phthalate (and hence doubly charged) species (Phth²⁻) becomes the dominant species in solution. Distribution curves for phthalic acid species were calculated using the Visual MINTEQ ver. 2.60 modelling software.

The spectrum of the fully protonated phthalic acid species (the neutral H₂Phth molecule) has two prominent bands with peak frequency positions at 1287 cm⁻¹ and 1707 cm⁻¹ which arise from the C-OH (ν_{C-OH}) and C=O ($\nu_{C=O}$) stretching vibrational modes of the protonated carboxyl group, respectively. Two shoulder bands at about 1300 and 1261 cm⁻¹ can also be seen on the absorption band originating from the carboxyl ν_{C-OH} mode, and are associated with benzene ring vibrations (Loring et al., 2001; Rosenqvist et al., 2003). Absorption bands originating from pure benzene ring vibrational modes occur at 1449, 1493 and 1603 cm⁻¹. Some other minor features in the spectrum of H₂Phth (e.g. 1555 and 1403 cm⁻¹) are attributed to minor contributions from the singly protonated hydrogen phthalate species (HPhth¹⁻). As seen in the species distribution diagram of aqueous phthalic acid (Figure 3-2), at the pH value in which the H₂Phth spectrum was collected (pH 2.05) the solution is comprised of about 10% of HPhth¹⁻.

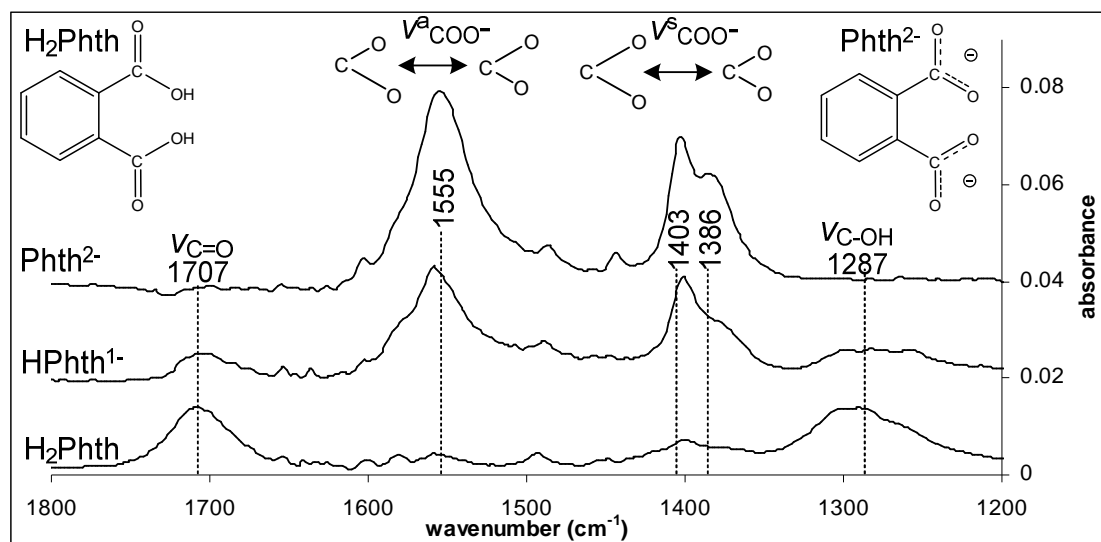


Figure 3-3 Representative IR spectra of aqueous phthalic acid (H_2Phth), hydrogen phthalate (HPhth^{1-}), and phthalate (Phth^{2-}). Absorption bands associated with the vibrational modes of the deprotonated carboxylate group (1555 , 1403 , and 1386 cm^{-1}) dominate the IR spectrum of Phth^{2-} , whereas the bands associated with the vibrational modes of the protonated carboxylic group (1707 and 1287 cm^{-1}) dominate the spectrum of H_2Phth . In the spectrum of HPhth^{1-} , vibrational contributions from both a deprotonated and a protonated carboxylic group are observed.

Hydrogen phthalate (HPhth^{1-}) contains features of both a protonated and a deprotonated carboxyl group. When compared to the IR spectrum of phthalic acid, the $\nu_{\text{C-OH}}$ and $\nu_{\text{C=O}}$ bands decrease in intensity and there is a concurrent emergence of three bands with peak positions at about 1559 , 1401 and 1380 cm^{-1} . These new bands are assigned to the vibrational modes of the deprotonated carboxylate group which exists in a resonant state between the C-O and C=O bonds. This causes a delocalisation of the negative charge which leads to two equivalent C-O bonds within the carboxylate group that give rise to carboxyl symmetric ($\nu^{\text{s}}_{\text{COO}^-}$) and asymmetric ($\nu^{\text{a}}_{\text{COO}^-}$) stretching vibrations.

In the completely deprotonated molecule (Phth^{2-}) both carboxyl groups exist in a resonant state resulting in the complete loss of the C=O and C-OH character and therefore in the disappearance of the C=O and C-OH bands from the IR spectrum. At the same time the intensity of the bands assigned to the stretching vibrations of the deprotonated carboxyl group further increase relative to the intensities of the same bands found in the spectrum of HPhth^{1-} species.

In the carboxylate symmetric stretching region phthalate exhibits two absorption bands with peak positions located at 1403 and 1386 cm^{-1} . Although the position of these two peaks is very similar to those reported previously, there is a disagreement in the literature on their proposed assignments (see table 3-2). Some authors have attributed the band at 1403 cm^{-1} to a benzene ring stretching mode and the band at 1386 cm^{-1} to a

carboxylate symmetric stretching mode (Dobson and McQuillan, 2000; Tejedor-Tejedor et al., 1992; Tunesi and Anderson, 1992); whereas others have assigned both bands to the carboxylate symmetric stretching mode (Hwang et al., 2007; Klug and Forsling, 1999; Loring et al., 2001; Nordin et al., 1997). Based on the complete disappearance of the 1403 cm⁻¹ band in the Raman spectra of aqueous phthalic acid, under acidic conditions, Klug and Forsling (1999) and Nordin et al. (1997) concluded that this band is more likely arising from a carboxylate stretching mode. Based on the findings by Klug and Forsling (1999) and Nordin et al. (1997), and in accordance to the theoretical frequency calculations of Loring et al. (2001), in the present study both bands are assigned to a carboxylate stretching mode. This assignment is further supported by the IR spectra collected in this study which show that both bands are significantly affected by the pH of the solution, and thus suggesting a common origin for the two bands.

In addition to two symmetric stretching modes, it is possible that phthalate also exhibits two asymmetric stretching modes. By obtaining the second derivative of the 1555 cm⁻¹ band, Nordin et al. (1997) were able to identify a second contributing band positioned at 1564 cm⁻¹ and suggested that the most probable origin of this second band is a second carboxylate asymmetric stretching mode. The occurrence of two asymmetric and two symmetric stretching modes is attributed to the effects of cooperative and opposing motions of the two adjacent carboxyl groups in the phthalate molecule (Nordin et al., 1997). The exact peak position of the second asymmetric stretching mode could not be identified in the present study.

Table 3-2 Literature absorption band maxima (cm⁻¹) and assignments for the aqueous phthalate ion (Phth²⁻), in the frequency region of the carboxylate stretching vibrations.

(Tejedor-Tejedor et al., 1992)		(Nordin et al., 1997)		(Dobson and McQuillan, 2000)		(Rosenqvist et al., 2003)		(Hwang et al., 2007)	
Peak	Asgmt	Peak	Asgmt	Peak	Asgmt	Peak	Asgmt	Peak	Asgmt
1382	$\nu^s_{\text{COO}^-}$	1385	$\nu^s_{\text{COO}^-}$	1381	$\nu^s_{\text{COO}^-}$	1381	$\nu^s_{\text{COO}^-} + \nu_{\text{C-C}}(\text{ring})$	1384	$\nu^s_{\text{COO}^-}$
1405	$\nu_{\text{C-C}}(\text{ring})$	1403	$\nu^s_{\text{COO}^-}$	1402	$\nu_{\text{C-C}}(\text{ring})$	1403	$\nu^s_{\text{COO}^-} + \nu_{\text{C-C}}(\text{ring})$	1403	$\nu^s_{\text{COO}^-}$
1552	$\nu^a_{\text{COO}^-}$	1550	$\nu^a_{\text{COO}^-}$	1550	$\nu^a_{\text{COO}^-}$	1555	$\nu^a_{\text{COO}^-} + \nu_{\text{C-C}}(\text{ring})$	1553	$\nu^a_{\text{COO}^-} + \nu_{\text{C-C}}(\text{ring})$
1580	$\nu_{\text{C-C}}(\text{ring})$	1583	$\nu_{\text{C-C}}(\text{ring})$	-	-	1584	$\nu^a_{\text{COO}^-} + \nu_{\text{C-C}}(\text{ring})$	1585	$\nu^a_{\text{COO}^-} + \nu_{\text{C-C}}(\text{ring})$
1603	$\nu_{\text{C-C}}(\text{ring})$	1603	$\nu_{\text{C-C}}(\text{ring})$	1600	$\nu_{\text{C-C}}(\text{ring})$	1604	$\nu^a_{\text{COO}^-} + \nu_{\text{C-C}}(\text{ring})$	1603	$\nu^a_{\text{COO}^-} + \nu_{\text{C-C}}(\text{ring})$

The asymmetric stretching mode of the carboxylate group ($\nu^{\text{as}}_{\text{COO}^-}$) is assigned to the band positioned at 1555 cm⁻¹. A shoulder on the high wavenumber side of this

band is also apparent, at about 1580 cm^{-1} . The presence of this band in all three species suggests that this band is associated with a benzene ring vibration and in accordance with previous studies (e.g. Klug and Forsling, 1999; Loring et al., 2001; Nordin et al., 1997) this band is assigned to a ring vibration. The peak frequency positions of the main absorption bands observed for the three phthalic acid species and respective assignments are summarised in Table 3-3.

Table 3-3 Absorption band peak positions for the three aqueous phthalic acid species, in the frequency region between 1200 to 1800 cm^{-1} obtained in the present study.

Vibrational Mode	Wavenumber (cm^{-1})		
	Phthalate (Phth^{2-})	Hydrogen phthalate (HPhth^{-1})	Phthalic acid (H_2Phth)
$\nu_{\text{C-C}}$ (ring)	-	1258	1261
$\nu_{\text{C-OH}}$	-	1282	1287
$\delta_{\text{C-H}}$ (ring)	-	1300	1301
$\nu_{\text{COO}^-}^{\text{s}}$	1386	≈ 1380	-
$\nu_{\text{COO}^-}^{\text{s}}$	1403	1401	-
$\nu_{\text{C-C}}$ (ring)	1444	1447	1449
$\nu_{\text{C-C}}$ (ring)	1487	1489	1493
$\nu_{\text{COO}^-}^{\text{a}}$	1555	1559	-
$\nu_{\text{C-C}}$ (ring)	≈ 1580	≈ 1577	1581
$\nu_{\text{C-C}}$ (ring)	1603	1602	1603
$\nu_{\text{C=O}}$	-	1707	1708

(B) Aqueous salicylic acid species

In the pH conditions where the IR adsorption measurements were carried out (pH 3-6), aqueous salicylic acid is primarily present in the form of the singly charged salicylate monoion (HSal^{1-}) (Figure 3-4). Figure 3-5 shows a representative IR spectrum of HSal^{1-} and also includes the assignment of its absorption bands to specific vibrational modes. The obtained IR spectrum of aqueous salicylic acid is in good agreement with the IR spectra of aqueous salicylic acid reported in the literature (Biber and Stumm, 1994; Dobson and McQuillan, 1999; Humbert et al., 1998; Tunesi and Anderson, 1992; Yost et al., 1990). The absorption bands located at 1620 , 1593 , 1486 and 1459 cm^{-1} are assigned to the C-C stretch vibrations ($\nu_{\text{C-C}}$) of the benzene ring. The bands with peak frequencies at 1388 and 1344 cm^{-1} are assigned to the coupled effect of the carboxylate symmetric stretching vibration ($\nu_{\text{COO}^-}^{\text{s}}$) and the bending vibration of the phenolic C-OH bond ($\delta_{\text{C-OH}}$) (Dobson and McQuillan, 2000; Tunesi and Anderson, 1992; Yost et al., 1990). The asymmetric stretching mode of the deprotonated carboxylic acid ($\nu_{\text{COO}^-}^{\text{a}}$) is attributed to the band located at about 1577 cm^{-1} . Finally the band at 1252 cm^{-1} arises from a phenolic stretching vibration ($\nu_{\text{C-OH}}$).

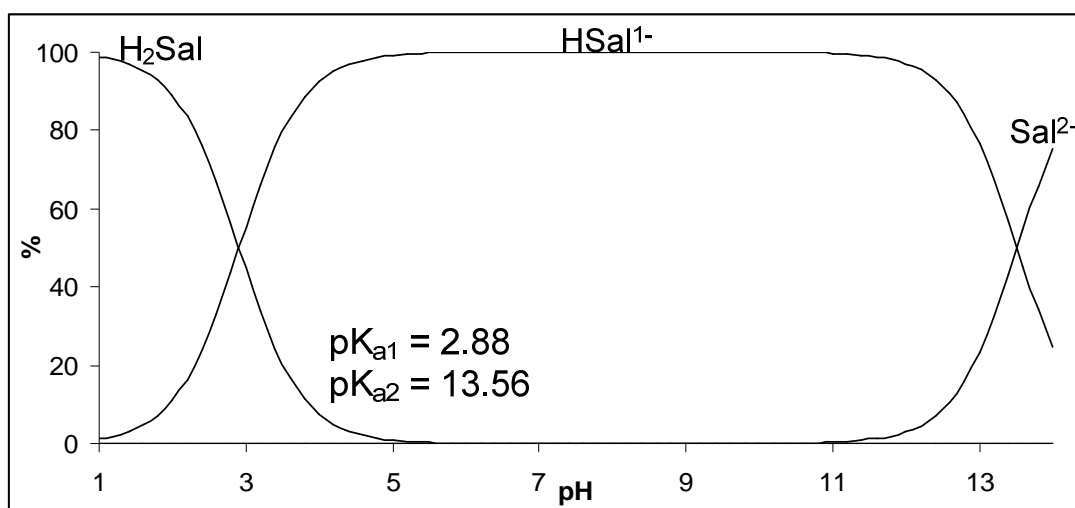


Figure 3-4 Species distribution of a 0.02 M salicylic acid solution over the pH range 1 to 14. Distribution curves for salicylic acid species were calculated using the Visual MINTEQ ver. 2.60 modelling software.

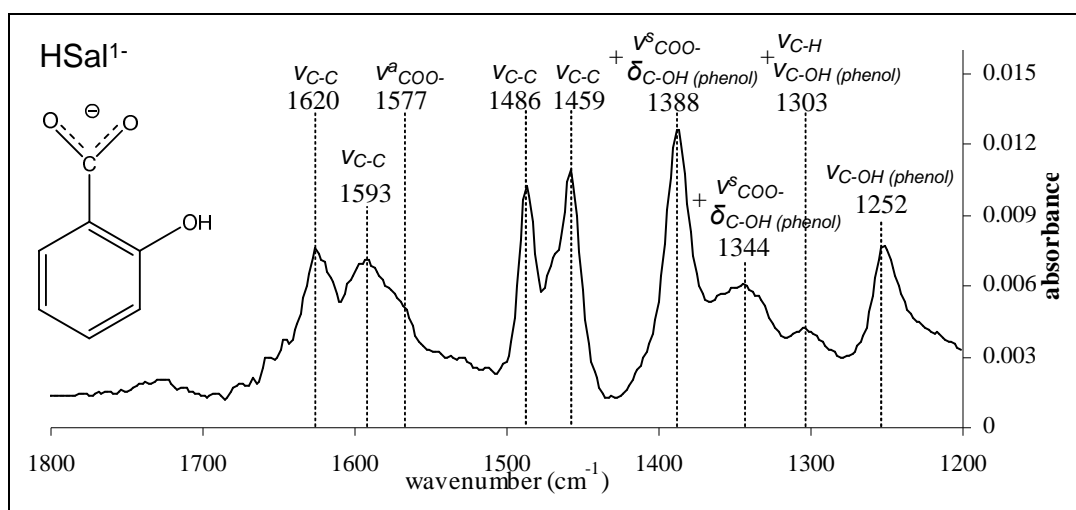


Figure 3-5 Representative IR spectrum of the aqueous salicylate monoion (HSal¹⁻), collected at pH 5.95. ν denotes a stretching vibrational mode and δ a bending vibrational mode.

Adsorbed species

(A) Adsorbed phthalic acid species

The IR spectra of adsorbed phthalic acid on different mineral surfaces have been reported and discussed by various authors (Das and Mahiuddin, 2007; Dobson and McQuillan, 2000; Hwang et al., 2007; Klug and Forsling, 1999; Kubicki et al., 1999; Morris and Wogelius, 2008; Nordin et al., 1997; Persson et al., 1998; Rosenqvist et al.,

2003; Tejedor-Tejedor et al., 1992; Tunesi and Anderson, 1992). Despite the extensive spectroscopic literature on adsorbed phthalate species, there is no general agreement on the binding and/or coordination mode of surface bound phthalic acid, even for similar mineral substrates. With reference to the type of surface complex formed, adsorbed phthalic acid has been explained by the formation of either a single inner sphere complex (Dobson and McQuillan, 2000); or two inner sphere complexes (Tejedor-Tejedor et al., 1992); or one inner and one outer sphere complex (Klug and Forsling, 1999; Persson et al., 1998) or two inner sphere complexes and an outer sphere complex (Hwang et al., 2007).

Furthermore, different coordination modes, including both monodentate and bidentate structures, have been proposed for inner sphere complexed phthalic acid. These contradictory results may be related to a surface effect, in which the type and local coordination environment of surface cations can affect the binding mode of the resulting surface complex. It is therefore likely that a connection exists between the coordination mode and the nature of the adsorbing surface. There are, however, other possible explanations for the discrepancies among previous studies. For example, Noren and Persson (2007) proposed that previous contradictory results in the literature may arise from differences in the interpretation of IR spectroscopic data rather than from the ability of organic ligands to adopt a range of different surface coordination modes. This suggestion is not surprising if one considers the structure of phthalic acid. The presence of two carboxylic groups allows phthalic acid to exhibit inter- and intra-molecular hydrogen bonding interactions in both the aqueous and the adsorbed phase. Furthermore, some carboxylate vibrational modes are coupled to benzene ring vibrational modes. Such interactions could potentially give rise to complex IR features that cannot be unambiguously assigned to specific molecular vibrations and this in turn can lead to different spectral interpretations.

Another source of discrepancy may be associated with the experimental approach and conditions employed for the collection of the IR spectra which may also account, at least in part, for the different findings in these studies. Particular IR spectroscopic methods may be more sensitive than other methods and therefore may reveal spectroscopic features that cannot be detected by other IR spectroscopic methods. In addition, adsorbed phthalic acid species were examined under a wide range of different experimental conditions and this can also affect the number and type of surface complexes formed. All the above factors can significantly influence IR measurements and/or the interpretation of the IR spectra obtained and hence the binding and coordination modes inferred for surface bound phthalic species.

The spectra of adsorbed phthalic acid on kaolinite, from a 1×10^{-3} M phthalic acid solution, from pH 3 to 6 are given in Figure 3-6. The obtained IR spectra share common spectroscopic features and with the exemption of the spectrum recorded at pH 3, all spectra exhibit remarkable similarities with regard to the number and peak frequency positions of the absorption bands observed. This indicates that surface speciation and binding mode of phthalic acid on kaolinite is practically identical at pH values above 3.

In the carboxylate stretching region, phthalate surface species give rise to three prominent absorption bands at about 1555, 1403, and 1385 cm^{-1} . The band centred at 1555 cm^{-1} corresponds to the carboxylate asymmetric stretching mode ($\nu^{\text{as}}_{\text{COO}^-}$) and the band doublet near the 1400 cm^{-1} region to the carboxylate symmetric stretching mode ($\nu^{\text{s}}_{\text{COO}^-}$). The two additional low intensity absorption bands located at 1487 and 1444 cm^{-1} originate from C-C stretching modes of the benzene ring. At pH 3, in addition to the abovementioned absorption bands, a relatively low intensity band at about 1700 cm^{-1} region is observed and denotes the presence of a C=O bond. Due to their strong similarities, the spectra obtained at pH values above 3 will be discussed together. Later on, the spectrum obtained at pH 3 will be discussed separately.

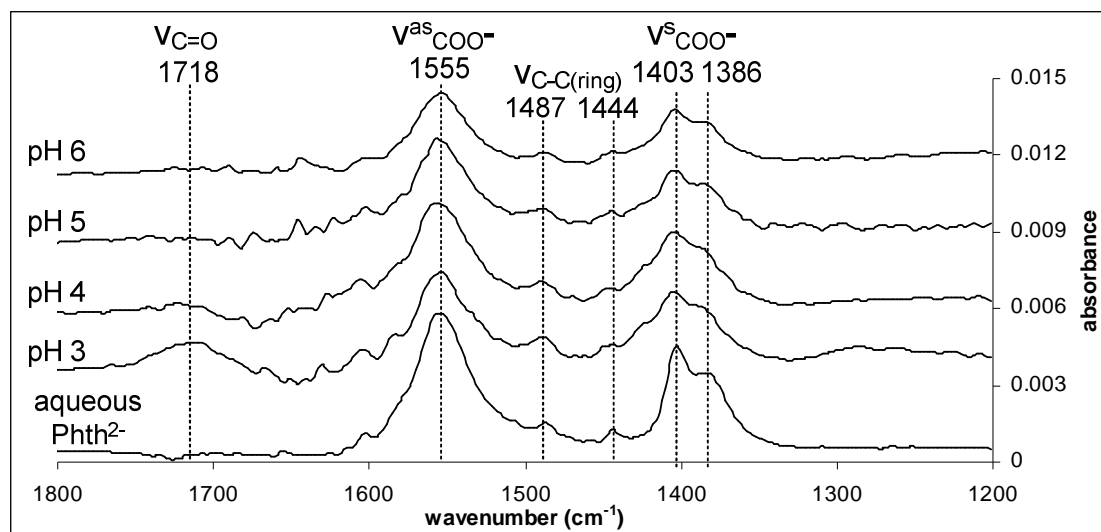


Figure 3-6 IR spectra of adsorbed phthalate on kaolinite as a function of pH, from a 1×10^{-3} M phthalic acid solution. The spectrum of aqueous phthalate is included for comparison. Spectra have been offset for clarity.

The frequency positions and relative intensities of the absorption bands exhibited by interfacial phthalic acid are not greatly affected by adsorption, as indicated by their similarity to those of the uncomplexed aqueous phthalate (Phth^{2-}) ion. Strong similarities between the IR spectra of surface complexes and of free aqueous species are

a characteristic feature of weak interactions between interfacial species and surface groups. Moreover, at pH values above 3, the IR spectra of surface bound phthalic acid do not show any absorption bands in the spectral region above 1700 cm^{-1} and below 1300 cm^{-1} . That would indicate the presence of C=O and of C-OH group vibrations respectively. The absence of such bands indicates that the adsorbed phthalic acid species are completely deprotonated. Based on the above observations it can be concluded that at pH values above 3, phthalic acid adsorbs on the surface of kaolinite primarily as a fully deprotonated, outer sphere complexed species.

It is interesting to note the fact that, at pH above 3, phthalic acid binds to the surface not only in a similar binding mode (i.e. outer sphere complexation) but also in a similar protonation state (i.e. as Phth^{2-}). Although at pH 4 and 5 the dominant species in solution is the singly protonated hydrogen phthalate species (HPhth^{1-}), the spectroscopic data show that phthalic acid binds to the surface in the fully deprotonated form, Phth^{2-} . This suggests that the interactions between the surface and outer sphere complexed phthalic acid molecules have an effect on the protonation state of phthalic acid. Such a phenomenon where adsorption promotes the deprotonation of surface bound ligands has been reported previously for other mineral-organic ligand systems (e.g. Johnson et al., 2004a; Lackovic et al., 2003b; Yoon et al., 2004a). The lower degree of protonation experienced by outer sphere complexed molecules may be the result of a combination of two factors. Firstly, the bonding environment of surface bound ions is expected to be considerably different than that of ions present in the aqueous phase and therefore the protonation constants of adsorbed species can be affected. Secondly, the pH at the mineral-water interface is different than the pH of the bulk solution (Johnson et al., 2004a).

Although phthalic acid binds predominantly as an outer sphere surface complex other minor surface species may also be forming on the surface of kaolinite. For example previous studies that have investigated the adsorption of phthalic acid on simple oxide minerals were able to identify IR absorption features that could be assigned to inner sphere complexed species (Hwang et al., 2007; Klug and Forsling, 1999; Nordin et al., 1997; Persson et al., 1998; Rosenqvist et al., 2003). The occurrence of inner sphere adsorbed phthalic acid species is expected to yield C-O stretching vibrations in the carboxylate stretching region with peak positions deviating from those of the aqueous phthalate species.

To identify the number of structurally different surface complexes in the IR spectra of adsorbed phthalic acid, the frequency region of the carboxylate symmetric stretching mode ($\approx 1400\text{ cm}^{-1}$) was studied in more detail. Analysis of this region for the

determination of the number of contributing absorption bands is more suitable because the absorption bands are better resolved and less sensitive to interference originating from water vapour and the water subtraction method (Klug and Forsling, 1999; Nordin et al., 1997). Mathematical processing of the IR spectra, including spectral deconvolution and calculation of the inverse second derivative spectra, was also employed to help identify the number of overlapping bands and their frequency positions at maximum. As already mentioned aqueous phthalate gives rise to two absorption bands in the symmetric carboxylate stretching region, located at 1403 and 1386 cm^{-1} . Therefore the occurrence of more than two bands in this spectral region can confirm the existence of additional surface species.

Although the two main adsorption bands in the $\nu^{\text{s}}_{\text{COO}^-}$ region are located in similar frequency positions to the two bands seen for the aqueous phthalate species, a third absorption band present as a shoulder, at about 1423 cm^{-1} , can also be observed (Figure 3-7). This third band located in the symmetric stretching region of the IR spectrum of adsorbed phthalic acid is indicative of the presence of an additional surface complex. The relatively large upward shift of the 1423 cm^{-1} band as compared to the frequency position of carboxyl symmetric stretch of the aqueous phthalate species (1403 cm^{-1}) suggests direct chemical bonding between the carboxyl group and the surface. Therefore the analysis of the $\nu^{\text{s}}_{\text{COO}^-}$ frequency region revealed that at least two different surface complexes coexist on the surface of kaolinite at the experimental conditions examined. The higher wavenumber component with a maximum located at about 1423 cm^{-1} can be attributed to the C-O stretching mode of an inner sphere complex and the two bands located at about 1403 and 1385 cm^{-1} to the C-O stretching modes of an outer sphere complex.

From Figure 3-7 it can be seen that at different pH values there is a change in the relative intensities between the two absorption bands found at 1423 and 1403 cm^{-1} , an observation which further supports the assignment of these two bands to two structurally different surface complexes. If these two bands were originating from the same surface complex then such a change should not have been observed. The relative intensity of the 1423 cm^{-1} band gradually increases as the pH is lowered, suggesting that the formation of the surface complex associated with the 1423 cm^{-1} band (i.e. the inner sphere complex) is favoured by acidic conditions. At pH 6 there is a complete predominance of the outer sphere complexed species since the band at 1423 cm^{-1} is almost absent from the IR spectrum. The effect of pH on the relative intensity of the spectral features arising from the two surface complexes isolated shows that a change in phthalic acid

speciation and/or surface charge has an effect, albeit small, on the binding mode of phthalic acid.

In conclusion, the IR spectra of adsorbed phthalic acid are dominated by absorption bands that can be associated with an outer sphere complex, suggesting a dominant outer sphere adsorption mechanism. However some spectroscopic features provide evidence for an additional minor surface species. The surface species is coordinated to the surface in an inner sphere complex mode and its formation is favoured by lower pH values.

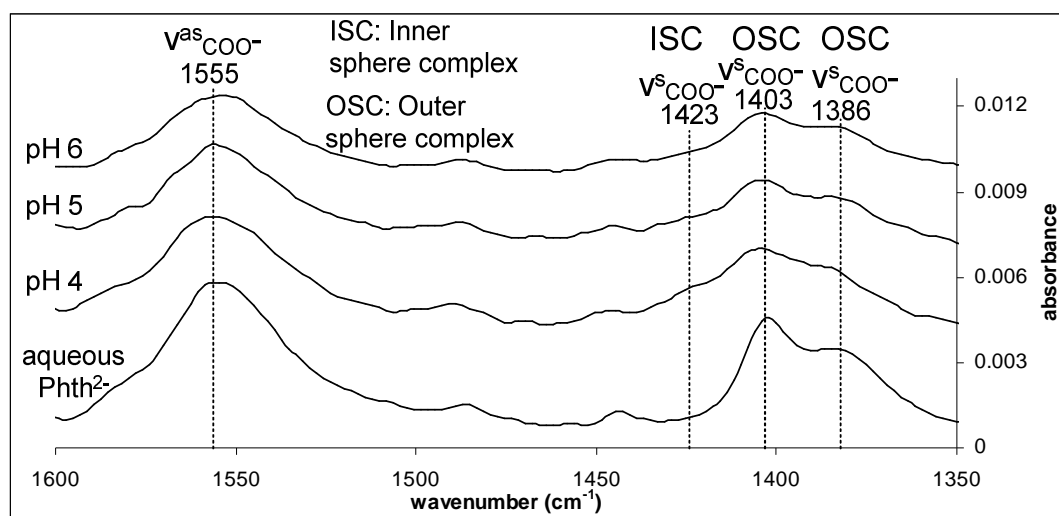


Figure 3-7 Comparison of the carboxylate stretching region for the spectra of adsorbed phthalic acid displayed in figure 6. With increasing pH the intensity of the band located at about 1423 cm^{-1} (attributed to an inner sphere complex) decreases relative to the intensity of the band at 1403 cm^{-1} (attributed to an outer sphere complex).

In order to confirm the assumption that the band increasing in intensity with decreasing pH values (1423 cm^{-1}) originates from an inner sphere complex, the spectra of adsorbed phthalic acid at pH 5 were collected at various ionic strengths. The relative intensities of the bands arising from an inner sphere complex are expected to increase at higher background electrolyte concentrations since outer sphere complexes typically exhibit strong ionic strength dependence with decreasing concentrations at higher ionic strengths (Persson et al., 1998). As expected, Figure 8 shows that as the ionic strength of the solution increases, the intensity of the band at 1423 cm^{-1} also increases relative to the intensity of the band at 1403 cm^{-1} . This is in accordance with the conclusions drawn earlier which indicated the coexistence of an inner and an outer sphere complex on the surface of kaolinite. One important observation that has to be pointed out here is that even at the higher ionic strength examined the overall intensity of the 1423 cm^{-1} band is

still weaker relative to that of the 1403 cm^{-1} . Therefore although the relative importance of the inner sphere complex increases at higher ionic strengths, outer sphere complexation is still the predominant adsorption mechanism, at least for pH 5.

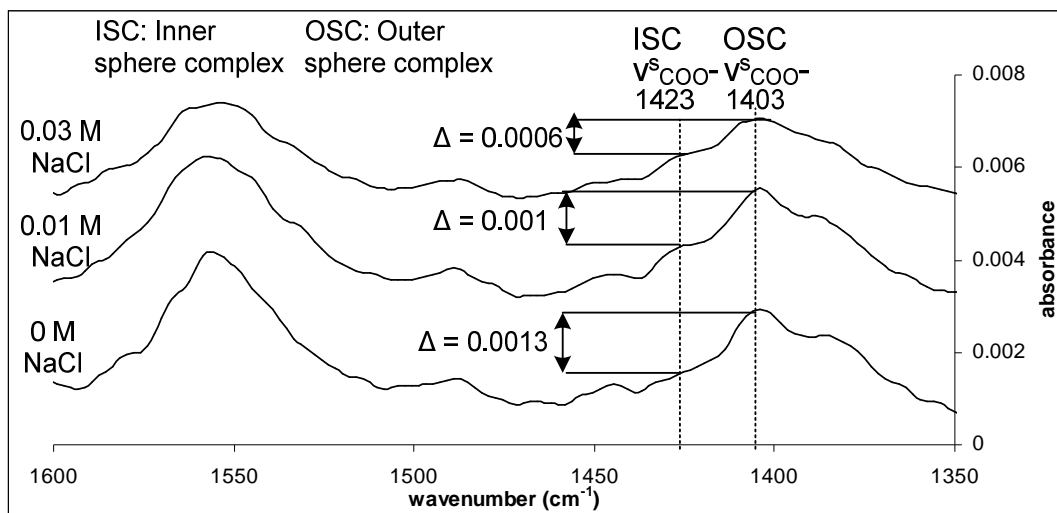


Figure 3-8 IR spectra of adsorbed phthalic acid on kaolinite at pH 5, as function of ionic strength, from a 1×10^{-3} M phthalic acid solution. At higher ionic strengths the intensity of the band at 1423 cm^{-1} increases relative to the intensity of the band at 1403 cm^{-1} . Δ quantifies the difference in intensity between the 1403 and 1386 cm^{-1} bands. Spectra have been offset for clarity.

A similar adsorption behaviour in which a fully deprotonated outer sphere complex dominates adsorption while a second minor inner sphere complex increases in relative importance at lower pH has been previously observed for other mineral-phthalate systems. Corresponding literature values for the $\nu^s_{\text{COO}^-}$ mode of the inner sphere complex identified are: 1420 cm^{-1} for gibbsite (Rosenqvist et al., 2003); 1422 cm^{-1} for boehmite (Nordin et al., 1997); 1424 cm^{-1} for aged $\gamma\text{-Al}_2\text{O}_3$ (Persson et al., 1998); $1427\text{-}1431\text{ cm}^{-1}$ for nonaged $\gamma\text{-Al}_2\text{O}_3$ (Klug and Forsling, 1999); 1418 cm^{-1} for goethite (Boily et al., 2000b); and 1417 cm^{-1} for haematite (Hwang et al., 2007). The similarity in peak frequency positions of these bands with those of the present study ($\approx 1423\text{ cm}^{-1}$) suggests that phthalate inner sphere surface complexes on kaolinite are structurally related to those found in simpler iron and aluminium hydr(oxides). It can be therefore concluded that the adsorption behaviour of phthalic acid is relatively insensitive to the nature of the mineral substrate, at least for aluminium- and iron-bearing minerals.

It is of interest to determine the coordination mode of the inner sphere surface complex formed on kaolinite. Possible coordination modes of inner sphere bound

phthalic acid are shown in Figure 3-9. The band separation between the carboxylate symmetric and asymmetric stretching modes ($\Delta\nu$) of adsorbed phthalate species can potentially provide some indication for its coordination mode (e.g. Dobson and McQuillan, 2000; Duckworth and Martin, 2001). While the $\nu^s_{\text{COO}^-}$ mode of the surface bound species shifts to lower wavenumbers when compared to the $\nu^s_{\text{COO}^-}$ mode of the aqueous species (by about 20 cm^{-1}), the peak frequency of the $\nu^{\text{as}}_{\text{COO}^-}$ mode is not clear due to overlapping by the more intense band exhibited by the outer sphere complex. A closer examination of the spectra collected in the presence of a background electrolyte, where a higher proportion of inner sphere complexes is expected, reveals a band shoulder at about 1530 cm^{-1} . Assuming that this band corresponds to the $\nu^{\text{as}}_{\text{COO}^-}$ mode of the inner sphere complex then the band separation between the $\nu^s_{\text{COO}^-}$ and the $\nu^{\text{as}}_{\text{COO}^-}$ modes of the adsorbed species ($\Delta\nu \approx 107$) is lower than that of aqueous phthalate species ($\Delta\nu \approx 150$). Such band separation is consistent with a bidentate geometry with respect to the coordination mode of the carboxylic group. However such a finding cannot be justified on the basis of band separations alone and the applicability of these rules to dicarboxylic acids can be subject to uncertainties. As noted by several authors other intramolecular interactions, such as hydrogen bonding and the coupling of vibrational modes, could be more important in determining band separations than the coordination environment of the carboxylate group (e.g. Nilsson et al., 1996).

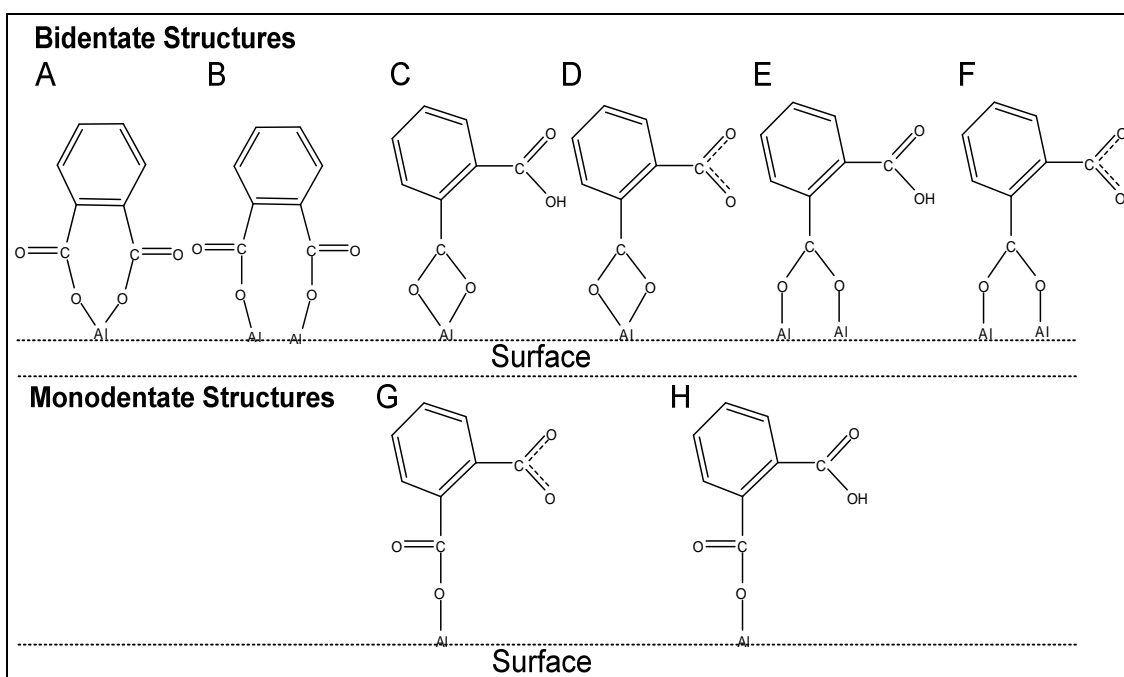
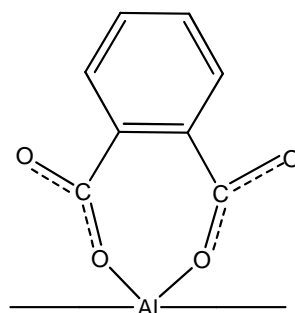


Figure 3-9 Possible coordination modes for inner sphere complexed phthalic acid with a surficial aluminium cation. Bidentate structures are directly bonded to the surface via two Al-O bonds whereas monodentate structures are coordinated to the surface with only one Al-O bond.

In addition to the direct comparisons made between the IR spectra of adsorbed and solution species, information regarding the binding mode of the surface species can be obtained by comparing the IR spectra of aqueous and surface metal complexes. The IR spectra of aqueous complexes between phthalate ions and large divalent cations (such as calcium) have been previously used as model spectra for outer sphere complexed phthalic acid. Conversely the IR spectra of aluminium and iron ions coordinated to phthalate in solution have been used as model spectra for inner sphere complexes (Hwang et al., 2007; Nordin et al., 1997).

The spectra of aqueous iron- and strontium-phthalate complexes have been presented in chapter 2 (Figure 2-4). Phthalic acid bonded to iron in solution exhibits a $\nu^s_{\text{COO}^-}$ mode with a peak at about 1420 cm^{-1} which is in a similar frequency position to the $\nu^s_{\text{COO}^-}$ mode attributed to the inner sphere complex identified in the spectra of adsorbed phthalic acid (1423 cm^{-1}). A similar peak frequency can also be observed for the aluminium-phthalate aqueous complex. The similarity in the frequency positions of the two $\nu^s_{\text{COO}^-}$ modes found for the aqueous and surface metal complexes strongly suggests that phthalate adopts a similar coordination mode with aqueous metal cations and with surface metal cations. Because the most probable structure of aqueous Fe- and Al-Phthalate complexes is a mononuclear bidentate chelate complex (Figure 3-9; structure A), absorption bands isolated near the 1420 cm^{-1} region in the IR spectra of interfacial phthalate species have been previously assigned to a mononuclear chelate structure (Boily et al., 2000b; Nordin et al., 1997; Persson et al., 1998; Rosenqvist et al., 2003). In accordance to these studies the inner sphere complex forming on the surface of kaolinite is most probably a mononuclear bidentate chelate complex. Although such a structure is expected to give rise to bands in the C=O stretching region ($\approx 1700\text{ cm}^{-1}$), the absence of the double bond character can be explained if the adsorbed species are bound to the surface via delocalised carboxylate groups (Dobson and McQuillan, 2000; Tunesi and Anderson, 1992) as shown below:



To further investigate how the relative intensity of the 1423 cm^{-1} band (and thus the importance of the inner sphere complex) is influenced by different experimental conditions, the intensity of this band relative to that of the 1403 cm^{-1} band was examined as a function of initial phthalate concentrations and reaction time. Figure 3-10 shows the IR spectra of adsorbed phthalic acid obtained from three different initial phthalic acid concentrations, at pH 4. Although solution concentration appears to favour outer sphere complexation its effect is not as significant as that of pH or of ionic strength. Other spectroscopic features which can be assigned to additional surface complexes could not be observed in the range of phthalate concentrations examined. Time-dependent IR spectra of adsorbed phthalic acid, at different solution conditions, were examined in order to resolve any dynamic changes occurring as the adsorption reaction progresses. Neither of the two surface species identified appeared to be favoured by increasing reaction time, at least within the time span of the experimental measurements (between two to three hour period). Furthermore, the frequency positions of the absorption bands remained unaltered during the course of the experiments, indicating that no changes are occurring in the coordination environment of phthalic acid, following initial adsorption.

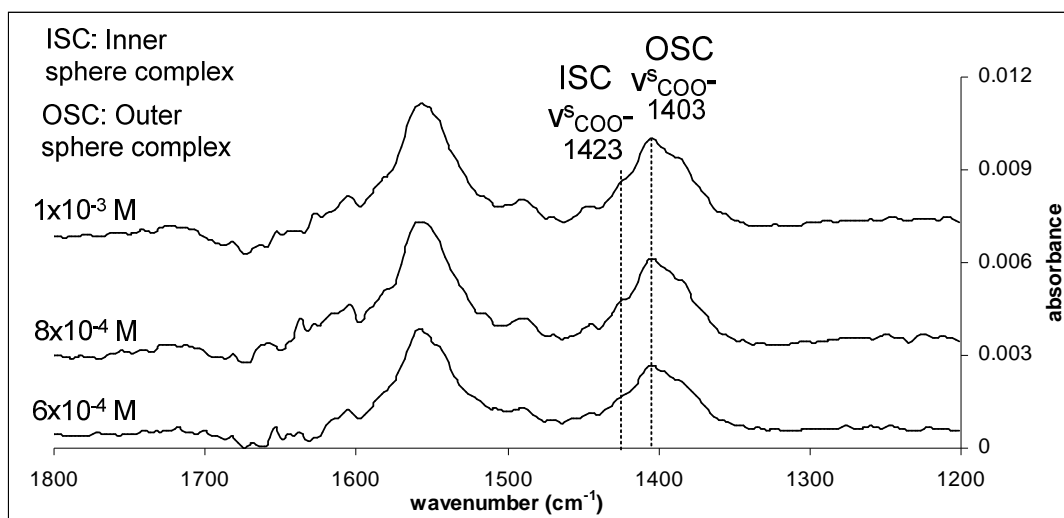


Figure 3-10 IR spectra of adsorbed phthalic on kaolinite, at pH 4, from three different initial phthalate concentrations. Spectra have been offset for clarity.

The above discussion examined the spectra of adsorbed phthalic acid at pH values from 4 to 6, and provided evidence about the binding and coordination mode of adsorbed phthalate species. Turning again to Figure 3-6, at pH 3 adsorbed phthalic acid yields three prominent absorption bands in the carboxylate stretching region with

similar peak frequency positions as those in the spectra obtained at higher pH values (1555, 1405, 1385 cm^{-1}). Accordingly, the origin of these three bands is attributed to the stretching vibrations of deprotonated carboxylate groups that are not directly bonded to the surface. Moreover the shoulder at about 1425 cm^{-1} is also present in the spectrum, indicating the existence of an inner sphere complexed surface species. In addition to the aforementioned bands, an absorption band with a peak position at about 1715 cm^{-1} which can be assigned to a C=O stretching vibration ($\nu_{\text{C=O}}$) is also present in the pH 3 spectrum.

The existence of a C=O bond suggests the presence of a protonated surface species. The concurrent presence of this band with the bands assigned to the deprotonated carboxylic group could thus indicate that at pH 3 phthalic acid coordinates to the surface as a singly protonated species ($\text{HPhth}^{\text{I-}}$). However the spectrum lacks absorption bands around 1290 cm^{-1} , the characteristic region of the C-OH stretching vibration ($\nu_{\text{C-OH}}$) of the protonated carboxylic group. The absence of a $\nu_{\text{C-OH}}$ mode precludes the possibility of a hydrogen phthalate species adsorbed in an outer sphere mode. Therefore, in accordance to the interpretation given for the spectra obtained at pH > 3, the three main bands located in the carboxylate stretching region originate from a fully deprotonated outer sphere phthalate complex.

The existence of the C=O group could imply the presence of an additional surface species which binds to the surface in an inner sphere mode. The assignment of this band to an inner sphere complex is substantiated further by the shift of the C=O vibration from 1707 cm^{-1} in the aqueous species to 1718 cm^{-1} in the adsorbed species. In addition to the C=O stretching vibration, the spectrum at pH 3 exhibits an absorption band in the carboxylate symmetric stretching region at about 1425 cm^{-1} . This band has a similar peak position to the absorption bands that were assigned to an inner sphere complex at higher pH values. Unfortunately these bands appear as low intensity shoulders and the exact peak positions cannot be determined accurately. Therefore it is not possible to state with confidence whether the band at pH 3 originates from the same type of inner sphere complex as that identified at higher pH values or whether this band originates from a structurally different surface complex. If these bands are originating from the same type of surface complex then the presence of the C=O band (1718 cm^{-1}) must be originating from a second inner sphere complex. However, additional peaks in the symmetric stretching region that could be associated with a third surface species could not be isolated in the spectrum at pH 3. It therefore seems unlikely that the C=O band originates from an additional inner sphere species. A more probable alternative explanation is that at pH 3 only one inner sphere complex exists on the surface and this

complex is associated with the bands at both 1718 and 1425 cm^{-1} . It follows that this inner sphere complex adopts a different coordination mode than that found at higher pH values and thus explaining the presence of the C=O bond.

It can be argued that, at pH 3, the three bands in the symmetric stretching region (1388, 1404 and 1425 cm^{-1}) originate from a single surface species where only one carboxyl group is attached to the surface in a monodentate coordination mode (Figure 3-9; structure G). Such a surface complex could explain all the principal features of the spectrum collected at pH 3. The bands at 1404 and 1388 cm^{-1} with very similar positions to those of the aqueous phthalate species could correspond to a deprotonated carboxylic group that is not involved in complexation whereas the bands at 1710 and 1425 cm^{-1} to the C=O and >Al-O-C stretching vibrations of the surface-bound carboxylic group respectively. In order to test this hypothesis the spectrum of adsorbed phthalic acid was collected in the presence of a background electrolyte. Figure 3-11 shows the IR spectrum of adsorbed phthalic acid at pH 3 and an ionic strength of 0.01 M NaCl. Although the absolute band intensities in this spectrum are significantly diminished it is still clear that the intensities of the bands at about 1720 and 1425 cm^{-1} increase significantly relative to the intensities of other bands. This finding supports the assignment of the bands at 1720 and 1425 cm^{-1} to an inner sphere surface complex and the assignment of the bands at 1388, 1404 and 1425 cm^{-1} to an outer sphere complex. The substantial reduction of band intensities at the carboxylate stretching region, at 0.01 M NaCl, suggests a significant reduction in the importance of the outer sphere adsorption mechanism at these conditions. It is very likely that the IR spectrum collected under these experimental conditions arises mainly from phthalate species coordinated to the surface in an inner sphere mode.

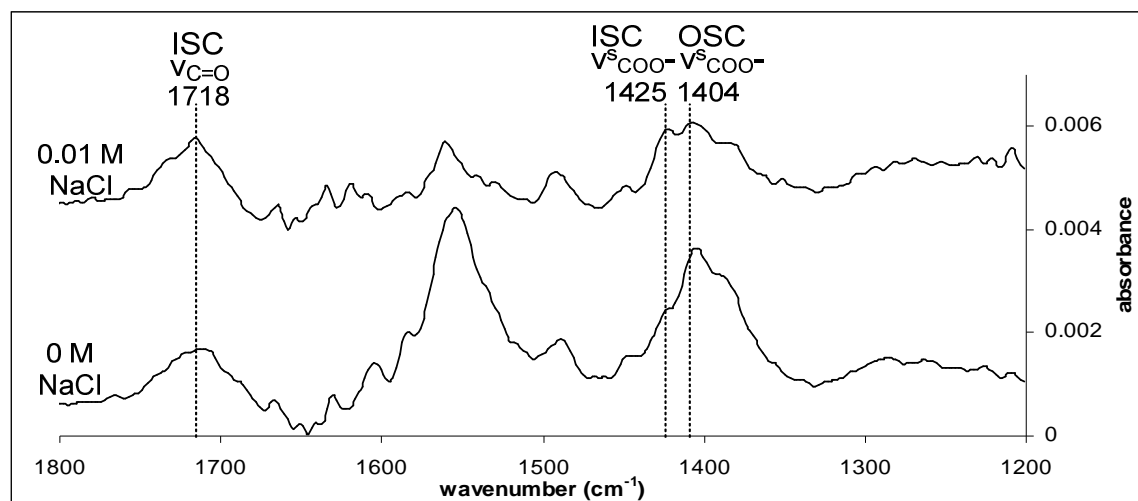
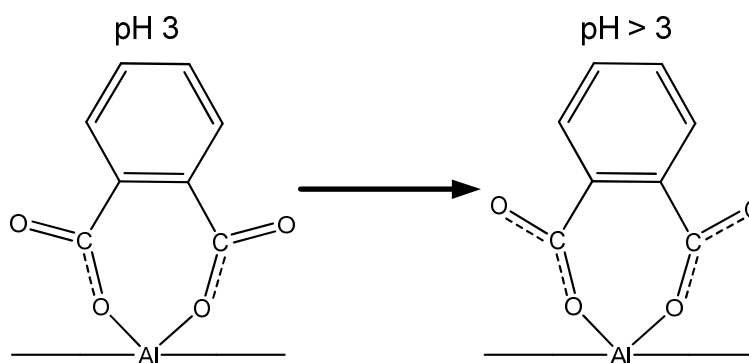


Figure 3-11 IR spectra of adsorbed phthalic acid on kaolinite, at I = 0 and 0.01 M NaCl, from a 1×10^{-3} M phthalic acid solution at pH 3. Spectra have been offset for clarity.

A coordination mode that is consistent with the IR spectrum at pH 3 is a bidentate coordination mode in which both carboxyl groups are directly bound to the surface, resulting in a seven membered ring structure (Figure 3-9; structures A or B). This coordination mode is very similar to that identified at higher pH values, thus explaining the similarity in peak positions of the $\nu^s_{\text{COO}^-}$ modes. As mentioned previously, the possible explanation for the loss of the C=O character in the interfacial species at pH > 3 is that at higher pH values the two coordinated carboxylate groups occur in a resonant state as shown below



Seven-membered ring chelate ring structures have been previously inferred from the IR spectra of adsorbed phthalic acid on aluminium oxide (Dobson and McQuillan, 2000); titanium oxide (Dobson and McQuillan, 2000; Tunesi and Anderson, 1992); and forsteritic olivine (Morris and Wogelius, 2008). Although the most probable structural geometry of surface bound phthalic acid on kaolinite is a mononuclear bidentate structure, the possibility of a binuclear bidentate structure cannot be excluded. Unfortunately it is not possible to differentiate between these two coordination modes from IR data alone.

Molecular orbital calculations can provide valuable help in the interpretation of the spectroscopic data since the experimental band frequency positions can be compared to the theoretical frequencies predicted for various model surface complexes. The assignment of the experimental IR peaks can be based on the IR spectrum of the theoretical surface complex that can best describe the obtained spectrum. Such theoretical studies are a valuable tool not only for the interpretation of IR bands but also for the structural determination of adsorbed species.

Two studies have determined the theoretical vibrational spectra of possible phthalate coordination modes using molecular orbital calculations, and related those to the experimental IR spectra of adsorbed phthalic acid (Hwang et al., 2007; Kubicki et

al., 1999). In the study by Hwang et al. (2007) the only complex examined that yielded only one significant band in the symmetric C-O stretching region was a binuclear bidentate complex in which both carboxylate groups are involved in the binding of phthalic acid (Figure 3-9; structure B). Furthermore the peak position of the calculated band showed an upward shift to higher wavenumbers (+14) when compared to the calculated peak position of the aqueous phthalate molecule. This moderate upward shift is consistent with the experimental frequencies obtained in this study. Other coordination modes examined (e.g. mononuclear bidentate modes through one or two carboxylic groups, binuclear bidentate mode through only one carboxylic group) predicted two absorption bands for the C-O symmetric stretching vibration. Therefore, according to the theoretical spectra of Hwang et al. (2007) a binuclear bidentate structure is more probable than a mononuclear bidentate. This is not surprising as these two coordination modes have similar structural features thus making it difficult to be differentiated by IR spectroscopy.

Kubicki et al. (1999) examined only three model phthalic acid surface complexes (one monodentate and two bidentate structures). Unfortunately assignments and relative intensities for the bands predicted by these model structures were not given, thus making it difficult to relate individual experimental bands to the calculated frequencies provided. Overall there is a bad agreement between the spectra obtained in this study and the predicted spectra calculated by Kubicki et al. (1999), and therefore no attempt was made to identify the most probable surface complex from the theoretical frequencies provided. However, interestingly enough, all three model surface complexes predicted an absorption band near 1420 cm^{-1} , which is in a similar position to the absorption band assigned to the C-O stretching vibration of the inner sphere complex identified in the present study.

(B) Adsorbed salicylic acid species

Figure 3-12 shows the IR spectra of adsorbed salicylic acid on kaolinite, from a 5×10^{-4} M salicylic acid solution in the pH range from 3 to 6. It is apparent from this graph that the spectra of adsorbed salicylic acid show a strong pH dependence in terms of relative band intensities. Absorption bands with peak frequency positions at 1629, 1593, 1485, 1348, 1305 and 1253 cm^{-1} gradually gain in intensity as the pH of the solution decreases from pH 6 to pH 3 (values shown in bold fonts in Fig 3-12). The changes in relative band intensities observed as a function of pH suggest that at least

two structurally different salicylate species coexist on the surface of kaolinite and that their relative distribution is pH dependent.

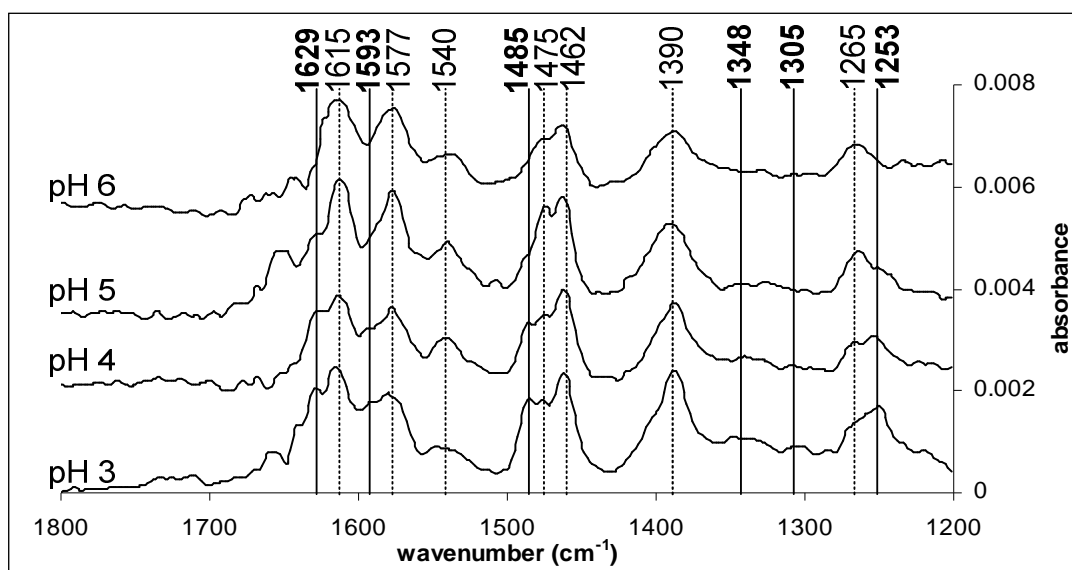


Figure 3-12 IR spectra of salicylic acid adsorbed on kaolinite from a 5×10^{-4} M salicylic acid solution as a function of pH. Solid lines and peak frequency positions in bold fonts indicate the absorption bands whose relative intensity increases with decreasing pH. The spectra have been offset for clarity.

For clarity, Figure 3-13 displays the spectra of interfacial salicylic acid at pH 3 and 6 (also shown in Fig 3-12) and the spectrum of aqueous HSal^{1-} species. It can be seen that the spectra of adsorbed salicylic acid exhibit a greater number of absorption bands as compared with the spectrum of aqueous HSal^{1-} . This further supports the presence of two different salicylate surface complexes on kaolinite in the pH range examined. At pH 6 the main absorption bands exhibited by adsorbed salicylic acid (1615, 1577, 1540, 1475, 1463, 1390, 1265 cm^{-1}) have peak frequency positions that are significantly different from those of aqueous salicylic acid. This difference in frequency positions strongly suggests significant changes in the chemical and structural environment of the salicylate ion upon adsorption, and hence is indicative of direct bonding to the surface. It can be therefore concluded that at pH 6, salicylic acid is coordinated to the surface primarily through an inner sphere mechanism.

At pH 3, additional absorption bands can be observed in the spectra of adsorbed salicylic acid (1629, 1593, 1485, 1348, 1305 and 1253 cm^{-1}). The emergence of these new bands indicates the occurrence of a second surface species, in addition to that identified at pH 6. The peak frequency positions of these new bands show strong similarities to those of aqueous HSal^{1-} species, suggesting that this second interfacial

species is not directly bonded to the surface and that it has a similar structural and coordination environment to that of aqueous HSal^{1-} . This second surface species identified can be therefore assigned to an outer sphere complex. Outer sphere complexation is favoured by acidic conditions as evidenced by the increase in relative intensity of the bands associated with outer sphere complexes salicylate species. This phenomenon is rather interesting as it contradicts previous studies which reported higher concentration of inner sphere complexed organic ligands at lower pH values (e.g. Persson and Axe, 2005; Yoon et al., 2004b).

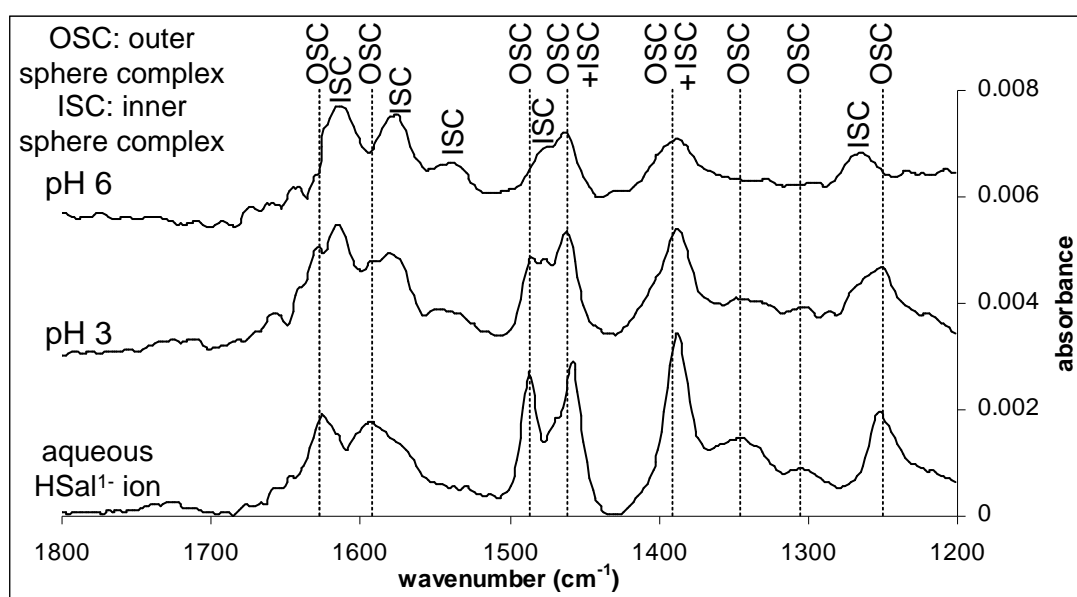


Figure 3-13 IR spectra of salicylic acid adsorbed on kaolinite at pH 3 and 6. The dashed lines serve as a guide to the eye and help to identify the peak frequency positions of the aqueous HSal^{1-} ion. The frequency positions of the main absorption bands at pH 6 are significantly different from those of aqueous salicylic acid are assigned to an inner sphere complex (ISC). The frequency positions of the absorption bands corresponding to the aqueous salicylate ion are in close agreement with the frequency positions of the additional absorption bands present in the spectrum at pH 3 and are thus assigned to an outer sphere complex (OSC). The spectra have been offset for clarity.

To further investigate the identity and spectroscopic features of the two surfaces complexes identified, the spectra obtained at pH 3 and 5 were examined in more detail. Figure 3-14 shows the spectra of adsorbed salicylic acid obtained at pH 3 and 5, as well as the difference spectrum obtained when the spectrum at pH 3 is subtracted from that at pH 5. The changes occurring as the pH of the solution decreases are evident by the difference spectrum obtained. The difference spectrum consists of absorption bands with peak frequency positions which are very similar to the bands exhibited by the aqueous HSal^{1-} species. The similarity in peak frequency positions of the difference

spectrum confirms the assumption that the bands growing in intensity with decreasing pH originate from an outer sphere surface complex. Furthermore this surface species binds to the surface as a singly protonated HSal^{-1} outer sphere complex. The strong resemblance of the difference spectrum with the spectrum of aqueous HSal^{-1} also indicates that the inter- and/or intra-molecular interactions occurring in the outer sphere bound salicylate complexes are similar to those occurring in the aqueous HSal^{-1} species. Furthermore the absence of additional bands other than those corresponding to outer sphere species precludes the existence of a third salicylate surface complex.

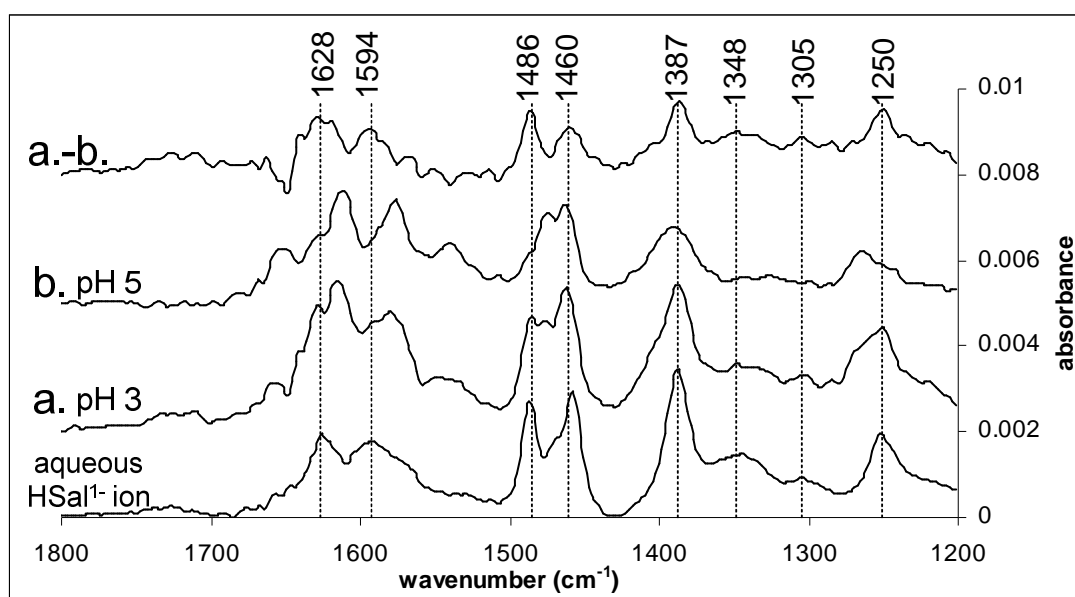


Figure 3-14 IR spectra of adsorbed salicylic acid from a 5×10^{-4} M salicylic acid solution on kaolinite, at pH 3 and 5. The spectrum labeled a-b is the difference spectrum obtained when spectrum b is subtracted from spectrum a. Spectrum peak frequencies provided correspond to the absorption maxima of the difference spectrum. The peak frequencies of the difference spectrum are related to the peak frequencies seen for the aqueous monoprotonated hydrogen salicylate ion (HSal^{-1}).

According to the above discussion salicylic acid forms two types of surface complexes on the surface of kaolinite, one inner sphere and one outer sphere complex. At pH 6 the spectroscopic features corresponding to the outer sphere complex are almost absent and hence this spectrum represents primarily the absorption profile of inner sphere complexed salicylic acid. Conversely, at pH 3 the spectrum includes spectral contributions of both inner and outer sphere complexed salicylic acid. The inner sphere complex identified is characterised by a spectrum with absorption maxima at about 1612, 1577, 1540, 1475, 1463, 1390, and 1264 cm^{-1} . The outer sphere complex, whose relative importance increases with decreasing pH, displays absorption bands at

about 1628, 1593, 1486, 1461, 1386, 1348, 1305, and 1250 cm^{-1} . The frequency positions at maximum for all the bands are insensitive to pH changes suggesting that each of the two surface complexes identified adopts the same coordination mode over the pH range from 3 to 6.

To examine the effects of experimental conditions on the relative surface concentrations of the two surface complexes isolated, the IR spectra of adsorbed salicylic acid were collected at different salicylate concentrations, ionic strengths and reaction times. Figure 3-15 shows the spectra of adsorbed salicylic acid at pH 5 obtained from a solution of 5×10^{-3} M salicylic acid in the presence of 0, 0.01 and 0.03 M NaCl. The absorption bands attributed to the outer sphere complex are reduced relative to those attributed to the inner sphere complex, indicating that outer sphere complexation is favoured by lower ionic strengths. The ionic strength dependence of these bands further confirms the assignment of these bands to outer sphere complexed salicylate species. In addition, the concurrent increase in dominance of the bands attributed to the inner sphere complex at higher ionic strengths supports the assignment of these bands to a single inner sphere complex.

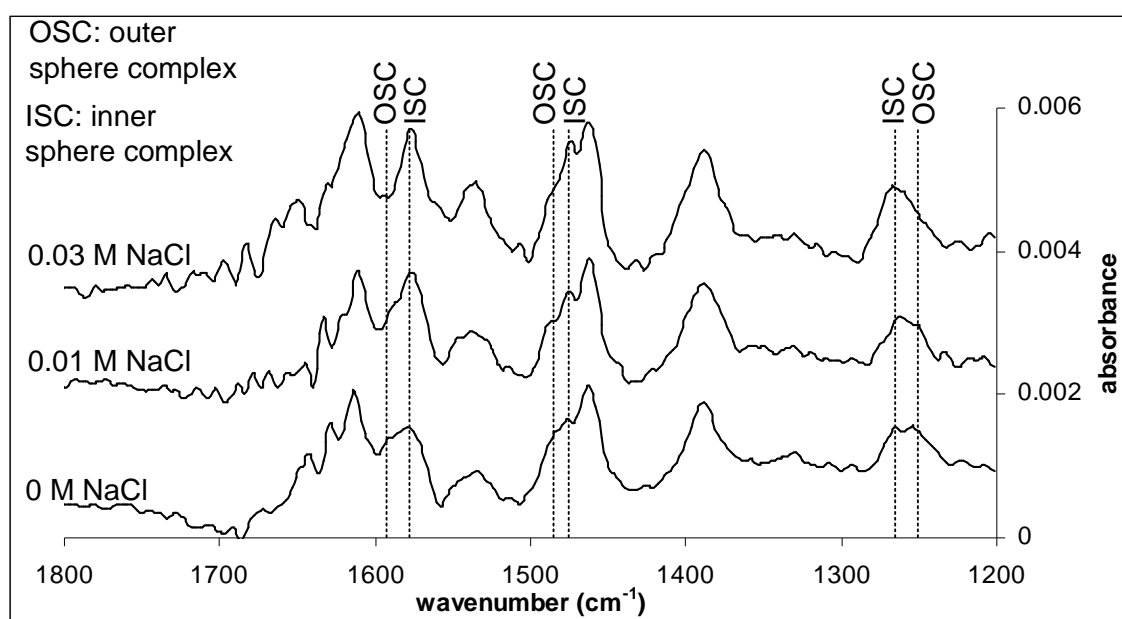


Figure 3-15 IR spectra of adsorbed salicylic acid on kaolinite from a 5×10^{-3} M salicylic acid solution at 0, 0.01 and 0.03 M NaCl, at pH 5. Lines show the change in relative intensity for specific adsorption bands corresponding to either an inner sphere complex (ISC) or an outer sphere complex (OSC). The spectra have been offset for clarity.

Contrary to the effect of increasing ionic strength and pH, higher initial salicylate concentrations favour outer sphere complexation as shown in Figure 3-16. At pH 4 the absorption bands originating from the outer sphere complex grow in intensity

as the initial concentration of salicylic acid changes from 5×10^{-4} to 1×10^{-3} M. A similar trend was observed for other pH values in the pH range from 3 to 6 (not shown). This behaviour suggests that at low concentrations salicylic acid binds to surface sites available for inner sphere complexation and once these sites become saturated, salicylic acid coordinates to the surface in an outer sphere mode. Increasing dominance of outer sphere complexed species at increasing concentrations have been previously reported for other organic ligands (Johnson et al., 2004b; Yoon et al., 2004b).

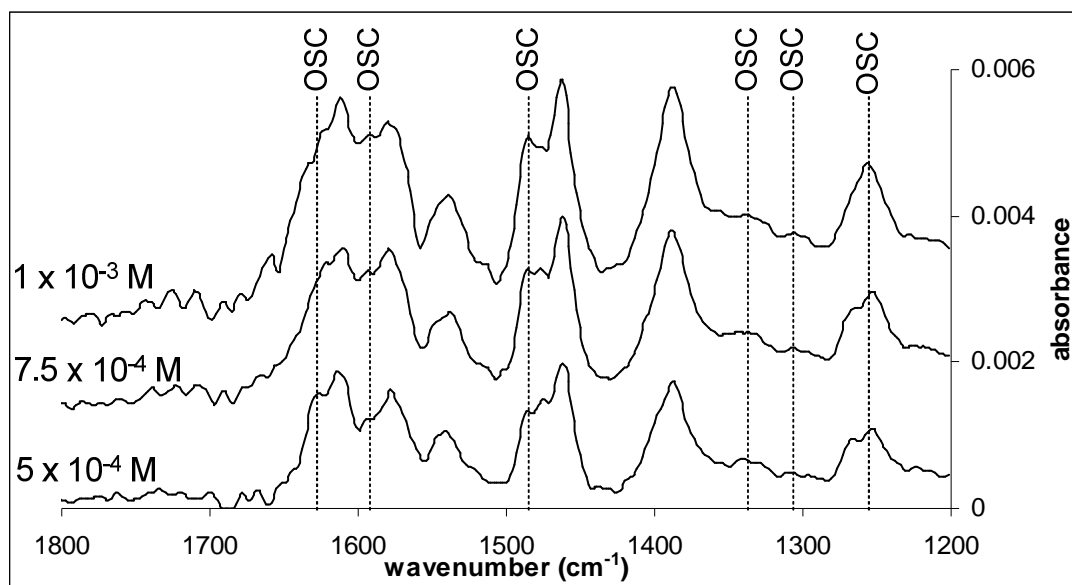


Figure 3-16 IR spectra of adsorbed salicylic acid on kaolinite at pH 4 as a function of total salicylate concentration in solution. The bands originating from the outer sphere complex (OSC) alone are marked with dashed lines. As the ligand concentration increases from 5×10^{-4} to 1×10^{-3} M the relative intensity of these bands increases, indicating increasing dominance of outer sphere complexed species. The spectra have been offset for clarity.

A close examination of the time-dependent IR spectra at the different solution concentrations studied did not reveal any shifts in the bands attributed to the vibrational modes of carboxyl and phenolic groups. Based on this observation it can be concluded that the adsorbed species maintain the initial coordination mode adopted throughout the duration of the experiments (typically up to 2 hours of reaction time). However, the relative band intensities of the two surface complexes were influenced by the reaction time indicating a change in relative concentrations for the two surface complexes. It is apparent from the increase in the relative intensities of the bands attributed to outer sphere complexes that the concentration of outer sphere complexed salicylic acid species increases with increasing time in the first 50 minutes (Figure 3-17). After this time period the relative concentrations of the two surface species remains constant.

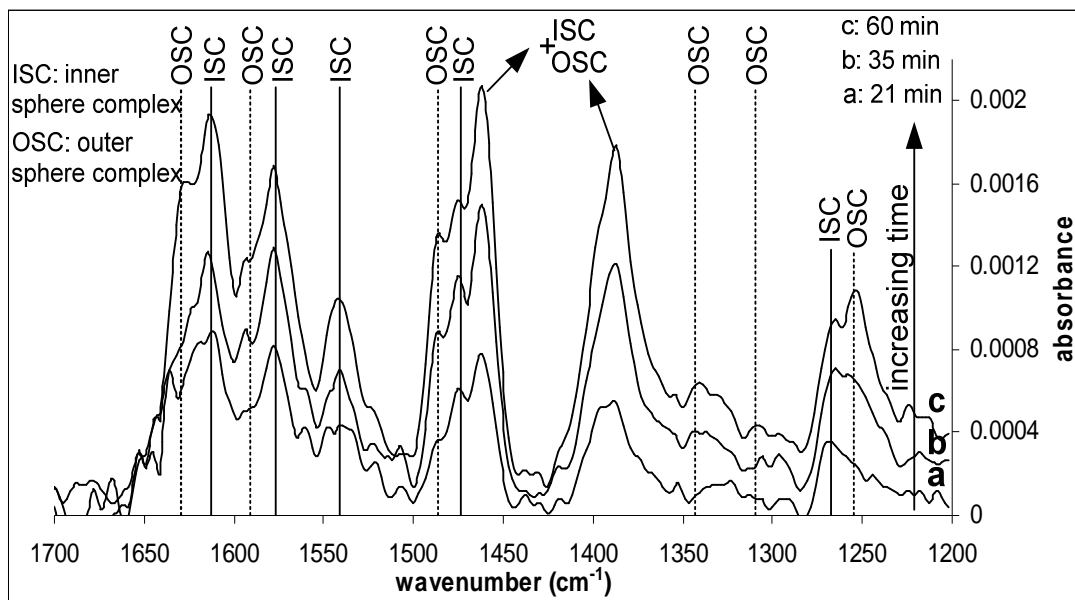


Figure 3-17 Time dependent IR spectra of adsorbed salicylic acid from a 5×10^{-4} M salicylic acid solution on kaolinite obtained at pH 4. As the reaction time is increased the intensity of the absorption bands associated with the outer sphere complex (OSC) increases relatively to the intensity of the bands associated with the inner sphere complex (ISC).

Because the IR spectra of adsorbed species are related to the structure of the surface complex formed, evidence about the coordination mode of inner sphere bound salicylic acid can be obtained from the characteristic absorption bands exhibited by this surface complex. Specific spectroscopic features of adsorbed salicylic acid have been previously used to infer the coordination mode of salicylic acid on different mineral surfaces (Biber and Stumm, 1994; Dobson and McQuillan, 2000; Kubicki et al., 1997; Kubicki et al., 1999; Molis et al., 2000; Tunesi and Anderson, 1992; Yost et al., 1990). Interpretation and band assignment of the spectrum corresponding to inner sphere complexed salicylic acid was based on previous IR spectroscopic studies of adsorbed salicylic acid and on direct comparisons between the spectra of adsorbed salicylate and those of aqueous salicylic acid. To aid the following discussion, the IR spectra of aqueous and adsorbed salicylic acid at pH 6 are given in Figure 3-18. Spectral contributions from outer sphere complexed salicylic acid in the IR spectrum of adsorbed salicylic acid at pH 6 are expected to be insignificant and therefore this spectrum is assumed to be representative of inner sphere complexed species.

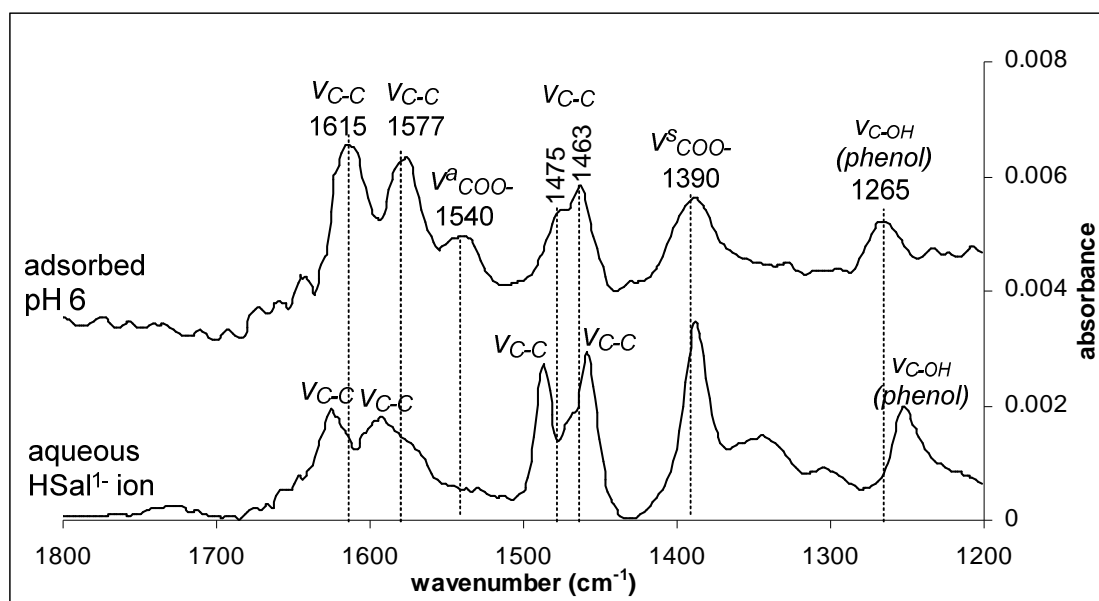


Figure 3-18 Differences in the spectroscopic features of aqueous salicylic acid (recorded at pH 6) and adsorbed salicylic acid on kaolinite obtained at pH 6 from a 5×10^{-4} M salicylic acid solution.

The bands with absorption maxima at 1615, 1577, 1475 and 1463 cm^{-1} are assigned to the benzene ring C-C vibrations ($\nu_{\text{C-C}}$). The frequency positions of these bands are different to those seen in the free salicylate ion, indicating that the electron distribution of the benzene ring is influenced by adsorption (Tunesi and Anderson, 1992; Yost et al., 1990).

The carboxylate asymmetric stretching mode ($\nu^{\text{a}}_{\text{COO}^-}$) of the surface bound carboxyl group is assigned to the 1540 cm^{-1} band. The frequency position of this vibrational mode is shifted to lower wavenumbers, by about 35 cm^{-1} , when compared to the corresponding mode of the aqueous HSal^{1-} species. Bands with similar frequency positions have also been observed and attributed to the $\nu^{\text{a}}_{\text{COO}^-}$ mode of inner sphere complexed salicylic acid, in previous studies (Biber and Stumm, 1994; Dobson and McQuillan, 2000; Molis et al., 2000; Tunesi and Anderson, 1992).

The symmetric stretching vibrational mode of the carboxyl group ($\nu^{\text{s}}_{\text{COO}^-}$) is assigned to the band positioned at 1390 cm^{-1} . This band replaces the two bands positioned at 1387 and 1344 cm^{-1} which were partly attributed to the symmetric stretching vibration of the aqueous salicylate ion. The absorption band at 1265 cm^{-1} is assigned to the stretching vibration of the phenolic C-OH group ($\nu_{\text{C-OH}}$). The corresponding $\nu_{\text{C-OH}}$ mode of aqueous HSal^{1-} is located at 1252 cm^{-1} . Finally one last point worth noting for the IR spectrum of adsorbed salicylic acid species is the absence of an absorption band near the 1700 cm^{-1} region which is characteristic of C=O stretch vibrational modes.

The direct bonding of the carboxylate group to the surface is indicated by the absorption band positioned at 1540 cm^{-1} . Because the band separation between the symmetric and asymmetric stretching modes of the adsorbed carboxyl group ($\Delta\nu = 150\text{ cm}^{-1}$) is lower than that of the free salicylate molecule ($\Delta\nu = 190\text{ cm}^{-1}$), it is tempting to assume that salicylic acid adsorbs on the surface in a bidentate coordination mode with respect to the carboxylic group. It has to be noted however that the $\Delta\nu$ value of the aqueous salicylic species can only be estimated because the coupling effect between the phenolic bending mode with the symmetric carboxylate stretching vibration obscures the “real” frequency position of the carboxylate symmetric stretching mode. Moreover, aqueous salicylic acid exhibits intramolecular hydrogen bonding which can influence the frequency positions of the carboxylate stretching vibrations and therefore structural assignment according to the frequencies of the carboxylate vibrational modes can be of limited use (Yost et al., 1990).

In addition to the carboxylate group, there is evidence that the phenolic group is also involved in surface coordination. The spectroscopic features which reveal the involvement of the phenolic group in surface coordination are (a) the shift of the phenolic stretching vibration to higher frequencies upon adsorption (from 1252 to 1265 cm^{-1}) and (b) the loss of absorption bands at about 1340 and 1305 cm^{-1} that have been partly attributed to phenolic vibrational modes (primarily bending modes) of the aqueous salicylate species.

From a structural point of view, tridentate coordination of salicylic acid is unlikely to occur due to steric constraints (Dobson and McQuillan, 2000; Yost et al., 1990). Therefore, given that the phenolic group coordinates to the surface, the carboxylate group can only bind to the surface in a monodentate coordination mode. Although a monodentate structure with respect to the carboxylate group is expected to exhibit a C=O stretching vibration (Figure 3-19; structures A, D and G), the absence of a C=O stretching band can be explained by a delocalised bonding arrangement of the surface bound carboxylate group. As already mentioned, surface coordination of salicylic acid changes the electronic distribution of the benzene ring as indicated by the shift in the peak frequency positions of the benzene ring C-C vibrations. Upon adsorption, propagation of the electron density disturbance from the benzene ring to the carboxylic group could explain the delocalised bonding arrangement of the surface bound carboxylate group and therefore the absence of a C=O bond vibration (Dobson and McQuillan, 2000).

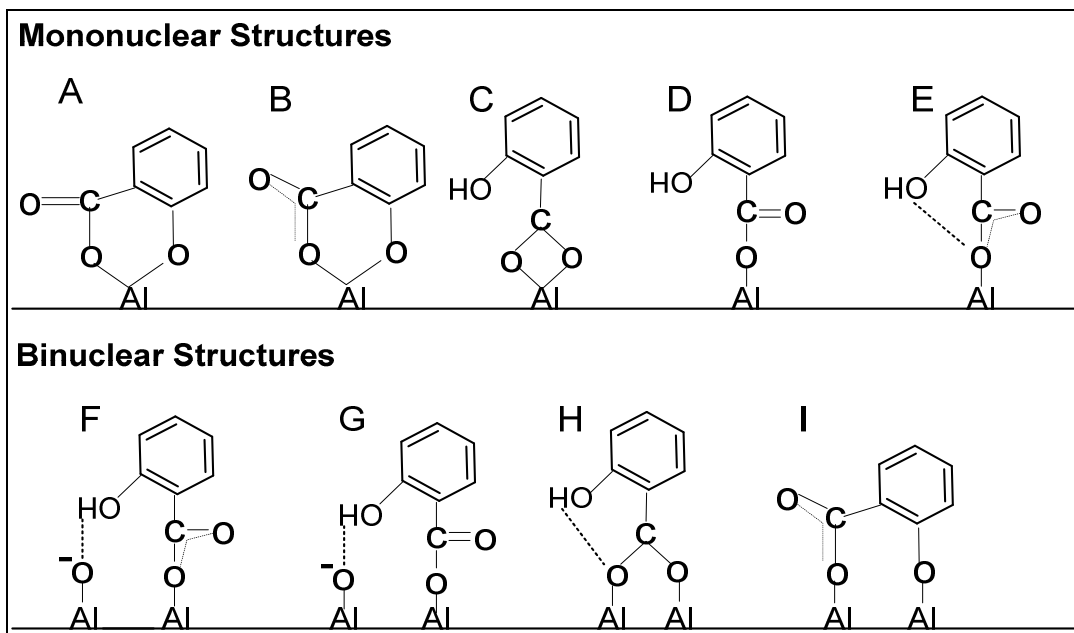


Figure 3-19 Possible coordination modes for adsorbed salicylic acid on a mineral surface. Mononuclear structures bond to a single surface cation whereas binuclear structures coordinate to two surface cations.

The comparison of the spectra of salicylate surface complexes with the spectra of aqueous metal-salicylate complexes with known coordination modes can help the structural assignment of the surface salicylate complex. Figure 3-20 compares the IR spectra of aqueous Fe- and Al-salicylate complexes with the spectra of free and adsorbed salicylic acid at pH 6, all obtained in this study. The absorption maxima of the bands in the spectrum of aqueous Fe-salicylate are different from those of Al-Sal, indicating a different coordination mode in the two aqueous complexes. The most striking difference to be seen is that the $\nu^s_{\text{COO}^-}$ and $\nu_{\text{C-OH}}$ modes shift to lower frequencies in the spectrum of Fe-salicylate and to higher frequencies in the Al-salicylate complex when these are compared to the spectrum of aqueous HSal^{1-} . These findings are consistent with those of Biber and Stumm (1994) who suggested that the structures of salicylate surface complexes formed on aluminium oxides are different from those on iron oxides. It is therefore evident that the type of metal cation (in solid or aqueous phase) has a significant effect on the coordination mode of salicylic acid.

The close similarity between the spectra of aqueous Al-salicylate complexes and surface salicylate complexes suggests that adsorbed salicylic acid adopts a similar coordination mode as that in the aqueous Al-salicylate complexes. One apparent difference, however, is that the absorption bands of the surface complex are broader than those of aqueous Al-salicylate complexes and of aqueous HSal^{1-} . The broadening of absorption features indicates adsorbed species, of similar binding and coordination mode, bound to surface sites of different nature. Coordination to different sites can give

rise to absorption bands with slightly different peak positions, and thus explain the broadened IR features of surface bound species (Boily et al., 2000b; Roddick-Lanzilotta and McQuillan, 2000). Band broadening in the IR spectra of adsorbed salicylate is therefore not surprising because salicylate may be bound to different surface sites on kaolinite, such as edge and basal plane sites.

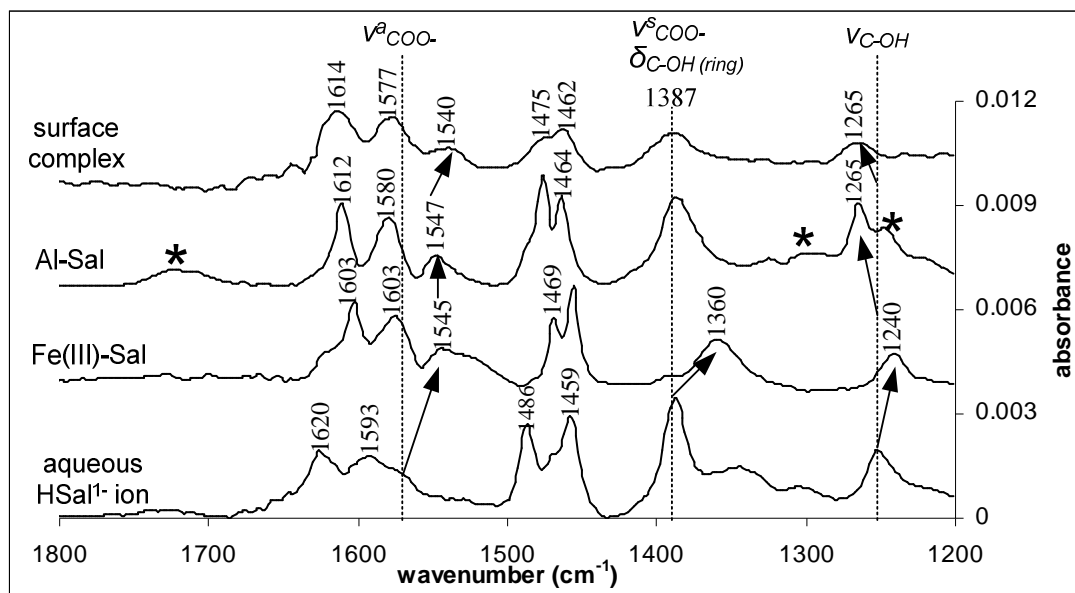


Figure 3-20 IR spectra of complexed salicylate with iron (III) and aluminium ions in solution, and on the surface of kaolinite (pH 6). The spectrum of aqueous HSaI^{1-} ion is also included for comparison. The IR spectra of aqueous metal-salicylate complexes were obtained at pH 3 in order to prevent precipitation. Dashed lines denote the position of the carboxylate and phenolic vibrational modes of the aqueous HSaI^{1-} ion and the arrows indicate the direction of shift of these vibrational modes following complexation. Bands marked with an asterisk in the IR spectrum of Al-Sal complex originate from uncomplexed $\text{H}_2\text{Sal}/\text{HSaI}^{1-}$ species.

For iron-bearing minerals it is generally accepted that salicylic acid forms a bidentate structure, with respect to the entire molecule, where both the carboxyl group and the phenolic group are involved in the binding of salicylic acid (Fig 3-19; structure A or B) (Biber and Stumm, 1994; Yost et al., 1990). Direct coordination of the phenolic group to surface iron has been inferred from the shift of the phenolic stretching vibration to lower wavenumbers following the complexation of salicylic acid (Yost et al., 1990). Conversely for aluminium-bearing minerals different structures have been proposed. Biber and Stumm (1994) suggested that adsorbed salicylic acid on aluminium oxide forms a six membered pseudochelate ring in which only the carboxylic group is directly coordinated to the surface and the phenolic group is hydrogen bonded to a neighbouring surface site (Figure 3-19; structure F or G). A similar monodentate structure has also been proposed by Kubicki et al. (1997) as a possible coordination mode for adsorbed salicylic acid on illite (Figure 3-19; structure E). In this surface

complex the phenolic group is hydrogen bonded to an Al-O-C moiety rather than to an adjacent surface site. An alternative structure also proposed by Kubicki et al. (1997) is a bridging bidentate complex with respect to the carboxylate group and the phenolic group is hydrogen bonded to an oxygen atom in an Al-O-C moiety (Figure 3-19; structure H). Finally, Dobson and McQuillan (2000) proposed a mononuclear five membered chelate ring structure (Figure 3-19; structure B) for adsorbed salicylic acid on Al₂O₃, TiO₂, ZrO₂, and Ta₂O₅.

The coordination mode of salicylic acid on Al₂O₃ proposed by Dobson and McQuillan (2000) is similar to that inferred for iron oxides and therefore is contradictory to previous investigations which suggested different binding modes for adsorbed salicylic acid on aluminium and iron oxides (Biber and Stumm, 1994). This contradictory finding may be explained by the difference in the interpretation of the IR spectra rather than by the differences in IR measurements. Dobson and McQuillan (2000) failed to consider the differences in the IR spectra of adsorbed salicylic acid obtained for the various mineral substrates examined in their study. As a result the authors assumed that salicylic acid adopts a similar coordination mode in all four mineral surfaces. However a close examination of the peak frequency positions reported in their study shows considerable differences between different adsorbed salicylate species. For example on Ta₂O₅ the carboxylate symmetric stretching vibration has a maximum at 1359 cm⁻¹ whereas on Al₂O₃ it is at 1387 cm⁻¹. The respective frequency position for the aqueous salicylate ion is at about 1384 cm⁻¹. In addition, the absorption maximum for the phenolic stretching vibration on Ta₂O₅ is at 1243 cm⁻¹, on Al₂O₃ at 1261 cm⁻¹ and for aqueous salicylic acid at 1251 cm⁻¹. This shows that upon adsorption the phenolic and carboxylic stretching vibrations shift to higher wavenumbers on aluminium oxide and to lower wavenumbers on tantalum oxide. It can be therefore clearly seen that adsorbed salicylic acid exhibits different peak frequency positions on these two different mineral substrates. This observed behaviour is comparable to that discussed above when Fe- and Al-salicylate complexes were presented.

The phenolic stretching mode of surface bound salicylic acid on kaolinite in this study has shifted from 1252 to 1265 cm⁻¹. As suggested by Biber and Stumm (1994), an increase in the frequency position of the phenolic stretching mode can be explained by a change in the strength of the intramolecular hydrogen bond or even by the breaking of the hydrogen bond (deprotonation of the phenolic group is expected to give a much higher upward shift). However the loss of the phenolic bending mode in the IR spectra of the interfacial species obtained in this study does not support the possibility of an unconstrained phenolic group which can vibrate freely in different modes. Therefore the

phenolic group in the present study is assumed to be coordinated to a surface site via hydrogen bonding interactions. According to the spectroscopic features presented here, either of the two structures E, F shown in Figure 19 are possible.

Macroscopic adsorption experiments showed that there is a significant adsorption of salicylic acid on kaolinite even at pH values as high as 10. In order to investigate whether at this higher pH adsorbed salicylate has the same binding mode as that observed at pH 6, the spectrum of adsorbed salicylic acid at pH 10 was collected. It can be seen in Figure 3-21 that the IR spectrum exhibited by interfacial salicylic species at pH 10 is significantly different from that obtained at pH 6, suggesting that salicylic acid does not form the same surface complex at pH 6 and pH 10. The shift of the band attributed to the phenolic vibration from 1252 cm^{-1} to 1273 cm^{-1} is consistent with a deprotonated phenolic group stretching mode $\nu_{\text{C-O}^-}$ (Yost et al., 1990). The occurrence of this band therefore indicates that at pH 10, interfacial salicylic acid is coordinated to the surface as the fully deprotonated salicylate species (Sal^{2-}).

This dramatic change in the IR spectrum of interfacial salicylic acid at pH 10 could be either attributed to a structurally different inner sphere surface complex or to a fully deprotonated outer sphere surface complex. Unfortunately the IR spectrum of aqueous salicylate ions (Sal^{2-}) could not be recorded because the extremely basic conditions required to obtain salicylate species in solution ($\text{pK}_{\text{a}2} = 13.5$) would damage the ZnSe crystal. A thorough review of the literature did not reveal any studies that reported the IR spectrum of aqueous Sal^{2-} species. However significant differences in the IR spectra of Sal^{2-} and HSal^{-1} are expected since once the phenolic group deprotonates the absorption bands originating or coupled with the phenolic group vibrations will be affected. In addition, the intra- and inter-molecular hydrogen bonds exhibited by the HSal^{-1} species will break causing further changes to the IR spectrum. Because these changes are not known it is not possible to comment whether the changes occurring in the spectrum of adsorbed salicylate at pH 10 are due to an outer sphere complexed salicylate species or to an inner sphere complex with a different coordination mode than that identified at pH 6.

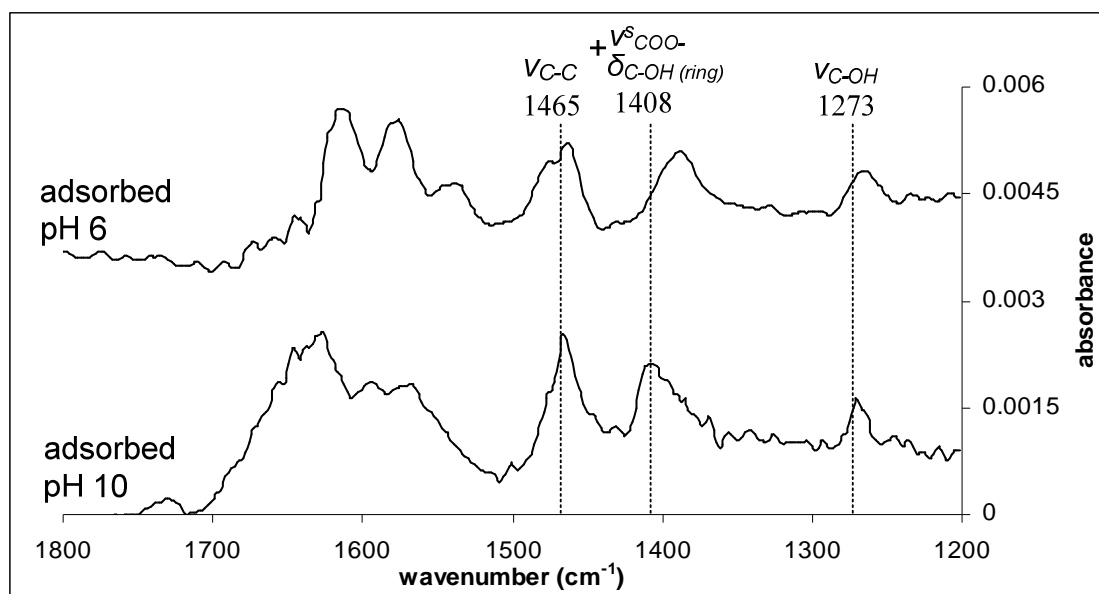


Figure 3-21 IR spectra of adsorbed salicylic acid from a 5×10^{-4} M salicylic acid solution on kaolinite, at pH 6 and 10.

Synopsis

This section has presented molecular level information, derived from IR spectroscopy, about the binding and coordination mode of the surface complexes formed following the adsorption of phthalic and salicylic acid onto kaolinite. Although IR spectroscopy can provide valuable information about the structure of the adsorbed species, the limitations associated with spectral interpretation must also be kept in mind. This is particularly true when trying to differentiate between surface structures with similar coordination modes. This limitation of unambiguous spectral interpretation does not allow one to draw definitive conclusions about the exact coordination mode of adsorbed molecules, but rather propose possible structures of surface species (Cooper and Vasudevan, 2009).

For phthalic acid the spectroscopic results revealed that two fully deprotonated phthalate species coexist on the surface of kaolinite, one that is coordinated to the surface through an outer sphere mechanism and one in an inner sphere mechanism. Although outer sphere complexation is the dominant adsorption mode under the experimental conditions examined, different solution conditions were found to influence the relative distribution between the two surface complexes. The inner sphere surface complex is favoured by lower pH values and higher ionic strength and the outer sphere complex by higher pH and lower ionic strength. This study has also shown that phthalic acid forms similar types of surface complexes on kaolinite (one inner and one outer sphere surface complex) to those proposed for iron and aluminium hydr(oxides). The

inner sphere complex adopts a bidentate coordination mode in which both carboxylic groups are involved in surface complex formation. This phthalate complex is most probably a mononuclear bidentate complex which results in a seven-membered chelate ring structure in which both carboxylate groups are directly bonded to the surface.

For salicylic acid, spectroscopic evidence indicated three main surface complexes on kaolinite. In the pH range from 3 to 6, one inner sphere complex and one outer sphere complex coexist on the surface. In these two surface complexes, salicylic acid exists as the singly protonated salicylic acid species. The relative concentration of these two complexes was significantly affected by the pH of the solution, ionic strength, initial salicylic acid concentrations and reaction times. Inner sphere complexation is favoured by higher pH, higher ionic strength, and lower initial salicylate concentrations whereas outer sphere complexation is favoured by lower pH, lower ionic strength and higher initial salicylate concentrations. The inner sphere complex identified is most probably a mononuclear monodentate complex where a single carboxylate oxygen is directly bonded to the surface and the phenolic group is hydrogen bonded to a neighbouring surface site. At pH 10, the IR spectrum of adsorbed salicylic acid indicated unsurprisingly that a different surface complex forms in which salicylic acid exists as the fully deprotonated salicylate species. Unfortunately the exact nature of this surface complex could not be determined as the spectrum of the fully deprotonated aqueous salicylate ion could not be obtained.

The IR spectroscopic results obtained regarding the number and type of surface complexes formed provide useful constraints that can be used in the development of realistic and reliable surface complexation models that describe the chemical reactions taking place at the interface. The following section will present surface complexation models that can describe the macroscopic adsorption behaviour of phthalic and salicylic acid on kaolinite.

Macroscopic adsorption properties

Adsorption as a function of pH

The macroscopic adsorption of phthalic and salicylic acid as a function of pH was studied in the pH range from 4 to 10, at three different total kaolinite surface area-to-initial ligand concentration ratios; [S.A (m^2): [ligand concentration (mol)]. The

results from these adsorption experiments are presented in Figures 3-22 and 3-23. For the range of experimental conditions examined the maximum adsorption density found for phthalic acid is 1.31×10^{-7} mol/m² and for salicylic acid is 1.27×10^{-7} mol/m². As expected these values are obtained at the higher ligand concentrations examined. Furthermore, at any given pH, the fractional adsorption decreases with higher initial ligand concentrations, a behaviour which is indicative of surface saturation effects. As the initial ligand concentration increases the surface binding sites become progressively occupied and thus the adsorption affinity of salicylic and phthalic acid for the surface of kaolinite is reduced.

Interestingly, for both organic ligands maximum adsorption densities were obtained at a pH of about 5.5. The similarity in maximum adsorption density values suggests that at pH 5.5 kaolinite exhibits a similar adsorption affinity towards salicylic and phthalic acid. However as the pH of the solution changes, the adsorption densities of the two ligands are no longer similar. For example, from the two datasets where the maximum adsorption densities were obtained, the corresponding adsorption density at pH 10 for phthalic acid is 4.11×10^{-8} mol/m² and for salicylic acid is 9.9×10^{-8} mol/m². The adsorption behaviour, as a function of pH, for each organic acid will now be discussed separately in more detail.

Phthalic acid adsorption on kaolinite as a function of solution pH and initial ligand concentration is shown in Figure 3-22. Although there is an overall decreasing adsorption trend as a function of pH, it can be clearly seen that for all three different acid concentrations phthalic acid adsorption reaches a maximum at about pH 5.5 and decreases at lower and higher pH values. This adsorption trend is somewhat different from the typical anion adsorption behaviour where adsorption either increases with decreasing pH until it reaches a plateau or keeps increasing throughout the pH range.

A pH-dependent adsorption behaviour can be explained in terms of the electrostatic interactions between surface sites and solute anions. As the pH of the solution increases, the negative surface charge also increases (or positive surface charge decreases) and thus leading to lower adsorption due to the increased electrostatic repulsions between the negatively charged surface sites and the negatively charged anions. Decreased adsorption at higher pH values could therefore indicate the importance of electrostatic forces of attraction in the binding of ions to mineral surfaces, i.e. outer sphere complexation. However, decreased adsorption as a function of increasing pH is also consistent with a ligand exchange mechanism. When surface sites and organic ligands carry an opposite charge, organic ligands can approach the surface in order for ligand exchange reactions to take place. Furthermore, neutral and positively

charged sites, expected at lower pH values, are more readily exchangeable than negatively charged sites because X-OH and X-OH₂⁺ bonds have a lower electron density (and thus are weaker) than X-O⁻ bonds (Evanko and Dzombak, 1998).

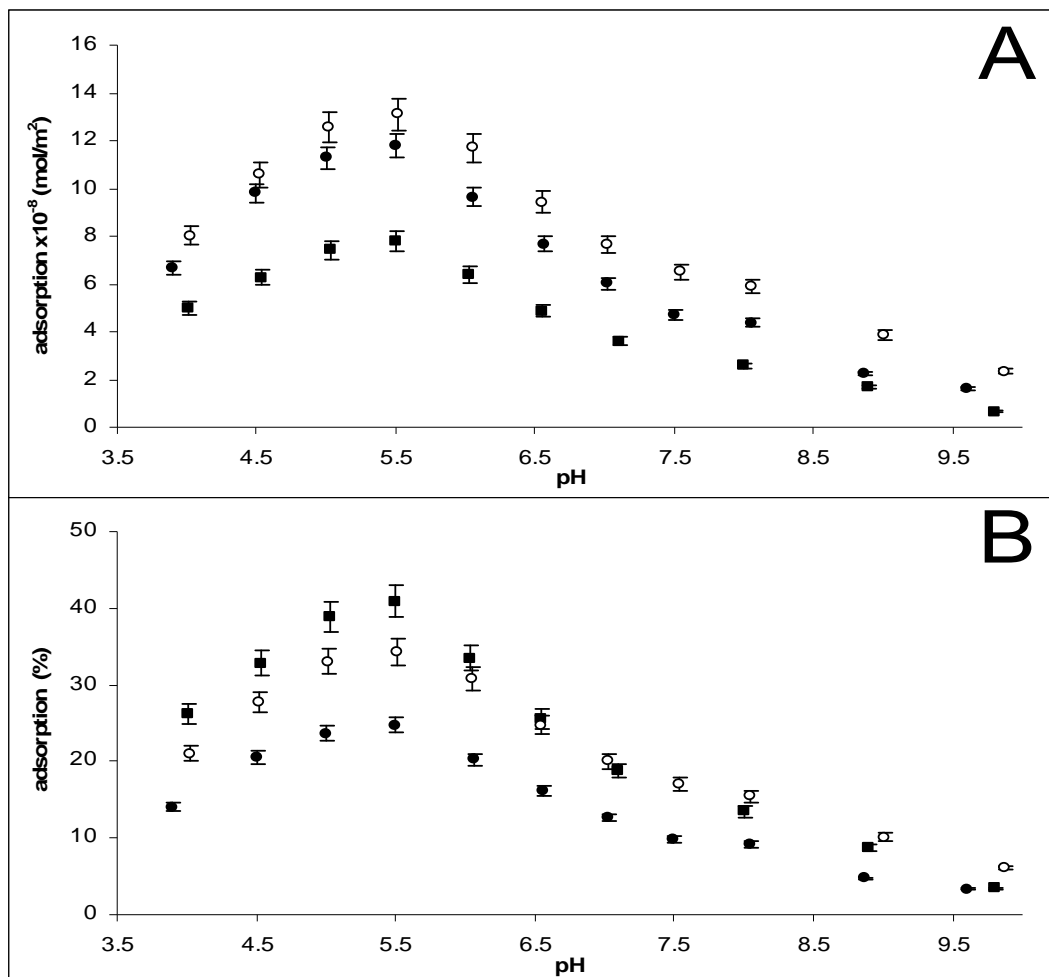


Figure 3-22 Adsorption of phthalic acid on kaolinite as a function of pH at an ionic strength of 0.01 M NaCl expressed as (A) adsorption density in mol/m² and (B) fractional adsorption. Symbols represent experimental data obtained for the following [total surface area (m²)] : [initial phthalate concentration (mmol)] ratios as follows: squares = [52.5] : [0.01] (5250); open circles = [52.5] : [0.02] (2625); closed circles = [42] : [0.02] (2100). Error bars represent an experimental error of 5% estimated from the triplicate measurements of several data points (see methods section).

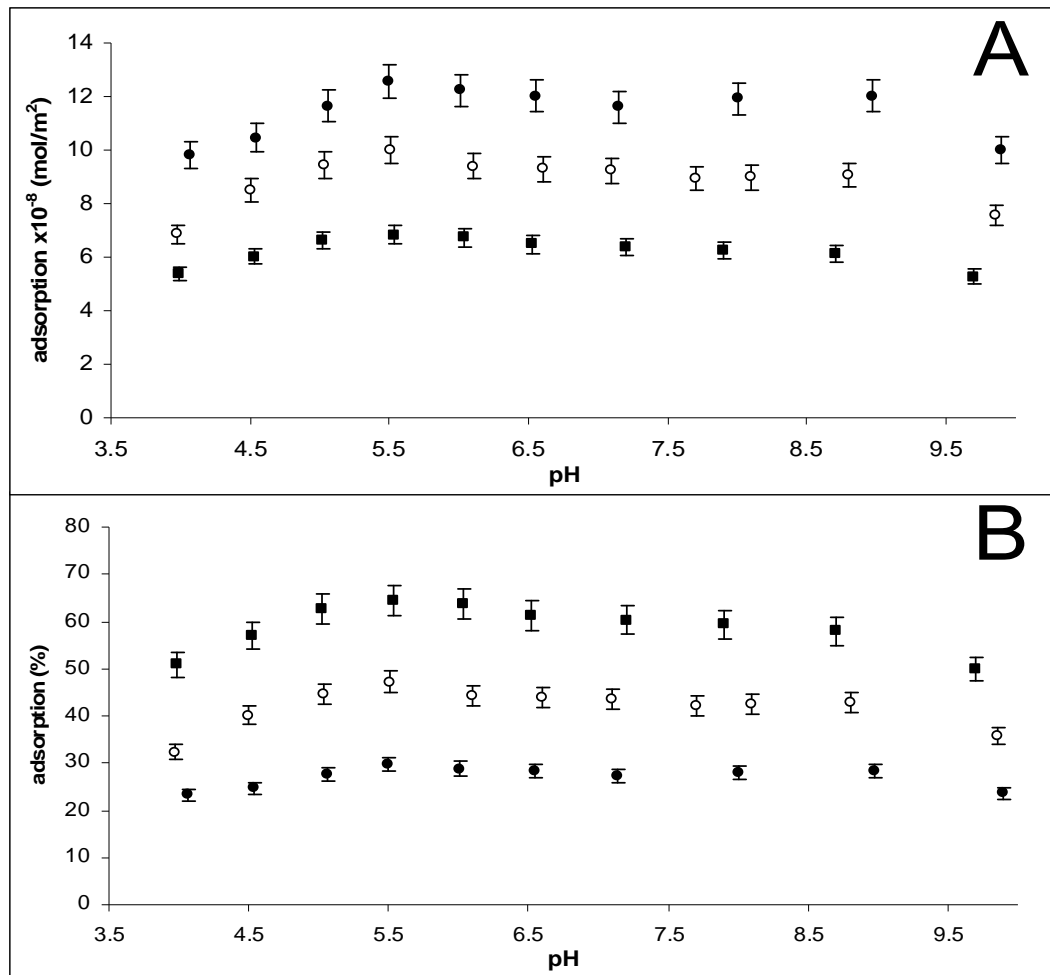


Figure 3-23 Adsorption of salicylic acid on kaolinite as a function of pH at an ionic strength of 0.01 M NaCl expressed as (A) adsorption density in mol/m^2 and (B) fractional adsorption. Symbols represent experimental data obtained for the following [total surface area (m^2)] : [initial phthalate concentration (mmol)] ratios as follows: squares = [47.3] : [0.005] (9460); open circles = [47.3] : [0.01] (4730); closed circles = [47.3] : [0.02] (2365). Error bars represent an experimental error of 5 % estimated from triplicate measurements of several data points (see methods section).

Accordingly, the adsorption behaviour of phthalic acid on kaolinite can be explained by taking into consideration how the charge of the surface and of the organic ligand varies with pH. Because phthalic acid carries two carboxylic groups it can exist in three ionic states, H_2Phth , HPhth^- , and Phth^{2-} . The $\text{pK}_{\text{a}1}$ and $\text{pK}_{\text{a}2}$ values of phthalic acid are 2.87 and 5.23 respectively, and therefore in the pH range where adsorption was examined (4 -10) phthalate ions will possess either a -1 (HPhth^{-1}) or a -2 (Phth^{-2}) charge. The point of zero net proton charge (pHpznpc) of kaolinite has been previously determined to be close to 5.5 (Huertas et al., 1998; Schroth and Sposito, 1997). Higher or lower pHpznpc values reported in the literature were attributed by Ganor et al. (2003) to the different ways by which the pHpznpc was determined.

As the pH of the solution increases from 4 to 10, the surface charge located at the edge sites of kaolinite changes from positive to negative, whereas phthalate ions are

negatively charged throughout the pH range. It appears that the charge of the ion is the most important parameter governing the extent of adsorption at pH values below the pH_{pznpc} (pH < 5.5) of kaolinite. Although from pH 4 to 5.5 the edge surface charge remains positive, the charge of phthalate ions becomes increasingly more negative since the dominant species in solution progressively changes from the singly protonated molecule (HPhth⁻¹) to the fully deprotonated molecule (Phth⁻²). These fully deprotonated molecules will be subject to higher attractive forces towards the positive surface and thus explaining the increased adsorption observed from 4 to 5.5. Once the charge of the surface edge sites reverts from positive to negative at pH > 5.5 then the adsorption starts decreasing due to the electrostatic repulsions between the negatively charged surface sites and the negatively charge phthalate ions. Figure 3-24 represents graphically the variations in surface charge, phthalic acid charge and adsorption as a function of pH.

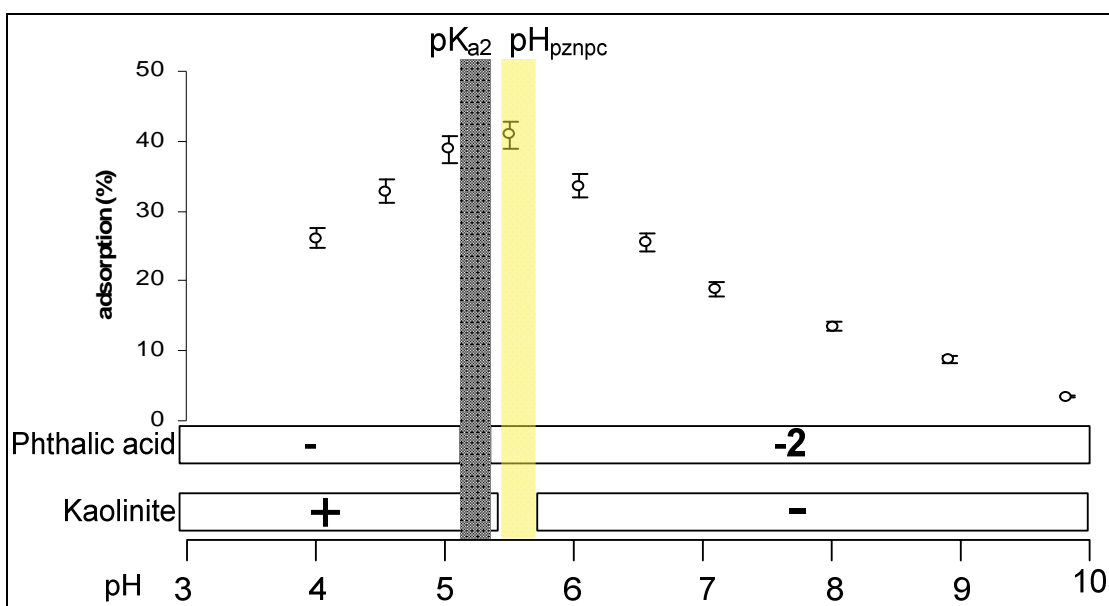


Figure 3-24 The dependence of surface charge and ligand charge on pH and how these parameters are related to the adsorption behaviour of phthalic acid on kaolinite. In the pH range below the point of zero net proton charge (pHpznpc), the net pH dependent surface charge of kaolinite is positive (pH < ≈5.5) and in the pH range above the pHpznpc this charge is negative (pH > ≈5.5). On the other hand, the net charge of phthalic acid is negative throughout the pH range shown here. The singly protonated species (HPhth⁻¹) is the major ion in solution below the pK_{a2} value (pH < 5.2) and the fully deprotonated species (Phth⁻²) is the major ion in solution above the pK_{a2} of phthalic acid (pH > 5.2). Symbols represent the adsorption behaviour of phthalic acid on kaolinite, in a system with initial phthalate concentration of 0.143 mM and a mineral surface area of 750 m²/L, at I = 0.01 M NaCl. These experimental conditions correspond to the [total surface area (m²)] : [initial phthalate concentration (mmol)] ratio of [52.5] : [0.01] shown in Figure 3-22.

Salicylic acid adsorption appears to be less dependent on pH variations as evidenced by the changes in absolute and percentage adsorption as a function of pH

(Figure 3-23). The amount of salicylic acid increases slightly from pH 4 to about 5.5 and gradually decreases, or even remains constant, at higher pH values. This lack of pH dependence suggests that interactions other than electrostatic forces of attraction are important in the adsorption of salicylic acid on kaolinite. A similar adsorption behaviour has been reported on goethite by Evanko and Dzombak (1998) for the adsorption of aromatic carboxylic acids which contained one carboxyl group and at least two adjacent phenolic groups. Interestingly, however, in the same study salicylic acid did not exhibit such an adsorption behaviour but rather showed a clear decreasing adsorption trend with increasing pH values.

Phthalic and salicylic adsorption behaviour presented in this study seem to be consistent with the observations of Pommerenk and Schafran (2005) regarding the role of different functional groups on the adsorption of aromatic diprotic organic acids on oxide surfaces. According to the authors at low pH values where the surface of the mineral is positive, deprotonated carboxylic groups increase adsorption whereas protonated phenolic groups increase adsorption at higher pH values. Similar results were reported by Evanko and Dzombak (1998) which found that additional functional groups located adjacent to a carboxylic acid enhanced adsorption of organic ligands on iron oxide. These findings strongly indicate the involvement of the phenolic group in the adsorption of salicylic acid on (hydr)oxide minerals. It therefore seems that the phenolic group also plays a role in the stabilisation of salicylate surface complexes on kaolinite surfaces.

Despite an extensive review of the literature, only one study was found in which the macroscopic adsorption behaviour of phthalic acid on kaolinite was reported (Angove et al., 2002). Similarly only one study was identified which examined the salicylic acid adsorption behaviour on kaolinite (Benyahya and Garnier, 1999). The observed trend in which the adsorption of phthalic acid reaches a maximum at about pH 5, and decreases in either direction is in good agreement with that reported by Angove et al. (2002). In contrast to the results obtained in this study, Benyahya and Garnier (1999) observed very low salicylic acid adsorption on kaolinite in the pH range between 3.5 - 9. This discrepancy may be explained by the different experimental conditions in which the adsorption of salicylic acid was examined. Two of the most important factors that can significantly influence the extent of adsorption are the mass of the substrate used (and hence available surface area for adsorption) and the ionic strength of the aqueous medium. The higher surface area-to-volume ratio of the mineral suspension ($675 \text{ m}^2/\text{L}$ vs $150 \text{ m}^2/\text{L}$) and the lower ionic strength (0.01 M vs 0.05 M) used in the

present study are more favourable experimental conditions for the uptake of salicylic acid.

Adsorption as a function of ionic strength

The dependence of ion adsorption on ionic strength is a criterion commonly used for distinguishing between inner and outer sphere adsorption mechanisms (e.g. Hwang et al., 2007; Nilsson et al., 1996; Nordin et al., 1997; Persson et al., 1998). It is generally assumed that anions adsorbing to the surface in an outer sphere mode have lower adsorption affinities at higher ionic strengths and this effect can be attributed to either (a) a reduction of the Coulombic attractive forces at pH values below the pH_{pznpc} due to decreased positive surface potential (Ali and Dzombak, 1996) and/or (b) the competition for available surface sites between adsorbing ions and outer sphere complexed background electrolyte ions such as NO_3^- and Cl^- (Persson et al., 1998). Conversely, ions coordinated in an inner sphere mode typically show little dependence on ionic strength or even exhibit higher adsorption with increasing ionic strength. Higher adsorption as a function of ionic strength is attributed to the higher concentration of counter ions at the interface which can compensate the charge generated on the surface as a result of inner sphere complexation (Goldberg and Johnston, 2001).

The effect of increasing ionic strength on the extent of salicylic and phthalic acid adsorption at pH 4 is shown in Figure 3-24. As the background electrolyte concentration is increased from 0 M (no added electrolyte) to 0.05M NaCl phthalic acid adsorption is reduced from 26% to 7% and salicylic acid adsorption from 27% to 19%. It can be seen that phthalic acid adsorption exhibits a strong dependence on the concentration of background electrolyte. This behaviour suggests that electrostatic interactions play a significant role in the binding of phthalate ions on the surface of kaolinite. Conversely salicylic acid adsorption shows a much less pronounced dependence on the ionic strength, suggesting that the surface complexes formed are mainly stabilised through direct chemical bonding.

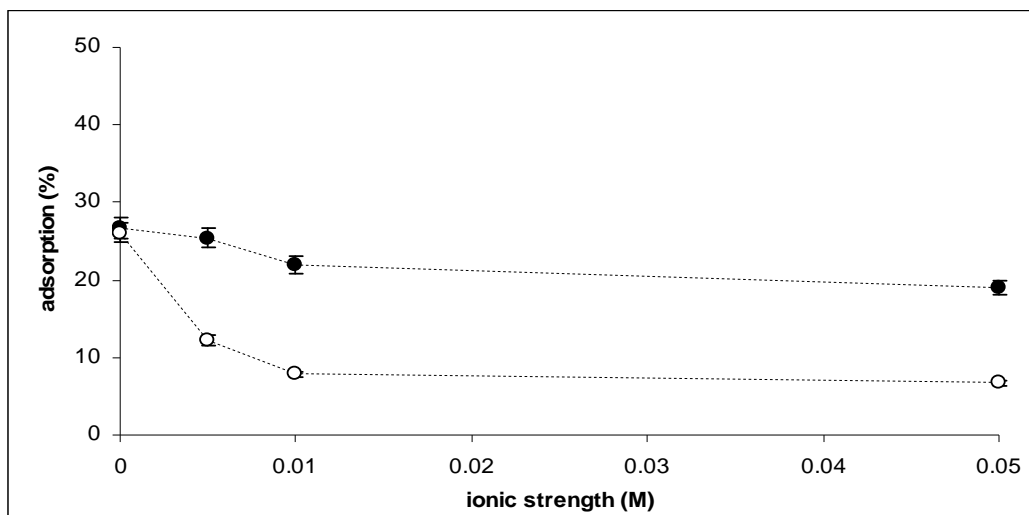


Figure 3-25 Fractional adsorption of phthalic acid (open circles) and salicylic acid (closed circles) as a function of ionic strength at pH 4. Dashed line is used as a guide to the eye to show the trend observed as the ionic strength increases from 0 M NaCl to 0.05 M NaCl.

Synopsis

Under the experimental conditions examined, salicylic and phthalic acid exhibit different adsorption behaviours. Phthalic acid adsorption shows a strong pH and ionic strength dependence with maximum adsorption occurring at low ionic strengths and at pH values near the pKa₂ value of phthalic acid (about pH 5.5). Salicylic acid adsorption is much less dependent on pH and ionic strength effects than phthalic acid. These differences strongly indicate that these two organic ligands adsorb on the surface of kaolinite via different adsorption mechanisms. The results obtained from the macroscopic adsorption experiments suggest that outer sphere complexation is the dominant adsorption mechanism for phthalic acid whereas inner sphere complexation is probably the dominant mechanism for salicylic acid. However, it must be noted that macroscopic data can only provide indirect evidence about the binding mechanisms between ions and surface sites. In addition such measurements fail to provide molecular level structural information for the interfacial species. The following section presents the results concerning the application of surface complexation modelling constrained by spectroscopic measurements in order to derive further information about the surface reactions taking place in the kaolinite-ligand systems examined.

Surface complexation modelling

Theoretical Background

Surface complexation models (SCMs) are semi-empirical chemical models that describe the adsorption behaviour of anionic and cationic species on mineral surfaces. In contrast to the traditional method of quantifying adsorption data from adsorption isotherms, SCMs can fit the experimental adsorption data by taking into account different chemical processes that can affect adsorption such as the speciation of solutes and of surface binding sites at different solution conditions, as well as the electrostatic effects of the interface.

All SCMs are based on the same four fundamental principles (Dzombak and Morel, 1990; Ganor et al., 2009): (1) Adsorption takes place at specific binding sites on the surface of the mineral, and surface complexation reactions are comparable to complexation reactions occurring in aqueous solutions, (2) adsorption is governed by the mass law and hence adsorption reactions can be quantitatively described by mass law equations, (3) surface charge develops as a result of ion adsorption reactions on surface sites, (4) an electrostatic correction factor derived from the EDL theory can be applied to these mass law equations in order to account for surface charge effects.

According to the surface complexation theory, all mineral surfaces are composed of functional groups that have the ability to interact with solute species to form surface species. Surface functional groups (or surface binding sites) are fundamental to surface complexation modelling, as the nature and density of these groups will influence the chemical and electrostatic properties of the mineral water interface, as well as the adsorbing capacity of the mineral (Davis and Kent, 1990).

Surface functional groups are generally represented by a generic surface hydroxyl group, >X-OH, which can undergo acid base reactions with hydrogen and hydroxyl ions, as well as adsorption reactions with other solute species. Acid-base equilibria of surface functional groups are often formulated using the 2-pK approach for which surface functional groups can either protonate or deprotonate according to the following surface reactions:



where >XOH represents a neutral surface hydroxyl group. The acid-base reactions of these functional groups are assumed to be the principal contributors to surface charge in solutions where only protons and hydroxyl groups are the only charge determining ions. The corresponding mass law equation and apparent equilibrium constant (K_1^{app}) for equation 1 can be written as:

$$K_1^{app} = \frac{(>XOH_2^+)}{(>XOH)\{H^+\}} \quad 3-6$$

and for equation 2 as:

$$K_2^{app} = \frac{(>XO^-)\{H^+\}}{(>XOH)} \quad 3-7$$

where () represents concentration and { } represents proton activity. The apparent equilibrium constant is dependent on the surface charge and can be determined experimentally from acid-base titrations. To derive an equilibrium constant which is independent of surface charge, an electrostatic term that accounts for the effect of surface charge on adsorption must be introduced in the mass law equations.

The total energy (ΔG_{tot}^o) of an adsorption reaction can be theoretically separated into two components, a chemical or intrinsic term (ΔG_{chem}^o) and a variable electrostatic or Coulombic term (ΔG_{coul}^o) as follows (Stumm, 1992)

$$\Delta G_{tot}^o = \Delta G_{chem}^o + \Delta G_{coul}^o \quad 3-8$$

where $\Delta G_{tot}^o = -RT \ln K$ and $\Delta G_{coul}^o = \Delta ZF\psi$. In these equations R is the ideal gas constant (8.314 J/mol K), T is the absolute temperature (K), ΔZ is the change in surface charge of the surface species due to adsorption, F is the Faraday constant (96490 C mol⁻¹) and ψ is the potential difference between the surface and the bulk solution. The intrinsic term is independent of surface charge and corresponds to the chemical energy required for an ion to bind to a surface site. The coulombic term accounts for the energy required to move a charged particle through an electric field generated by the electric charge on the surface. Therefore an equilibrium constant which is independent of surface charge, termed the intrinsic equilibrium constant, can be given by (Stumm, 1992)

$$K^{app} = K^{int} e^{-\frac{\Delta Z \psi F}{RT}} \quad 3-9$$

where K^{int} is the intrinsic equilibrium constant and K^{app} is the apparent equilibrium constant. This relationship enables the description of surface chemical equilibria through an equilibrium constant which includes an intrinsic equilibrium constant (represents the interaction of the ion with the surface in the absence of surface charge) and an electrostatic correction term (which accounts for the variable electric charge on the surface).

The intrinsic equilibrium constants for the protonation and deprotonation reactions 3-4 and 3-5 can now be expressed as

$$K_1^{int} = \frac{(>XOH_2^+)}{(>XOH)\{H^+\}} e^{\frac{\psi F}{RT}} = K_1^{app} e^{\frac{\psi F}{RT}} \quad 3-10$$

$$K_2^{int} = \frac{(>XO^-)\{H^+\}}{(>XOH)} e^{\frac{\psi F}{RT}} = K_2^{app} e^{\frac{\psi F}{RT}} \quad 3-11$$

In surface complexation modeling the intrinsic equilibrium constants of surface acid-base equilibria are expressed similarly to equations 3-10 and 3-11 and the electrostatic term, which is an exponential Boltzmann factor (unitless), is included as a separate component in model calculations. This electrostatic correction term allows for charge corrections and is also applied to the equilibrium constants describing the adsorption reactions of ions other than OH^- and H^+ . It must be noted that the electrostatic term is not constant because as the reaction progresses the surface charge will be affected. For example during deprotonation additional protons desorbing from the surface will experience increased attraction from the increasing negative charge building on the surface due to successive deprotonation. Similarly, for a protonation reaction as protonation progresses further adsorbing protons will be subject to higher electrostatic repulsion (or lower electrostatic attraction) due to the build-up of positive charge at the surface. Therefore this variable electrostatic correction term accounts for the energy required to transfer an ion through the potential gradient at the mineral water interface.

In all SCMs the effect of variable surface charge is corrected according to the electric double layer (EDL) theory which assumes an electrostatic charge separation at the surface-solution interface. The difference in SCMs lies in the physical description of the electrical double layer at the mineral water interface (Kraepiel et al., 1998; Sahai and Sverjensky, 1997). The two fundamental differences between different models are found in: (1) the electrostatic equations used to describe the surface charge-surface potential relationship and hence in the use of different electrostatic correction factors and, (2) the location of ions to different adsorption planes at the mineral water interface (Westall and Hohl, 1980). Three commonly used SCMs in the literature for the description of ion adsorption are briefly outlined.

The Constant Capacitance Model (CCM)

The constant capacitance model assumes that all ions are adsorbed to specific surface sites in only one plane positioned on the surface, the zero plane and hence the model accounts for only specifically adsorbed ions (inner sphere complexes). Because the capacitance of the mineral-solution interface is dominated by the compact inner layer, the diffuse layer of counter ions of the EDL is neglected (Lützenkirchen, 1999). The electrostatic charge-potential relationship, at the interface is linear and is given by

$$\sigma_0 = C\psi_0 \quad \text{3-12}$$

where σ_0 and ψ_0 are the surface charge and surface potential of the zero plane respectively, and C the capacitance of the mineral-water interface. The surface charge is therefore related to surface potential through a constant capacitance. At the zero plane, the σ_0 charge arises from the specific adsorption of ions, and the surface potential is fixed at ψ_0 . Because the surface potential is independent of the ionic strength of the solution, the capacitance used in this model is limited to a specific type and concentration of background electrolyte (Hayes et al., 1991; Westall and Hohl, 1980). Therefore the equilibrium constants describing the surface reactions, obtained with the CCM, are valid only for one particular ionic strength. The use of CCM is usually restricted to high ionic strength conditions ($>0.01M$) (Hayes et al., 1991).

The Triple Layer Model (TLM)

Unlike the CCM, this model allows the presence of both specifically and non-specifically adsorbed ions at the mineral-water interface. According to this model three

planes exist at the interface, the 0-plane, β -plane and d-plane. Strongly bound ions occupy the 0-plane on the surface of the mineral, while weakly bound ions occupy the β -plane which is positioned adjacent to the surface. The diffuse layer of counter ions is positioned in the d-plane. The overall charge balance equation at the surface-solution interface is given by

$$\sigma_0 + \sigma_\beta + \sigma_d = 0 \quad \text{3-13}$$

where σ_0 , σ_β and σ_d are the charges in the 0-plane, β -plane and the diffuse layer respectively. The charge-potential relations in the three planes can be described by the following equations

$$\sigma_0 = C_1(\psi_0 - \psi_\beta) \quad \text{3-14}$$

$$\sigma_\beta = C_1(\psi_\beta - \psi_0) + C_2(\psi_\beta - \psi_d) \quad \text{3-15}$$

$$\sigma_d = C_2(\psi_d - \psi_\beta) \quad \text{3-16}$$

where C_1 is the capacitance corresponding to the area occupied between the zero and beta plane and C_2 between the beta and d plane (Langmuir, 1997). Because the TLM allows the formation of ion pair complexes between the background electrolyte and surface sites (positioned in beta plane), the equilibrium constants derived are valid over a range of ionic strength conditions (Hayes et al., 1991).

Extended Constant Capacitance Model (ECCM)

This ECCM is similar to the CCM but it possesses two surface planes at the mineral-water interface. This allows the modelling of both inner and outer sphere complexes. The model assumes that the total capacitance of the interface is constant and is allocated into two planes, the inner (or 0-plane) and the outer (β -plane) plane. The relation of the total capacitance (C_{tot}) with respect to the capacitance values in each of the two surface planes is given by

$$\frac{1}{C_{tot}} = \frac{1}{C_1} + \frac{1}{C_2} \quad \text{3-17}$$

where C_1 is the capacitance of the inner plane (0-plane) and C_2 of the outer plane (β -plane). The charge potential relationship in the two planes is given by the following equations

$$\psi_0 - \psi_\beta = \sigma_0 / C_1 \quad \text{3-18}$$

$$\psi_\beta = (\sigma_0 + \sigma_\beta) / C_2 \quad \text{3-19}$$

where ψ_0 and ψ_β are the potential values at the 0-plane and beta plane respectively (Nilsson et al., 1996). Similarly to the CCM, the effect of counter ions can be neglected and thus the equilibrium constants derived are restricted to a particular ionic strength concentration. Effectively the ECCM can be visualised as the TLM without the diffuse layer. The main concepts discussed for the three models are illustrated in Figure 3-25.

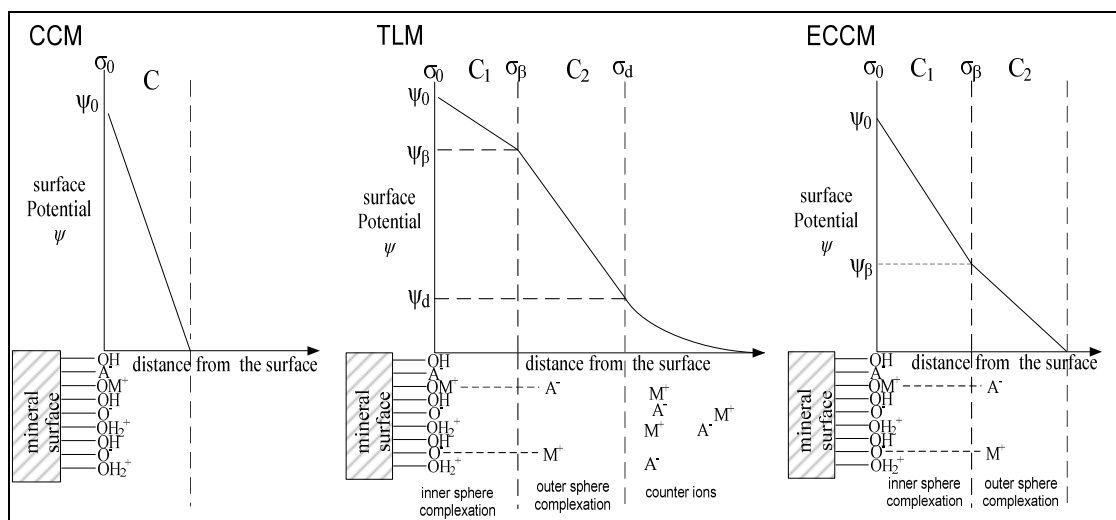


Figure 3-26 Schematic representation of the position of surface species at the surface-solution interface and of the relationship between surface charge (σ) and surface potential (ψ) according to the constant capacitance model (CCM); the triple layer model (TLM) and the extended constant capacitance model (ECCM).

Application of surface complexation modelling

SCMs are widely used for the description of ion adsorption on mineral surfaces. Determination of the acid-base properties of mineral surfaces is perhaps the most commonly used application of surface complexation models. The description of acid-base titration data using surface complexation modelling provides an atomic-level description of surface properties including surface site densities, acidity constants, and interfacial capacitance. Such information is required for the prediction of the charging behaviour of mineral surfaces and for the application of surface complexation models to ion adsorption data.

Although surface complexation modelling has become increasingly popular, there are still a number of drawbacks associated with the application of surface

complexation models. These drawbacks primarily arise from the different modelling approaches that can be used for the description of titration and adsorption data. Differences concerning the modelling approach include: the choice of a particular SCM over a number of available SCMs; the assumptions made regarding the chemical reactions taking place at the interface; methods used to determine the various input parameters required by the specific SCM chosen; and the parameter optimisation procedure employed. All these factors can give rise to significant variations in modeling results. Although the main problems and limitations associated with surface complexation modelling have been discussed elsewhere (e.g. Dzombak and Morel, 1990; Hayes et al., 1991; Lützenkirchen, 1999; Lützenkirchen, 1998; Zuyi et al., 2000), the aforementioned factors that need to be considered for the formulation of a modelling approach will be introduced in the following section. The aim of the following discussion is to show that surface complexation modelling should be used with caution and that modelling results should be confirmed or used in conjunction with other experimental techniques. The main problems of surface complexation modeling are categorised here in three broad groups relating to the different stages of the modelling procedure.

(1) Choice of surface model

The first decision one has to consider in surface complexation modeling is the choice of the type of surface complexation model to be used. It has been shown that different surface complexation models can simulate a particular experimental dataset equally well, but different model outputs may be determined by each model (e.g. Westall and Hohl, 1980). The degree of complexity required for the description of the chemical reactions taking place at the mineral water interface is an important factor for the choice of the particular SCM used. Although more complex models can be more successful in simulating adsorption data over a wider range of experimental conditions, they require a higher number of input parameters. From the common surface complexation models employed to simulate proton adsorption data, the triple layer model (TLM) requires the highest number of adjustable parameters and the diffuse layer model (DLM) the lowest.

Findings from other independent methods, such as spectroscopy, are fundamental in a successful modelling strategy because they can impose constraints on model parameters such as the number and type of surface species forming on the surface. Therefore prior information regarding the number of surface species formed can guide the selection of an appropriate model for a given system. For example the

constant capacitance model (CCM) can only model inner sphere complexes, whereas the triple layer model accommodates for both inner and outer sphere surface complexes and can also incorporate in model computations the interactions of background electrolyte ions with surface sites.

(2) Model parameters

Modelling of adsorption data requires the use of different number and type of input parameters which are dictated by the choice of the particular SCM used. Input parameters required include the specific surface area of the mineral, surface species, surface site densities, surface complexation constants and interfacial capacitance(s). Model input parameters can be obtained either by modelling the experimental data (i.e. adjustable parameters) and/or some can be estimated independently by other techniques. Adjustable parameters can be optimised according to the SCM used so that model outputs provide a satisfactory fit to the experimental data. If input parameters required by the model can be estimated by other independent techniques they may be introduced as fixed parameters in model calculations. For example the specific surface area of the mineral is usually determined by means of BET analysis and is therefore not regarded as an adjustable parameter.

In addition, the modeller needs to decide on other model factors required to fit the adsorption data such as the number of surface sites and the type of surface species involved in complexation reactions. According to surface complexation theory, surface sites are surface reactive groups which participate in proton donor-acceptor reactions, as well as, in other ion adsorption reactions. SCMs can account for the chemical heterogeneity of the mineral surface by allowing different types of surface sites, with different proton affinities, to participate in the adsorption of ions (multisite approach). Conversely in the single site approach all surface sites are assumed to be energetically identical and therefore there is no preferential adsorption of solute ions to particular surface sites (Sahai and Sverjensky, 1997).

The number of different types of surface sites, and their respective densities, are important model parameters which have to be estimated with some confidence in order to obtain reliable results. The number of different surface sites is typically determined by model fits of acid-base titration data and commonly the minimum number of discrete surface sites which can satisfactorily fit the experimental data is chosen. Despite the structural heterogeneity of mineral surfaces, one or two types of adsorption sites are usually found to satisfactorily describe the acid-base properties of common mineral (hydr)oxides such as iron and aluminium oxides and clay minerals such as kaolinite

(e.g. Angove et al., 1997; Du et al., 1997; Hwang and Lenhart, 2009; Nordin et al., 1998; Sahai and Sverjensky, 1997; Villalobos and Leckie, 2001; Westall and Hohl, 1980).

It has to be noted however that the number of surface sites used for the description of the acid-base titration data is only used for modelling purposes and therefore does not necessarily represent the exact number of different types of adsorption sites existing on the mineral surface. Furthermore, the proton active surface sites determined by fitting acid-base titration data, are also assumed to participate in surface complexation reactions with other ions. However the assumption that adsorbates can only bind to the proton active sites may not hold true and is an over-simplification because ions could interact with surface functional groups which are not proton active (Persson and Lövgren, 1996). Similarly ions may not have the ability to bind with all the surface sites that exhibit proton activity.

Because the number of surface sites is typically a fitted parameter, the number of surface sites estimated for the same mineral may vary depending on the experimental titration data and modelling approach. Clearly if a higher number of surface sites is used to describe a chemical equilibrium problem, then a higher number of adjustable parameters will be required (i.e. higher number of binding constants and site densities). While simplicity ought to be the guiding principle of any surface complexation model, physically realistic parameters which represent the mineral-solution interface must also be used. Therefore, there must be a compromise between model complexity (and hence computational complexity) and model validity. Computational complexity increases with the number of additional chemical reactions considered in the model.

Site densities can be estimated by different experimental or theoretical methods such as isotopic-exchange experiments, crystallographic parameters, potentiometric titrations (maximum proton adsorption), and adsorption isotherms (adsorption maxima at constant pH) obtained from various organic and inorganic ions. Due to the difficulties associated with determining the concentration of surface sites experimentally, surface site density is also commonly treated as an adjustable parameter in the data fitting process of acid-base titration data. It also follows that an accurate estimate of site densities implies that the surface area of the mineral must also be determined with confidence. Again different methods have been employed for surface area measurements, with the BET method being the most popular surface measurement method. Despite its widespread use, the accuracy of the results obtained by the BET method is also subject to criticism. More particularly it is argued that this method

underpredicts the surface area of some minerals, e.g. for kaolinite, by a factor of 10-20 (Xie and Walther, 1992).

Alternatively, surface site density for minerals with well defined crystal structures can be estimated from crystallographic considerations. It has been proposed that a fixed number of surface sites should be used in order to provide a consistent modelling approach and hence enable the comparison between the results obtained from different studies. For example a fixed site density value of 2.31 sites nm⁻² has been previously proposed for all minerals (e.g. Goldberg and Johnston, 2001).

Finally interfacial capacitance values may be introduced as either fixed or adjustable parameters. For example, for the TLM model a fixed capacitance value at 0.2 F/m² for the outer plane (C₂ layer) has been proposed (Sahai and Sverjensky, 1997). Alternatively the interfacial capacitance can be treated as an adjustable parameter and the exact value chosen will be based on the ability of the particular value to simulate titration data. In many cases, though, a range of capacitance values may provide similarly good fits.

The values chosen for the above mentioned parameters can have a significant effect on the modelling results obtained. For example, Hayes et al. (1991) showed that the optimised surface protonation constants (log K), evaluated by the CCM, are influenced by the site density and the interfacial capacitance used in the simulations of titration data. Unfortunately even for the simpler and well studied minerals there is still no universal agreement on the physical and electrostatic model input parameters to be used. In order to overcome this limitation and be able to compare surface complex formation constants obtained from different experimental data, the interfacial physical and electrostatic properties used in modelling must be the same for any given mineral (Westall and Hohl, 1980). More in depth discussions regarding model parameter evaluation of the surface protonation parameters can be found elsewhere (e.g. Hayes et al., 1991; Lützenkirchen, 1999; Sahai and Sverjensky, 1997; Westall and Hohl, 1980).

The choice of these surface protonation parameters (e.g. site densities, interfacial capacitance, protonation constants) can have a significant effect on the modelling results of ion adsorption data (e.g. Hwang and Lenhart, 2009; Johnson et al., 2004a). The importance of using model parameters that are able to predict results that are consistent with spectroscopic data is highlighted by Hwang and Lenhart (2009) which used the ECCM for the description of phthalate adsorption on haematite. Predicted surface speciation was highly dependent on the input model parameters used including site densities and interfacial capacitance. Therefore in addition to the choice of appropriate

surface complexation reactions, the reliability of surface complexation models depends on the choice of appropriate input model parameters (Hwang and Lenhart, 2009).

(3) Fitting procedure

Perhaps the most serious drawback in the application of surface complexation modelling is associated with the data fitting procedure. Model fits to experimental data are typically obtained using computer codes that incorporate all the model parameters required for the description of the chemical equilibrium problem. FITEQL, which uses a simultaneous nonlinear least squares fitting routine, is the most widely used computer program in surface complexation modelling. The equilibrium model defined for a chemical system is iteratively solved and model adjustable parameters are optimised in order to minimise the difference between model and data values at each experimental point. More details about the optimisation procedure in FITEQL will be given later on.

As discussed earlier, surface complexation models require many input parameters which in some cases cannot be independently determined and therefore are treated as adjustable parameters in the data fitting procedure. Westall and Hohl (1980) demonstrated that the simultaneous optimisation procedure of a large number of adjustable parameters cannot retrieve unique values for any of these parameters. This problem arises because various adjustable parameters are interdependent, for any single SCM, and therefore various combinations of the adjustable parameter values can give a satisfactory fit to the experimental data. The problem of determining a unique parameter set is further exacerbated if the model has a large number of adjustable parameters. FITEQL typically fails to converge when three or more adjustable parameters are optimised simultaneously. In such cases the adjustable model parameters have to be optimised in a stepwise fashion and depending on which parameters were first optimised the model may yield different optimised parameters. Therefore when a large number of adjustable parameters are required to model the acid-base titration data, then a universal systematic approach for the optimisation of different model parameters should also be employed. Although some studies provide information on how the different parameters have been optimised (e.g. Hayes et al., 1991; Lutzenkirchen, 1999; Peacock and Sherman, 2005) in most studies such information is not included. A standardised optimisation procedure is particularly important for the evaluation of the acid-base properties of mineral surfaces (site density, surface acidity constants, interfacial capacitance) since these properties are subsequently used as fixed parameters when modelling the adsorption behaviour of ions.

In summary, the ability of surface complexation modelling to describe ion adsorption behaviour is limited by a number of uncertainties and assumptions of the modelling procedure. SCMs require a number of input parameters, such as site densities, surface species, surface equilibrium constants, and interfacial capacitances that in many cases cannot be independently determined or verified. Because these model parameters are often poorly constrained, they are commonly evaluated on the basis of their ability to adequately simulate experimental titration and adsorption data. However, such a model fitting approach may not always lead to a unique set of model parameters since the use of different modelling approaches (e.g. electrostatic model used, number of adjustable parameters, and optimisation procedure) can provide different sets of optimised model parameters that can describe the same experimental data equally well. Unfortunately, although widely recognised, there is not a common modelling approach on how different model input parameters should be derived. This lack of common methodology can lead to significant inconsistencies in the reported model outputs derived for the description of adsorption data. Having discussed the three main obstacles involved in calculating models to describe adsorption, we now present details about the model algorithm and parameters used to describe the mineral surface before going on to the next section which will show the results of the modelling of our experimental data.

Overview of FITEQL

The non linear optimisation program FITEQL version 4.0 (Herbelin and Westall, 1999) was used to fit the proton and ligand adsorption behaviour of kaolinite. FITEQL is a geochemical equilibrium computer program that determines surface complexation parameters (e.g. surface site concentration, formation constants of surface species, interfacial capacitance) from experimental adsorption data. When modelling adsorption data, FITEQL optimises model parameters of a user-defined chemical equilibrium problem so that the difference between the experimental data and calculated model values is minimised.

The modelling procedure using the FITEQL algorithm consists of two main steps: (a) description of the chemical equilibrium problem, and input of model parameters (b) optimisation of adjustable model parameters. The chemical equilibrium problem is mathematically formulated using a tableau format which includes the chemical species that need to be considered in the problem, and the chemical components that define these species. An example of such a tableau format is given in

Table 3-4. The top row lists the chemical components required to define the chemical species of the equilibrium problem which are listed in the first column. The numbers across each row represent the exponents of component concentrations for each particular chemical species, and hence define the mass law equation describing the formation of the particular chemical species.

Table 3-4 Tableau format of the stoichiometric coefficients for the surface reactions relevant to the adsorption of an anionic species.

Species	Components				Reaction
	$\exp(-F\psi/RT)$	$>XOH$	L^{2-}	H^+	
H^+	-	-	-	1	
OH^-	-	-	-	-1	$H_2O \leftrightarrow OH^- + H^+$
HL^{-1}	-	-	1	1	$L^{2-} + H^+ \leftrightarrow HL^{-1}$
L^{2-}	-	-	1	-	
$>XOH$	-	1	-	-	
$>XOH_2^+$	1	1	-	1	$>XOH + H^+ \leftrightarrow >XOH_2^+$
$>XO^-$	-1	1	-	-1	$>XOH \leftrightarrow >XO^- + H^+$
$>XL^{1-}$	-1	1	1	1	$>XOH + L^{2-} + H^+ \leftrightarrow >XL^{1-} + H_2O$
XHL^0	0	1	1	2	$>XOH + L^{2-} + 2H^+ \leftrightarrow XHL^0 + H_2O$

Overall the input parameters required by the programme for the description of the chemical system include: surface area, site densities, number of surface species, surface protonation constants, stoichiometries of the surface complexation reactions, formation constants of surface species, and speciation reactions of aqueous ions. An electrostatic term describing the relationship between charge and potential at the interface, valid for the chosen electrostatic model, is included as a separate component in the input file as shown in Table 3-4 ($\exp(-F\psi/RT)$ component). In addition, depending on the electrostatic model used other input parameters may include background electrolyte binding constants and interfacial capacitance.

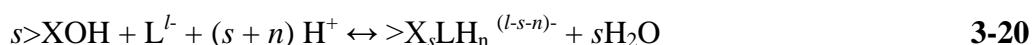
The different model input parameters can be assigned as either fixed values (known parameters) or adjustable values (unknown parameters to be optimised). It must be noted that the unknown model parameters are not calculated by the model but instead initial estimates are supplied by the user and these are optimised by the FITEQL code in order to obtain the best fit to the experimental data. In general, when modelling acid

base titration data of a particular mineral, site densities, interfacial capacitance and proton binding constants are the optimised model parameters. When modelling ion adsorption data these surface parameters are introduced as fixed parameters in the problem and the fitting procedure of the adsorption data is carried out by optimising the formation constants of the surface species assumed to exist on the surface.

The optimisation procedure is based on adjusting the model parameters in order to minimise the difference between experimental and predicted values for components whose total and free concentrations are known (assigned as Type II components in FITEQL). For acid-base titration data, both the total and free concentrations of H⁺ ions are known and therefore H⁺ is assigned as a Type II component. Conversely for modelling ion adsorption data, the adsorbing cationic or anionic species are assigned as Type II components.

The goodness of fit of model calculations is evaluated according to the overall variance, $V(Y) = WSOS/DF$, which is the weighted sum of squares of the residuals between calculated and experimental values ($Y = Y_{calc} - Y_{exp}$), divided by the degrees of freedom. A decrease in this value indicates a better fit, and generally a value less than 20 usually denotes a very good fit (Herbelin and Westall, 1999). On the other hand, $V(Y)$ values less than 0.1 typically indicate that the model has too many adjustable parameters (Dzombak and Morel, 1990).

A general equation which can be used for the description of different possible surface-ligand inner sphere species is:



where $>XOH$ denotes a surface site, s and n represent the number of surface sites and number of protons participating in the complexation reaction respectively, and l the ligand charge. The above equation shows that the formation of a particular surface species can be represented by the stoichiometric coefficients of three components, namely the number of surface sites, number of protons involved in the complexation reaction, and the charge of the ligand. These stoichiometric coefficients which are specified in the input file (as shown in Table 3-4) are systematically varied in different optimisation runs and the reaction (or combination of reactions) which gives the best model fits to the experimental data, following the optimisation of the adjustable mode parameters, is accepted as valid for the given system. During modelling all the different possible reaction stoichiometries must be considered, as well as the coexistence of two or more types of surface complexes.

Kaolinite structure and properties

Kaolinite's chemical formula can be written as $\text{Al}_2\text{Si}_2\text{O}_5(\text{OH})_4$ and based on its structural features it is classified as a 1:1 layer silicate mineral. The ideal structure of kaolinite consists of a sheet of tetrahedrally coordinated silicon atoms, bound to a sheet of dioctahedrally coordinated aluminium atoms (gibbsite-like sheet). The tetrahedral and dioctahedral sheets are linked together via common oxygen atoms (Al-O-Si) and successive layers are bound together via hydrogen bonds (Figure 3-27).

In each silica tetrahedron three oxygen atoms lie in the same plane, forming the base of the tetrahedron, and the fourth oxygen (termed apical oxygen) points in a direction perpendicular to the plane. Each silicon atom is bonded to three other silicon atoms via bridging oxygen atoms (Si-O-Si) and therefore the shared oxygen atoms are valency satisfied. The apical oxygen atoms, however, carry a negative charge which needs to be satisfied by coordinating to ions outside the tetrahedral sheet. In the aluminium octahedral sheet each aluminium atom shares four hydroxyl groups with neighbouring aluminium atoms and is also bonded to two apical oxygen atoms from the silicon sheet. One hydroxyl group (termed inner hydroxyl group) is facing towards the shared plane of the aluminium and silicon sheets whereas the remaining three hydroxyl groups (termed outer hydroxyl groups) are facing towards the external surface of the octahedral sheet. These outer hydroxyl groups generate the gibbsite-like surface in the aluminium octahedral sheet (Huertas et al., 1998).

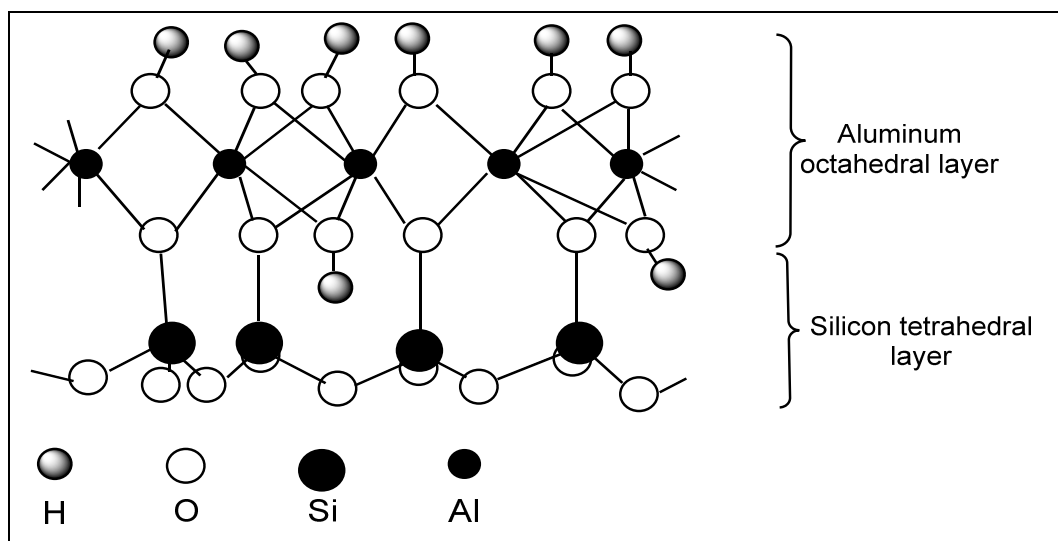


Figure 3-27 Idealised structural representation of kaolinite. Adopted from Warne et al. (2000).

The charge on the surface of kaolinite arises from the existence of both permanent and non permanent (pH dependent variable) charges. The non permanent surface charges develop from the acid-base behaviour of surface functional groups. Surface groups involved in protonation/deprotonation reactions include the Al-OH-Al groups of the octahedral basal plane and terminal hydroxyl groups at the edge sites (Si-OH and Al-OH) (Kraepiel et al., 1998). Hydroxyl groups located in the aluminium basal plane have a higher acidic character than aluminol edge group and hence protonate at lower pH values (Ganor et al., 2003; Huertas et al., 1998). Therefore edge hydroxyl groups are generally considered to be more reactive than basal hydroxide groups. Silanol edge groups can only deprotonate and contribute only to the negative charge (Brady et al., 1996). Due to the hydrophobic character of the oxygen atoms in Si-O-Si bonds and Si-O-Al bonds, these groups do not participate, at least significantly, in proton adsorption reactions (Huertas et al., 1998).

Besides the pH-dependent charge, the surface of kaolinite carries a permanent negative charge originating from isomorphous substitutions in the crystal lattice. For example aluminium can replace a silicon atom in the tetrahedral silica sheet ($[\text{Si-O-Si}]^0 \rightarrow [\text{Si-O-Al}]^{-1}$) resulting in a single negative charge for each substitution (Wieland and Stumm, 1992). Clay minerals generally have a net negative charge at all pH values due to the much higher area of the permanently negative sites relative to the area of edge sites. However in contrast to other common clays, the importance of the permanently negative charged sites in kaolinite is much lower. Therefore the amphoteric nature of edge hydroxyl groups and their associated charge is more important for kaolinite's net surface charge than in other clay minerals.

Modelling the acid base properties of kaolinite

Potentiometric acid-base titrations were performed to determine surface parameters that can adequately account for the surface acid-base reactions of kaolinite. These parameters include the number of discrete surface sites available for proton adsorption, site densities, protonation constants, and interfacial capacitance. Surface parameters obtained from titration data can then be used for the development of surface complexation models that can describe the adsorption of salicylic and phthalic acid on kaolinite.

The adsorption of protons on kaolinite as a function of pH and three different ionic strengths, obtained from the potentiometric acid-base titrations, is shown in Figure 3-28. As mentioned in the methodology section, the change in proton density at each titration point can be calculated according to

$$\Delta C_s = (C_a - C_b - [H^+] + [OH^-]) \frac{V}{S.A}$$

where ΔC_s is change in surface proton concentration (mol m^{-2}). This equation enables the calculation of the relative surface concentration of protons as a function of pH, rather than the absolute surface concentrations. The calculation of absolute proton surface concentrations requires prior knowledge about the pH_{pznpc} of the mineral surface (Schroth and Sposito, 1997). As discussed by Ganor et al. (2003) the main reason for the differences between the titration curves of kaolinite reported in the literature can be attributed to the different pH_{pznpc} values used. After the kaolinite titration curves were recalculated assuming a zero proton density at about pH 5, the authors obtained a good agreement between the titration curves. In the present study, a pH_{pznpc} value of 5.4 was assumed for the calculation of absolute surface proton concentrations. This value is similar to the pH used by Ganor et al. (2003) as a common reference point for the zero proton surface density. Furthermore pH 5.4 is also the pH_{pznpc} value estimated by Schroth and Sposito (1997) for the KGa-2 kaolinite reference sample used in the present study.

Figure 3-28 shows that a higher proton surface density is obtained at lower pH values and lower ionic strengths. Furthermore, it can be seen that there is no common intersection point of the titration curves at different electrolyte concentrations. A higher proton binding on kaolinite at lower background electrolyte concentrations is consistent with the findings of some previous studies which observed a small increase in the degree of protonation at lower ionic strengths (e.g. Heidmann et al., 2005; Huertas et al., 1998; Peacock and Sherman, 2005). Other studies, however, observed a more complex relationship between ionic strength and proton adsorption as a function of pH. Increased protonation at lower ionic strengths was only seen at acidic pH values whereas at basic pH this trend was reversed (i.e. higher ionic strength favouring protonation) in the potentiometric titrations reported by Kraepiel et al. (1998) and Carroll-Webb and Walther (1988). Furthermore, Kraepiel et al. (1998) observed that ionic strength had a significant effect on protonation only for electrolyte concentrations between 0.1 to 0.01 M whereas at higher concentrations (0.1-1 M) the ionic strength had

a negligible effect on the acid base titration curves of kaolinite. Contrary to these findings, Tertre et al. (2006) could not identify a distinct trend between ionic strength and proton adsorption as the titration curves obtained at $I = 0.5, 0.1,$ and 0.025 M NaClO_4 , were essentially superimposed.

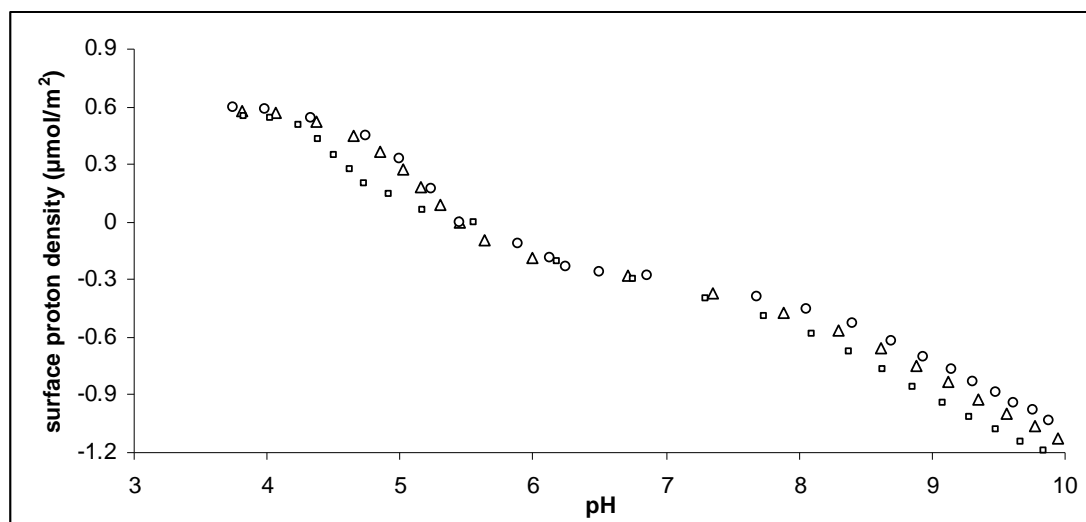


Figure 3-28 Proton surface density on kaolinite at 0.1 M (squares), 0.01 M (triangles) and 0.001M (circles), obtained from acid-base titrations. The background electrolyte is NaCl.

Common to most kaolinite studies, however, is the absence of a common intersection point between the titration curves obtained at different ionic strengths, a feature typically seen for simple (hydr)oxides. The lack of a common intersection point is attributable to the presence of permanent surface charge on kaolinite (Kraepiel et al., 1998; Tertre et al., 2006). The existence of both permanent and variable surface charge can also explain the variability in the effects of ionic strength on proton uptake observed in different studies. Different kaolinite samples are expected to exhibit different proton consumption behaviours (i.e. shapes of titration curves) since ionic strength-induced effects can be significantly influenced by the relative magnitude of variable and permanent surface charges (Kraepiel et al., 1998). Therefore kaolinite samples having different cation exchange capacity will give rise to acid-base titration curves of different shapes and responses to ionic strength effects.

Kaolinite is a well studied mineral and its surface properties and chemistry have been investigated for a long time by numerous researchers, and surface titration data obtained for different kaolinite samples have been successfully fitted to various surface complexation models (e.g. Angove et al., 1998; Brady et al., 1996; Heidmann et al., 2005; Huertas et al., 1998; Ikhsan et al., 1999; Peacock and Sherman, 2005; Tertre et

al., 2006; Wieland and Stumm, 1992). However the models proposed for the description of the acid-base titration curves show a considerable variation and as a result different findings have been reported regarding the surface properties and chemistry of kaolinite. Several reasons could explain the disparity in the reported results including differences in the morphology of the samples used, experimental procedures, and data treatment. Furthermore, and most importantly, the modelling approach employed for the determination of surface parameters varied significantly in different studies. The main differences include the number and nature of available proton binding sites, the density of each of these sites, and the electrostatic models used to fit the experimental data.

Table 3-5 shows examples of different modelling approaches employed in the literature for the description of the acid-base reactions taking place at the surface of kaolinite. It can be seen that there is a wide variety of surface reactions used for the description of kaolinite's acid-base properties. Proton binding sites include both edge and basal surface active sites, as well as cation exchange sites. This list is not exhaustive but it does give an indication of the diverse set of surface reactions that have been previously proposed for the acid-base properties of kaolinite.

In light of previous findings regarding the proton adsorption behaviour of kaolinite, a multi-site modelling approach was adopted. The main objective of fitting the acid-base titration data of kaolinite was to identify the minimum number of types of surface sites (i.e. the simplest model) that could give a satisfactory fit to the data. As already mentioned the proton adsorption/desorption reactions on the surface of kaolinite primarily take place onto (a) the permanently charged sites mainly occurring on the siloxane basal plane, (b) aluminol groups which are located at both edge and basal plane sites and, (c) silanol groups located at edge surface sites.

A number of different models were tested in order to obtain the model that gives the best fit to the experimental data. These models included a combination of different number and types of surface sites that could participate in proton uptake reactions. Initially a two-site model was examined which assumed a silanol site and an aluminol site (model 1). According to this model aluminol groups have an amphoteric character (can protonate and deprotonate) and no distinction between basal and edge aluminol sites was made. Furthermore, in accordance with previous studies (Brady et al., 1996; Brady and Walther, 1989), silanol groups could only dissociate because of their strong acidic character.

Table 3-5 Examples of varying modelling approaches employed for the description of the acid-base properties of kaolinite.

Surface site	Density $\mu\text{mol}/\text{m}^2$	Surface reactions	log K	SCM	Study
AlOH (edge or basal)	1.5	$>\text{AlOH} + \text{H}^+ \leftrightarrow >\text{AlOH}_2^+$ $>\text{AlOH} \leftrightarrow >\text{AlO}^- + \text{H}^+$	4.08 -10.25	CCM	(1)
Al ₂ OH (basal plane)	5	$>\text{Al}_2\text{OH} + \text{H}^+ \leftrightarrow >\text{Al}_2\text{OH}_2^+$ $>\text{Al}_2\text{OH} \leftrightarrow >\text{Al}_2\text{O}^- + \text{H}^+$	1.85 -10.25		
SiOH (edge site)	1.4	$>\text{SiOH} \leftrightarrow >\text{SiO}^- + \text{H}^+$	-7.13		
AlOH (edge site)	0.7-1	$>\text{AlOH} + \text{H}^+ \leftrightarrow >\text{AlOH}_2^+$ $>\text{AlOH} \leftrightarrow >\text{AlO}^- + \text{H}^+$	6.5 -8.5	CCM	(2)
AlOH (basal plane)	1.2-2	$>\text{AlOH} + \text{H}^+ \leftrightarrow >\text{AlOH}_2^+$ $>\text{AlOH} \leftrightarrow >\text{AlO}^- + \text{H}^+$	3.4 -8.4		
XO (siloxane layer-permanent charge)	2.7	$\text{XOH} + \text{Na}^+ \leftrightarrow \text{XONa} + \text{H}^+$ $2\text{XOH} + \text{Al}^{3+} \leftrightarrow (\text{XO})_2\text{Al}^+ + 2\text{H}^+$	-2.9 -0.34		
SOH (general site)	3.25	$>\text{SOH} + \text{H}^+ \leftrightarrow >\text{SOH}_2^+$ $>\text{SOH} \leftrightarrow >\text{SO}^- + \text{H}^+$	3.96 -7.24	CCM	(3)
X ⁻ (siloxane layer-permanent charge)	2.25	$\text{XH} + \text{K}^+ \leftrightarrow \text{XK} + \text{H}^+$	-2.85		
SOH (general site)	18.3 ^a	$>\text{SOH} + \text{H}^+ \leftrightarrow >\text{SOH}_2^+$ $>\text{SOH} \leftrightarrow >\text{SO}^- + \text{H}^+$	2.52 -7.51	ECCM	(4)
XH (siloxane layer-permanent charge)	1.6 ^a	$\text{X}^-\text{---H}^+ + \text{Na}^+ \leftrightarrow \text{X}^-\text{---Na}^+ + \text{H}^+$	-3.06		
AlOH (edge site)	0.83	$>\text{AlOH} + \text{H}^+ \leftrightarrow >\text{AlOH}_2^+$ $>\text{AlOH} \leftrightarrow >\text{AlO}^- + \text{H}^+$	4.8 -6.1	DDLMM	(5)
SiOH (edge site)	0.83	$>\text{SiOH} \leftrightarrow >\text{SiO}^- + \text{H}^+$	-7.7		
XH siloxane layer	3.7	$\text{XH} + \text{Na}^+ \leftrightarrow \text{XNa} + \text{H}^+$	-7.2		
AlOH (edge + basal)	1.31 ^b	$>\text{AlOH} + \text{H}^+ \leftrightarrow >\text{AlOH}_2^+$ $>\text{AlOH} \leftrightarrow >\text{AlO}^- + \text{H}^+$	2.33 -5.28	CCM	(6)
SiOH (edge + basal)	2.26 ^b	$>\text{SiOH} \leftrightarrow >\text{SiO}^- + \text{H}^+$	-8.23		

(1) Huertas et al. (1998). Sample used was from Twiggs County, Georgia (Ward's Natural Science Establishment. Values reported are averaged for three ionic strengths, I= 0.1, 0.01 and 0.001M KClO₄.

(2) Wieland and Stumm (1992). Commercial china clay from St. Austell/Cornwall U.K (English Lovering Pochin & Co). I= 0.1M NaNO₃

(3) Ikhsan et al. (1999). Acid washed commercial kaolinite (Ajax chemicals). I= 0.05 M KNO₃.

(4) Peacock and Sherman (2005). Sample from the ECC International Lee Moor China Clay Pit, Cornwall, U.K. I= 0.1 M NaNO₃.

(5) Tertre et al. (2006). Commercial sample from St Austell, U.K (English China Clays). I= 0.5 M NaClO₄.

(6) Brady et al. (1996). Poorly crystallised kaolinite reference sample KGa-2 from Washington County, Georgia (Clay Minerals Society). I= 0.1 M NaCl.

(^a) study reported site densities in mol/g. Site densities were converted to mol/m² by using the B.E.T. surface area (m²/g) given in the study.

(^b) study reported site densities in mol/L. Site densities were converted to mol/m² by using values provided in the paper (i.e. S.A of 10.5 m²/g and a kaolinite suspension of 80g/L)

Once the titration data was modelled according to model 1 then additional surface sites were added to this model in order to investigate whether better fits could be obtained. Two different three-site models were tested, one where an additional aluminol group was considered (model 2) and one model where an additional permanent negatively charged site was considered (model 3). In model 2 one aluminol site corresponds to an edge site and one aluminol site to a basal site. For this model, the site density of aluminol and silanol edge sites ratio was kept constant (1:1) in order to be

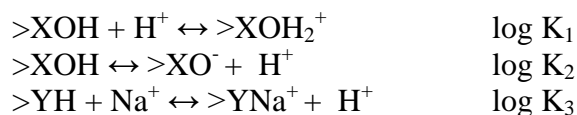
consistent with the ratio of aluminium and silicon atoms in kaolinite's structure. The use of these three-site models did not offer any advantage over the two-site model as the goodness of fit calculated by FITEQL was similar for all three models.

A different surface model examined included only one pH dependent surface site (no distinction between silanol and aluminol groups) and one permanent negatively charged site (model 4). Such a two-site surface model has been previously used (see table 3-5; studies 3 and 4) and also produced model fits that were similar to those obtained for models 1-3. Despite the similarities in model fits obtained from all the different models examined, model parameters estimated by model 4 were used for the modelling of ligand adsorption data for two reasons.

(1) For consistency with models previously derived for the adsorption of organic ligands and metal cations on kaolinite (Angove et al., 2002; Angove et al., 1997; Angove et al., 1998; Ikhsan et al., 2004b; Lackovic et al., 2003a; Lackovic et al., 2003b). These previous studies also used a two-site model consisting of one variable-charge site and one permanently charged site. Proton binding constants used in these studies are in very good agreement with those calculated by the model in the present study.

(2) The optimised model parameters calculated by the present model provided the best fit to the experimental adsorption data when they were subsequently introduced as fixed parameters for the kaolinite-ligand systems. Other models examined either produced poorer model fits or the surface speciation predicted was inconsistent with the IR spectroscopic data.

The ability of the proposed model to describe the proton adsorption data is shown in Figure 3-29 and the optimised acid-base properties of kaolinite, at 0.01 M, as calculated by the model are listed in Table 3-6. According to this model, two types of surface active sites participate in surface protonation reactions, represented by the following reactions



where >XOH represents a pH dependent surface charge site. Although no distinction is made between aluminol (AlOH) and silanol (SiOH) groups, it is expected that the XOH groups involved in adsorption reactions are primarily AlOH surface groups located at the edge sites and on basal planes of kaolinite (Angove et al., 1998; Peacock and

Sherman, 2005; Wieland and Stumm, 1992). Y^- represents a permanent negatively charged site which can exchange a proton with a background electrolyte sodium ion.

The model required the optimisation of 5 adjustable parameters for any given capacitance value: surface densities for the two proton-active sites (XOH and Y^-), two proton binding constants for the pH-dependent surface site ($\log K_1$ and $\log K_2$), and one equilibrium constant for the ion exchange reaction of the permanent negatively charged site ($\log K_3$). Simultaneous optimisation of all five parameters could not be carried out as FITEQL would not converge when all five parameters were assigned as optimised parameters. Therefore a sequential optimisation procedure was employed where site densities were optimised first while the protonation constants were fixed to values obtained by Lackovic et al. (2003a). Then the proton binding constants were optimised in a second optimisation run in which the optimised site density values were used as fixed parameters. It must be noted that different optimisation procedures were found to influence the optimised model parameters.

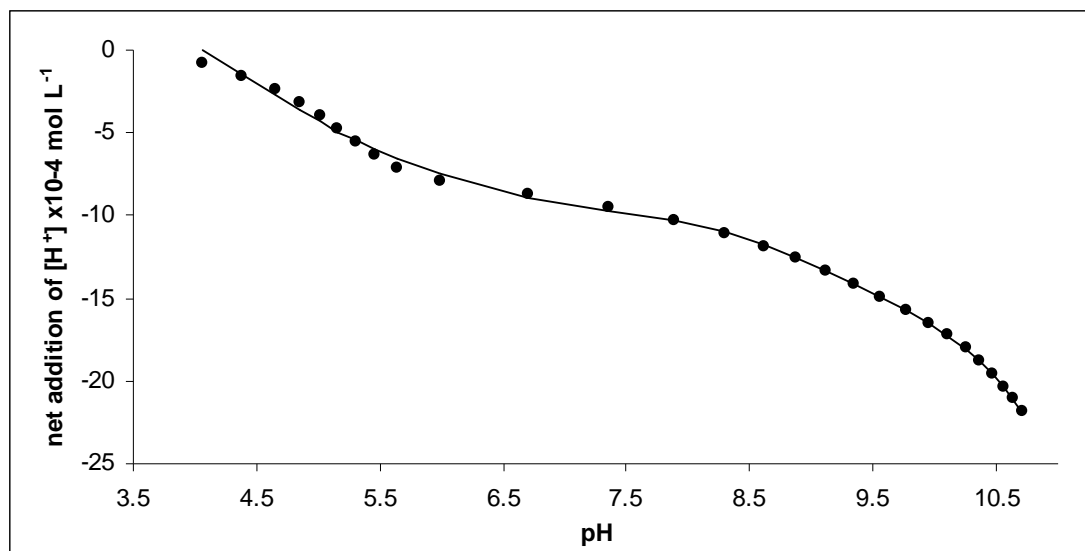


Figure 3-29 Potentiometric titration data for a kaolinite suspension, at $I = 0.01$ M, shown as net hydrogen ions added (negative values denote addition of hydroxyl ions). Symbols represent experimental data points and the line represents the theoretical titration curve calculated by the constant capacitance surface complexation model according to the model proposed using the parameters given in Table 3-6.

The capacitance of the interface was also treated as an adjustable parameter. Because the capacitance can not be optimised by FITEQL, the optimisation procedure described above was carried out at different capacitance values in order to obtain the value that provided the best fit. Model fits to the titration data were relatively insensitive for capacitance values from 1 to 2.5, when all the other parameters were allowed to vary

with the overall $V(Y)$ ranging from 25 to 16. However different capacitance values resulted in different optimised values, with site density being the most sensitive parameter to changes in interfacial capacitance. A range of interfacial capacitances has been previously used when modelling the acid-base titrations of kaolinite. Although a capacitance value of 2.1 has been previously used in a number of kaolinite studies (e.g. Angove et al., 2002; Ikhsan et al., 2004b; Lackovic et al., 2003b), a capacitance value of 1.1 was chosen and used throughout our calculations because it provided much better fits to the kaolinite-ligand experiments than a value of 2.1.

Table 3-6 Best-fit model parameters for the acid-base titration data of kaolinite according to the CCM.

Surface parameters	I = 0.01 M NaCl	
<i>Surface area ($m^2 g^{-1}$)^a</i>	21	
<i>Mass to volume ratio ($g L^{-1}$)</i>	40	
<i>Interfacial capacitance</i>	1.1	
<i>Site density^b</i>	<i>mmol m^{-2}</i>	<i>sites nm^{-2}</i>
>XOH	1.42	0.85
>YH	1.25	0.75
Surface reactions		
>XOH + $H^+ \leftrightarrow >XOH_2^+$	$\log K_1 = 4.17^b$	
>XOH $\leftrightarrow >XO^- + H^+$	$\log K_2 = -7.41^b$	
>YH + $Na^+ \leftrightarrow >YNa^+ + H^+$	$\log K_3 = -2.88^b$	
V_y^c	18	

^a obtained from BET analysis in this study

^b optimised parameters of the surface complexation model in FITEQL

^c goodness of fit of the proposed model as calculated by FITEQL. V_y is the weighted sum of squares (SOS) of residuals divided by the degrees of freedom (DF), $V_y = SOS/DF$

Modelling phthalic and salicylic acid adsorption on kaolinite

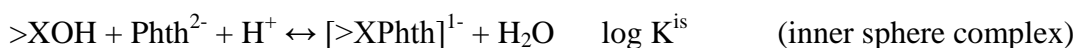
Phthalic and salicylic acid adsorption data were modelled according to the extended constant capacitance model (ECCM). The acid-base parameters of kaolinite determined by fitting the titration data (see Table 3-6) were used as fixed parameters in the surface complexation models developed for the kaolinite-ligand systems. Furthermore, the number, type, and protonation state of the surface complexes identified by the IR spectroscopic part of this study were used as constraints in the modelling

procedure. Therefore two surface complexes were included in the model describing the kaolinite-phthalate system and three surface complexes in the model describing the kaolinite-salicylate system. Surface complexation was assumed to occur only on the pH dependent surface charge sites (>XOH).

The modelling procedure consisted of identifying the set of surface reactions that could provide the best fit to the experimental data. Model fits were judged according to the goodness of fit parameter calculated by FITEQL after the optimisation procedure had converged. For each kaolinite-ligand system the equilibrium constants of the surface complexation reactions were the only adjustable parameters. Several combinations of surface reactions which could represent the surface species identified by spectroscopy were examined at different optimisation runs, including both mononuclear and binuclear surface complexes. In some cases different sets of surface reactions could fit the experimental adsorption data equally well. Consequently the models were further refined by requiring that model predictions could also simulate the pH dependence and relative concentrations of the individual surface species according to the spectroscopic results.

Kaolinite-Phthalic acid

The model which produced the best fit to the experimental data involved two surface complexes which can be represented by the following equations:



Model parameters for this model are summarised in Table 3-7 and the agreement between experimental and calculated data can be seen in Figure 3-30. The symbols are experimental data points and solid lines represent model fits to the experimental data according to the model parameters listed in Table 3-7. Although the model describes the adsorption data well over the entire pH range, for the three individual datasets better fits could be obtained if different equilibrium constants and/or interfacial capacitances were used. However the model parameters presented here could give the best overall fits for all three datasets. It has to be noted that the intrinsic equilibrium constants of the surface reactions presented are only valid for the experimental conditions of the present study.

Table 3-7 Model parameters used for the description of phthalate adsorption data on kaolinite according to the extended constant capacitance model.

Solution Reactions	log K
$\text{H}_2\text{O} \leftrightarrow \text{OH}^- + \text{H}^+$	-14
$\text{Phth}^{2-} + \text{H}^+ \leftrightarrow \text{HPhth}^{1-}$	5.23 ^a
$\text{Phth}^{2-} + \text{H}^+ \leftrightarrow \text{H}_2\text{Phth}^0$	8.10 ^a
Surface reactions	
$>\text{XOH} + \text{H}^+ \leftrightarrow >\text{XOH}_2^+$	4.17 ^b
$>\text{XOH} \leftrightarrow >\text{XO}^- + \text{H}^+$	-7.41 ^b
$>\text{YH} + \text{Na}^+ \leftrightarrow >\text{YNa}^+ + \text{H}^+$	-2.88 ^b
$>\text{XOH} + \text{Phth}^{2-} + \text{H}^+ \leftrightarrow [>\text{XPhth}]^{1-} + \text{H}_2\text{O}$	8.17 +/- 0.07 ^c
$>\text{XOH} + \text{Phth}^{2-} \leftrightarrow [>\text{XOH}---\text{Phth}^{2-}]^{2-}$	4.45 +/- 0.05 ^c
Other parameters	
Site density XOH ($\mu\text{mol}/\text{m}^2$)	1.42 ^b
Site density YH ($\mu\text{mol}/\text{m}^2$)	1.25 ^b
Inner layer capacitance (F/m^2)	2.2 ^c
Outer layer capacitance (F/m^2)	2.2 ^c

^a Evanko and Dzombak (1999).

^b Fixed parameter

^c Optimised parameter

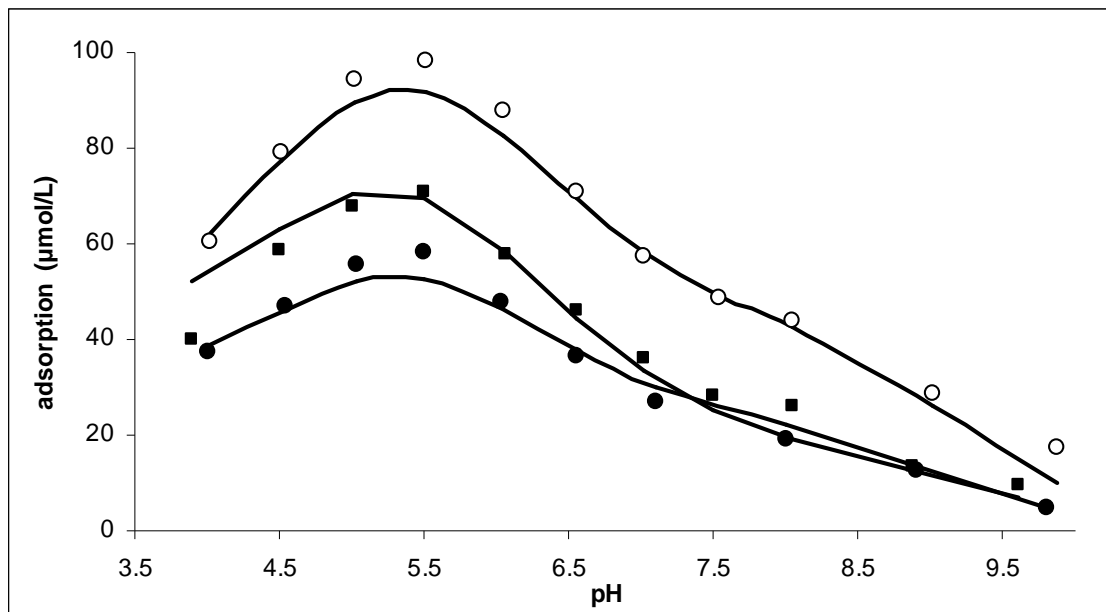


Figure 3-30 Phthalate adsorption on kaolinite as a function of pH, at I = 0.01 M NaCl and three systems with different initial phthalate concentration to surface area ratios (Phth : S.A). Open circles 2 x 10⁻⁵ mol : 52.5 m²/g; squares 2 x 10⁻⁵ mol : 42 m²/g; closed circles 1 x 10⁻⁵ mol : 52.5 m²/g.

In accordance with the spectroscopic results presented, the proposed model predicts two surface complexes, one inner and one outer sphere complex with formation constants of $\log K^{\text{is}} = 8.17$ and $\log K^{\text{os}} = 4.45$ respectively. The use of a binuclear inner

sphere surface complex, instead of a mononuclear complex in the proposed model neither improved model fits nor changed significantly the relative distribution of the two surface complexes as a function of pH. The only difference obtained in model outputs was an increase in the formation constant of this surface species from 8.2 for the mononuclear complex to about 16 for the binuclear complex. Corresponding literature values for phthalate formation constants from studies that have described the adsorption of phthalic acid assuming one inner and one outer sphere complex are: $\log K^{is} = 6.54$ and $\log K^{os} = 4.34$ for boehmite (Nordin et al., 1997); $\log K^{is} = 15.37$ (binuclear complex) and $\log K^{os} = 18.24$ for goethite (Boily et al., 2000b); $\log K^{is} = 17.43$ (binuclear complex) and $\log K^{os} = 23.0$ for haematite (for 5 sites/nm² and a C1/C2=1.9/1.7) (Hwang and Lenhart, 2009).

Figures 3-31 and 3-32 display the calculated species distribution of phthalic acid at two different initial phthalate concentrations. It can be seen that the outer sphere complex is the dominant surface species over the entire pH range. The inner sphere complex contributes to the overall adsorption only at pH values above about 5.5 and its fractional concentration increases at lower pH values. These model predictions are in good agreement with the IR spectroscopic data. It can be argued however that there is a disagreement between model and spectroscopic results with regards to the relative concentration between inner and outer sphere complexes. For example, at pH 4, for the system depicted in Figure 3-30, the model predicts that about 60% of the adsorbed species are outer sphere complexes and 40% are inner sphere complexes. The calculated relative concentration of inner sphere complexes is somewhat higher than that estimated from the spectrum of adsorbed phthalic acid, at pH 4, which strongly suggests an even more predominant outer sphere complex. This discrepancy can be attributed to two main factors. Firstly the macroscopic adsorption experiments were carried out at different experimental conditions than those in which the IR measurements were obtained. For example in the macroscopic adsorption experiments a much higher mineral surface area was used and this can have a significant effect on the relative distributions between inner and outer sphere complexes. In addition all the adsorption experiments were undertaken in a 0.01 M NaCl background electrolyte solution whereas solutions with no added electrolyte were used for most of the IR spectroscopic experiments. IR results showed that ionic strength can have a significant effect on the relative distribution of inner and outer sphere complexed species, with higher ionic strengths favouring inner sphere complexation. The second factor that could explain the observed discrepancies between model predictions and IR data is related to the

relatively simple surface complexation model used for the description of surface reactions and electrostatic properties of the kaolinite-solution interface.

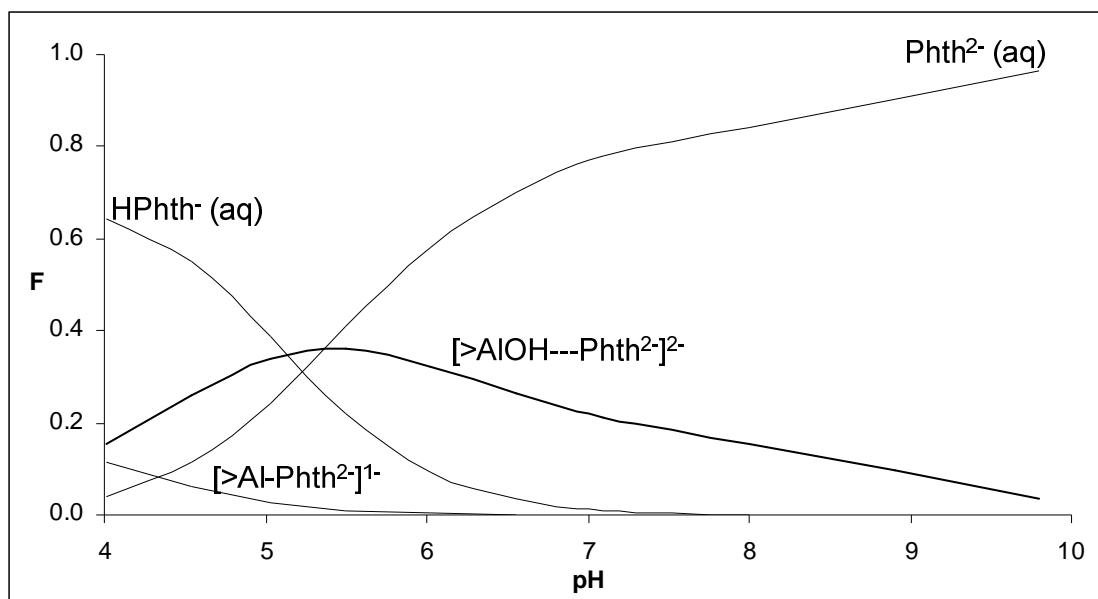


Figure 3-31 Predicted phthalate speciation in a kaolinite-phthalate system as a function of pH using the parameters listed in Table 3-7. System consisted of a 1.43×10^{-4} M phthalic acid solution (1×10^{-3} mol) and a surface area of $52.5 \text{ m}^2/\text{g}$. F denotes the fractional distribution of phthalate species in the system.

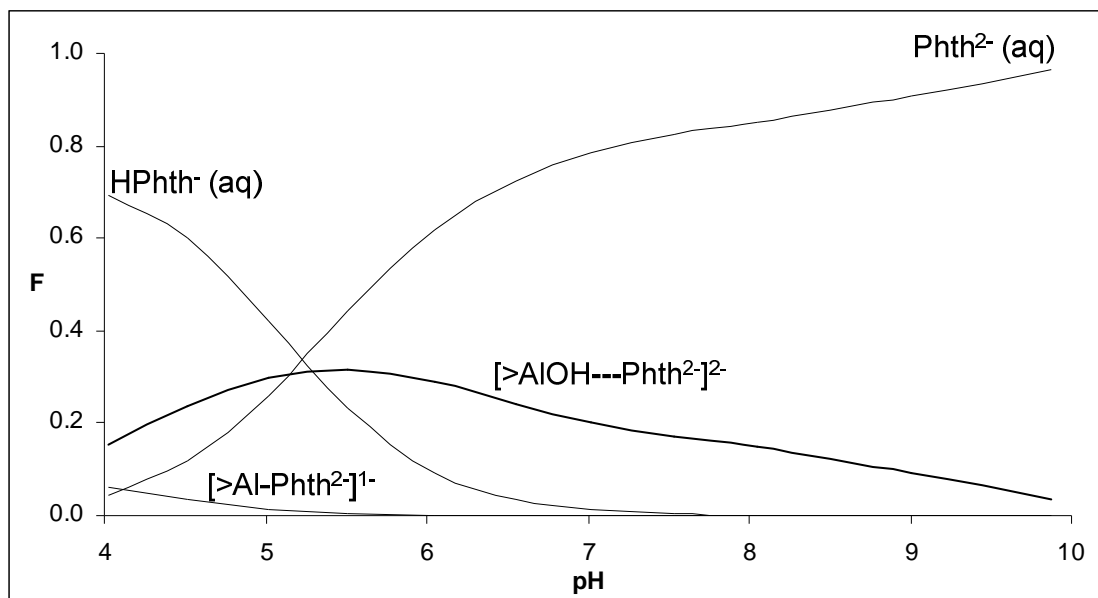
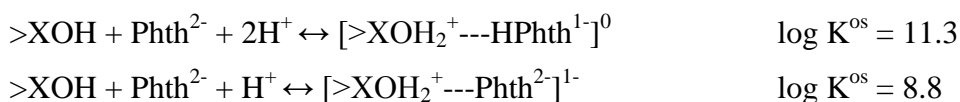


Figure 3-32 Predicted phthalate speciation in a kaolinite-phthalate system as a function of pH using the parameters listed in Table 3-7. System consisted of a 2.86×10^{-4} M phthalic acid solution (2×10^{-3} mol) and a surface area of $52.5 \text{ m}^2/\text{g}$. F denotes the fractional distribution of phthalate species in the system.

Phthalate adsorption on kaolinite was also modelled by Angove et al. (2002), using the ECCM, assuming two outer sphere complexes represented by the following two surface reactions:



Despite the similar kaolinite acid-base parameters used in the present study and that of Angove et al. (2002), the two models predict the formation of different types of phthalate surface species. In Angove's et al. (2002) study both surface complexes are outer sphere complexes and both involve protonated surface hydroxyl groups. Conversely in the present study adsorption data was modelled using one inner and one outer sphere complex in which both surface reactions involve a neutral hydroxyl group interacting with a fully deprotonated phthalate molecule. These significant differences in model predictions can be explained by two factors: the modelling approach and the disagreement in the adsorption profiles of phthalate obtained in the two studies.

The surface species used in the model proposed by Angove et al. (2002) were not related to spectroscopic data and thus their model was solely based on its ability to best describe the macroscopic adsorption data. However in the present study, IR data indicated the existence of an inner sphere complex which was included in the model. The second factor is associated with the different experimental adsorption data obtained in the two studies. Although the adsorption envelopes in the two studies exhibited similar shapes, Angove's et al (2002) dataset showed that phthalate adsorption is negligible at pH values above about 7, whereas in this study adsorption is negligible only at pH values above pH 10. According to the model proposed by Angove et al. (2002), the surface complex $[>\text{XOH}_2^+ \text{---Phth}^{2-}]^{1-}$ is the dominant species at $\text{pH} > 4$ and its concentration as a function of pH follows a similar trend as that found for the dominant outer sphere complex $[>\text{XOH} \text{---Phth}^{2-}]^{2-}$ proposed in the present study. When the $[>\text{XOH}_2^+ \text{---Phth}^{2-}]^{1-}$ species is included in the present model, its concentration falls sharply at $\text{pH} > 5.5$ as it follows the concentration of $>\text{XOH}_2^+$ groups. Therefore such a surface species fails to properly fit phthalate adsorption data as it underpredicts adsorption at $\text{pH} > 6$. Conversely $>\text{XOH}$ surface sites assumed to interact with phthalate ions, in the present model, are the dominant surface species in the pH range examined and can account for the phthalate adsorption found at higher pH. Figure 3-32 displays how the concentration of surface functional groups relates to the concentration of phthalate species, according to the proposed model in the present study.

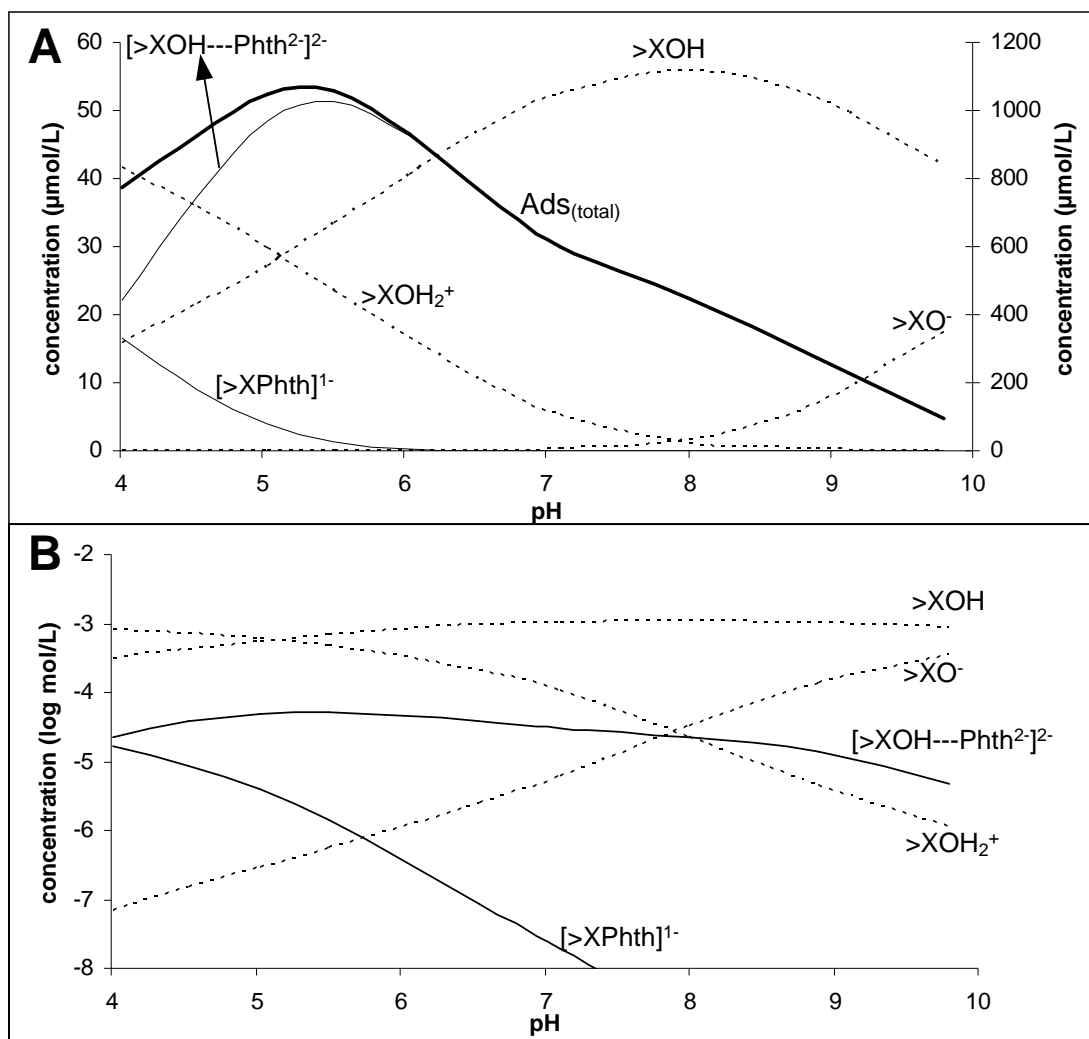


Figure 3-33 The distribution of surface functional groups and phthalate surface complexes according to the proposed model in (A) concentrations expressed as mol/L and (B) in logarithmic scale. Surface complexes are denoted by solid lines and surface functional groups by dashed lines. Note that for diagram A the left axis values correspond to the concentrations of the phthalate surface complexes and the right axis values for the concentration of the surface functional groups. The bold solid line represents the total phthalate adsorption for the kaolinite-phthalate system with a $[\text{Phth}] : [\text{S.A}]$ ratio of $1.5 \times 10^{-5} \text{ mol} : 52.5 \text{ m}^2$.

The effect of interfacial capacitance on the model outputs predicted by the ECCM have been discussed previously (e.g. Hwang and Lenhart, 2009; Johnson et al., 2004a). Therefore it was deemed appropriate to choose a total capacitance value that not only predicts surface speciation but that is also consistent with the IR measurements. The choice of capacitance values used for the inner (C_1) and outer (C_2) plane of the interface were a compromise between the model's ability to best fit the adsorption data and the ability to provide model outputs that are consistent with the spectroscopic data. Table 3-8 shows the effect of varying C_1 and C_2 values on the overall model fits and on the optimised phthalate complexation constants for the system with a $[\text{Phth}] : [\text{S.A}]$ ratio of $1.5 \times 10^{-5} \text{ mol} : 52.5 \text{ m}^2/\text{g}$. Various combinations tested could provide a satisfactory fit to the experimental data (e.g. optimisation runs 3-9). As seen in Table 8, the lowest

values for V(Y), and therefore the best model fits, were obtained in optimisation runs 8 and 9.

Table 3-8 The effect of varying C_1 and C_2 values on the optimised surface complexation constants ($\log K_{is}$ and $\log K_{os}$) and on the overall model fits (VY). Total capacitance ($C_T = 1/C_1 + 1/C_2$) was set to 1.1.

Optimisation run	C_1 ($F\ m^{-2}$)	C_2 ($F\ m^{-2}$)	$\log K_{is}$	$\log K_{os}$	V(Y)
1	1.7	3.1	8.62	3.87	34.7
2	1.8	2.8	8.56	4.0	24.2
3	1.9	2.6	8.49	4.13	15.9
4	2.0	2.4	8.42	4.22	10.6
5	2.1	2.3	8.33	4.32	6.6
6	2.2	2.2	8.24	4.40	4.2
7	2.3	2.1	8.11	4.48	2.42
8	2.4	2.0	7.89	4.56	1.4
9	2.6	1.9	7.12	4.66	1.4
10	2.8	1.8	No convergence		
11	3.1	1.7			

In addition to model fits, the relative distribution between the inner and outer sphere complexes predicted by the model was also very sensitive to varying C_1 and C_2 values. Figure 3-34 shows examples of the resulting surface speciation of adsorbed phthalate predicted for different C_1 and C_2 values. At pH 4, C_1/C_2 values of 2.1/2.3 and 2.2/2.2 (i.e. optimisation runs 5 and 6 in Table 3-8) predict almost equal concentrations of inner and outer sphere complexes. As C_1 decreases the concentration of inner sphere complexes relative to that of outer sphere complexes whereas as C_1 increases the concentration of inner sphere complexes is decreased dramatically. It can be therefore seen that the choice of capacitance values used in the model is not only important for the quality of model fits but also for the ability of the model to predict surface speciation. Therefore it was deemed appropriate to choose capacitance values that not only provided satisfactory model fits but also predicted surface speciation which is in agreement with the IR results.

Unfortunately, as already mentioned, different ligand to surface area ratios were used for the collection of adsorption data and IR measurements. Therefore the expected relative distribution between inner and outer sphere complexation in the macroscopic adsorption experiments cannot be obtained accurately from the IR spectra by calculating the peak areas of bands corresponding to inner and outer sphere complexes. It is, however, feasible to limit the possible combinations of C_1/C_2 values. At pH 4, the

optimisation runs that are closer to the IR spectroscopic data are 5 (2.1/2.3), 6 (2.2/2.2) and 7 (2.3/2.1). Other combinations either predict a higher concentration of inner sphere complexes than outer sphere complexes or predict very low concentrations for inner sphere complexed species at pH 4. For example the two optimisation runs which provided the best model fits (8 and 9) predicted insignificant concentrations of inner sphere complexes at pH 4, a finding that is inconsistent with the spectroscopy data. As a result, a C_1/C_2 of 2.2/2.2 was chosen to model the adsorption data. From the above discussion it can be seen that spectroscopic results can constrain the values of interfacial capacitances. Therefore an experimental setup that allows IR and macroscopic adsorption measurements to be obtained at similar concentration to surface area ratios could be used as an independent method for the determination of optimal interfacial capacitances.

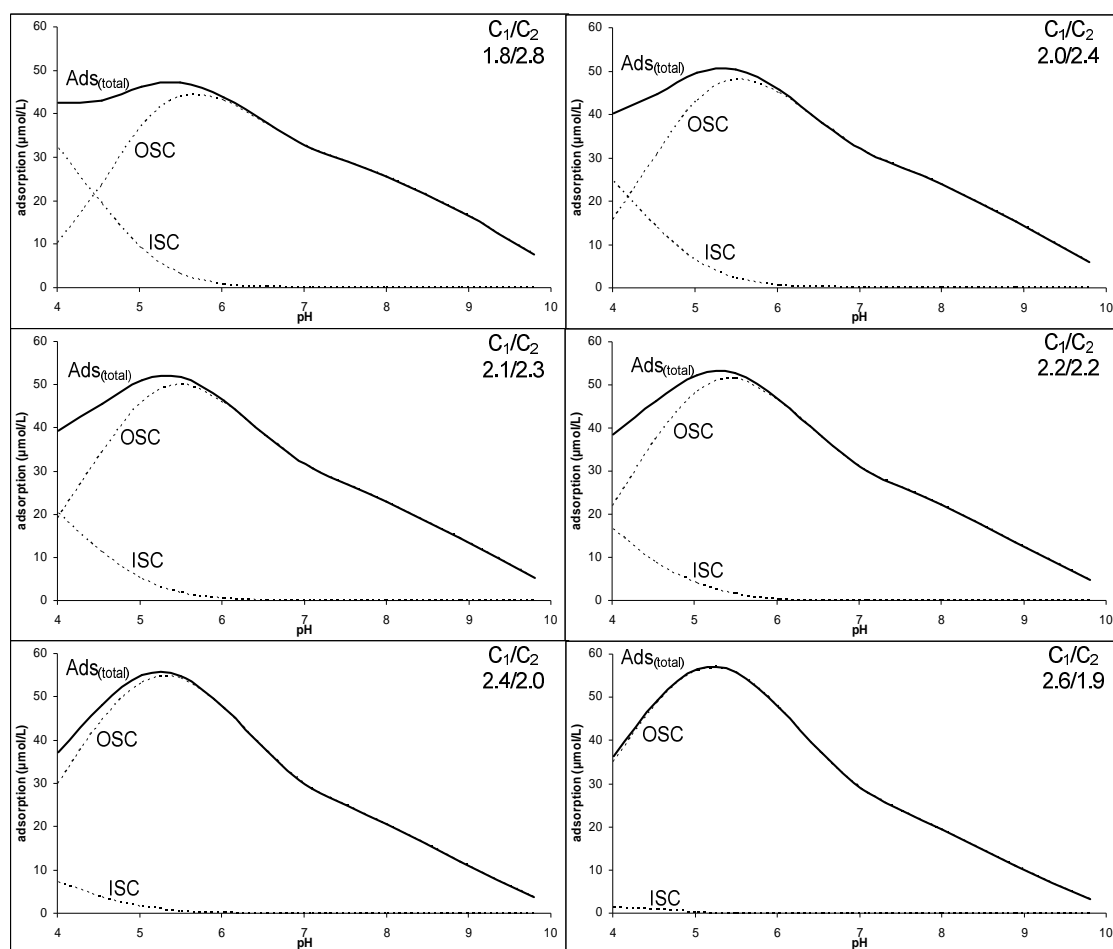


Figure 3-34 The effect of varying C_1 and C_2 values on the predicted relative ratios of the inner and outer sphere complexes. Solid lines represent the total adsorption ($\text{Ads}_{\text{total}}$), ISC denotes inner sphere complexes and OSC outer sphere complexes.

Considering the very good fit of the data to the model it can be concluded that the proposed model involving two phthalate surface complexes gives an appropriate representation of the kaolinite-phthalate system. The fact that the model does not only describe the data quantitatively but is also consistent with the spectroscopic results, adds further confidence to the model's applicability. While the two surface reactions included in the proposed model provide a very good description of the experimental data, other surface reaction schemes could be fitted equally well to the experimental data. For instance, FITEQL yielded a similar goodness of fit parameter for a model consisting of two outer sphere complexes. This finding is similar to Nordin's et al. (1997) findings which showed that the adsorption of phthalate on boehmite could be described equally well using either two outer sphere complexes or one inner and one outer sphere complex. These observations highlight the problem of using the goodness of fit as the only criterion to select an appropriate surface complexation model. It is therefore important to obtain molecular level information about the surface species formed prior to the application of surface complexation modelling for the description of macroscopic adsorption data.

IR spectroscopy is particularly suited for the development of surface complexation modelling as it provides information about the surface species formed including their protonation state and binding mode. On the other hand, however, it is important to note that even by combining spectroscopic data with macroscopic adsorption data it is still possible that a unique solution may not always be found. An example of such a case has been encountered in this study. A binuclear inner sphere complex could reproduce the same goodness of fit to the data as a mononuclear complex. Unfortunately it is very difficult to differentiate between mononuclear and binuclear coordination modes using IR spectroscopy.

Kaolinite- salicylic acid

A number of possible surface species, both mononuclear and binuclear, were examined in order to find the reaction scheme that best described the adsorption data of salicylic acid. In agreement with the IR results, three surface complexes were included in the model. As discussed earlier, at $\text{pH} < 6$ two singly protonated salicylate surface species were found to coexist on the surface, one inner and one outer sphere. At higher pH values, $\text{pH} = 10$, the IR spectra showed the presence of a third fully deprotonated surface species that replaces the two singly protonated species identified at lower pH values. Because the binding mode of this surface species could not be determined, both

inner and outer sphere binding modes species were considered for the for this surface species.

The following reactions were found to best describe the adsorption of salicylic acid on kaolinite

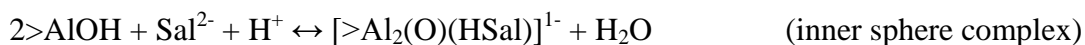


Table 3-9 lists the model parameters used to fit the adsorption data of salicylic acid on kaolinite. Although other reaction schemes could also provide satisfactory fits to the experimental adsorption data, the model proposed below was the only one that could predict the adsorption behaviour of the individual surface species, as obtained by the spectroscopic data.

Table 3-9 Model parameters used for the description of phthalate adsorption data on kaolinite according to the extended constant capacitance model.

Solution Reactions	log K
$H_2O \leftrightarrow OH^- + H^+$	-14
$Sal^{2-} + H^+ \leftrightarrow HSal^{1-}$	13.56 ^a
$Sal^{2-} + H^+ \leftrightarrow H_2Sal^0$	16.44 ^a
Surface reactions	
$>AlOH + H^+ \leftrightarrow >AlOH_2^+$	4.17 ^b
$>AlOH \leftrightarrow >AlO^- + H^+$	-7.41 ^b
$>YH + Na^+ \leftrightarrow >YNa^+ + H^+$	-2.88 ^b
$2>XOH + Sal^{2-} + H^+ \leftrightarrow [X_2(O)(HSal)]^{1-} + H_2O$	20.5 +/- 0.2 ^c
$2>XOH + Sal^{2-} + 2H^+ \leftrightarrow [(>XOH)(>XOH_2^+)---HSal^{1-}]^0$	23.8 +/- 0.2 ^c
$2>XOH + Sal^{2-} \leftrightarrow [(>XOH)_2---Sal^{2-}]^{2-}$	12.7 +/- 0.2 ^c
Other parameters	
Site density AlOH ($\mu\text{mol}/\text{m}^2$)	1.42 ^b
Site density YOH ($\mu\text{mol}/\text{m}^2$)	1.25 ^b
Inner layer capacitance (F/m^2)	4.0 ^c
Outer layer capacitance (F/m^2)	3.3 ^c

^a Evanko and Dzombak (1999).

^b Fixed parameter

^c Optimised parameter

Salicylic acid adsorption data and model fits are shown in figure 3-35. A satisfactory fit is obtained for all three datasets but the model slightly overestimates adsorption at pH below pH 5. The speciation of salicylic acid as calculated by the

proposed model is shown Figures 3-36 and 3-37. The species distribution diagram shows that at acidic conditions salicylic acid adsorption can be explained by the formation of two surface complexes, one inner and one outer sphere. These two surface complexes have a reverse concentration trend as a function of pH, with the concentration of the inner sphere complex increasing as the pH increases from 4 to 6 and the concentration of the outer sphere complex decreasing at the same pH range.

The inner sphere complex can be visualised as a surface bound singly protonated salicylate ion which is directly coordinated to one surface site and hydrogen bonded to the second deprotonated surface hydroxyl group. Such a surface species is in accordance with the coordination mode inferred from the IR spectroscopic results presented earlier. For the outer sphere complex, salicylate ion interacts with two surface groups, one neutral and one positively charged hydroxyl group. The involvement of a protonated surface hydroxyl group explains decreasing surface concentration of the outer sphere complex as the pH of the solution increases.

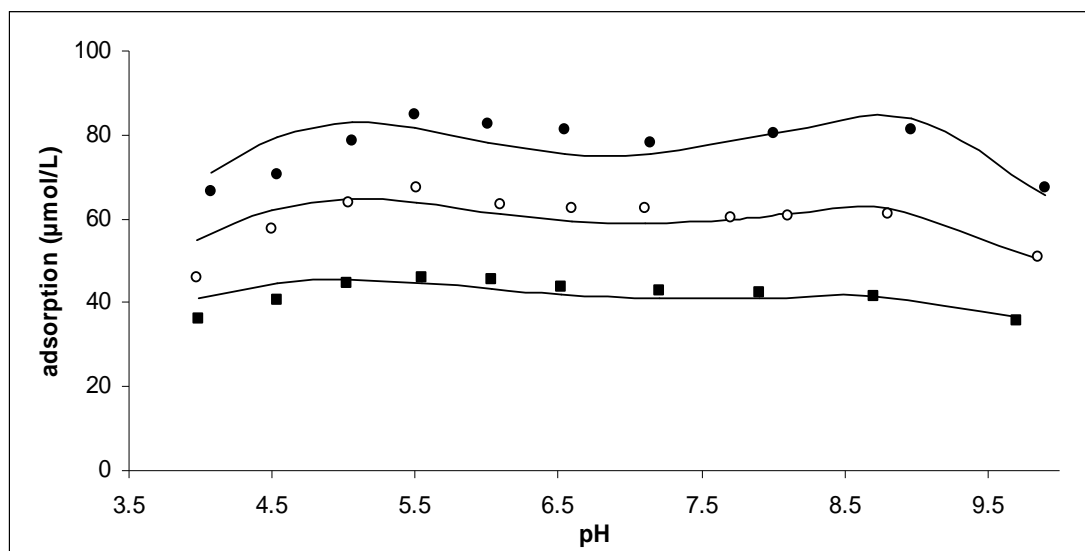


Figure 3-35 Salicylate adsorption on kaolinite as a function of pH, at $I = 0.01$ M NaCl and three systems with different initial salicylate concentration to surface area ratios (Sal : S.A). Closed circles 2×10^{-5} mol : 47.25 m^2/g ; open circles 1×10^{-5} mol : 47.25 m^2/g ; squares 5×10^{-6} mol : 47.25 m^2/g .

Overall the predicted concentration trend as a function of pH for the two surface complexes identified in the acidic region is consistent with the spectroscopic results which showed an increase in dominance for the inner sphere complex at higher pH values. However, the predicted relative concentrations of these two surface species appear to differ from those estimated by IR spectroscopy. The proposed model

underpredicts the relative importance of outer sphere complexation, especially at pH 4 and 5 where significant contributions of outer sphere complexed salicylate species were determined from the IR spectra. As previously explained, this discrepancy between model and spectroscopic results can be attributed to the different experimental conditions in which the adsorption and IR measurements were carried out and to the relatively simple model used for the description of the kaolinite-salicylate system.

The inner sphere complexed surface species dominates adsorption up to pH 7 and at higher pH values is progressively replaced by a binuclear outer sphere complex involving two neutral surface sites and one fully deprotonated salicylate ion. Above pH 8 this outer sphere complex is the dominant surface species and grows in importance up to pH about 9. This behaviour is consistent with the spectroscopic results in that at pH 10 a different surface complex than that identified at pH < 6 was present in the IR spectra. Although the type of this complex was unclear by spectroscopy the proposed binuclear outer sphere complex was the only one that could yield a satisfactory data fit to the experimental data.

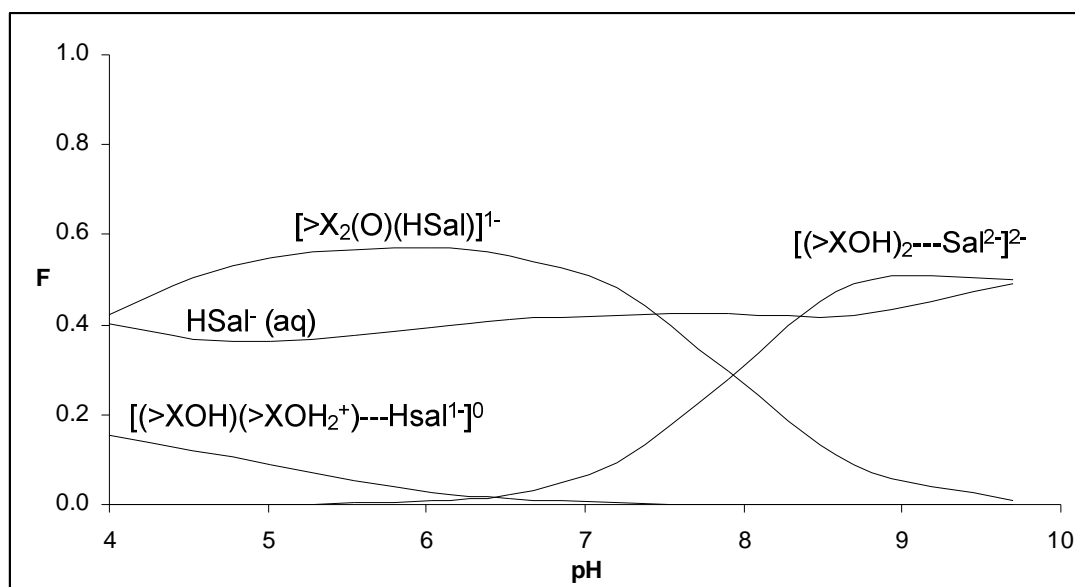


Figure 3-36 Predicted salicylate speciation in a kaolinite-salicylate system as a function of pH using the parameters listed in Table 3-9. System consisted of a $7.14 \times 10^{-5} M$ salicylic acid solution ($5 \times 10^{-6} \text{ mol}$) and a surface area of $47.25 \text{ m}^2/\text{g}$. F denotes the fractional distribution of salicylate species in the system.

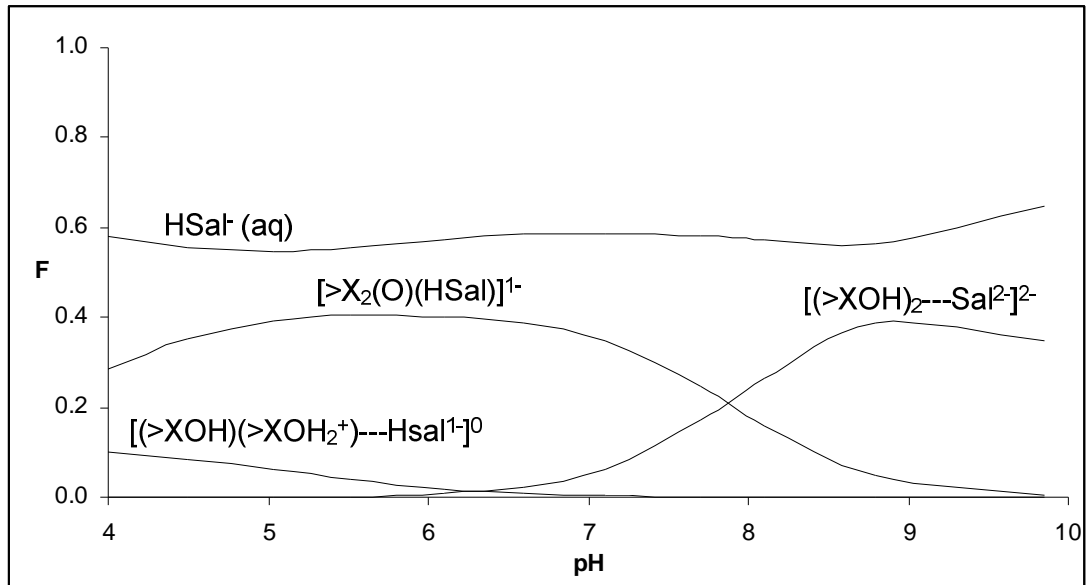


Figure 3-37 Predicted salicylate speciation in a kaolinite-salicylate system as a function of pH using the parameters listed in Table 3-9. System consisted of a 1.43×10^{-4} M salicylic acid solution (1×10^{-5} mol) and a surface area of $47.25 \text{ m}^2/\text{g}$. F denotes the fractional distribution of salicylate species in the system.

Finally, it has to be mentioned that the adsorption of salicylic acid was modelled using a different total interfacial capacitance value ($C_T = 1.8$) than that used for the modelling of the acid-base titration data and of phthalate adsorption data ($C_T = 1.1$). When a total capacitance of 1.1 was used the model produced poor fits to the data and also the predicted distribution of salicylate surface species was inconsistent with the spectroscopic results. At this point it is unknown why a different interfacial capacitance was required to model the adsorption data of salicylic acid.

Synopsis

Proton adsorption on kaolinite was modelled according to the constant capacitance model, assuming two proton binding sites: a pH dependent charge site (XOH) and a permanent negatively charged site (Y). This model produced a satisfactory fit to the acid-base titration data of kaolinite and the surface parameters optimised included site densities, protonation constants and the capacitance of the interface. These optimised model parameters were used as fixed parameters when modelling the adsorption of phthalic and salicylic acid on kaolinite.

Macroscopic salicylic and phthalic acid adsorption data was modelled according to the extended constant capacitance model using constraints from IR spectroscopic data. The pH-dependent charge XOH sites were considered as the main adsorption sites

on the surface of kaolinite. For phthalic acid the model assumes two surface species: one is coordinated in an inner sphere mode $[>XPhth]^{1-}$, and one in an outer sphere mode $[>XOH---Phth^{2-}]^{2-}$. The outer sphere species is the dominant surface species over the entire pH range, whereas the inner sphere species is only present at pH values below 6. For salicylic acid the model found to best describe the adsorption data included three surface complexes: one inner sphere complex $[X_2(O)(HSal)]^{1-}$, and two outer sphere complexes $[(>XOH)(>XOH_2^+)---HSal^{1-}]^0$ and $[(>XOH)_2---Sal^{2-}]^{2-}$. In the acidic region $[X_2(O)(HSal)]^{1-}$ is the dominant species and $[(>XOH)(>XOH_2^+)---HSal^{1-}]^0$ contributes to adsorption only at $pH < 6$. At about $pH 6.5$, the $[(>XOH)_2---Sal^{2-}]^{2-}$ starts forming and at $pH > 8$ becomes the dominant surface species.

In the acidic region, following the adsorption of either salicylic and phthalic acid, two surface complexes coexist on the surface, one inner and one outer sphere complex. For phthalic acid, the concentration of outer sphere complexed phthalate increases with increasing pH from 4 to 5.5 and then decreases at higher pH values. In contrast, the concentration of outer sphere complexed salicylic acid is at maximum at pH 4 and decreases as the pH increases. This reverse adsorption behaviour is attributed to the different surface species involved in the formation of these two outer sphere complexes.

For the kaolinite-phthalate system the outer sphere complex is stabilised by the interactions between phthalate ions and neutral surface sites. As the pH of the solution increases from 4 to 6, the concentration of neutral surface sites increases and thus favours the formation of the phthalate outer sphere complex. In addition, at higher pH values, outer sphere complex formation is also favoured because the concentration of the fully deprotonated phthalate ions (species involved in complexation) in solution increases. The decrease in surface concentration of these species at even higher pH values is explained by the increased electrostatic repulsions experienced between negatively charged site and negatively charged phthalate molecules.

For the kaolinite-salicylate system, the outer sphere complex is stabilised by the association between salicylate ions and positively charged surface sites. Therefore the formation of the salicylate outer sphere complex is favoured by lower pH values where a higher concentration of positively charged surface sites exists.

There is generally a very good agreement between the proposed surface complexation models and spectroscopic results which gives confidence in the reliability of model outputs. Small discrepancies in the results obtained by model outputs and IR spectroscopy are attributed to the different experimental conditions used in these experiments and the simple surface complexation model used.

Summary and Conclusions

The complexation reactions of phthalic and salicylic acid on kaolinite were studied by combining the results obtained from macroscopic and microscopic adsorption experiments. *In situ* MIR-FTIR spectroscopy was employed to obtain molecular level information on the surface complexes formed. The IR findings were then combined with the results obtained from the macroscopic adsorption measurements in order to derive surface complexation models that can describe the adsorption reactions in the two kaolinite-ligand systems.

The first section of this chapter presented IR spectroscopic data about the structure and binding mode of the surface species forming. According to the analysis of the IR spectra, phthalic and salicylic acid were found to form two and three different types of surface complexes on kaolinite respectively. Phthalic acid adsorption occurs through a dominant outer sphere adsorption mechanism over the entire pH range examined (pH 3-6). An additional minor inner sphere phthalate surface species is also present and its formation is favoured by lower pH and higher ionic strengths. Phthalate was present as the fully deprotonated phthalate ion in both surface species.

In the pH range from 3-6, salicylic acid was found to form one inner and one outer sphere complex. In both surface complexes salicylic acid exists as the singly protonated salicylate ion. The relative concentration of these two complexes is governed by the pH, ionic strength, salicylate concentration and reaction time. The relative concentration of inner sphere complexed species increases at higher pH, higher ionic strength, lower initial salicylate concentration and shorter reaction times. At pH 10 a different fully deprotonated salicylate species could be observed in the IR spectra, indicating that a different surface complex is forming at higher pH values

Macroscopic adsorption experiments showed that the two ligands exhibit very different adsorption behaviours on kaolinite, in the pH range from 4 to 10. In general, the pH-dependent adsorption profile of phthalic acid is characterised by an adsorption maximum at a pH value of about 5.5 and decreases at higher and lower pH values. In contrast salicylic acid adsorption is less influenced by variations in the pH of the solution. Additionally phthalic acid adsorption is significantly reduced as the ionic strength of the solution, whereas salicylic acid adsorption is less influenced by ionic strength effects.

The adsorption of both organic ligands as a function of pH was successfully described according to the extended constant capacitance model (ECCM) using the

surface species identified by spectroscopy. Model fits to the experimental data and optimised surface complexation constants were obtained by the computer program FITEQL. The complexation of phthalate on kaolinite was described by one inner sphere complex, $[>XPhth]^{1-}$ ($\log K^{is} = 8.17$), and one outer sphere complex: $[>XOH---Phth^{2-}]^{2-}$ ($\log K^{os} = 4.45$). A similar adsorption mechanism has been previously proposed for phthalate surface complexes on simple aluminium and iron oxides. Salicylate complexation on kaolinite was described by three surface complexes: one inner sphere $[X_2(O)(HSal)]^{1-}$ ($\log K^{is} = 20.5$), and two outer sphere complexes $[(>XOH)(>XOH_2^+)---HSal^{1-}]^0$ ($\log K^{os} = 23.8$) and $[(>XOH)_2---Sal^{2-}]^{2-}$ ($\log K^{os} = 12.7$).

Chapter 4 The adsorption of humic acid on kaolinite and gibbsite

Introduction

Mineral particles and natural organic matter (NOM) represent the major reactive phases of soils, and as a result they can play an important role in the binding and transport of metal cations, inorganic and organic anions, and anthropogenic pollutants. Numerous studies have investigated the adsorption properties of mineral surfaces and related those to the physicochemical properties of mineral surfaces. However, in natural systems mineral surfaces are at least partially coated by organic matter (Mayer and Xing, 2001). Because the interactions between organic matter and mineral surfaces can affect the environmental behaviour of the two individual components, the effect of organic matter adsorption on mineral surfaces has been the subject of considerable scientific interest.

Numerous studies have identified the importance of adsorbed organic matter in regulating several geochemical and environmental processes such as adsorption, dissolution, and contaminant transport. In particular, the interactions between mineral surfaces and organic matter can modify many of the physicochemical properties of mineral surfaces. Significantly, upon adsorption organic matter has been shown to have a great effect on the charging behaviour of minerals by introducing a negative charge on the surface of oxides and clay minerals (Gu et al., 1995; Tipping, 1981; Tombácz et al., 2004). This change in surface charge characteristics imposed by these organic molecules will in turn influence several important surface dependent processes such as adsorption, contaminant transport, colloidal stability and particle flocculation.

To gain a better understanding of sorption processes in natural systems there is a requirement to investigate the interactions between organic matter and mineral surfaces. Early work has indicated that ligand exchange is an important mechanism for the adsorption of humic substances on mineral surfaces, particularly metal (hydr)oxides (Gu et al., 1994; Parfitt et al., 1977b; Tipping, 1981). In more recent studies, other adsorption mechanisms have also been proposed for the uptake of humic substances including anion exchange, cation bridging, hydrophobic interactions and van der Waals interactions (Arnarson and Keil, 2000; Yoon et al., 2005). Much of what we know about the interactions between humic substances and mineral surfaces has been typically

derived from the macroscopic adsorption behaviour in these systems and from the study of low molecular organic compounds (LMW) compounds that have been used as general humic substance analogues. However experimental measurements concerning the macroscopic adsorption behaviour can only give indirect evidence about the adsorption mechanisms.

Although several spectroscopic investigations have been undertaken for the study of organic matter interactions with mineral surfaces, the majority of these studies have dealt with simple low molecular weight (LMW) organic compounds. To date only a few studies have investigated explicitly the molecular level interactions of humic substances with mineral surfaces. Furthermore, simple mineral (hydr)oxides are commonly used as mineral substrates amongst these studies. In contrast to mineral (hydr)oxides, clay minerals have received little attention and hence there is a limited number of studies reporting the microscopic interactions between humic substances and clay minerals.

The aims of this study were to investigate the adsorption behaviour of humic acid on two aluminium bearing minerals (kaolinite and gibbsite), and propose likely adsorption mechanisms. Both IR spectroscopic and macroscopic adsorption methods were employed to examine the interactions between humic acid and these two mineral substrates. The main objectives of this study were: (1) examine the macroscopic adsorption properties of humic acid over a wide range of experimental conditions including different pH, initial humic acid concentration, ionic strength, type of background electrolyte, (2) identify adsorption mechanisms that are consistent with the macroscopic adsorption behaviour of humic acid, (3) examine the molecular level interactions of humic acid molecules with kaolinite and gibbsite using *in situ* MIR (multiple internal reflection) FTIR spectroscopy, (4) combine the macroscopic and spectroscopic data in order to identify the most likely mechanisms involved in the adsorption of humic acid on kaolinite and gibbsite.

Kaolinite was chosen as a representative clay mineral in order to examine the adsorption behaviour and binding mechanisms of humic acid on clay minerals. Although the adsorption properties of humic acid on kaolinite have been previously investigated, adsorption measurements have been mainly restricted to the collection of adsorption isotherm data under limited experimental conditions (Elfarissi and Pefferkorn, 2000; Feng et al., 2005; Hur and Schlautman, 2003; Murphy et al., 1992; Murphy et al., 1994; Tombácz et al., 2004; Zhou et al., 1994). To date no systematic studies investigating humic acid adsorption on kaolinite under a wide range of solution conditions have been undertaken. Furthermore, there have not been any IR

spectroscopic studies of adsorbed humic acid on kaolinite in the literature. Gibbsite was chosen as a model aluminium hydroxide surface, which is also structurally related to kaolinite, in order to examine whether humic acid binds to the surface of the two minerals through a similar adsorption mechanism. To the best of our knowledge no studies have yet investigated the adsorption properties of humic acid on gibbsite, either at the macroscopic or microscopic level.

Methodology

Materials

Commercial kaolinite (KGa-2, Clay Minerals Society) and gibbsite (SF-11E, Alcan) were used in this study. The identity and purity of the mineral phases was confirmed by X-ray diffraction (XRD) analysis. The mineral samples used in the experiments were washed three times in de-ionised water and allowed to dry at room temperature with no further treatment. The surface area of the kaolinite and gibbsite samples are 21 +/- 2 and 10.5 +/- 1.2 m²/g respectively, as measured by the BET nitrogen adsorption method, using a Micrometrics Gemini surface area analyser. Mean surface area values and errors at the 95% confidence level were obtained from triplicate measurements.

Two 1-litre humic acid solutions were prepared from a commercial humic acid sample (Acros Organics) by dissolving 1 g of humic acid in 1 litre of 15 MΩ UV treated water, at pH 8. To ensure maximum dissolution, the solutions were initially shaken vigorously by hand repeatedly and then sonicated for 2 hours in an ultrasonic water bath. The non dissolved fraction (estimated at about 50% of the dry weight of humic acid added) was removed by centrifugation. The two 1-litre solutions were then mixed together to give a final volume of a two-litre humic acid stock solution with a concentration of 1 g/L. This was stored in the dark at 4°C and was subsequently used in all the experiments of the present study within two months. The total organic carbon concentration (TOC) of the stock solution was determined to be 55.6 mg/L by a TOC analyser.

Humic acid titrations

Acid-base titrations were performed to determine the proton binding capacity of the humic acid sample used in the present study. Separate titrations were carried out for three different ionic strengths using NaCl as the background electrolyte. All titration experiments were carried out using a computer-controlled titrator (Mettler Toledo DL 67) in titration vessels sealed in an airtight chamber. Titrant addition, pH measurement, and data recording were controlled by the titrator. The temperature was kept constant (25°C +/- 0.05) by placing the reaction vessel into a water jacket connected to a circulating temperature controlled water bath. Humic acid solutions were continuously stirred by a propeller stirrer connected to the automatic titrator.

The concentration and volume of humic acid titrated in each experiment was 0.5 g/L and 50 mL respectively. The ionic strength was adjusted to initial background electrolyte concentrations of 0.1, 0.01 and 0.001 M by diluting 25 mL of the humic stock solution with 25 mL of 0.2, 0.02 and 0.002 M NaCl solutions respectively. The pH electrode was calibrated using three standard buffer solutions at pH 4, 7 and 10 and pH readings were accurate to within 0.01 unit. The acid and base solutions used as titrants were from 0.1 M HCl and 0.1M NaOH volumetric solutions respectively.

Titrations were carried out according to the following procedure. Humic acid solutions were initially stirred and bubbled with moisturised nitrogen gas for about an hour to remove dissolved CO₂ species. The titration vessel was then sealed with the pH electrode, the nitrogen line and the burettes in place. The nitrogen line was placed immediately above the solution so that an inert atmosphere could be maintained in the reaction vessel for the duration of the experiment. A known volume of NaOH was then added to the system to increase the pH to about 10. Following the addition of base, the pH of the solution was allowed to equilibrate for about 3 more hours until a stable pH reading could be obtained. After this equilibration period, incremental additions of HCl were added to lower the pH down to about pH 3.5. After each addition of acid titrant (0.035 mL), the solution was allowed to equilibrate and the resulting pH was recorded. Equilibrium conditions were assumed according to a criterion set for electron potential stability over a one minute interval. The criterion for electron potential stability was a drift in electrode potential by less than 0.05 mV/min for a minimum equilibration time of 10 minutes. If this criterion was not met, equilibrium conditions were assumed after an equilibration time of 20 minutes. In most cases equilibrium was achieved between the first 10-15 minutes and the maximum equilibration time was only reached for only few points at near neutral pH values.

The concentration of protons participating in the protonation/deprotonation reactions with humic acid [H^+_{ads}] was calculated from the titration data according to the following equation:

$$[H^+_{ads}] = \frac{[H^+] - [OH^-] - 10^{-pH} + 10^{(-14+pH)}}{[HA]} \quad 4-1$$

where at each titration point [H^+_{ads}] has units in mol/g, [H^+] and [OH^-] represent the concentration of proton and hydroxide ions (mol/L) calculated from the volume of strong acid and base added in the system, and [HA] is the concentration of humic acid (g/L).

Modelling

The concentrations and acidity constants of humic acid functional groups (i.e. proton binding sites) were obtained by modelling the acid base titration data, using the optimisation program FITEQL Version 4.0 (Herbelin and Westall, 1999). Experimental data required for modelling the titration data is the total hydrogen ion concentration (T_H) added and the resulting pH at each titration point. T_H can be determined at each titration point by (Westall et al., 1995)

$$T_H = C_a - C_b + T_H^0 \quad 4-2$$

where C_a and C_b are the concentrations of acid and base added in the solution (mol/L) respectively, and T_H^0 the concentration of acid or base added initially.

The acid-base titration data were modelled using the discrete site distribution model which assumes that humic acid consists of a mixture of monoprotic acids and the protonation/dissociation reaction for each proton binding site can be written as



where HL represents an acidic functional group and K the equilibrium constant of the protonation/dissociation reaction which relates to the acidity of the functional group.

A non electrostatic model (NEM) was used for the optimisation of model parameters. For each different proton binding site, initial estimates (i.e. adjustable parameters) required by the non electrostatic model include the concentration of acidic functional groups and the proton binding equilibrium constant (K). Consequently the overall number of adjustable parameters is dictated by the number of proton binding sites chosen to fit the data. A simultaneous, unconstrained optimisation procedure of all the adjustable parameters was allowed during model runs.

Because of the heterogeneous and complex nature of humic acids there is limited information concerning the physicochemical properties of humic acids that could guide the selection of the input parameter set. Therefore the modelling procedure adopted was to derive the simplest model (i.e. the least number of adjustable parameters) which could satisfactorily fit the experimental data. Initially titration data were modelled assuming the presence of only one proton binding site (one-site model) which requires the least number of adjustable parameters. Then additional sites were included until the model was capable to satisfactorily reproduce the titration data at the three different background electrolyte concentrations. The improvement brought about by increasing the number of surface sites was judged by the goodness of fit parameter calculated by FITEQL, and by visual inspection for the agreement between model and experimental data. The goodness of fit of the model to the experimental data is given by the fitting parameter, $V(Y)$, which is evaluated by the weighted sum of squares of the residuals between calculated and experimental values.

Model outputs obtained by the NEM were compared with model outputs obtained when the electrostatic effects were explicitly considered using the diffuse layer model (DLM). It has to be noted that by taking into account the electrostatic effects more input parameters are required by the model such as the specific surface area of humic acid and capacitance. Unfortunately these values are not *a priori* known and have to be treated as adjustable parameters, thus increasing the overall number of adjustable, and thus unknown, model parameters in model calculations. In addition when the DLM was used the optimisation procedure did not converge if all the adjustable parameters were optimised simultaneously. Therefore in the discussion section the model parameters obtained by the NEM will be considered.

Adsorption experiments

A series of adsorption experiments were carried out to quantify the extent of humic acid adsorption on gibbsite and kaolinite as a function of pH, initial humic concentration, ionic strength, and ionic composition. All adsorption experiments were undertaken using a computer-controlled titrator (Mettler Toledo DL 67) in 100 ml airtight titration vessels. An inert atmosphere in the titration vessel was maintained by a continuous flow of water-saturated nitrogen gas above the suspension and the mineral-humic suspensions were continuously stirred by the help of a propeller stirrer. The temperature of the suspensions was maintained at 25°C +/- 0.05 by the use of water jacket around the reaction vessel.

A typical experiment carried out to determine humic acid adsorption, at a particular pH, initial humic acid concentration, and ionic strength was conducted as follows: A pre-weighted mass of mineral was first suspended in 50 ml of a sodium chloride electrolyte solution and stirred until a stable pH reading was observed. The pH of the suspension was then adjusted to the required value by small additions of hydrochloric acid or sodium hydroxide. While stirring, the appropriate volume of humic acid stock solution (1 g/L) was added in the mineral suspension in order to get the desired starting humic acid concentration. The humic acid-mineral suspension was allowed to equilibrate while stirring for two hours. The pH of the solution was continuously monitored and maintained at the required value within 0.01 pH units by small additions of HCl or NaOH accordingly. Because the adsorption reaction was found to be very fast, with higher adsorption at lower pH values, care was taken so that the pH of the suspension never fell below the target pH during the addition of the stock humic solution or during the course of the experiment.

Following equilibration, the suspensions were centrifuged, and the supernatant filtered using a 0.45 µm syringe filter. The remaining humic acid concentration in solution was measured by UV absorbance at 330 nm using a UV-VIS spectrophotometer. Filtration of the supernatants was necessary because for some samples (particularly those obtained at high pH and low ionic strengths) the centrifugation step failed to completely remove all the suspended particles from the aqueous phase. The presence of these very fine suspended particles would increase the UV absorbance of the solution and this in turn would overestimate the concentration of humic acid calculated. Prior to U.V analysis all the samples were basified to about pH 10, by adding a small volume of concentrated sodium hydroxide solution (0.1 M), in order to eliminate the influence of pH on UV absorption.

The same experimental procedure was repeated for different humic acid-mineral systems at specific humic acid concentrations, pH values and ionic strengths. Although more time consuming such a method was preferred to typical batch adsorption experiments conducted in the literature where the system components are added in closed reaction vessels and allowed to react for the duration of the experiment without further pH adjustment. Following initial pH adjustment, preliminary experiments showed a large difference between initial and final pH values. Because the pH of the suspension is an important parameter for the adsorption process, it was deemed necessary to control the pH throughout the duration of the experiment.

Several control experiments at various solution conditions were conducted in the absence of the mineral phase in order to quantify the losses of humic acid due to other process such as precipitation and/or adsorption on container walls and/or adsorption on the filter medium. Losses due to the filtration process and due to adsorption on the container walls were negligible whereas humic acid precipitation was found to occur in systems where divalent cations were present in the background electrolyte solution. Calibration standards for UV analysis were prepared by diluting the solutions obtained from control experiments performed at different pH and salt levels. For the range of humic acid concentrations used, a linear relationship between absorbance and humic acid concentration was obtained, and equilibrium humic acid concentrations were determined according to the straight line equation yielded from the calibration lines obtained at different solution parameters.

Humic acid adsorption was calculated from the difference between initial humic acid concentration and the equilibrium concentration in solution according to the following equation

$$q = (C^0 - C) \frac{V}{m \times S.A} \quad 4-4$$

where q is the mass of humic acid adsorbed (g/m^2), C^0 and C are the initial and equilibrium concentrations of humic acid respectively (g/L), V the volume of the suspension (L), $S.A$ is the surface area of the mineral (m^2/g), and m the mass of solid in suspension (g).

Triplicate experiments were performed in selected experiments in order to obtain the random error associated with the experimental procedure. The experimental error was estimated at about 5% or less and therefore a 5% error was assumed for all the adsorption measurements.

Reaction kinetics

The reaction kinetics of humic acid adsorption on gibbsite and kaolinite were investigated in preliminary experiments carried out in 0.001 M NaCl background electrolyte, at pH 4 and 7. The rate of adsorption was examined by measuring the extent of humic acid adsorption at different mixing times, which varied from 2 minutes to 4 hours. For both minerals the results showed a very rapid adsorption process, and an apparent equilibrium was established within the first 10 minutes. Because of the very fast reaction kinetics observed, the reaction time for all adsorption experiments was set at 2 hours.

Adsorption as a function of pH

The effect of pH on humic acid adsorption onto kaolinite and gibbsite was examined over the pH range between 4 and 10, in 0.001 M NaCl solutions. A new mineral suspension was used for each pH value examined. For the kaolinite systems, 12 g/L mineral suspensions were used at two different initial humic acid concentrations of 0.019 or 0.038 g/L. The adsorption as a function of pH was also examined in kaolinite-humic acid systems consisting of a 6 g/L kaolinite suspensions and an initial humic acid concentration of 0.057 g/L. For gibbsite systems, 12 g/L mineral suspensions were used at three different initial humic acid concentrations of 0.038, 0.057, and 0.074 g/L. Depending on the initial humic acid concentrations required, the total volume of the mineral suspensions varied from 51 to 54 mL.

Adsorption isotherms

Adsorption isotherms were determined by adding various initial humic acid concentrations in suspensions of constant mineral concentration, constant ionic strength (0.01 M NaCl) and a constant pH. Mineral suspensions of 6 g/L for kaolinite and of 4 g/L for gibbsite were used. A new mineral suspension was used for each particular initial humic acid concentration. At pH 5, adsorption isotherms at 0.05 and 0.1 M ionic strength were also obtained for both minerals.

Adsorption as a function of ionic strength and type of background electrolyte

Several experiments were undertaken to determine the effect of ionic strength on humic acid adsorption. The effect of ionic strength on adsorption was evaluated using NaCl as the background electrolyte at pH 5, 7 and 9. The effect of different types of electrolytes was evaluated using NaCl, KCl, MgCl₂, SrCl₂ and MgSO₄ at 0.01 M. In all these experiments the initial humic acid concentration was 0.057 g/L in mineral suspensions of 6 g/L and 4 g/L for kaolinite and gibbsite respectively. All adsorption experiments were carried out in triplicates in order to determine whether significant differences (at the 95% confidence level) existed in the extent of humic acid adsorption obtained with the different background electrolyte ions.

IR spectroscopy

IR measurements of adsorbed humic acid species at the mineral-water interface were obtained using a Biorad FTS 6000 spectrometer equipped with a deuterated triglycine sulphate (DTGS) detector. Each spectrum recorded consisted of 256 co-added scans, obtained at a spectral resolution of 4 cm⁻¹. The flow through *in situ* IR spectroscopic method used to obtain the IR spectra of humic acids at the mineral-water interface, is described in Chapters 2 and 3. The deposition method consisted of distributing 1 mL of the mineral suspension (0.02 g of either kaolinite or gibbsite in 20 mL of D/I water) across the surface of the ZnSe crystal and allowing it to air dry at room temperature.

The IR spectra of surface bound humic acid species reported were obtained using a subtraction procedure also detailed in Chapter 2. Briefly two subtraction steps were required in order to isolate the spectra arising by the adsorbed humic acid species alone. In the first step the background spectrum, containing IR contributions from the mineral phase and the internal reflection element, was subtracted. In the second step, a water spectrum taken prior to the addition of the humic acid solution was subtracted from the sample spectra in order to remove the strong water absorption bands that dominate the spectra recorded in the presence of water. Separate experiments were carried out for each pH and ionic strength value examined and some experiments were replicated to check the reproducibility of the acquired IR spectra.

Results and Discussion

Acid-base properties of humic acid

In common with other organic acids, the acid-base properties of humic acid are governed by the proton affinity of the various acidic functional groups present in its structure. Although humic acids possess several different types of functional groups, the proton binding sites in humic acid are considered to be dominated by carboxylic and phenolic moieties (Ritchie and Perdue, 2003). It is therefore important to determine the concentration and acidity constants of these functional groups in order to help understand and describe the behaviour of humic acids in the natural environment.

Due to the significance of the carboxylic and phenolic content of humic acids, numerous studies have been carried out in an attempt to estimate the concentrations and acidity constants of these two functional groups in humic acids (De Wit et al., 1993b; Gustafsson, 2001; Marshall et al., 1995; Masini et al., 1998; Milne et al., 1995; Milne et al., 2001; Ritchie and Perdue, 2003; Westall et al., 1995; Zhou et al., 2005). Acid-base titration is by far the most commonly used method for the determination of proton binding site concentrations in humic acids. A great variation in experimental procedures and data treatment can be found in the literature including (a) the experimental conditions in which the titrations were conducted, such as the pH range and ionic strengths examined, (b) equilibration times allowed for the incremental titrant addition, (c) equations and correction factors used to calculate the concentration of adsorbed hydrogen ions, (d) numerical models used to describe the proton binding equilibria of humic acid.

The lack of universally accepted systematic analysis of humic acid titration data coupled to the inherently complex and heterogeneous nature of humic acids can have a significant effect on the acid-base properties determined. The method used for the determination of acid-base parameters can in fact produce a greater variation in the results obtained than the physicochemical heterogeneity between different humic acid samples (Leenheer et al, 1995). As a result a wide range of humic acid parameters relating to the number, concentration and acidity of proton binding sites have been previously reported. Table 4-1 provides examples of humic acid acid-base parameters proposed in the literature.

Table 4-1 Summary of the acid-base properties of humic acid reported in the literature.

Study	sample type	Model used to fit data	Concentration of acidic groups (mmol g ⁻¹)			Proton binding constants					
			Carboxylic	Phenolic	Total	pKa ₁	pKa ₂	pKa ₃	pKa ₄	pKa ₅	pKa ₆
Marshall et al. (1995) ^a	natural	Model A ^b	-	-	3.21	3.33	5.98				
Marshall et al. (1995) ^a	natural	Model V ^c	-	-	-	2.72	4.23	5.74	8.17	9.53	10.89
Westall et al. (1995)	IHSS reference	Nonelectrostatic	4.2	1.2	6.3 ^d	4	6	8	10		
Masini et al. (1998)	commercial	Nonelectrostatic	3.6	1.3	4.9	2.83	4.66	6.12	7.46	8.7	9.88
Masini et al. (1998)	commercial	Nonelectrostatic	3.3	1.5	4.8	3.26	5.25	6.42	7.5	8.82	10.23
Milne et al. (1995)	natural ^e	EDL	3.08	2.19	5.27	3.69	8.38				
Boily and Fein (2000)	commercial	Nonelectrostatic	-	-	7.43	2.6	6.1	8.8			
Gustafsson (2001)	purified peat ^f	Stockholm Humic Model	2.5	2.5	5.0	3.9	8.9				
Gustafsson (2001)	commercial ^g	Stockholm Humic Model	2.5	2.5	5.0	4.4	8.9				
Milne et al. (2001)	commercial ^h	NICA-Donnan	2.94	2.40	5.34	3.76	8.07				
Milne et al. (2001)	commercial ⁱ	NICA-Donnan	2.31	5.34	7.65	2.87	8.00				
Janos et al.(2008)	natural (raw) ^j	None- pH based	4.05	2.90	6.95						
Janos et al.(2008)	natural (purified) ^j	None- pH based	4.95	2.10	7.05						

a Values reported are mean values obtained for ten different humic acid samples.

b Calculations based on a simple electrostatic model using only two types of functional groups, a carboxyl and an acid hydroxyl group.

c Based on model V suggested by Tipping and co-workers which allows for the addition of multiple carboxyl and hydroxyl groups. pKa₁₋₃ constants represent the dissociation constants of carboxyl groups and pKa₄₋₆ of hydroxyl groups.

d The remaining 0.9 mmol g⁻¹ were assigned to an amino acid group (pKa₃ = 8)

e peat humic acid

f purified peat humic acid (dataset HH-09).

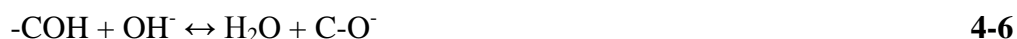
g purified Aldrich humic acid (dataset HH-18). Same dataset used by Milne et al (2001) with code HH-18

h purified Aldrich humic acid (dataset HH-18). This dataset provided one of the best model fits in this study.

i Aldrich humic acid (dataset HH-24).

j similar to leonardite humic acid, prepared from young brown coal

Previous researchers have employed simple, empirical rules in order to estimate the type and concentration of acidic functional groups from humic acid titration curves. For example carboxylic and phenolic groups have been operationally distinguished in the titration curves by assuming that each group is responsible for the base (or acid) consumption up to a specific pH value. Base consumption by carboxylic and phenolic groups can be represented by the following reactions:



All carboxylic groups (and no phenolic groups) are generally assumed to consume base up to pH 7 or 8, whereas base consumption between pH 8 and 10 is attributed to one half of the phenolic group concentration of the humic acid (Janos et al., 2008; Ritchie and Perdue, 2003; Santos et al., 1999).

According to the abovementioned rules, initial estimates for the concentration of carboxylic and phenolic groups can be obtained by plotting the concentration of adsorbed protons on a relative scale, in which proton uptake is assumed zero ($[\text{H}^+_{\text{ads}}] = 0$) at pH 10 (Figure 4-1). Table 4-2 shows the apparent carboxylic and phenolic group concentrations derived from the titration data shown in Figure 4-1. The total number of carboxylic sites on humic acid was assumed to be equal to the number of protons adsorbed up to pH 8, and the total number of hydroxyl sites was assumed to be twice the proton adsorption density between pH 8 and 10.

Table 4-2 Carboxylic and phenolic group concentrations for the humic acid used in the present study, estimated from the titration curves shown in Figure 4-1.

Ionic strength (M)	Site Density (mmol g^{-1})		
	Carboxylic	Phenolic	Total
0.001	2.29	2.70	4.99
0.01	1.98	1.70	3.68
0.1	2.21	1.42	3.63

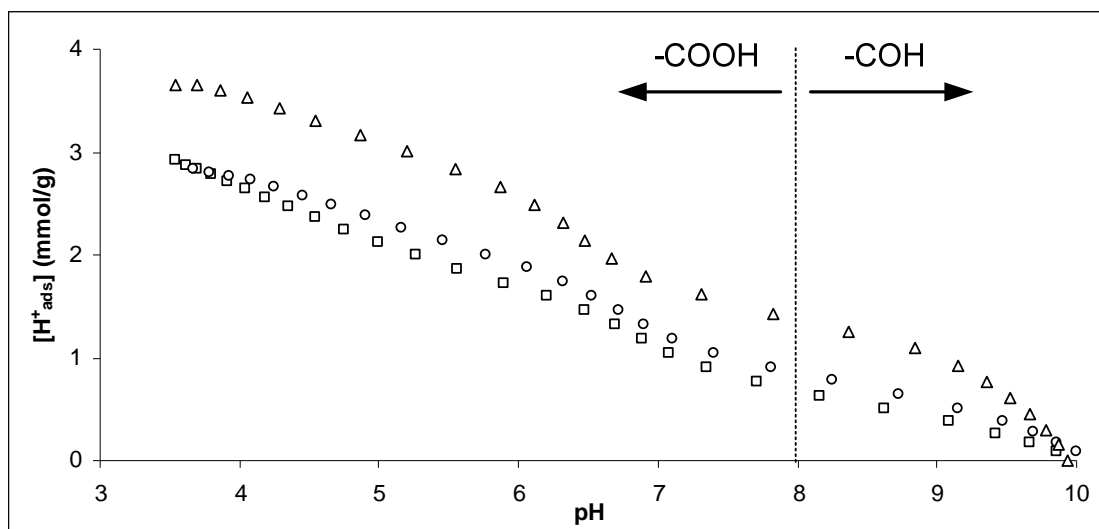


Figure 4-1 Acid-base titration curves for the humic acid sample used in the present study, obtained at 0.001 M (triangles), 0.01 M (circles), and 0.1 M (squares) NaCl. The proton adsorption density (H^+_{ads}) expressed as mmol of hydrogen ions adsorbed per gram of humic acid is given on a relative scale assuming $[H^+_{ads}] = 0$ at pH 10. At pH values lower than 8, carboxylic groups are assumed to be responsible for proton adsorption, whereas at pH values higher than 8 phenolic groups are assumed to be involved in proton adsorption reactions.

The acid-base properties of humic acids can also be obtained by fitting the titration data to one of the several chemical equilibrium models developed to model adsorption reactions occurring in aqueous species and on mineral surfaces. Such models simulate the experimental data by using best-fit values for a set of adjustable parameters. The number of adjustable parameters and model assumptions depend on the type of model used to fit the experimental data. Each model has its own limitations and advantages and it is therefore not surprising that no single model is widely accepted.

For example non electrostatic models (NEMs) do not take into account the electrostatic effects of proton binding reactions and hence the results obtained are limited to the particular experimental conditions of the system under investigation. Although electrostatic models are more likely to successfully describe titration data over a wider range of experimental conditions, they require a higher number of input parameters. Furthermore some of the more sophisticated models developed require input parameters that may not be readily available such as charge spreading around the humic acid molecule, the geometry of molecules (e.g. cylinder vs sphere), and interactions of binding sites with background electrolyte ions (Avena et al., 1999; Christensen et al., 1998; De Wit et al., 1993a; Gustafsson, 2001).

Differences in modelling results may not only originate from the different types of models used but also on the assumptions made regarding some important physicochemical properties of humic acids. The number of different types of available binding sites used in the modelling of titration data will have a significant effect on

model outputs. Unfortunately there is no general consensus in the literature on the number of different binding sites required to model proton adsorption, with values ranging from two sites up to eight sites. Site densities and their respective concentrations are typically treated as adjustable parameters when modelling the proton-binding properties of humic acids.

Furthermore, the dissociation of acidic groups may be modelled as a collection of discrete proton affinity constants or as a continuous distribution of pKa values. For the discrete-site approach, humic acid is assumed to be composed of either a mixture of different monoprotic acids or as a polyprotic acid which undergoes a series of protonation/deprotonation steps (Boily and Fein, 2000). Conversely the continuous distribution approach aims to describe the functional group heterogeneity of humic acids by assuming a continuous distribution of acidity in humic acid molecules. The pKa values obtained represent the mean values derived from a numerical function which describes the site distribution within the humic acid molecule (Fukushima et al., 1995). Again there is no agreement which representation is more appropriate for modelling humic acid titration data.

From the above discussion it is evident that the structural and chemical complexity of humic acids presents several problems for the description of the proton binding chemistry. Ideally a model should be able to adequately describe the acid-base equilibria over a wide range of experimental conditions (such as pH and ionic strength) with the least number of adjustable parameters. For the present study the aim was to derive a simple chemical model that represents the chemical behaviour of the humic acid sample used, which in turn will enable the description of humic acid adsorption behaviour on kaolinite and gibbsite. Hence an accurate representation of the binding properties of humic acid is beyond the scope of the present study and the reader is referred to the literature for studies which explicitly consider the physicochemical properties of humic acids.

A non electrostatic model with three different proton binding sites was found to give a satisfactory description to the acid-base titration data and therefore the proton binding properties of humic acid were estimated according to this simple model. It has to be noted that such a model does not necessarily represent the “real” physicochemical properties of humic acid which is expected to have a much higher number of binding sites with a wide range of proton binding constants. Furthermore, a non electrostatic model can only provide apparent equilibrium constants for the proton binding reactions of humic acidic functional groups. However, even the more complex electrostatic models require several input parameters that can be subject to significant uncertainties

such as the geometry of humic molecules, surface area, charge accumulation and background electrolyte permeability in the humic molecule (Westall et al., 1995). For comparison purposes, the diffuse layer model, a relative simple electrostatic model, was also used for modelling the titration data of humic acid.

Figure 4-2 presents the titration curves of humic acid, obtained at three different ionic strengths, together with model fits calculated by the nonelectrostatic model. Model fits obtained using two proton binding sites (dashed lines) and three proton binding sites (solid lines) are included for comparison. As can be seen, the model consisting of three binding sites provides a better fit to the experimental data and therefore model outputs from this model are chosen for the present study. The proton binding properties optimised according to the three site model are given in Table 4-3. The calculated fractional distribution of the three proton binding sites, as a function of pH, at I= 0.001 and 0.01 M are shown in Figure 4-3. The dissociation reactions of these three structurally different binding sites are represented by the following reaction



where HL represents a protonated functional group, for n=1,2,3.

Table 4-3 Optimised model parameters describing the acid-base behaviour of humic acid, at three ionic strengths, according to the three site nonelectrostatic model proposed. Concentrations of acidic functional groups are given in mmol per litre of humic acid solution and mmol per gram of humic acid. Binding sites have been assigned to phenolic or carboxylic groups according to their acidity constants.

Ionic Strength	Surface group	Site density		Proton reaction	log K	V(Y)*
		mmol L ⁻¹	mmol g ⁻¹			
0.1 M	HL1 (-COOH)	0.572	1.144	HL1 ↔ H ⁺ + L1 ⁻	-4.45	0.7
	HL2 (-COH)	0.288	0.576	HL2 ↔ H ⁺ + L2 ⁻	-9.13	
	HL3 (-COOH)	0.603	1.206	HL3 ↔ H ⁺ + L3 ⁻	-6.77	
	Σ^{COOH}	1.175	2.350			
	Σ^{COH}	0.288	0.576			
0.01 M	HL1 (-COOH)	0.472	0.944	HL1 ↔ H ⁺ + L1 ⁻	-4.67	0.6
	HL2 (-COH)	0.323	0.646	HL2 ↔ H ⁺ + L2 ⁻	-9.27	
	HL3 (-COOH)	0.624	1.248	HL3 ↔ H ⁺ + L3 ⁻	-6.76	
	Σ^{COOH}	1.096	2.192			
	Σ^{COH}	0.323	0.646			
0.001 M	HL1 (-COOH)	0.401	0.802	HL1 ↔ H ⁺ + L1 ⁻	-3.86	2.8
	HL2 (-COH)	0.591	1.182	HL2 ↔ H ⁺ + L2 ⁻	-9.50	
	HL3 (-COOH)	0.659	1.318	HL3 ↔ H ⁺ + L3 ⁻	-6.37	
	Σ^{COOH}	1.060	2.120			
	Σ^{COH}	0.591	1.182			

*Goodness of fit parameter calculated by FITEQL.

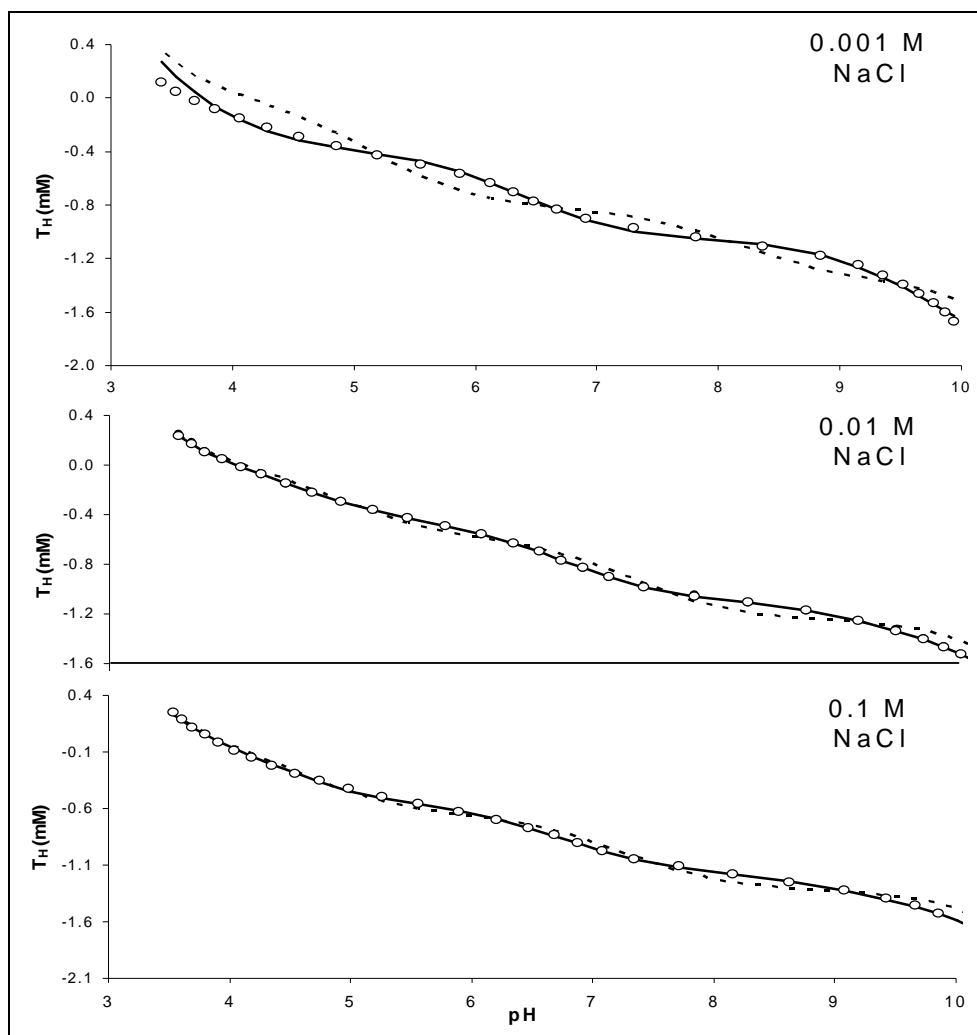


Figure 4-2 Acid-base titration data for humic acid at $I = 0.001, 0.01$ and 0.1 M NaCl, shown as total hydrogen (T_H) in mM added in the solution. Symbols represent experimental datapoints and lines represent model fits according to the non electrostatic model. Solid lines represent the model consisting of 3 binding sites and dashed lines a model consisting of two binding sites.

Based on the pKa values ($-\log K$ of the proton binding constants) derived from the modelling results, each binding site could be assigned to a specific functional group. Previous studies related the modeled pKa values to pKa values of known functional groups found in simpler organic molecules such as carboxylic and phenolic groups. Typically the strongest acidic sites are thought to mainly represent carboxylic groups and the weaker acidic sites are thought to represent phenolic groups (Gustafsson, 2001; Westall et al., 1995; Zhou et al., 2005). Accordingly, for the present study, the two binding sites with pKa values around 4 and 6.5 can be ascribed to carboxylic groups and the binding site with a pKa value at about 9 to a phenolic group. However, depending on the stereochemical arrangement of acidic functional groups within the humic acid molecule, the acidity constants of specific functional groups may exhibit uncharacteristically high values when compared to those found in simpler organic acids

(Davis, 1982). This is particularly true for neighbouring carboxylic groups where the dissociation of the first group can significantly increase the dissociation constant of an adjacent group. The higher than expected pKa values exhibited by such carboxylic groups would result in falsely being categorised as phenolic/hydroxyl groups. Therefore the concentrations of carboxylic and phenolic groups given in Table 4-3 are only estimates.

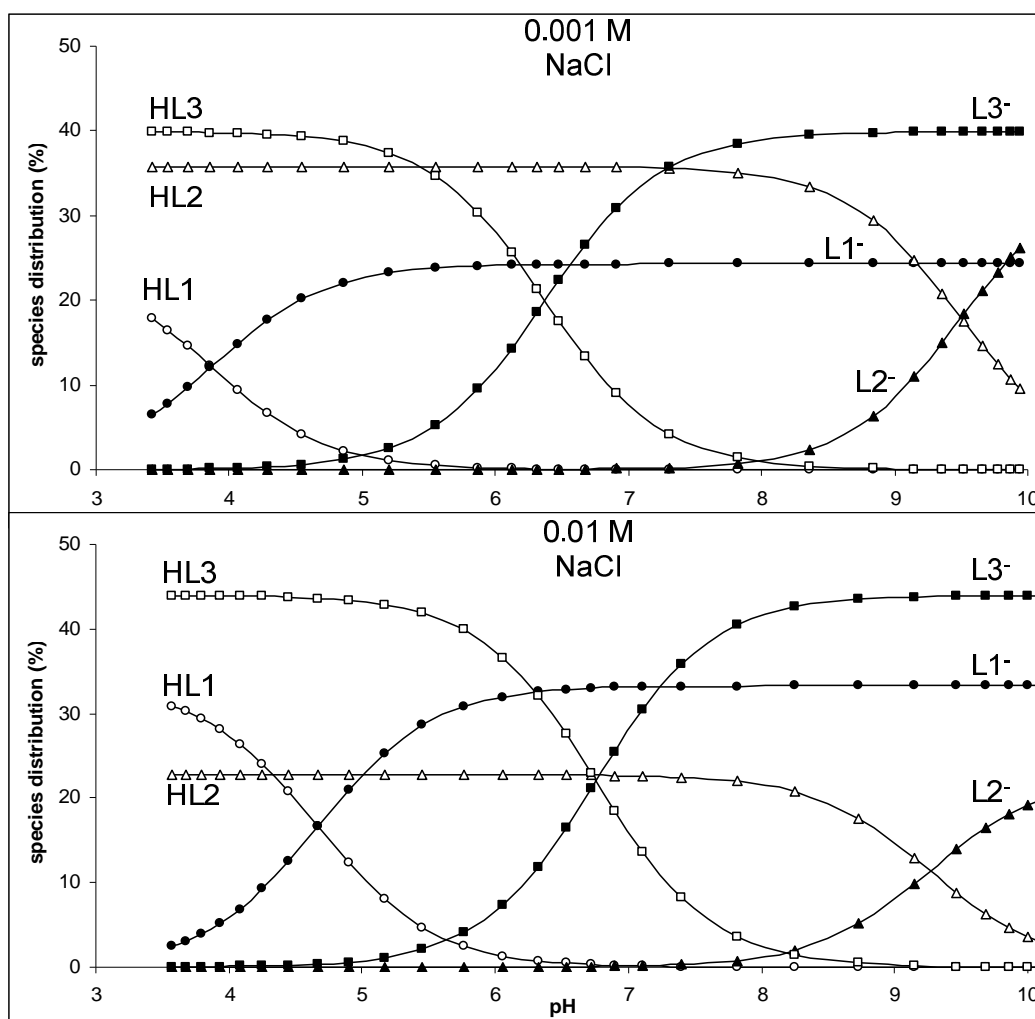


Figure 4-3 Fractional concentration of the three proton binding sites according to the non electrostatic model summarised in Table 3, at $I = 0.001$ and 0.01 M NaCl. HL denotes neutral functional groups and L^- denotes deprotonated functional groups.

Differences in the concentration of functional groups obtained at different ionic strengths could be attributed to either the highly heterogeneous nature of humic acid sample or to modelling artefacts due to the simple model used. Major sources of uncertainty related to the study of humic acid acid-base properties have been

investigated in detail elsewhere (Santos et al., 1999) and uncertainty contributions include sample heterogeneity and errors in pH measurements. Furthermore, differences in the concentration of functional groups obtained could also reflect the effects of ionic strength on the structural conformation of humic acid molecules. In turn, changes in the structural conformation may influence the relative and absolute concentrations of the different types of functional groups exposed to the solution

The concentrations of acidic groups found in the present study appear to be lower than those reported in previous studies (see Tables 4-1 and 4-3). The different humic acid samples used is a major factor that can explain the lower proton binding capacity found in the present study. Moreover, the concentrations of humic acid solutions assumed and hence reported here are not on an ash-free weight basis, whereas in most studies concentrations are given on ash-free weight basis. According to the chemical specifications of the particular sample used in this study, humic acid has an ash content of about 50%. Although the insoluble fraction was removed from the humic acid stock solution by centrifugation, the concentration assumed was for the initial mass of humic acid added (i.e. 1 g/L). This high ash content therefore overestimates the true concentration of humic acid in the stock solution by about 50%, and this in turn underestimates the concentration of proton binding sites determined. Recalculating the humic acid concentration in the stock solution on an ash free basis gives a value of about 0.5 g/L. Consequently the site density concentrations (mmol/g of humic acid) reported in Table 4-3 can be doubled to account for the new humic acid concentration value. These new values obtained for the concentrations of proton binding sites are within the range of concentrations reported in the literature.

Table 4-4 compares the modelling results obtained from the non electrostatic model with selected modelling results obtained using the Diffuse Layer Model (DLM). The DLM requires two additional adjustable parameters, namely interfacial capacitance and specific surface area of the humic acid. The specific surface area of humic substances is typically calculated mathematically from the estimated radius and density of humic acid (De Wit et al., 1993a; Tipping, 2002; Zhou et al., 2005). The different surface area values examined in Table 4-4 are within the estimated range of 2000 to 10500 m²/g suggested for humic acids (Zhou et al., 2005). It can be seen that for the titration curve obtained at 0.1 M, the results estimated according to the DLM, using a humic surface area of 10000 m²/g, are in a very good agreement with those estimated by the non electrostatic model. The DLM does not offer any advantage over the NEM in terms of goodness of fit since the error parameters calculated by FITEQL for both models are very low for both models. Moreover, the use of DLM introduces further

variability in model outputs because the surface area of humic acid cannot be calculated with confidence.

Table 4-4 Comparison of the optimised model parameters obtained using the Diffuse Layer Model (DLM) and the non electrostatic model (NEM).

Humic acid proton binding properties						Other model parameters		
Ionic Strength	Surface group	Site density		Proton reaction	log K	Model	Surface area	
		mmol L ⁻¹	mmol g ⁻¹				m ² g ⁻¹	V _Y
0.1 M	HL1	0.572	1.144		-4.45	NEM	N/A	0.7
	HL2	0.288	0.576	HL _n ↔ H ⁺ + L _n ⁻	-9.13			
	HL3	0.603	1.206	n= 1,2,3	-6.77			
0.1 M	HL1	0.643	1.286		-3.97	DLM	2000	1.6
	HL2	0.296	0.592	HL _n ↔ H ⁺ + L _n ⁻	-7.83			
	HL3	0.586	1.172	n= 1,2,3	-5.50			
0.1 M	HL1	0.584	1.168		-4.27	DLM	6000	0.4
	HL2	0.291	0.582	HL _n ↔ H ⁺ + L _n ⁻	-8.54			
	HL3	0.627	1.254	n= 1,2,3	-6.23			
0.1 M	HL1	0.577	1.154		-4.33	DLM	10000	0.3
	HL2	0.289	0.578	HL _n ↔ H ⁺ + L _n ⁻	-8.75			
	HL3	0.622	1.244	n= 1,2,3	-6.43			

Adsorption experiments

Adsorption as a function of pH

The adsorption of humic acid as a function of pH and different initial humic acid concentrations on gibbsite and kaolinite is shown in Figures 4-4 and 4-5 respectively. At a fixed ionic strength (0.001 M NaCl) the extent of humic acid adsorption is dependent on both the pH of the solution and initial humic acid concentrations, with increased adsorption densities at lower pH and higher initial humic acid concentrations. The strong pH dependence of humic acid adsorption on both mineral surfaces is consistent with the findings reported for the adsorption of humic substances to various mineral surfaces (e.g. Arnarson and Keil, 2000; Au et al., 1999; Davis, 1982; Filius et al., 2000; Gu et al., 1996; Murphy et al., 1992; Tipping, 1981; Wang et al., 1997; Yoon et al., 2004a; Zhou et al., 1994)

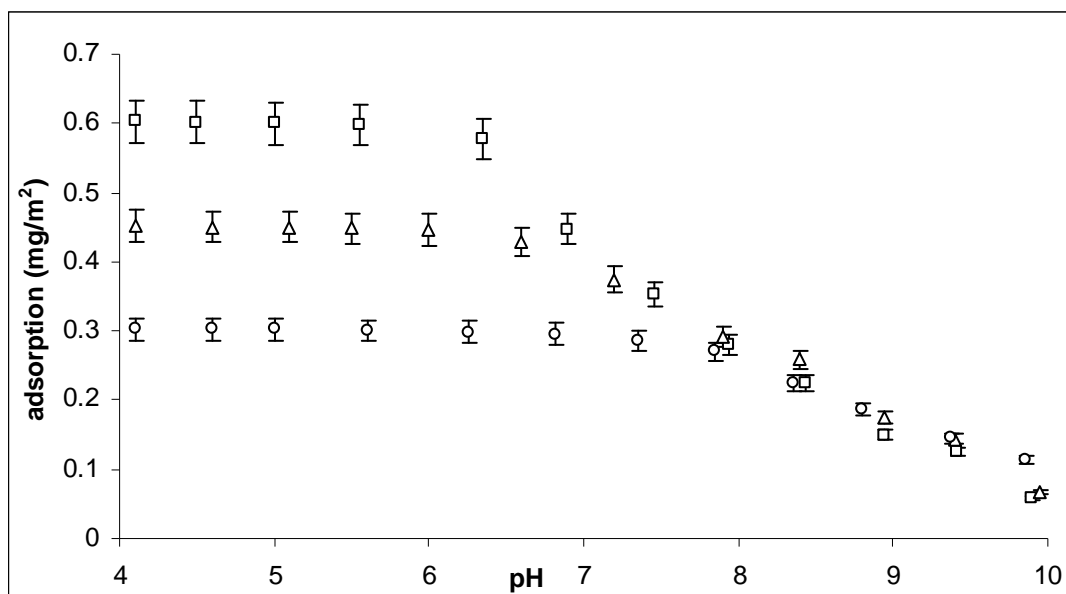


Figure 4-4 Adsorption of humic acid on gibbsite as a function of pH, expressed in mg of adsorbed humic acid per m² of gibbsite. Gibbsite suspension concentration is 12 g/L at a background electrolyte concentration of 0.001 M NaCl. Initial humic acid concentrations used are 0.074 g/L (squares), 0.057 g/L (triangles), and 0.038 g/L (circles). Error bars of 5% represent the random error associated with the experimental procedure.

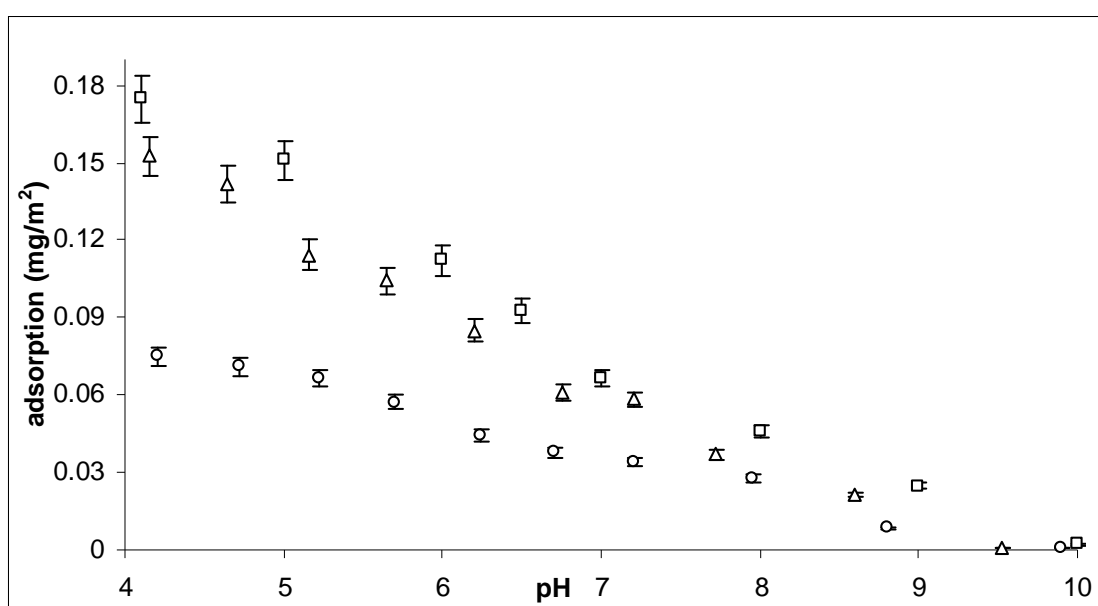


Figure 4-5 Adsorption of humic acid on kaolinite as a function of pH, expressed in mg of adsorbed humic acid per m² of kaolinite. Squares represent humic acid adsorption from a kaolinite suspension of 6 g/L and initial humic acid concentration of 0.057 g/L. Kaolinite suspension concentration for the other two datasets is 12 g/L and initial humic acid concentrations are 0.038 g/L (triangles) and 0.019 g/L (circles). In all systems a background electrolyte of 0.001 M NaCl is used. Error bars of 5% represent the random error associated with the experimental procedure.

At acidic conditions all the available humic acid is adsorbed on gibbsite indicating that adsorption is limited by the concentration of humic acid rather than the available surface sites and that maximum surface coverage has not been reached. At

near neutral pH conditions and basic conditions, a gradual decrease in adsorption is observed as the pH of the solution increases and at pH values higher than about 8 the adsorption appears to be independent of the starting humic acid concentration.

The adsorption data for the kaolinite-humic acid systems are more scattered probably due to the lower adsorption densities obtained which are subject to bigger experimental error. Humic acid adsorption on kaolinite shows a greater pH-dependence, than on gibbsite, and a gradual decrease in adsorption over the entire pH-range studied can be observed. At pH values above 9 the adsorption becomes negligible in all three kaolinite-humic acid systems investigated. The adsorption behaviour of humic acid on kaolinite suggests that even in acidic conditions, the availability of surface sites is the limiting factor for adsorption rather than humic acid concentration.

The pH-dependent adsorption behaviour observed, suggests that adsorption is controlled, or at least favoured, by the electrostatic interactions between charged surface sites and ionised humic acid functional groups. The pH of the solution is an important parameter in the adsorption process because it controls the charge of both the surface sites and of the humic acid molecules, and therefore governs the type of electrostatic interactions between the surface and humic acid. In general, adsorption will be favoured within the pH-range where surface sites and humic acid molecules carry opposite electrical charges.

The pH-dependent charge on mineral surfaces originates from the amphoteric character of surface hydroxyl groups which can either dissociate, at high pH, or protonate, at low pH. Below the pH_{pzc} , the surface has a net positive charge and above the pH_{pzc} the surface has a net negative charge. Therefore the surface charge of a mineral will change from positive to negative with increasing pH. Similarly, the pH of the solution controls the extent of dissociation of acidic functional groups within humic acid molecules and this in turn governs the overall charge of these molecules. At low pH values ($pH < 1^{st}$ acid pK_a of humic acid), the majority of these functional groups are undissociated resulting in an overall neutral or low negative charge. As the pH of the solution increases, more acidic functional groups dissociate and the net charge of the humic molecules becomes increasingly more negative.

The effect of pH on the type of electrostatic interactions occurring between humic acid molecules and the surfaces of kaolinite and gibbsite can therefore explain the observed humic acid adsorption trend as a function of pH. Over the entire pH range examined, humic acid molecules possess a negative charge which originates from the dissociation of strong acidic functional groups (estimated $pK_{a1} \approx 4$; Figure 4-3). Conversely, for kaolinite the net surface charge becomes negative at pH values above

about 5.1 and for gibbsite at pH values above about 9 (kaolinite $pH_{pzc} = 5.1$, gibbsite $pH_{pzc} = 9$; Sverjensky and Sahai, 1996). Consequently at pH values below the pH_{pzc} of the two minerals, adsorption can be driven by the electrostatic attraction between the surface and the humic acid molecules. As the pH of the solution increases, the negative charges on both the surface and the humic molecule increase and this results in lower adsorption due to the reduced electrostatic attractions (or increased electrostatic repulsions) between humic acid molecules and the surface.

It has to be noted, however, that a pH-dependent adsorption trend does not necessarily indicate that the interactions between adsorbed humic acid molecules and surface sites involve only simple Coulombic forces of attraction. At low pH, electrostatic attractions allow humic acid molecules to come in contact with the surface and this in turn can increase the possibility of other adsorption mechanisms to take place (Arnarson and Keil, 2000; Ganor et al., 2009). As a result regardless of the adsorption mechanisms involved in the uptake of humic acids, adsorption is expected to be significantly influenced by the pH of the solution.

According to the results obtained in the preset study, humic acid exhibits a higher adsorption affinity for gibbsite than for kaolinite over the entire pH examined. Figure 4-6 compares the adsorption of humic acid on kaolinite and on gibbsite as a function of pH, obtained under the same experimental conditions (0.001 M NaCl, mineral suspension of 12 g/L and an initial humic acid concentration of 0.038 g/L). The surface concentration of humic acid on gibbsite is always higher than that on kaolinite for the entire pH range examined. An increase in pH from 4 to 10 results in decreased adsorption from 0.3 to 0.12 mg of humic acid/m² for gibbsite and from 0.15 to almost 0 mg of humic acid/m² for kaolinite. Corresponding percentage adsorption values are from about 99% to 38% for gibbsite and from about 96% to 0.5% for kaolinite.

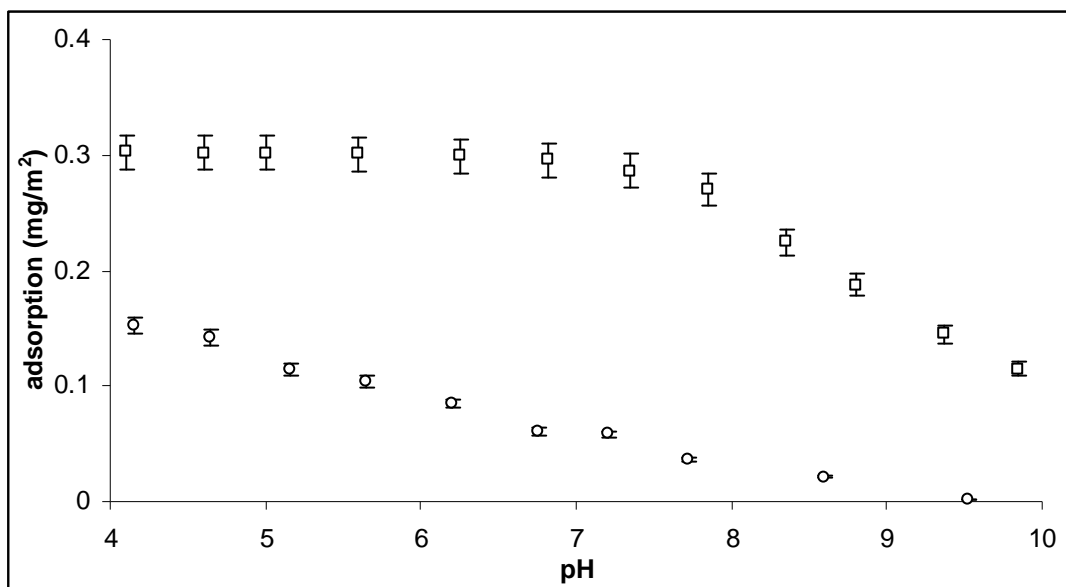


Figure 4-6 Humic acid adsorption density on kaolinite (circles) and gibbsite (squares), expressed as mg of humic acid adsorbed per m² of mineral surface. The mineral-humic acid systems consisted of kaolinite or gibbsite suspensions of 12 g/L and an initial concentration 0.038 g/L of humic acid. Error bars of 5% represent the random error associated with the experimental procedure.

The higher adsorptive capacity of gibbsite can be attributed to the different structural and chemical properties of the two mineral substrates such as surface area, surface charging properties, density of surface sites, and affinity of these surface sites for humic acid. As already mentioned a pH-dependent adsorption behaviour observed reflects the importance of electrostatic effects on humic acid adsorption. It is therefore expected that the different surface charging properties of the two minerals (i.e. the acidity of surface hydroxyl groups) will significantly affect the extent of adsorption. The pH_{pzc} values of kaolinite (5.1) and gibbsite (9) indicate that the net surface charge of gibbsite is positive over a wider range of pH values and, that at each particular pH, the surface of gibbsite will always be more positive (or less negative) than the surface of kaolinite. As a result this higher positive charge can enhance the adsorption of negatively charged humic acid molecules on gibbsite.

Furthermore the concentration of binding sites involved in humic acid adsorption reactions may be different for the two mineral surfaces. It has been suggested that it is primarily the aluminium hydroxyl groups located at the edge surface of kaolinite (about 20-30 % of the total surface area) which participate in surface adsorption reactions (Brady et al., 1996; Namjesnik-Dejanovic et al., 2000) and hence this may explain the lower humic acid adsorption densities on kaolinite. Another possible explanation that can account for the differences in adsorption densities is that the different coordination environment of aluminium in kaolinite and gibbsite may be

affecting the affinity of humic acid for the surface. This factor, however, is not expected to have a significant effect on adsorption since aluminium atoms in the octahedral sheet of kaolinite are coordinated in a similar manner as the aluminium atoms in gibbsite. Finally different adsorption densities could be explained if humic acid is adsorbing via different adsorption mechanisms on the surface of these two minerals. Again this explanation seems improbable since the macroscopic adsorption behaviour and spectroscopic data (presented later) indicate a similar binding mode for both minerals.

Adsorption isotherms

Adsorption isotherms describing the adsorption density of humic acid as a function of humic acid concentration remaining in solution after equilibration, at fixed pH, are shown in Figures 4-7 and 4-8. For both mineral substrates, the adsorption isotherms determined exhibit a steep slope at low equilibrium concentrations, and a plateau section at elevated equilibrium concentrations where adsorption density reaches a maximum and becomes independent of equilibrium concentration. The initial steep slope at low concentrations indicates a high affinity type interaction between surface binding sites and humic acid (Gu et al., 1995; Hur and Schlautman, 2003). The plateau section of the isotherms indicates that maximum adsorption on both gibbsite and kaolinite is reached for the range of humic acid concentrations used.

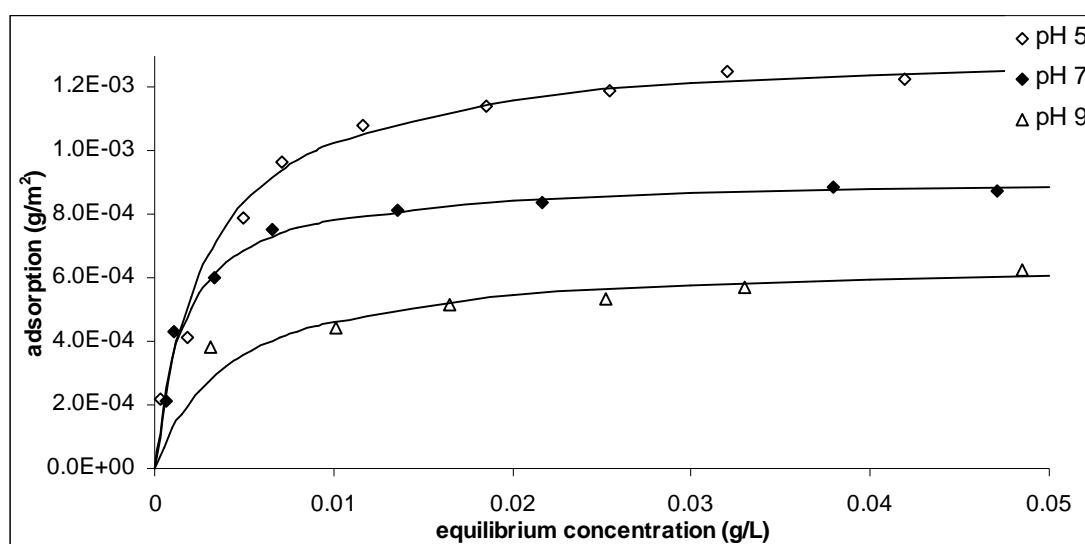


Figure 4-7 Adsorption isotherms of humic acid onto gibbsite at pH 5, 7, 9 and a background electrolyte of 0.01 M NaCl. Adsorption density is expressed in grams of humic acid adsorbed per meter squared of available gibbsite surface area (gibbsite S.A = 10.5 m²/g). Solid lines represent the Langmuir fit for the experimental data (points) using model parameters in Table 5.

For each mineral, the pH of the solution influences the slope of the curves and the maximum sorption density, with lower pH values yielding steeper slopes and higher adsorption maxima. In addition, at each particular pH value, maximum adsorption on the surface of kaolinite is reached at lower humic acid concentrations than on the surface of gibbsite. These observations are in agreement with the results obtained from the adsorption edge experiments (adsorption as a function of pH) and hence the same interpretation can be applied to the adsorption isotherm data. Consequently, increased adsorption maxima at lower pH can be explained by the increased electrostatic attraction between the surface and humic acid molecules. The higher adsorption density observed for gibbsite can be attributed the different surface properties of kaolinite and gibbsite.

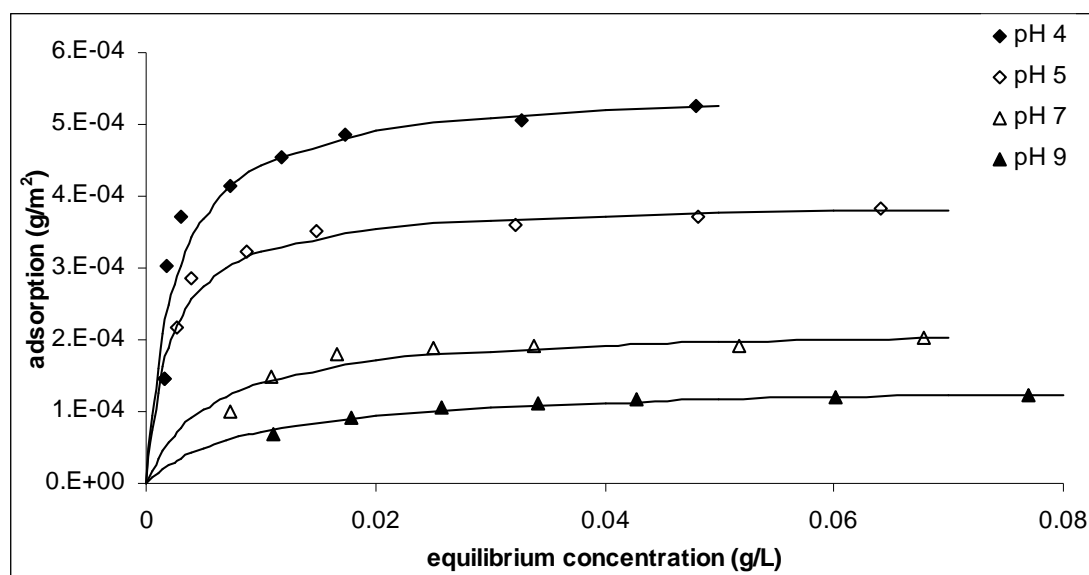


Figure 4-8 Adsorption isotherms of humic acid onto kaolinite at pH 4, 5, 7, 9 and a background electrolyte of 0.01 M NaCl. Adsorption density is expressed in grams of humic acid adsorbed per meter squared of available kaolinite surface area (kaolinite S.A = 21 m²/g). Solid lines represent the Langmuir fit for the experimental data (points) using model parameters in Table 5.

The ionic strength of the solution also has an effect on the adsorption isotherms obtained at pH 5 as illustrated in Figures 4-9 and 4-10. The steeper initial slopes of the isotherms obtained at higher ionic strengths indicate that humic acid exhibits a higher affinity for the surface of kaolinite and gibbsite as the ionic strength of the solution increases. Furthermore, higher quantities of humic acid can adsorb on the surface as the concentration of background electrolyte increases. The effects of ionic strength on humic acid adsorption will be discussed in the following section.

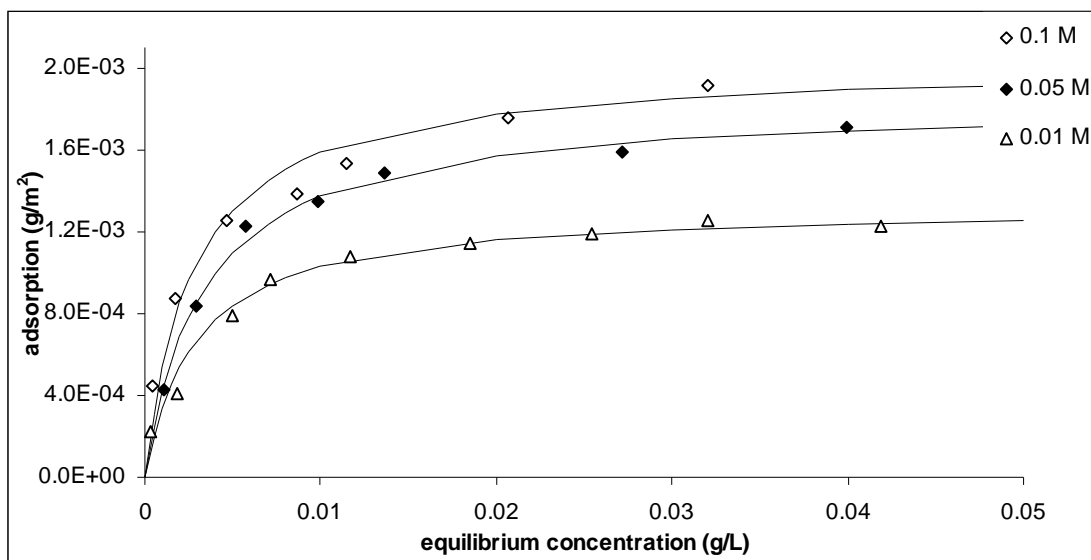


Figure 4-9 Adsorption isotherms of humic acid on gibbsite at pH 5 in 0.01, 0.05 and 0.1 M NaCl. Adsorption density is expressed in grams of humic acid adsorbed per meter squared of available gibbsite surface area (gibbsite S.A = 10.5 m²/g). Solid lines represent the Langmuir fit for the experimental data (points) using model parameters in Table 4-5.

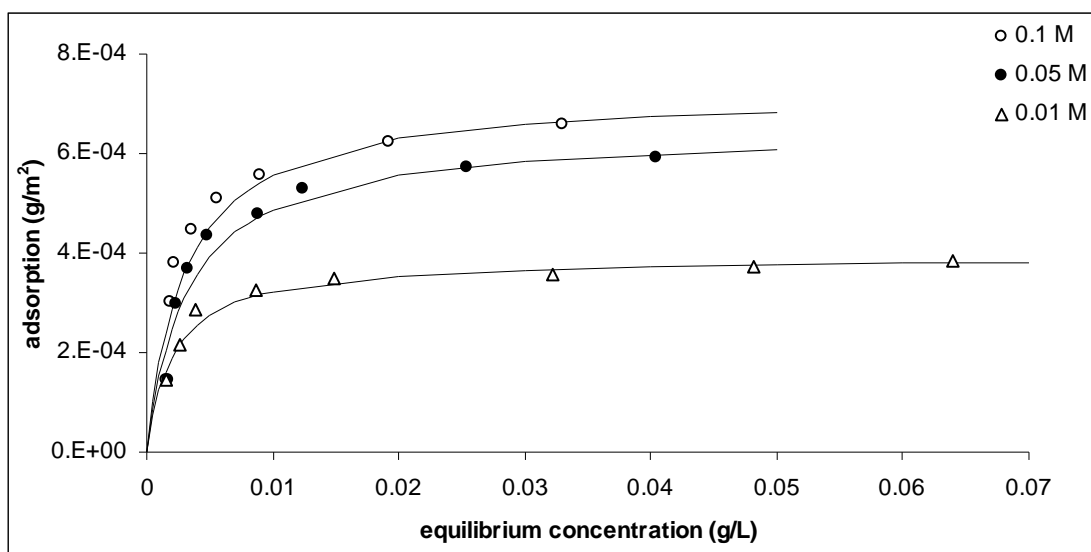


Figure 4-10 Adsorption isotherms of humic acid on kaolinite at pH 5 in 0.01, 0.05 and 0.1 M NaCl. Adsorption density is expressed in grams of humic acid adsorbed per meter squared of available kaolinite surface area (kaolinite S.A = 21 m²/g). Solid lines represent the Langmuir fit for the experimental data (points) using model parameters in Table 4-5.

The general shape of the adsorption isotherm curves obtained in the present study is consistent with the adsorption isotherms reported in the literature for the adsorption of humic substances on oxides (Illés and Tombacz, 2003; Namjesnik-Dejanovic et al., 2000; Saito et al., 2004; Tombacz et al., 2000; Vermeer et al., 1998; Wang et al., 1997) and clay minerals (Majzik and Tombacz, 2007; Murphy et al., 1992; Murphy et al., 1994; Saada et al., 2003a; Tombacz et al., 2004; Vreysen and Maes,

2006). Despite a thorough review of the literature, humic acid adsorption isotherms for gibbsite could not be found for comparison with the present results. For kaolinite, the shape of humic acid adsorption isotherms obtained here are in very good agreement with previously reported humic acid adsorption isotherms (e.g. Jones and Tiller, 1999; Murphy et al., 1994; Saada et al., 2003a; Tombácz et al., 2004). However, it must be noted that Elfarissi and Pefferkorn (2000) reported a different isotherm shape for humic acid adsorption on kaolinite. In their study adsorption reaches a pseudo-plateau region at low initial concentrations and at higher humic acid concentrations there is a further increase in adsorption. Enhanced adsorption at higher concentrations was attributed to hydrophobic bonding between humic molecules and oxygen groups positioned in the basal phase.

For both mineral substrates the humic acid adsorption isotherms obtained at different solution conditions resemble Langmuir-type adsorption isotherms. Adsorption isotherms exhibiting a Langmuir-type behaviour, have been previously used as indicators of monolayer surface coverage. Monolayer surface coverage, however, does not necessarily represent saturation of surface binding sites (Day et al., 1994; Murphy et al., 1992; Murphy et al., 1994). Because of the large size of humic acid molecules, molecular segments which are not directly associated with the surface may be covering neighbouring surface sites and thus inhibiting the involvement of these sites in adsorption reactions.

Because the adsorption of humic acid follows a Langmuir-type isotherm, adsorption isotherms obtained in the present study were fitted according to the Langmuir model. The mathematical description of the adsorption isotherms obeying the Langmuir model is given by the general Langmuir adsorption equation which is given by

$$q = \frac{Kq_{\max}C}{1 + KC} \quad 4-8$$

where q is the adsorption density of humic acid (g of HA/m²); K is the adsorption constant (L/g), which can be used as a relative measure of surface affinity for the adsorbate; q_{\max} is the maximum adsorption density (g of HA/m²); and C the equilibrium concentration in solution (g of HA/L). The linear form of the Langmuir equation is given by

$$\frac{C}{q} = \frac{1}{Kq_{\max}} + \frac{C}{q_{\max}} \quad 4-9$$

Humic acid adsorption maxima (q_{\max}) and adsorption constants (K) were determined from the slope and y-intercept, respectively, of the straight line obtained by plotting C/q vs C as described in equation 4-9. The Langmuir model produced very good fits to the adsorption isotherm data and the estimated model parameters are given in Table 4-5. Theoretical adsorption isotherms calculated according to the estimated Langmuir model parameters are shown as solid lines in Figures 4-7 to 4-10. Although the obtained adsorption isotherms show a very good agreement with the Langmuir adsorption equation, it must be noted that the Langmuir model is a very simple model that can only offer limited information about the adsorption process. The Langmuir model assumes that the surface affinity for humic acid is independent of surface coverage, there are no interactions between the adsorbed species, and the limiting factor for adsorption is the number of reactive surface sites. However due to the heterogeneous and macromolecular character of humic acids these assumptions do not probably hold true. Nevertheless the Langmuir model is a useful tool for estimating the maximum adsorption capacity of mineral surfaces for solute ions.

Table 4-5 Langmuir model parameters obtained from the adsorption isotherm data. K represents the adsorption constant (L/g) and q_{\max} the maximum humic acid adsorption density in milligrams of adsorbed humic acid per unit area of adsorbent surface (mg/m^2) and in micrograms of adsorbed organic carbon per unit area of adsorbent surface ($\mu\text{g C}/\text{m}^2$).

Solution Parameters		Gibbsite				Kaolinite			
I (M)	pH	q_{\max}		K	R^2	q_{\max}		K	R^2
		mg/m^2	$\mu\text{g C}/\text{m}^2$			mg/m^2	$\mu\text{g C}/\text{m}^2$		
0.01	4	-	-	-	-	0.551	30.64	408	0.99
	5	1.33	73.95	342	0.99	0.393	21.85	468	0.99
	7	0.914	50.82	610	0.99	0.219	12.18	177	0.99
	9	0.663	36.86	232	0.99	0.138	7.67	111	0.99
0.05	5	1.84	102.3	297	0.99	0.645	35.86	310	0.98
0.1	5	2.02	112.3	362	0.99	0.725	40.31	329	0.98

Because many studies have reported humic acid adsorption densities in terms of grams of adsorbed organic carbon, Table 4-5 also includes adsorption densities in micrograms of adsorbed organic carbon per meter squared area. It must be noted however that these values were not obtained by direct total organic carbon (TOC) analysis of supernatant solutions. Instead they were obtained by the conversion of mg of humic acid (calculated from UV-Vis spectroscopy) to μg of organic carbon using the total organic carbon concentration measured for the humic acid stock solution (55.6

mg/L). As a result these values are only estimates that allow the comparison of the results obtained here with the results reported in the literature. This is because previous studies provided evidence for the fractionation of humic substances during adsorption on mineral surfaces, with mineral surfaces exhibiting selective adsorption for different humic acid fractions (Feng et al., 2005; Hur and Schlautman, 2003; Illés and Tombacz, 2003; Namjesnik-Dejanovic et al., 2000; Wang and Xing, 2005). If preferential adsorption of either higher or lower molecular weight fractions occurs in the present systems then the linear relationship between grams of humic acid in solution and grams of organic carbon in solution may no longer hold true and therefore the conversion of humic acid concentration to organic carbon concentration may be inaccurate.

Maximum adsorption densities for natural organic matter, or for its individual components (such as humic and fulvic acids), determined from the Langmuir isotherm fitting parameters, have been previously reported for various mineral substrates (e.g. Gu et al., 1996; Gu et al., 1995; Hur and Schlautman, 2003; Illés and Tombacz, 2003; Saada et al., 2003b; Saito et al., 2004; Shen, 1999; Tombacz et al., 2000; Vreysen and Maes, 2006; Wang et al., 1997). Literature values for maximum humic acid adsorption densities on kaolinite are listed in Table 4-6. Comparisons between studies should be interpreted with caution since adsorption maxima were determined under various different solution conditions. In addition, adsorption density values reported are in different units, making direct comparisons difficult.

Adsorption densities obtained in this study appear to be somewhat lower than the adsorption densities listed in Table 4-6. For example at pH 5 and 0.01 M NaCl, Tombacz et al. (2004) obtained a maximum adsorption density of about 12 mg of humic acid per gram of kaolinite. For the same experimental conditions adsorption density in the present study is estimated at about 8 mg of humic acid per gram of kaolinite. Murphy et al. (1994) reported a maximum density of about 13 $\mu\text{mol C}/\text{m}^2$ (i.e. 0.156 mg C/m²) at pH 4.5 and a salt concentration of 0.1 M. The maximum adsorption density estimated in the present, at pH 5 and I= 0.1 M, is about 0.04 mg C/m². Several factors could be responsible for this variation in adsorption densities including different morphology of kaolinite samples, experimental procedures (e.g. equilibration times, determination of solute concentrations), and different humic acid samples used.

Table 4-6 Humic acid maximum adsorption densities on kaolinite reported in the literature.

Study	Solution conditions		Adsorption density	Humic Acid
	pH	Ionic strength		
Hur and Schlautman (2003)	7	0.1 M NaCl	0.114 mg C/m ²	commercial, purified
Tombácz et al. (2004)	4-5	0.01M NaCl	≈12 mg HA/g	natural brown coal, purified
Murphy et al. (1994)	4.5	0.1 M NaClO ₄	≈13 μmol C/ m ² (0.156 mg C/ m ²)	reference peat humic acid
Murphy et al. (1994)	4.5	0.005 M NaClO ₄	≈ 7 μmol C/ m ² (0.084 mg C/ m ²)	reference peat humic acid
Saada et al. (2003a)	-	0.01 M CaCl ₂	≈4 mg C/g	commercial, no treatment
Saada et al. (2003a)	-	0.01 M CaCl ₂	≈ 2.5 mg C/g	purified peat humic acid
Saada et al. (2003b)	5.3-5.8	0.002 NaCl	1.24 mg C/g (0.09 mg C/m ²)	commercial, no treatment
Saada et al. (2003b)	4.8-5.3	0.001 CaCl ₂	4.17 mg C/g (0.3 mg C/ m ²)	commercial, no treatment

Another interesting feature observed in the adsorption behaviour of humic acid is that surface area-normalised maximum adsorption densities (q_{\max}) on kaolinite range approximately from 20% - 30% of the q_{\max} values on gibbsite. Perhaps not coincidentally, kaolinite edge surface sites are also estimated to make up about 20-30% of the total surface area (Brady et al., 1996; Sutherland et al., 1999). This could therefore be an indirect indication that humic acid adsorption on kaolinite occurs only on edge surface sites. A similar observation was made by Hur and Schlautman (2003) where the maximum adsorption density of purified peat humic acid on kaolinite was found to be only about 27% of that obtained on haematite.

Adsorption at different ionic strengths and type of background electrolyte

The concentration of background electrolyte has a significant effect on the adsorption of humic acid on both gibbsite and kaolinite, in all three pH values examined (Figures 4-11 and 4-12). The two main findings concerning the effect of ionic strength on humic acid adsorption are: (a) an increase in adsorption density at higher ionic strengths and (b) at higher ionic strengths the effect of pH on adsorption is less pronounced. Enhanced adsorption at higher salt concentrations is also evident from the adsorption isotherms obtained at pH 5 and different ionic strengths (Figures 4-9 and 4-10).

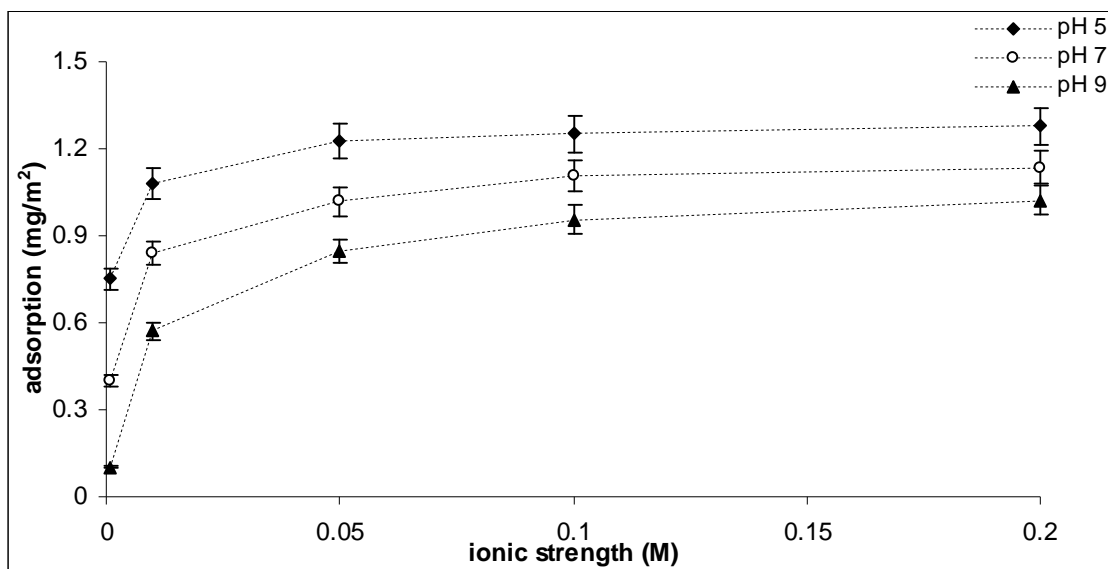


Figure 4-11 Humic acid adsorption on gibbsite as a function of background electrolyte (NaCl) concentration at pH 5, 7 and 9. Error bars of 5% represent the random error associated with the experimental procedure. Dashed lines are a guide for the eyes.

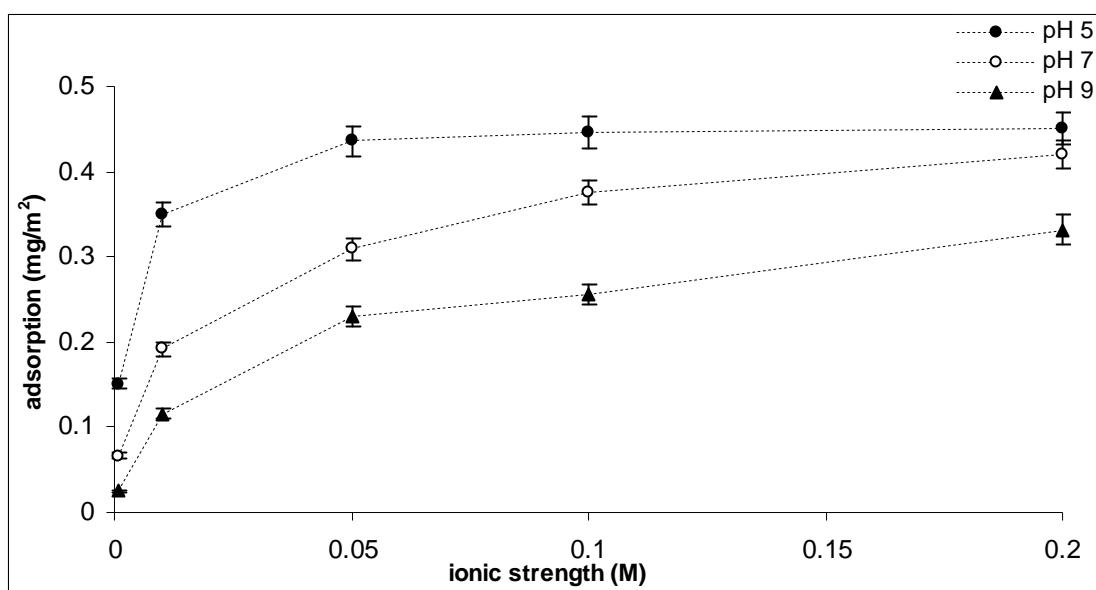


Figure 4-12 Humic acid adsorption on kaolinite as a function of background electrolyte (NaCl) concentration at pH 5, 7 and 9. Error bars of 5% represent the random error associated with the experimental procedure. Dashed lines are a guide for the eyes.

The ionic strength effect on humic acid adsorption is much more marked for background electrolyte concentrations between 0.001 - 0.05 M, as evidenced by the steep increase in adsorption within this range. At ionic strengths higher than 0.05 M, adsorption densities either remain similar (pH = 5) or continue to gradually increase up to 0.2 M (pH 7 and 9). Increased adsorption to ionic strengths up to 0.2 M is more evident for the kaolinite-humic acid systems at pH 7 and 9. Furthermore, the effect of ionic strength on adsorption was measurable only at electrolyte concentrations above

I=0.001 M. Adsorption experiments undertaken in solutions with no added electrolyte yielded similar results to the adsorption experiments at 0.001 M, for both kaolinite and gibbsite.

For both minerals the effect of ionic strength on the extent of humic acid adsorption is more pronounced at higher pH values. At pH 9, an increase in ionic strength from 0.001 to 0.2 M NaCl resulted in a tenfold increase in humic acid adsorption on gibbsite, from 0.1 mg/m² (7.5 % adsorbed) to 1 mg/m² (75% adsorbed). The corresponding increase in adsorption at pH 5 is from 55 % to 94%. For kaolinite, at pH 9, humic acid adsorption increases from 0.025 to 0.33 mg/m² as the ionic strength increases from 0.001 to 0.2 M NaCl, representing an increase in percentage adsorption from 5% to 70%. At pH 5 and the same ionic strength range, humic acid adsorption increases from 32% to 95%.

The ionic strength effects on the adsorption of humic substances on mineral (hydr)oxides and clay minerals reported in the literature vary. Although several studies have reported increased adsorption as a function of increasing ionic strength (Arnarson and Keil, 2000; Feng et al., 2005; Illés and Tombacz, 2003; Vermeer et al., 1998; Vermohlen et al., 2000; Zhou et al., 1994), in some studies different adsorption patterns have been reported. For example Davis (1982) observed that the adsorption of natural organic matter on γ -Al₂O₃ was similar in solutions with less than 0.01 M NaCl concentrations and slightly reduced in 0.1 M NaCl solutions. Weng et al. (2005) and Vreysen and Maes (2006) did not observe a significant effect of ionic strength on the adsorption of fulvic acid on goethite and bentonite respectively. Abate and Masini (2003) on the other hand observed that higher ionic strengths increased adsorption of humic acid on vermiculite only at pH 5 whereas at pH 7 the adsorption decreased at higher ionic strengths.

The influence of the type of background electrolyte on humic acid adsorption at different pH values and I = 0.01 M is shown in Figure 4-13. Humic acid adsorption is significantly enhanced in the presence of divalent cations (magnesium, strontium and calcium) in comparison to humic acid adsorption in the presence of monovalent cations (sodium and potassium). Enhanced adsorption in the presence of calcium ions, as opposed to sodium or potassium ions has also been observed in other studies (Arnarson and Keil, 2000; Day et al., 1994; Feng et al., 2005; Jones and Tiller, 1999; Majzik and Tombacz, 2007; Vreysen and Maes, 2006).

Results from the control experiments showed that in the presence of divalent ions, a significant proportion of humic acid removed from the solution was due to precipitation rather than adsorption. Humic acid precipitation was greater in the

presence of calcium and strontium than in the presence of magnesium. This precipitation effect was accounted for in the calculations by employing corrections based on the amount of humic acid that had precipitated in the control experiments. It is therefore possible that the adsorption data shown in Figure 4-13 underestimate the actual amount of humic acid adsorbed if some of the humic acid precipitating in the control experiments can in fact adsorb on the surface when the mineral phase is present in the system. Previous studies reporting adsorption in the presence of divalent cations did not report whether this effect was observed and whether the adsorption results were corrected for precipitation losses.

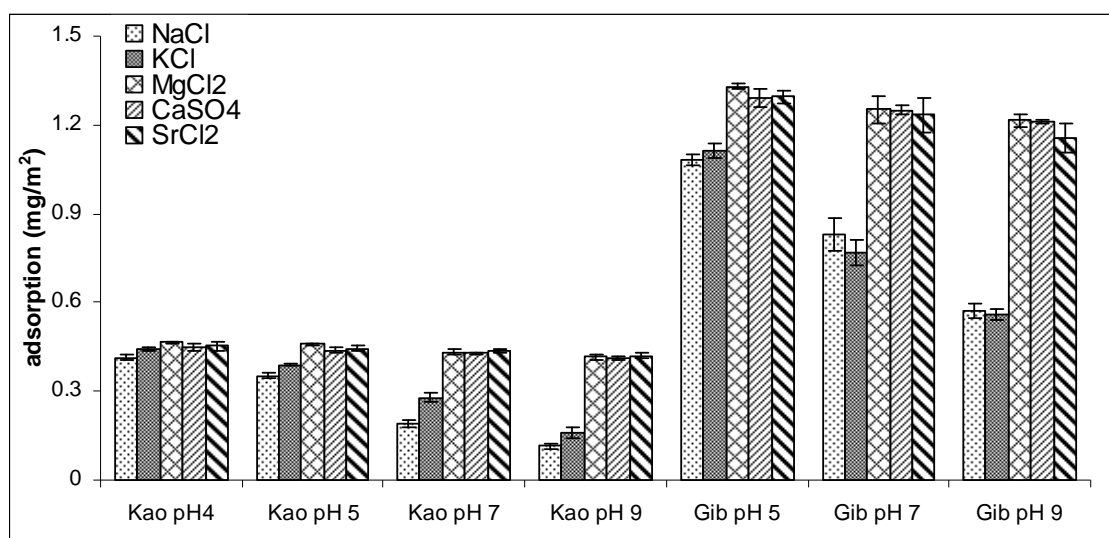


Figure 4-13 Effect of cation type on the extent of humic acid adsorption on kaolinite (Kao) and gibbsite (Gib). Adsorption data represent mean values of triplicate experiments and error bars indicate 95% confidence limits.

Factors affecting humic acid adsorption

It has been shown in the previous sections that solution chemistry has a major influence on the extent of humic acid adsorption on kaolinite and gibbsite. The response of adsorption affinity to changes in solution conditions can be related to specific adsorption mechanisms, and thus can provide indirect information about the principal mechanism(s) involved in humic acid adsorption. The influence of solution chemistry on various adsorption mechanisms will be discussed in detail in the following section. However other factors than those related to particular adsorption mechanisms may play an important role in the amount of humic acid adsorbed as different solution parameters change.

As already mentioned the pH of the solution plays an important role in the adsorption of solute ions as it governs the speciation and charging behaviour of surface sites and of humic acid molecules and hence the nature of electrostatic interactions between humic acids and mineral surfaces. In general, for the adsorption of humic acids, higher adsorption is expected at pH values below the pHPzc of mineral surfaces where the net surface charge is positive.

Increased adsorption at higher ionic strengths can be explained by a charge screening effect by which solution cations can neutralise the electrostatic repulsions between negatively charged humic acid molecules and surface sites. Therefore higher ionic strengths can increase adsorption by allowing humic acid molecules to approach the surface even when both surface sites and humic molecules carry the same charge. Divalent ions are more effective in screening the negative charge developed on the surface and thus explaining the increased effect of divalent cations.

Moreover higher concentrations of electrolyte ions can screen the excess negative charges on the surface induced by humic acid adsorption and thus enabling more humic acid molecules to adsorb. Adsorbed humic molecules induce a negative charge on the surface which originates from anionic groups that are not directly involved in surface coordination (Tipping, 1981; Tombácz et al., 2004). This excess negative charge can repel further humic acid molecules from approaching the surface of the mineral. The steeper initial slopes seen in the adsorption isotherms obtained at higher ionic strengths (Figures and 4-9 and 4-10), are consistent with the a negative surface charge induced by the adsorption of humic acid.

Because humic acids exhibit a polyelectrolyte character, some authors interpreted the adsorption behaviour of humic acid on mineral surfaces according to the theories developed for the adsorption of anionic polyelectrolytes (e.g. Vermeer et al., 1998; Vermohlen et al., 2000). Accordingly the adsorption trends observed in this study as a function of humic acid concentration, pH, and ionic strength can also be explained by assuming that humic acid behaves as a flexible anionic polyelectrolyte.

The pH and ionic strength play a central role in the adsorption behaviour of polyelectrolytes by controlling the structural conformation of these molecules. Solution pH controls the charge of the polyelectrolyte and this in turn will affect its structural conformation. At high pH values where the majority of acidic functional groups within the molecule are deprotonated, the electrostatic repulsions between negatively charged sites give rise to an open or stretched structural configuration. Conversely, at low pH values these macromolecules adopt a more compact structural configuration (coiled

structure) because of the reduced intramolecular electrostatic repulsions between different segments within the molecule.

Because the structural conformation can be retained in the adsorbed state (Meadows et al., 1988), the structure of the humic molecule in solution can have a significant effect on the extent of adsorption. As the pH increases and the humic acid charge becomes progressively more negative, adsorption can be reduced because the adsorbed molecules adopt a more flat configuration on the surface. This open configuration allows a strong interaction with surface sites resulting in a higher fraction of segments in contact to the surface (termed trains). In contrast, as the pH decreases, higher adsorption can take place because the adsorbed molecules extend further in the solution with more segments attached on the surface as loops and tails (Vermeer et al., 1998), and hence allowing more humic acid molecules to coordinate to the surface.

The presence of background electrolyte has a dual effect on adsorption by screening the electrostatic interactions between the polyelectrolyte and the surface (either attractive or repulsive) as well as the intramolecular electrostatic interactions (repulsive) between charged segments of polyelectrolyte molecules. Van de Steeg et al. (1992) proposed that polyelectrolyte adsorption can be distinguished in to two regimes, a screening-reduced and a screening-enhanced adsorption regime. For a screening-reduced adsorption, polyelectrolytes are coordinated to the surface primarily through electrostatic forces of attraction between molecule segments and surface sites. Adsorption decreases with increasing ionic strength because the higher concentrations of electrolyte ions screen the segment-surface site electrostatic attractions.

For a screening-enhanced adsorption, polyelectrolyte segments are mainly coordinated to the surface via non electrostatic interactions. In this case adsorption increases with increasing ionic strength due to the screening of the segment-segment electrostatic repulsions within the polyelectrolyte molecule. The reduction of these (lateral) intramolecular repulsions enable polyelectrolytes to adopt surface structures with a higher fraction of loops and tails and this closer configuration in turn enables more molecules to adsorb on the surface. If the respective contributions from electrostatic and nonelectrostatic interactions on adsorption are similar then no significant change in adsorption at various salt concentrations is expected (Van de Steeg et al., 1992).

The theory of polyelectrolyte adsorption can also be used to explain the general shape of the adsorption isotherms obtained in this study. Adsorbed polyelectrolytes are typically found to compensate or even overcompensate the surface charge and as a result the excess negative charge induced by these compounds can minimise further

adsorption. Similar findings have been reported for humic acids where electrophoretic results showed a surface charge reversal upon adsorption of humic acids on mineral surfaces (Au et al., 1999; Davis, 1982; Tipping and Cooke, 1982; Tombacz et al., 1999; Tombacz et al., 2004; Vermohlen et al., 2000). Furthermore, the importance of the charge reversal effect is dependent on the charge density of the polyelectrolyte and this in turn can affect the maximum adsorption density. As shown by Vermohlen et al. (2000) organic polyanions with higher charge density exhibited lower maximum adsorption densities on the surface of aluminium oxide and goethite. Therefore adsorption at higher humic acid concentrations may be limited by the electrostatic repulsions between adsorbed and solution humic molecules rather than the availability of surface sites assumed by the Langmuir model.

The adsorption properties of polyelectrolytes have only been introduced in this study in order to stress the inherent complexities associated with the study of humic acid adsorption and the reader is referred to other sources for more detailed discussions on the theory of polyelectrolyte adsorption (e.g. Cohen Stuart et al., 1991; Van de Steeg et al., 1992; Vermeer et al., 1997).

Regardless of the adsorption mechanism(s) involved in the adsorption of humic acid, the effect of ionic strength on adsorption can be explained by three factors: (1) Higher ionic strength can impose changes to the structural conformation, due to a charge screening effect on the intramolecular electrostatic repulsions within the humic acid molecules (Abate and Masini, 2003; Murphy et al., 1992; Tombacz et al., 2000; Tombacz et al., 2004). At high pH values, and low ionic strengths, the humic molecules adopt an open configuration due to the repulsive forces between negatively charged functional groups within the molecule. At higher ionic strengths, however, the additional cations can neutralise these repulsive forces and the humic acid molecules tend to have a more coiled configuration. Because of the smaller molecular size each adsorbed molecule occupies a smaller surface area and therefore more humic molecules can coordinate to the surface.

(2) As the ionic strength of the solution increases, the thickness of the diffuse double layer is compressed and this enables humic molecules to be in a closer proximity to the surface. As the distance between solution molecules and the surface decreases, increased humic acid adsorption could result from the enhancement of short ranged attractive forces such as van de Waals interactions (Arnarson and Keil, 2000; Zhou et al., 1994). In fact enhanced humic acid adsorption with increasing concentration of monovalent cations has been previously attributed solely to van der Waals interactions (Arnarson and Keil, 2000; Feng et al., 2005).

(3) Adsorbed organics can introduce a negative charge on the surface which acts as an electrostatic barrier and minimises further adsorption due to the increased electrostatic repulsions between the surface and aqueous humic acid molecules (Vermeer et al., 1998). However, the presence of additional cations in solution can decrease the negative electrostatic potential which develops in the surface-water interface, following the adsorption of humic molecules on the mineral surface. The higher concentration of cations in solution can therefore diminish or even neutralise the repulsive forces between adsorbed and aqueous humic molecules and hence enables additional humic molecules to coordinate on the surface.

Similarly divalent cations can be more effective in enhancing humic acid adsorption than monovalent cations because: (1) Divalent ions are more effective in screening the intramolecular electrostatic repulsions of humic molecules and therefore humic molecules may adopt a more compact configuration in the presence of divalent ions than in the presence of monovalent ions of similar ionic strength. (2) Divalent ions are more effective in screening the negative charge developed on the surface following humic acid adsorption and thus allowing further molecules to approach the surface and adsorb. For example, the effect of calcium ions in changing the electrostatic properties of goethite, when compared to sodium, was calculated by Weng et al. (2005) according to the Ligand and Charge Distribution (LCD) model. It was shown that in a 0.1 M NaNO_3 solution, a high loading of fulvic acid maintained a negative electrostatic potential on the surface over the entire pH range (3-11). The addition of 1mM calcium ions in the electrolyte solution resulted in less negative potential values at high pH. Moreover, in the absence of fulvic acid or at low concentrations, the electrostatic potential was kept positive for all pH values.

The above discussion shows that the complex structural and chemical characteristics of humic acids present difficulties in interpreting their macroscopic adsorption data. The following section will discuss possible adsorption mechanisms that can explain the observed humic acid adsorption trends as a function of solution chemistry. Generally in the absence of spectroscopic data, adsorption mechanisms of organic anions onto mineral surfaces can be predicted on the basis of macroscopic adsorption behaviour. However due to the complex nature of humic acids, conclusions drawn regarding the adsorption mechanisms of simple organic anions, from macroscopic adsorption data, may not apply for humic acids even if they exhibit similar adsorption behaviours.

Humic acid adsorption mechanisms based on the macroscopic adsorption properties

pH-dependent adsorption behaviour

As illustrated in Figures 4-4 and 4-5, humic acid adsorption is significantly influenced by the pH of the solution. A trend of decreased adsorption at higher pH values is consistent with both a ligand exchange reaction and an anion exchange adsorption mechanism (Gu et al., 1994; Tipping, 1981). These two adsorption mechanisms will be briefly outlined here.

Anion exchange

Adsorption via an anion exchange mechanism involves electrostatic interactions between surface sites and humic acid molecules. The adsorption reaction results in outer-sphere complexation where negatively charged functional groups are bound to positively charged surface sites through weak electrostatic forces of attraction. This reaction is termed anion exchange because the adsorbing anions (in this case humic acid) exchange for inorganic anions that had been previously bound to surface sites as outer sphere complexes. The following equation describes an anion exchange reaction (Schlautman and Morgan, 1994)



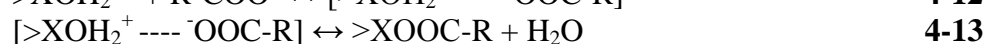
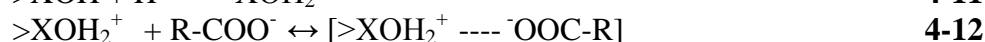
where A^- represents a background electrolyte anion, $>XOH_2^+$ a positively charged site, and $R\text{-COO}^-$ a carboxylate group attached to a humic acid molecule. Lower adsorption is expected as the pH increases because the concentration of positively charged sites decreases. As a result this adsorption mechanism is significant only at pH values below the pH_{pzc} of the mineral where the surface and humic acid molecules carry opposite charges.

Ligand Exchange Reaction

Ligand exchange between humic acid carboxylic groups and surface hydroxyl groups has been traditionally considered as a major mechanism for the adsorption of humic substances onto mineral surfaces (e.g. Gu et al., 1994; Murphy et al., 1992; Tipping, 1981). This reaction results in inner sphere complexation where direct chemical bonds form between carboxylic groups (and possibly phenolic) and metal centres on the surface of minerals. Acidic functional groups present in simpler organic

molecules have also been shown to form surface complexes through a ligand exchange mechanism (Axe and Persson, 2001; Biber and Stumm, 1994; Duckworth and Martin, 2001; Yoon et al., 2004b).

It has been suggested that ligand exchange takes place through a series of reactions which includes the formation of a precursor outer-sphere complex. The adsorption process is believed to proceed in the following sequence of surface reactions (Murphy et al., 1992; Schlautman and Morgan, 1994)



where $>\text{XOH}$ represents a neutral surface hydroxyl group, and R-COO^- represents a humic acid carboxylate group. The inner sphere complex forms by the exchange between a surface OH_2^+ moiety with a humic COO^- group (equation 4-13).

The dependence of a ligand exchange reaction on pH can be partly explained by the protonation reaction shown in equation 4-11. Acidic conditions favour the ligand exchange adsorption mechanism because the increased electrostatic attraction between humic acid functional groups and surface sites allow humic acid molecules to approach the surface and increase the possibility of ligand exchange (Feng et al., 2005). Once the humic acid molecules approach the surface, ligand exchange reactions can also take place between humic acid carboxyl groups and neutral surface hydroxyl groups as shown below (Murphy et al., 1992)

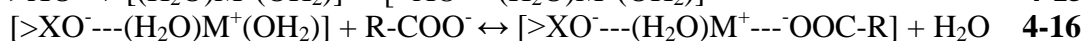
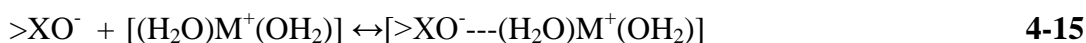


Furthermore, lower adsorption at higher pH values can also be explained by the lower concentration of available ligand exchangeable surface sites. Neutral and positively charged surface sites ($>\text{XOH}$ and $>\text{XOH}_2^+$) are more readily exchangeable than negatively charged sites and thus ligand exchange reactions are favoured by lower pH values where the concentration of neutral and positively charged sites is higher (Tipping, 1981).

Ionic strength dependence on adsorption behaviour

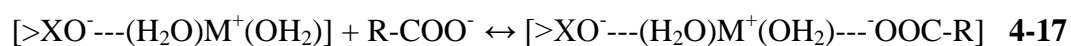
The enhanced humic acid adsorption observed at higher ionic strengths suggests that the background electrolyte ions are involved in the interactions between humic acid and surface sites. Also, importantly, the increased adsorption trend at higher ionic strengths indicates that an anion exchange reaction is not an important adsorption mechanism, at least for higher ionic strengths. If anion exchange was of major importance then a higher concentration of background electrolyte ions would have resulted in lower adsorption densities because inorganic anions can compete with humic acid functional groups for available surface sites (Arnarson and Keil, 2000; Gu et al., 1994).

The two adsorption mechanisms which are consistent with increased adsorption at higher ionic strengths are cation bridging and water bridging. Cation bridges form when cations at the mineral-water interface bind (or bridge) humic organic anions to negatively charged surface sites as shown below (Schlautman and Morgan, 1994)



where M^+ represents a cation in solution and the two surrounding water molecules represent its hydration sphere. According to the reaction sequence given above, background electrolyte cations are attracted to the negatively charged surface sites by electrostatic forces of attraction (equation 4-15). The positive charge of these surface bound cations can then attract the negatively charged humic acid molecules on the surface, thus bridging the repulsive forces between negatively charged surface sites and negatively charged organic functional groups (equation 4-16).

During cation bridging humic acid forms an outer sphere complex with a surface bound cation by displacing a water molecule from the hydration sphere of the cation. If the water molecule remains between the organic anion and the metal cation then the adsorption mechanism is referred to as water bridging. In this case the humic acid molecule is bonded via hydrogen bonding. A typical water bridging reaction can be represented by the following reaction



From the above reactions it can be seen that inorganic cations in solution can mediate the adsorption of humic acid at pH values above the pHpzc of the mineral by counterbalancing the electrostatic repulsions between negatively charged surface sites and humic acid molecules. The importance of cation and water bridging adsorption mechanisms increases at higher ionic strengths due to the higher concentration of cations that can participate in cation/water bridging reactions.

As shown earlier, enhanced humic acid adsorption at higher ionic strengths is more pronounced at pH 9 when compared to pH 5 (Figures 4-11 and 4-12). This observation is consistent with the cation/water bridging mechanisms. At pH 9 the concentration of surface sites which can be involved in cation/water bridging (i.e. negatively charged sites) is higher, and moreover, humic acid adsorption is at a minimum because of the increased electrostatic repulsions. Therefore, at higher pH values, the presence of additional cations in solution can favour humic acid adsorption through cation/water bridging reactions.

A cation/water bridging mechanism is further supported by the enhanced adsorption observed in the presence of divalent ions in the background electrolyte solution. Figure 4-13 shows that higher adsorption densities are obtained in solutions containing polyvalent cations (Mg^{2+} , Sr^{2+} , Ca^{2+}) as opposed to solutions with monovalent cations (Na^+ , K^+). Furthermore, similarly to the effect of ionic strength on adsorption, enhanced adsorption in the presence of divalent cations is more evident at higher pH values. The reason for this increased humic acid affinity for surface sites is the higher positive charge carried by divalent cations which enables them to be more effective in bridging the repulsive forces between like charged surface sites and humic functional groups (Feng et al., 2005).

Operative adsorption mechanisms

Based on the humic acid adsorption behaviour as a function of ionic strength, water/cation bridging mechanism appears to be an important mechanism for the adsorption of humic acid on kaolinite and gibbsite. However other adsorption mechanisms must also be involved in the uptake of humic acid on kaolinite and gibbsite. This can be inferred from the influence of ionic strength on adsorption over the entire pH examined. Enhanced adsorption is observed even at pH values where the surface of kaolinite and gibbsite are expected to be positively charged. However, water/cation bridges can be significant adsorption mechanisms only at pH values above the pHpzc of the mineral. Furthermore at low ionic strengths and in the presence of

monovalent cations, cation bridging is not expected to be a significant adsorption mechanism (Arnarson and Keil, 2005; Feng et al., 2005). Therefore other mechanisms must be contributing to humic acid adsorption, and the relative importance of these mechanisms could be depended on solution chemistry (e.g. pH, ionic strength and cation composition).

Based on the influence of various solution conditions on the extent of humic acid adsorption, previous studies proposed dominant adsorption mechanisms. For example, Feng et al. (2005) suggested that humic acid adsorption on kaolinite and montmorillonite is consistent with three main adsorption mechanisms; ligand exchange, van der Waals interactions and cation bridging. The relative contribution of these three mechanisms to overall adsorption was estimated by the influence of different solution conditions on the maximum adsorption capacity as follows: At an ionic strength of 0.001 M NaNO₃, the effect of pH was attributed solely to a ligand exchange mechanism. At higher sodium concentrations (0.01 M NaNO₃) increased adsorption was explained by the involvement of van der Waals interactions due to the compression of the double-layer. Cation bridges in the presence of sodium ions were considered negligible. Finally the increased adsorption observed when calcium ions (0.001 and 0.01 M Ca(NO₃)₂) were used as the background electrolyte ions was attributed to cation bridges.

Arnarson and Keil (2000) also used the adsorption behaviour of organic matter on montmorillonite in order to derive the relative importance of different adsorption mechanisms. Consistent with Feng et al. (2005) the three main adsorption mechanisms identified were van der Waals interactions, ligand exchange and cation bridging. The relative importance of different mechanisms was obtained from the effect of ionic strength (0.05-0.7 M) and type of solution cations on adsorption. At an ionic strength of 0.7 M adsorption obtained in the presence of Na₂SO₄ was attributed solely to van der Waals interactions since cation bridging was considered to be minimal in the presence of sodium ions and SO₄⁻ were considered to completely inhibit ligand exchange. In the presence of NaCl, adsorption was attributed to both van der Waals interactions and ligand exchange. Finally in the presence of CaCl₂ all three adsorption mechanisms were assumed to be involved.

Accordingly, in this study the major adsorption mechanisms that can be inferred from the adsorption behaviour of humic acid, on both minerals, include ligand exchange, anion exchange, and cation/water bridging mechanisms. At low ionic strengths (0.001 M NaCl) ligand exchange is the most probable adsorption mechanism since at such low sodium concentrations, and especially at low pH values, the effect of

cation/water bridging on humic acid adsorption is expected to be minimal. In addition, hydrophobic and van der Waals interactions may also be contributing to adsorption. From the adsorption behaviour alone it is not possible to identify which of these adsorption mechanisms is involved or their relative importance if all mechanisms are operative simultaneously.

At higher ionic strengths, or in the presence of divalent cations, cation/water bridging and van der Waals interactions are expected to be the dominant adsorption mechanisms, particularly at high pH values. However it must be kept in mind that the effect of solution conditions on adsorption behaviour may not be reflecting only the adsorption mechanisms responsible of humic acid. For instance the polyelectrolyte nature of humic acids is also likely to affect the adsorption behaviour of humic acid.

As mentioned above, at low ionic strengths a ligand exchange mechanism may be involved in humic acid adsorption. To further investigate this possibility two different sets of adsorption experiments were performed in order to determine the importance of the ligand exchange mechanism. First, a series of experiments were carried out in order to estimate the effect of adsorption on the pH of the solution. Second a series of adsorption experiments were carried out in the presence of Na₂SO₄ as the background electrolyte.

A rise in pH during the adsorption of humic substances has been previously associated with a ligand exchange mechanism (e.g. Chorover and Amistadi, 2001; Illés and Tombacz, 2003; Murphy et al., 1992). This is due to the release of hydroxyl ions into solution following the exchange of a surface hydroxyl group for a humic acid functional group (see equation 4-14). An upward pH drift was also observed in most of the adsorption experiments (pH < 8) performed in the present study. However, control experiments carried out either in the absence of the mineral phase or in the absence of humic acid revealed that a pH change could be partly attributed to the buffering capacity of humic acid and/or of the mineral itself. Especially for humic acid, following an initial pH adjustment to values below about 7.7 (equilibrium pH of the humic acid stock solution), a steady upward pH drift was observed and long equilibration times were required in order to stabilise the humic acid solution at a target pH. It is possible, therefore, that the upwards pH drift observed originated from the tendency of humic acid to return to its natural equilibration pH. A similar effect was observed for gibbsite suspensions with pH values below and above about 8 drifting towards pH 8, after an initial pH adjustment.

In order to investigate the effect of adsorption on solution pH, a set of independent adsorption experiments designed specifically for determining the change in

pH following adsorption were carried out. A 50 mL mineral suspension was equilibrated at pH 5.00 for six hours, under a nitrogen atmosphere, and then aliquots of the humic acid stock solution (1g/L), also equilibrated to pH 5.00 for 24 hours, were introduced to the suspension at successive time intervals. After the addition of each dose of humic acid (1 mL) the suspension was allowed to equilibrate and the pH change was monitored. Before the next addition, the pH of the suspension was adjusted back to the initial pH value (i.e. pH 5.00). The change in solution pH, following adsorption, was investigated at different ionic strengths and mineral suspensions of different concentrations.

The change of pH following the addition of humic acid in a mineral suspension containing 1 g of gibbsite in a 50 mL 0.001 M NaCl solution is shown in Figure 4-14. The effect of humic acid in a blank system containing only a 0.001 M NaCl solution at pH 5 is also shown. After the addition of the first 1 mL of humic acid, the pH of the suspension increases from 5.00 to about 5.50. This increase in pH could be indicative of a ligand exchange adsorption mechanism, where humic acid functional groups exchange for surface hydroxyl groups. The lower increase in pH as more humic acid is added in the suspension is also consistent with the occurrence of a ligand exchange mechanism. As more humic acid is added to the system the surface becomes progressively more saturated and less humic acid molecules can exchange for available sites and therefore the increase in pH is reduced.

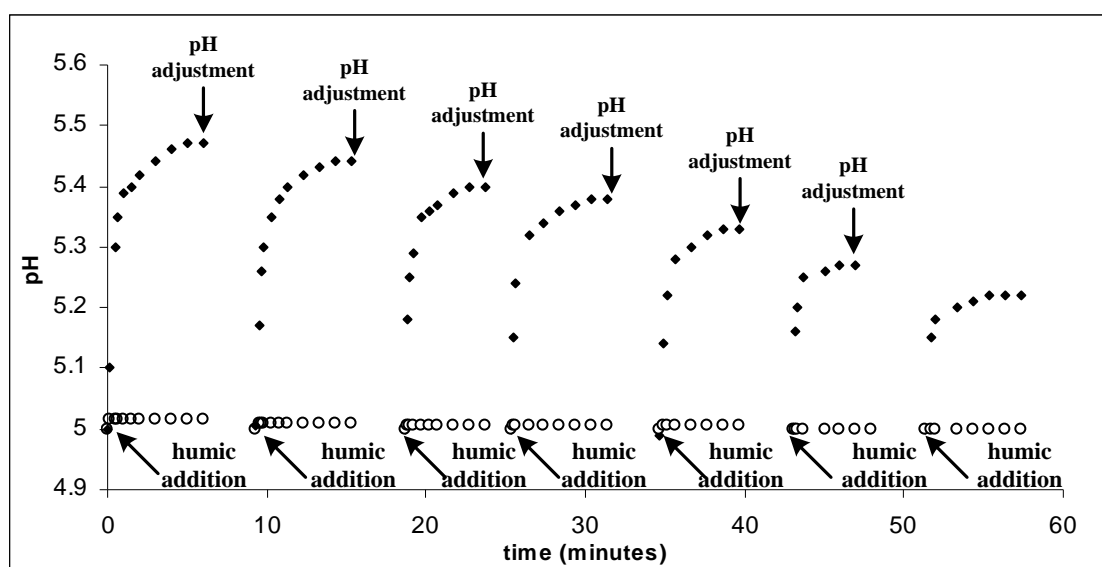
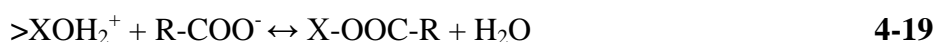


Figure 4-14 The change in solution pH during successive 1 mL additions of humic acid (1 g/L) in a 20 g/L gibbsite suspension, at 0.001 M NaCl (solid symbols). Prior to the addition of the next aliquot of humic acid the pH of the suspension was adjusted back to pH 5.00. The change in pH for a blank experiment (no gibbsite) during successive additions of humic acid is also shown by the open symbols.

It should be noted however that observations of pH changes following adsorption should be treated with caution. This is particularly true for the study of humic acid adsorption reactions where various factors can affect the pH of the solution. The change in pH, for ligand exchange reactions, will depend on the speciation of surface groups and of humic acid functional groups involved as shown by the following equations (Vreysen and Maes, 2006)



According to the above reactions only the exchange of deprotonated humic acid functional groups for neutral surface groups will lead to an increase in pH. As a result the observed change in pH will depend on the relative importance of the four reactions, and this in turn will depend on the solution conditions. Although at a particular pH the relative distribution of protonated and neutral surface hydroxyl groups can be estimated with confidence, for humic acid functional groups this is not possible due to the wide range of pKa values exhibited by these groups. Therefore it is very difficult to estimate the importance of a ligand exchange mechanism from changes in pH upon adsorption.

For the same experimental conditions a very small decrease in pH was observed in the case of kaolinite (data not shown). The much smaller effect of humic acid adsorption in kaolinite systems could be attributed to the lower adsorption capacity of kaolinite and/or to the different charging behaviour of kaolinite. Additionally a ligand exchange mechanism may be a more dominant adsorption mechanism for the gibbsite-humic acid system than for the kaolinite-humic acid system.

It has to be noted, however, that a pH rise following the adsorption of humic acid cannot be necessarily taken as direct evidence of a ligand exchange mechanism as is the case for the adsorption of low molecular weight ligands. The complex interactions of humic acids with the surface can give rise to other processes which can influence the uptake or release of hydrogen ions. In addition to the effect of ligand exchange reactions, the total amount of protons released or adsorbed, following the binding of humic molecules on the surface, is controlled by two other competing mechanisms. The interactions between humic acid molecules and the surface weaken the binding of hydrogen ions on the molecule, resulting in the release of hydrogen ions into the

solution (Saito et al., 2004; Weng et al., 2005). At the same time however, the adsorption of humics increases the surface affinity for protons because the negative charge of the adsorbed molecules screens the repulsive forces between protons in solution and the positively charged surface sites (Weng et al., 2005). Moreover, Davis (1982) and Tipping (1981) suggested that ionised functional groups present in adsorbed humic molecules that are not directly involved in surface complexation are also able to be involved in proton uptake reactions. As a result all these processes which are not related to the ligand exchange mechanism can also influence the pH of the solution.

The effect of sulphate ions on the extent of humic acid adsorption can also be used as an indirect evidence for the occurrence of ligand exchange reactions. Decreased adsorption in the presence of sulphate ions, as opposed to chloride or nitrate ions in the background electrolyte, has been previously used for determining whether ligand exchange is a significant adsorption mechanism (Arnarson and Keil, 2000; Gu et al., 1994). This is based on the assumption that sulphate ions can also form inner sphere surface complexes through a ligand exchange mechanism and can thus compete with humic acid functional groups for available surface sites.

Figure 4-15 shows that the effect of sodium sulphate concentration on humic acid adsorption is similar to that observed for sodium chloride, i.e. humic acid adsorption increases with increasing ionic strength. At low ionic strengths ($I < 0.01$ M), humic acid adsorption densities on gibbsite appear to be higher in sodium sulphate solutions than in sodium chloride solutions as illustrated in Figure 4-16. A similar effect is also observed for the kaolinite systems. The higher adsorption observed in Na_2SO_4 solutions at these lower ionic strengths is attributed to the higher concentration of sodium ions present in solution, since at a given ionic strength the concentration of sodium ions in Na_2SO_4 solution is twice as high as that in NaCl solutions. The importance of Na^+ concentration on humic acid adsorption, especially at ionic strengths between 0.001-0.05 M has been shown previously (Figures 4-11 and 4-12).

Although at higher ionic strengths ($I > 0.01\text{M}$) adsorption densities in sodium sulphate appear to be somewhat lower than in sodium chloride, the differences obtained are within the experimental error (5%). This finding suggests that a ligand exchange mechanism does not play an important role in humic acid adsorption on gibbsite and kaolinite.

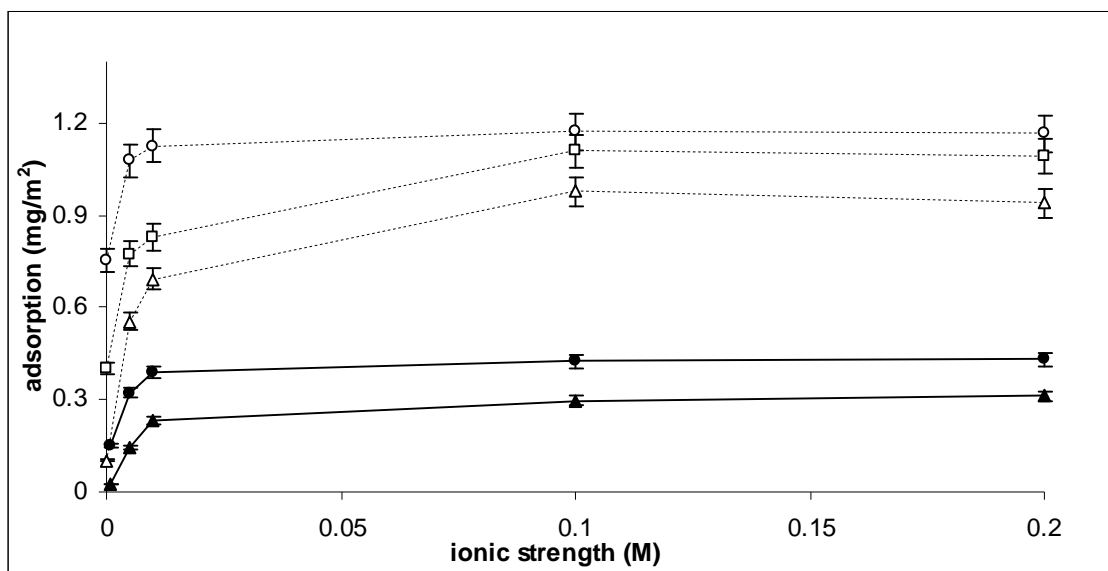


Figure 4-15 Effect of sulphate ions on the extent of humic acid adsorption onto gibbsite (open symbols) and kaolinite (solid symbols), at pH 5 (circles); pH 7 (squares); and pH 9 (triangles). Gibbsite systems consisted of a 4 g/L mineral suspension and an initial humic acid concentration of 0.057 g/L. Kaolinite systems consisted of a 6 g/L mineral suspension and an initial humic acid concentration of 0.057 g/L. Na₂SO₄ was used as a background electrolyte. Dashed lines are a guide for the eyes.

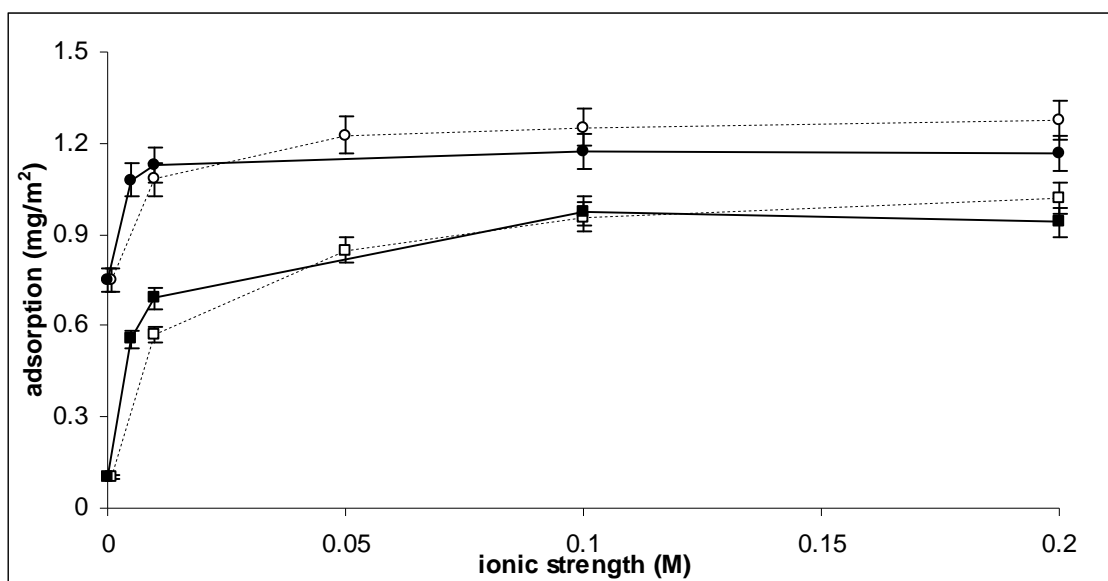


Figure 4-16 Comparison of humic acid adsorption densities on gibbsite obtained in sodium sulphate solutions (solid symbols; also shown in Figure 4-15) and sodium chloride solutions (open symbols; Also shown in Figure 4-11), at pH 5 (circles) and pH 9 (squares).

The conclusions drawn from these two different sets of experiments offer contradictory evidence regarding the importance of ligand exchange, particularly for gibbsite. Although the increase in pH following adsorption would lead one to conclude that ligand exchange is involved in the adsorption process, the effect of sulphate ions on adsorption indicates to the contrary. Therefore it is difficult to obtain reliable

information about the operative adsorption mechanisms of humic acids based on macroscopic adsorption experiments alone.

In summary, macroscopic adsorption data can provide indirect evidence regarding the binding mechanisms of ions onto mineral surfaces. Results obtained in the present study suggested that different mechanisms may be involved in the adsorption of humic acid on kaolinite and gibbsite. Based on the results obtained from the macroscopic adsorption experiments presented here, humic acid adsorption on kaolinite and gibbsite is most consistent with cation/water bridging and van der Waals interactions. At low ionic strengths however (0.001 M NaCl), the possibility of other adsorption mechanisms contributing to adsorption, such as ligand exchange, cannot be excluded. In addition, the adsorption behaviour of humic acids is further complicated by the complex nature of these compounds and therefore information obtained regarding the binding mechanisms must be treated with caution. This shows the importance of spectroscopic evidence in order to obtain more robust results about the type of reactions taking place between mineral surfaces and humic acids. The following section presents the results concerning the use of *in situ* multiple internal reflection (MIR)-FTIR spectroscopy in order to derive molecular level information regarding the binding mechanisms of humic acid.

IR measurements

IR spectra of humic acid in aqueous solution

Despite the complex macromolecular and polyfunctional character of humic acids, the IR spectra obtained for aqueous humic acid exhibit a relatively low number of absorption bands, as seen in Figure 4-17. At pH 3.5 six prominent absorption bands are evident in the carboxyl region (1200-1800 cm^{-1}) with peak frequency positions at 1755, 1712, 1615, 1440, 1382, and 1275 cm^{-1} . Most of these bands are strongly influenced by the pH of the solution and therefore can be attributed to the vibrational modes of carboxyl functional groups. The two absorption bands located between the 1700-1750 cm^{-1} region are characteristic of C=O stretching modes. The intensity of the 1712 cm^{-1} band is strongly dependent on the pH of the solution and hence it is assigned to the C=O stretching mode of protonated carboxylic groups ($\nu_{\text{C=O}}$). Conversely the 1755 cm^{-1} band

is present in all three pH values examined and in accordance with previous studies it is assigned to C=O bonds of ketone and ester moieties (Lumsdon and Fraser, 2005; Yoon et al., 2004a). The intensity of the band with a peak frequency position at 1275 cm^{-1} is also highly influenced by the pH and is assigned to the stretching vibrational modes of C-OH bonds ($\nu_{\text{C-OH}}$) of protonated carboxyl groups.

The absorption bands located at 1615 and 1383 cm^{-1} are assigned to the asymmetric ($\nu^{\text{a}}_{\text{COO}^-}$) and symmetric ($\nu^{\text{s}}_{\text{COO}^-}$) stretching modes of deprotonated carboxylate groups respectively. At pH 7 these two bands dominate the IR spectra of humic acid, indicating that the majority of carboxyl groups in humic acid exist in the deprotonated form (COO^-). The relative intensity of the bands corresponding to protonated carboxyl groups (i.e. C=O and C-OH) is indicative of the protonation state of both aqueous and adsorbed humic acid species.

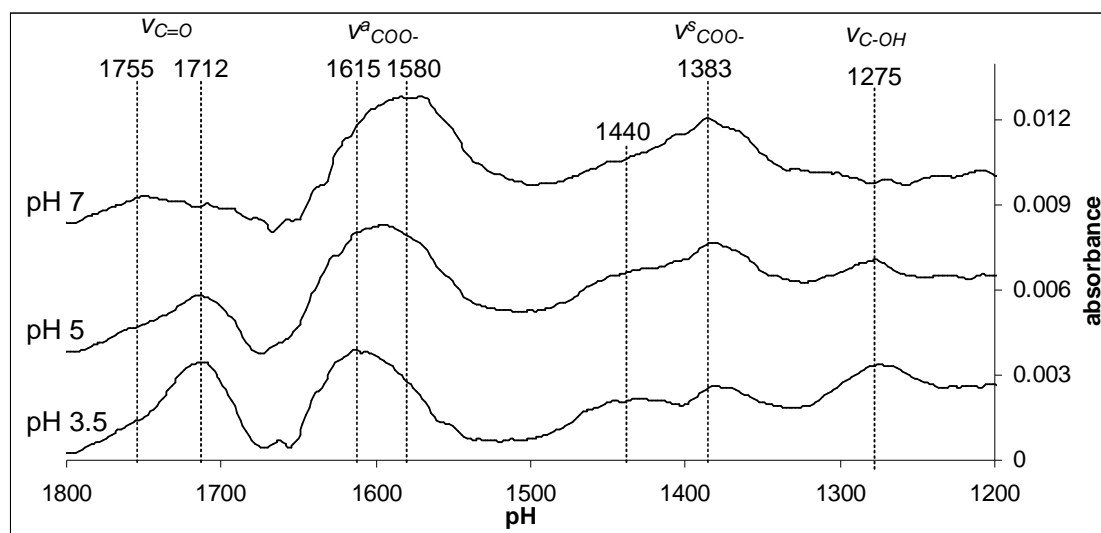


Figure 4-17 IR spectra of aqueous humic acid in aqueous solution at pH 3.5, 5 and 7. Spectra have been offset for clarity.

In addition to an increase in intensity, the peak frequency position of the 1615 cm^{-1} , attributed to $\nu^{\text{a}}_{\text{COO}^-}$, shifts to lower wavenumbers as the pH of the solution increases from pH 3.5 to 7. The corresponding peak frequency position of this band is about 1580 cm^{-1} at pH 7. Yoon et al. (2005) attributed this shift to the effects of pH on the extent of intramolecular hydrogen bonding between neighbouring carboxylic moieties. It must also be noted that the peak intensity of this band is relatively high at pH 3.5. Initially this observation is inconsistent with the assignment of the $1580\text{--}1615\text{ cm}^{-1}$ to the carboxyl asymmetric stretching vibration since the majority of the carboxyl

groups will be protonated at pH 3.5. However, Lumsdon and Fraser (2005) suggested that other functional groups are also contributing to the absorption profile of this band such as quinones and olefinic groups. Therefore, the complex absorption profile of this band could explain its response to pH changes, including the lower effect of pH on the band's intensity and the shift to lower wavenumbers at higher pH values.

Finally, the origin of the broad band centred at about 1440 cm^{-1} is unclear. It could be argued that it arises from the symmetric stretching modes of carboxylate groups with different structural environment than those exhibiting the absorption band at 1383 cm^{-1} . However its peak frequency position is higher than typical symmetric modes exhibited by carboxylate groups found in LMW carboxylic acids and humic substances (Hay and Myneni, 2007). Furthermore the intensity of this band does not appear to be influenced by changes in the pH. A most probable origin for the 1440 cm^{-1} band is from skeletal vibrations of the humic acid molecules. Absorption bands with similar frequency positions, in the spectra of aqueous humic acid, have also been reported previously and were attributed to lignin components by Lumsdon and Fraser (2005) and to C-H deformation modes of CH_3 - and CH_2 - groups by Kaiser et al. (1997).

IR spectra of interfacial humic acid

The *in situ* IR spectra of adsorbed humic acid on kaolinite from a 0.1 g/L humic acid solution, at pH 3, 5 and 7, and an ionic strength of 0.01 M NaCl are shown in Figure 4-18. The peak frequency positions and corresponding assignments to specific vibrational modes are also included. Similar spectral results were also obtained from solutions with lower humic acid concentrations (0.05 and 0.08 g/L) or lower ionic strengths (0.001 M). As expected, however, at lower initial humic acid concentrations and lower ionic strengths, the band intensities were considerably weaker, particularly at higher pH. This finding is in accordance with the macroscopic adsorption behaviour presented earlier which showed increased adsorption densities at higher ionic strengths and higher initial humic acid concentrations.

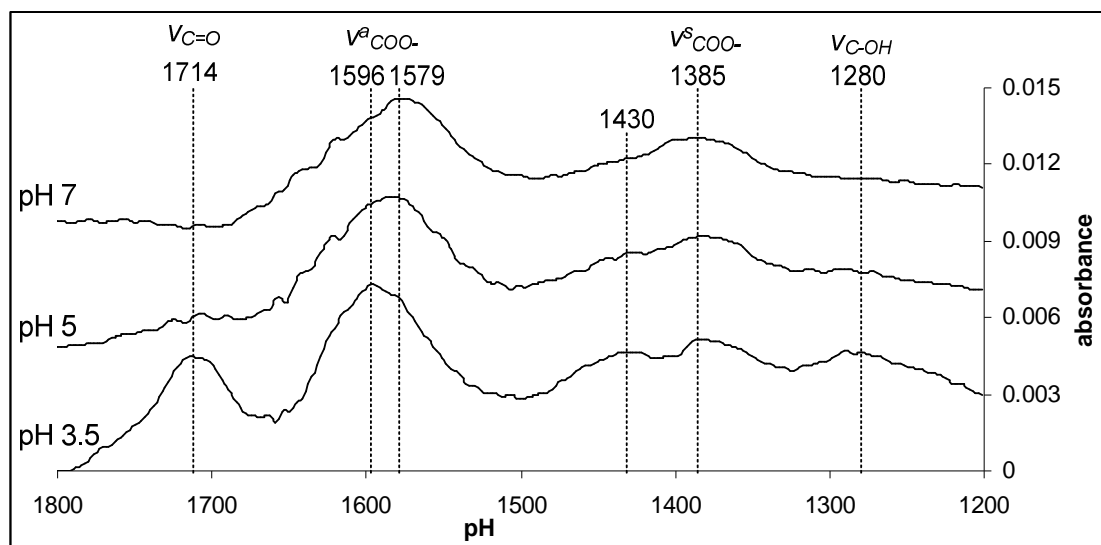


Figure 4-18 IR spectra of adsorbed humic acid, from a 0.1 g/L humic acid solution, on kaolinite. Spectra have been offset for clarity.

The spectra of adsorbed humic acid onto kaolinite are dominated by absorption bands associated with the carboxylate stretching modes, indicating the involvement of the carboxyl groups in surface adsorption. Coordination to the surface primarily through carboxyl interactions was also suggested by Yoon et al. (2005) for the adsorption of peat humic acid on boehmite and by Kaiser et al. (1997) for the adsorption of organic matter on iron and aluminium (hydr)oxides. At pH 3.5, the spectrum shows six prominent absorption bands with absorption maxima at 1714, 1596, 1445, 1431, 1385 and 1280 cm^{-1} . The frequency positions and relative intensities of these bands show a strong pH dependence similar to that observed for aqueous humic acid. More specifically, as the pH increases, the intensities of the bands located at 1714 ($\nu_{\text{C-OH}}$) and 1280 cm^{-1} ($\nu_{\text{C-OH}}$) diminish; the intensity of the band positioned at 1385 cm^{-1} ($\nu^{\text{s}}_{\text{COO}^-}$) is increased; and there is a concurrent shift in the peak position of the band located in 1596 cm^{-1} ($\nu^{\text{a}}_{\text{COO}^-}$) to lower wavenumbers. All these spectroscopic features are associated with a higher degree of deprotonation of interfacial humic acid molecules at higher pH values.

In terms of peak frequency positions the spectra of adsorbed humic acid show strong similarities with the spectra of aqueous humic acid. A difference that can be observed, however, is a change in the relative intensity between the C=O ($\approx 1715 \text{ cm}^{-1}$) and COO^- ($\approx 1615\text{-}1580 \text{ cm}^{-1}$) bands (Figure 4-19). The relative intensity of these two bands in the spectrum of adsorbed humic acid on kaolinite at pH 3.5 is more comparable to that obtained for aqueous humic acid at pH 5. Because these absorption

bands are strongly correlated with the protonation state of humic acid, this finding reveals that the degree of protonation of humic acid is affected by adsorption.

The higher extent of deprotonation is also evidenced by the peak frequency position of the $\nu^{\text{a}}_{\text{COO}^-}$ mode exhibited by adsorbed humic acid at pH 3.5 (1596 cm^{-1}). The frequency position of this absorption band is closer to that of aqueous humic acid spectrum at pH 5 (1595 cm^{-1}) than that of aqueous humic acid at pH 3.5 (1615 cm^{-1}). As observed in the spectra of aqueous humic species, the position of the $\nu^{\text{a}}_{\text{COO}^-}$ mode is very sensitive to pH changes and thus to the degree of protonation. Therefore the spectroscopic results strongly indicate that adsorption on kaolinite promotes deprotonation of the humic acid. This observation is consistent with previous investigations which observed enhanced deprotonation of organic ligands coordinated to mineral surfaces via outer sphere adsorption modes (e.g. Johnson et al., 2004a; Lackovic et al., 2003b; Yoon et al., 2004a; Yoon et al., 2005). As suggested by Yoon et al. (2004a), at acidic conditions two mechanisms can explain the increased resistance to protonation of surface bound organic ligands. First, at the mineral-water interface there is a lower proton activity (higher pH) than in the bulk aqueous phase due to the repulsion of protons from the interface by the positive surface charge. Second, protons may be transferred from the adsorbed organic ligand to the surface via a charge induction mechanism. This charge induction results in a lower degree of protonation for the adsorbed molecules and an increased positive surface charge.

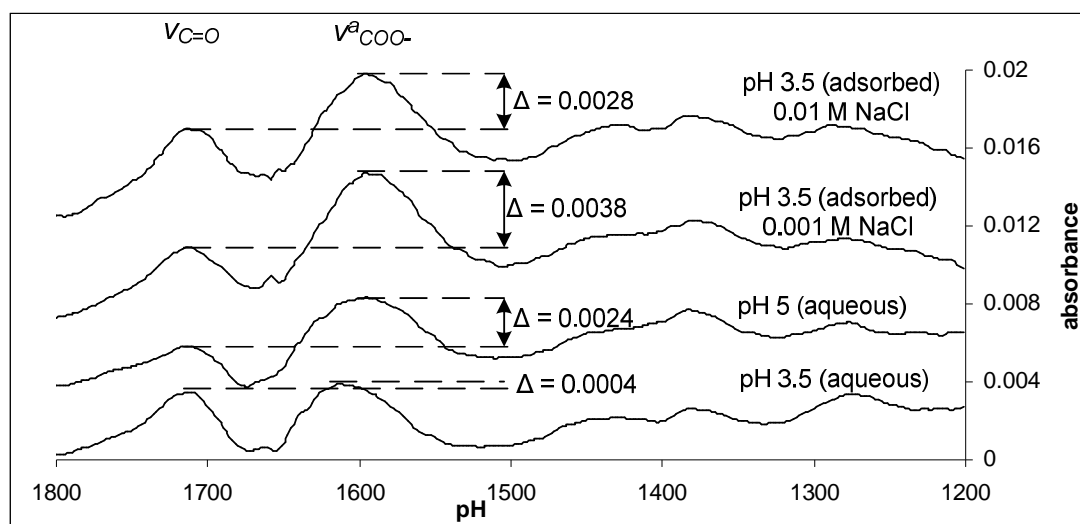


Figure 4-19 The difference in relative intensity of the bands arising from C=O and COO⁻ stretching vibrations observed in aqueous and adsorbed humic acid. The difference in intensity (Δ) is given in absorbance units. A smaller Δ value indicates a higher protonation state. Spectra have been offset for clarity.

In Figure 4-19 it can also be seen that the ionic strength of the solution influences the protonation state of adsorbed humic acid. At pH 3.5 and 0.01 M NaCl, the difference in intensity between the C=O and COO⁻ bands is very similar to that observed for aqueous humic acid at pH 5. However at a lower ionic strength (0.001M), the difference in intensities is greater than that found at 0.01 M NaCl, indicating an even greater extent of deprotonation.

The absence of additional bands in the spectra of adsorbed humic acid when compared to the spectra of aqueous humic acid is consistent with an outer sphere adsorption mechanism in which humic acid functional groups are not bound to surface sites via direct chemical bonding. The predominance of outer sphere complexation is also supported by the close similarity in the absorption band peak positions exhibited by adsorbed and aqueous humic acid species. Remarkably small shifts in peak positions following adsorption were also observed by Yoon et al. (2004a) and Yoon et al. (2005) for the adsorption of fulvic and humic acid on boehmite. Furthermore, Yoon et al. (2004a) observed that the peak shifts exhibited by fulvic acid, upon adsorption, are significantly smaller when compared to the shifts seen for simpler outer sphere complexed organic ligands. The authors attributed this effect to the small fraction of carboxylic groups that are involved in outer sphere complexation reactions relative to the overall number of carboxylic groups present. As a result the IR spectra of adsorbed species are dominated by spectral contributions of solution-facing carboxylic groups and thus explaining the smaller band shifts obtained for outer sphere complexed organic macromolecules (Yoon et al., 2004a).

The IR spectra of adsorbed humic acid on gibbsite are very similar to those obtained for adsorbed humic acid on kaolinite. Additionally, similar changes were observed in the spectra of adsorbed humic acid on kaolinite and on gibbsite as a function of pH. These spectral similarities suggest that humic acid can coordinate to the surface of kaolinite and gibbsite in a similar binding mode (i.e. outer sphere complexation). The peak frequency positions of the absorption bands exhibited by adsorbed humic acid on gibbsite and kaolinite, at different pH values are given in Table 4-7.

Table 4-7 Peak frequency positions of the absorption bands originating from carboxyl vibrational modes of aqueous and adsorbed humic acid at 0.01 M NaCl

Assignment	Wavenumber (cm^{-1})								
	Aqueous			Kaolinite			Gibbsite		
	pH			pH			pH		
	3.5	5	7	3.5	5	7	3.5	5	7
$\nu_{\text{C-OH}}$	1275	1277	-	1280	-	-	1276	1278	-
$\nu_{\text{COO}^-}^{\text{s}}$	1382	1382	1385	1383	1382	1385	1386	1388	1388
$\nu_{\text{COO}^-}^{\text{a}}$	1615	1595	1580	1596	1584	1579	1604	1590	1582
$\nu_{\text{C=O}}$	1712	1714	-	1714	-	-	1715	1716	-

Figure 4-20 compares the IR spectra of adsorbed humic acid on kaolinite and on gibbsite at pH 3.5. One important difference that can be immediately observed is the higher relative intensity of the C=O band (1715 cm^{-1}) in the spectra of adsorbed humic acid on gibbsite. This suggests that, at the same pH, adsorbed humic acid on gibbsite exists in a higher protonation state than on kaolinite. The higher extent of protonation is also indicated by the higher intensity of the band at about 1280 cm^{-1} , which is attributed to the stretching mode of carboxyl C-OH bonds. This shows that the different charging behaviour of the two mineral surfaces has an effect on the extent of humic acid protonation state, with adsorption on kaolinite leading to a higher degree of deprotonation than adsorption on gibbsite. Finally, it can be seen that the protonation state of adsorbed humic acid on gibbsite also appears to be influenced by the ionic strength of the solution, with higher ionic strengths favouring protonation.

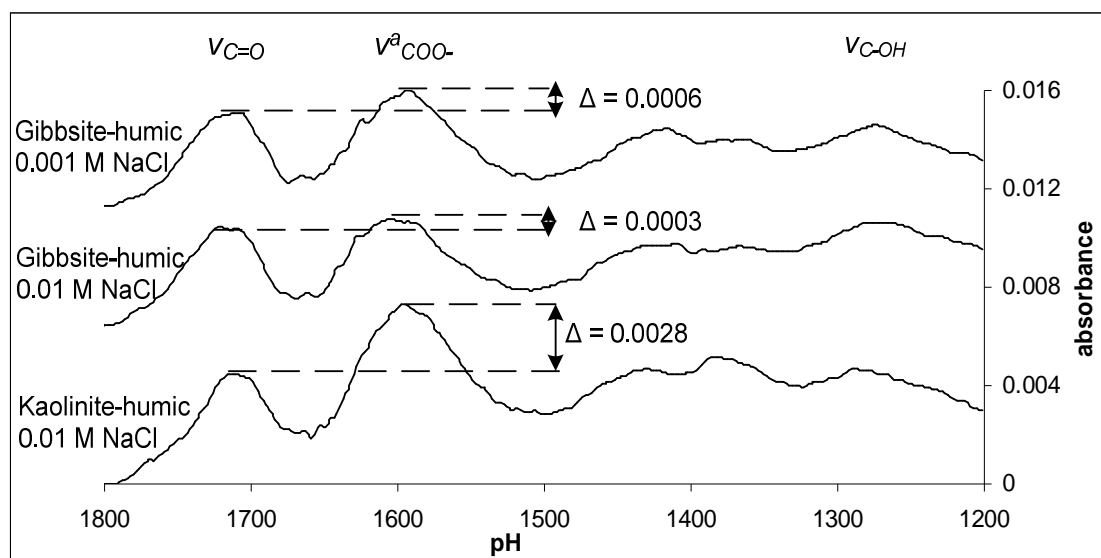


Figure 4-20 Comparison of adsorbed humic acid spectra on kaolinite and gibbsite at pH 3.5. The difference in intensity (Δ) is given in absorbance units. A smaller Δ value indicates a higher protonation state. Shifts in peak frequency positions of the $\nu_{\text{COO}^-}^{\text{a}}$ band are also associated with the different degree of protonation of humic acid surface complexes. Spectra have been offset for clarity.

In summary, interfacial humic acid on kaolinite and gibbsite gives rise to similar IR spectra indicating a similar binding adsorption mode on both mineral substrates. The strong resemblance of the IR spectra of aqueous and adsorbed humic acid species strongly suggests a dominant outer sphere adsorption mechanism under the experimental conditions examined. Differences in relative band intensities observed for the two minerals reflect mineral specific effects on the protonation state of adsorbed humic acid molecules.

In addition to the effects of mineral substrate on the binding mode of humic acid, it is also interesting to examine whether different humic acid samples exhibit different binding properties on similar mineral substrates. Such behaviour would not be unsurprisingly given the highly heterogeneous nature of humic acids. Humic acids are complex macromolecules and carboxyl groups can be attached to different segments within the humic acid molecule including both aliphatic and aromatic components. Therefore, even though humic acids interact primarily through carboxyl functionalities, the different structural environment of carboxyl groups in humic acid samples from different sources may also be influencing the binding mode of humic acid. Unfortunately comparisons with literature data are not possible due to the limited number of studies that have reported IR spectra of adsorbed humic acids. To date only one study has reported *in situ* IR spectra of adsorbed humic acid (Yoon et al., 2005). In accordance with the spectroscopic results obtained in the present study, Yoon et al. (2005) suggested that humic and fulvic acid are predominantly adsorbed as outer sphere complexes at the boehmite-solution interface.

To examine the effect of structural and chemical heterogeneity on the binding mode of humic acid, a limited number of IR experiments were carried out using a different humic acid sample. The additional humic acid used was also a commercial sample purchased from Fluka (hereinafter referred to as FHA). To allow direct comparisons, the spectra of adsorbed FHA were obtained using the same experimental procedure and conditions as that used previously for the ACROS humic acid (hereinafter referred to as AHA).

The spectra of aqueous FHA and AHA are shown in Figure 4-21. At the same pH, FHA has more protonated carboxylic groups, as evidenced by the higher intensity of C=O bands, indicating a stronger acidic character for the AHA sample. This difference in acidic character reflects the different local structural environments for the carboxylic groups in the two samples (e.g. type of moieties attached to carboxyl groups, neighbouring functional groups), which can influence their chemical behaviour including the proton binding properties. Moreover, the two humic acid samples show

absorption bands in the carboxylate asymmetric stretching region ($\approx 1620\text{-}1570\text{ cm}^{-1}$) with different peak frequency positions and different absorption band widths (AHA sample exhibits broader absorption features in the $\nu^a_{\text{COO}^-}$ region). These differences can also be attributed to the different structural characteristics of the two humic acid samples. Typically samples with a wide range of carboxyl structural types will give rise to broader absorption bands (Hay and Myneni, 2007).

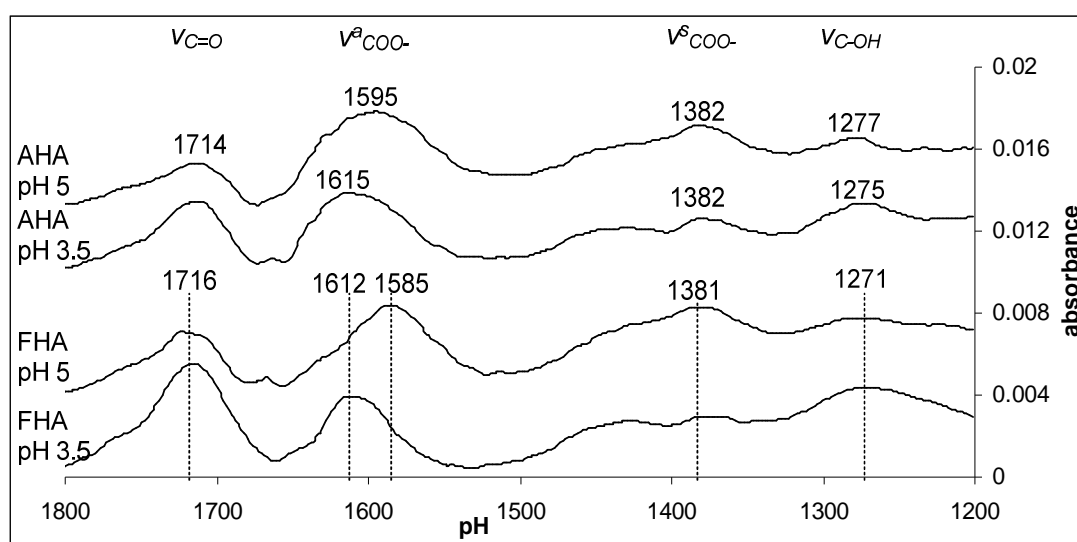


Figure 4-21 IR spectra of aqueous Fluka humic acid (FHA) and ACROS humic acid (AHA; also shown in Figure 4-18). Spectra have been offset for clarity.

In addition to the structural heterogeneity of carboxylic groups other functional groups within the humic acid molecules may be contributing to the bands obtained in the carboxylate stretching region. As a result these additional vibrational modes, which may be different in the two humic acid samples, could also be responsible for the difference in peak frequency position and width observed for the COO^- band. To isolate the absorption bands corresponding to carboxyl vibrational modes the spectra of aqueous humic acid collected at pH 3.5 were subtracted from the aqueous spectra collected at pH 7. Because a change in pH is expected to primarily affect the absorption bands originating from the carboxyl groups, the difference spectra obtained from this subtraction procedure will comprise of absorption bands primarily originating from the carboxyl stretching modes.

Figure 4-22 shows the difference spectra obtained for the two humic acid samples. As expected, each spectrum includes two positive bands corresponding to the symmetric and asymmetric stretching modes of the deprotonated carboxyl group, and two negative bands corresponding to the vibrational modes of the protonated carboxyl group (i.e. C-OH and C=O). The negative intensity bands develop because the

concentration of protonated carboxyl groups is significantly reduced as the pH changes from pH 3 to pH 7. Conversely the concentration of deprotonated carboxyl groups increases as the pH changes from 3 to 7 and thus explaining the positive bands obtained.

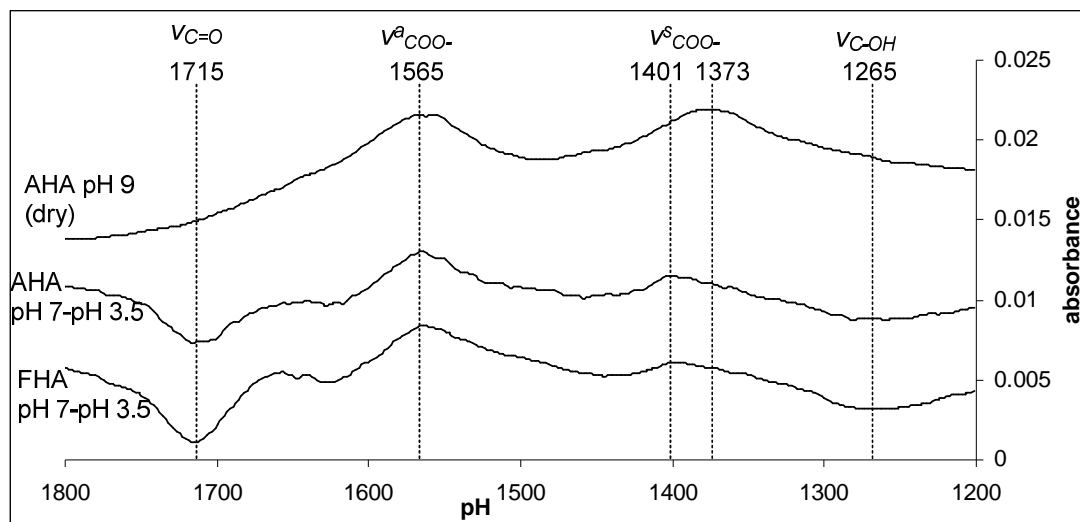


Figure 4-22 pH-dependent absorption features for AHA and FHA obtained from the subtraction of the aqueous humic acid spectra collected at pH 3.5 from the aqueous spectra collected at pH 7. Positive features correspond to the stretching vibrations of deprotonated carboxylic groups ($\nu^a_{\text{COO}^-}$ and $\nu^s_{\text{COO}^-}$) and negative features to the stretching vibrations of protonated carboxylic groups ($\nu_{\text{C=O}}$ and $\nu_{\text{C-OH}}$). The dry AHA spectrum collected at pH 9 is also included for comparison. Spectra have been offset for clarity.

A striking feature of Figure 4-22 is that the number and frequency positions of the absorption bands obtained from the subtraction procedure show remarkable similarities in the two humic acid samples. This observation is in agreement with the findings of Hay and Myneni (2007), who reported that carboxylic acid groups in different types of NOM samples (humic or fulvic acids; fluvial or soil) exhibit a narrow range of peak frequency positions. The range of peak frequency positions reported for the different types of NOM examined by Hay and Myneni (2007) were 1585-1590 cm^{-1} and 1368-1382 cm^{-1} for the carboxylate asymmetric and symmetric stretching modes respectively. Corresponding peak frequency positions obtained in the present study are 1565 cm^{-1} and 1396-1401 cm^{-1} . It should be noted, however, that the IR spectra reported by Hay and Myneni (2007) were collected under dry conditions and this can influence the frequency positions of the carboxylate stretching vibrations.

The spectrum of dry AHA humic acid adjusted to pH 9 was collected in order to observe the differences occurring in the IR spectra of humic acid upon drying (Figure 4-22). The dry spectrum at pH 9 has only two prominent absorption bands with peak positions at 1563 and 1373 cm^{-1} corresponding to the carboxylate asymmetric and

symmetric stretching vibrations respectively. Upon drying the asymmetric stretching mode did not change significantly (about 2 cm^{-1}) whereas the symmetric stretching mode shifted by about 20 cm^{-1} from 1396 cm^{-1} in the aqueous spectrum to 1373 cm^{-1} in the dry spectrum. Although the new peak frequency position of the symmetric stretching mode is within the range of frequency values reported by Hay and Myneni (2007), the frequency position of the asymmetric mode falls outside the range reported. However the frequency position of the asymmetric mode found in the present study for the two aqueous samples is similar to those reported by Yoon et al. (2005) for aqueous Pahokee peat humic acid (1571 cm^{-1}) and Lumsdon and Fraser (2005) for aqueous humic acid extracted from an organic surface horizon soil (1573 cm^{-1}).

The spectra of adsorbed AHA and FHA on kaolinite at pH 3 and 5 from 0.1 g/L humic acid solutions (0.001 M NaCl) are shown in Figure 4-23. The IR spectra of FHA are also dominated by the spectroscopic features of carboxyl groups, with absorption bands attributed to both protonated (1719 and 1285 cm^{-1}) and deprotonated carboxyl groups (1583 - 1585 , 1380 cm^{-1}). The peak frequency positions of these bands have very similar peak frequency positions to those exhibited by adsorbed AHA humic acid indicating similar carboxyl binding modes for both humic acid samples. The difference in peak frequency positions of the band associated with the carboxyl asymmetric stretching vibration (1580 - 1600 cm^{-1}) is attributed to the differences in the protonation state of the two humic acid samples. These spectroscopic findings suggest that despite the structural heterogeneity of different humic acid samples their binding properties on mineral surfaces can be remarkably similar.

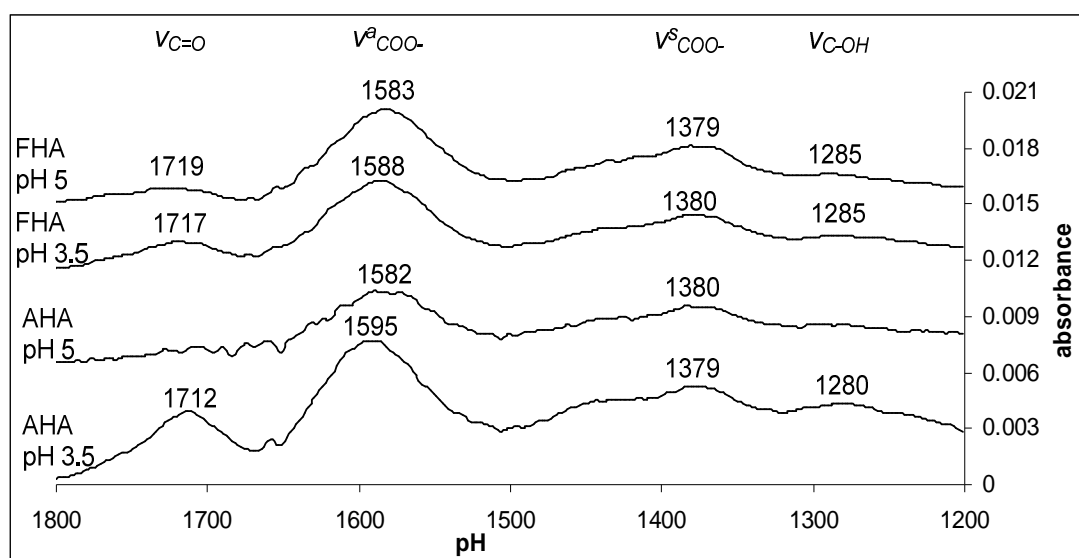


Figure 4-23 Adsorbed humic acid spectra on kaolinite at 0.001 M NaCl , obtained from 0.1 g/L solutions of ACROS humic acid (AHA) and Fluka humic acid (FHA). Spectra have been offset for clarity.

Proposed binding mechanisms from the combined study of spectroscopic and macroscopic adsorption data

In a previous section it has been shown that it is very difficult to assess the importance of individual adsorption mechanisms of humic acids from the macroscopic adsorption behaviour of humic acid. However, using the macroscopic adsorption data in tandem with the spectroscopic measurements it is possible to obtain more conclusive evidence regarding the adsorption mechanisms. IR data showed that humic acid is adsorbed on gibbsite and kaolinite primarily through non specific interactions (i.e. outer sphere complexation). These spectroscopic results validate the macroscopic adsorption data which indicated that ligand exchange (i.e. inner sphere complexation) is not an important mechanism for adsorption at $>0.001\text{M}$ NaCl. However, even at the lower ionic strengths (0.001M NaCl) examined, there is still no spectroscopic evidence of inner sphere complexation. This is an interesting finding because it contradicts the generally held view that ligand exchange can be an important mechanism of humic adsorption on mineral surfaces.

Unfortunately IR spectroscopy cannot differentiate between different adsorption mechanisms that result in outer sphere complexation such as van der Waals interactions, anion exchange and cation bridging. Nevertheless, the macroscopic adsorption behaviour of humic acid can further refine these spectroscopic findings. It has been shown that adsorption increases with increasing ionic strength and that divalent cations are more efficient in enhancing humic acid adsorption. As discussed previously these two findings are more consistent with cation (or water) bridging and van der Waals interactions. Although both mechanisms could be contributing to adsorption their relative importance is expected to vary with solution conditions. For example at low pH values ($\text{pH} < \text{pH}_{\text{pzc}}$) and in the presence of sodium or potassium ions, humic acid adsorption will be dominated by van der Waals interactions. Conversely at high pH values ($\text{pH} > \text{pH}_{\text{pzc}}$) and in the presence of divalent cations, cation/water bridging is expected to be the main adsorption mechanism.

Finally, at low ionic strengths the possibility of small contributions from other adsorption mechanisms such as ligand exchange and anion exchange cannot be excluded completely. However according to the results presented these mechanisms are not believed to be of significant importance. Regarding a ligand exchange mechanism this conclusion is based on the absence of spectroscopic evidence for inner sphere complexation and regarding anion exchange this conclusion is based on the enhanced humic acid adsorption as a function of ionic strength. This is a significant finding which

suggests that humic acids can coordinate to mineral surfaces via different binding modes than those found for simpler organic ligands. For example anion exchange and ligand exchange have been found to be major adsorption mechanisms for other smaller carboxyl-containing organic ligands (e.g. Axe and Persson, 2001; Duckworth and Martin, 2001; Evanko and Dzombak, 1999). One implication of this finding concerns the appropriateness of using simple LMW organic acids as analogues to humic substances.

Conclusions

The adsorption of humic acid onto kaolinite and gibbsite was quantified for a wide range of experimental conditions including pH, humic acid concentration, ionic strength, and type of background electrolyte. Although gibbsite exhibited a higher adsorption density towards humic acid than kaolinite, similar adsorption trends were observed for both minerals with higher adsorption occurring at lower pH, higher ionic strength, and in the presence of divalent ions. The wide range of solution conditions in which humic acid was found to occur coupled with the rapid adsorption kinetics observed (equilibrium was reached within minutes) suggests that kaolinite and gibbsite particles will be at least partially coated with humic substances in natural systems with significant concentrations of organic matter.

The macroscopic adsorption behaviour of solute ions can be related to the adsorption mechanism(s) involved in the binding of humic acid on mineral surfaces. However due to the complex nature of humic acids the information obtained from the macroscopic adsorption properties can be subject to uncertainties. Factors that can complicate the interpretation of the adsorption results are associated with the polydisperse, polyfunctional and polyelectrolytic character of humic acids. According to the adsorption data, any of the following adsorption mechanisms could play an important role in humic acid binding with kaolinite and gibbsite: ligand exchange, cation/water bridging, and van der Waals interactions. Increased humic acid adsorption at higher ionic strengths indicates that anion exchange is not a significant adsorption mechanism.

Because it is important to differentiate whether non specific binding (cation/water bridging, van der Waals interactions) or specific binding (ligand exchange) is occurring between humic acid and mineral surfaces, *in situ* IR

spectroscopy was employed to examine the binding mode of adsorbed humic acid. The five main findings of the IR spectroscopic analysis are: (1) The IR spectra of adsorbed humic acid on both kaolinite and gibbsite confirmed the importance of carboxylic groups on surface complexation by humic acids. (2) Adsorbed humic acid on both substrates exhibited similar IR spectra suggesting a similar humic acid binding mode. (3) The absence of shifts in band positions of the carboxyl vibration modes, following adsorption, indicated a dominant outer sphere sorption mechanism consistent with cation/water bridging or van der Waals interactions. (4) The protonation state of humic acid is influenced by the adsorption reaction with adsorbed humic acid exhibiting a lower degree of protonation when compared to aqueous humic acid at the same pH. This finding was more evident for the kaolinite-humic acid systems than for the gibbsite-humic acid systems. (5) Despite the structural heterogeneity of humic acid samples, the IR spectra of adsorbed humic acids obtained from different sources can be remarkably similar.

Contrary to expectations, the combined results of macroscopic and spectroscopic measurements showed that ligand exchange and anion exchange are not important mechanisms for the adsorption of humic acid on kaolinite and gibbsite. Humic acid adsorption is more consistent with either cation/water bridging and/or van der Waals interactions. The results of this investigation indicate that adsorbed humic acid does not form direct chemical bonds with the surface and therefore may have a smaller impact on surface reactivity than previously thought.

Chapter 5 General discussion and conclusions

The work presented in this thesis was motivated by the need to better understand the role of organic ligand surface complexation reactions in the natural environment. Knowledge about the interactions of organic ligands with mineral surfaces, and particularly the molecular level adsorption mechanisms, can provide insights into the effects of surface bound ligands on the adsorption properties, charging behaviour and reactivity of mineral surfaces. This in turn can increase our understanding of several important geochemical processes such as dissolution and precipitation reactions; colloidal stability and flocculation; transport and fate of both organic and inorganic chemicals in soils and waters; nutrient cycling; and the carbon biogeochemical cycle.

Natural organic matter (NOM), the major source of organic ligands in the environment, is composed of a mixture of organic molecules with a wide range of molecular weights and chemical properties. Although the predominant fraction of NOM is composed of ill defined organic macromolecules (collectively termed humic substances), we still have a limited understanding of the environmental behaviour and effects of these compounds. Much of our understanding regarding the interactions of humic substances with mineral surfaces has come from the study of model, well defined, low molecular weight organic acids which are generally used as analogs for humic substances. Humic substances and other low molecular weight organic ligands are believed to exhibit similar adsorption mechanisms because their chemical behaviour is governed by the same type of functional groups, that is, carboxyl and phenolic groups.

Due to the environmental importance of organic ligands, much scientific effort has been devoted, for many years, to the study of organic ligand surface complexation reactions. Information regarding mineral surface-organic ligand interactions has been obtained by a variety of macroscopic and microscopic adsorption methods. However research to date has tended to focus on mineral (hydr)oxides and far too little attention has been paid to organic ligand adsorption on clay minerals. For this reason the purpose of the current study was to investigate the adsorption of organic ligands on kaolinite, a relatively simple aluminosilicate clay mineral.

To investigate the interactions of organic ligands with kaolinite surfaces, three common low molecular weight organic acids (oxalic, phthalic, and salicylic acid) and a commercial humic acid were chosen for this study. Molecular level information

regarding the structure and binding mode of adsorbed species was obtained using *in situ* MIR FTIR spectroscopy. Other experimental techniques including adsorption experiments, surface titrations, and surface complexation modelling were also employed in order to determine and describe the macroscopic adsorption behaviour of the organic ligands examined.

The layout of this thesis may be initially perceived as a collection of isolated studies, with each chapter addressing a unique aspect of organic ligand surface complexation. However, the objectives of each chapter have been set in such a way so as to meaningfully contribute to the improvement of our understanding of fundamental aspects of organic ligand complexation reactions. Consequently the present chapter is meant to synthesise the main findings drawn from each chapter, to relate these to the existing literature, and finally to address the main contributions of this study to the current knowledge.

To begin with, the introductory chapter was aimed at presenting the fundamental aspects of adsorption process and the effects of organic ligand adsorption on surface dependent phenomena with a specific emphasis on mineral dissolution reactions.

In **Chapter 2** the flow through *in situ* IR spectroscopic technique used for the study of organic ligand complexations is presented. Because this technique has received considerable attention in this work, a significant part of this chapter deals with presenting its main advantages and limitations. A general discussion on how IR spectroscopy can contribute to the molecular level understanding of mineral surface-organic ligand interactions is also included. Finally, to demonstrate the application of the flow through IR method presented for the study of organic ligand surface complexation, a case study investigating the adsorption of oxalic acid on kaolinite is provided. The main conclusions derived from chapter 2 are:

(1) The current experimental method was successful in providing direct experimental evidence regarding the binding and coordination mode of the surface complexes formed in real time. However some limitations arise in the application of this method to the study of surface complexation. Most notably the degradation of the mineral films deposited on the ZnSe crystal during the course of the experiments has limited the quantitative analysis of the IR spectra obtained. Due to the degradation of the mineral coating, the integrated absorbance of particular bands obtained at different reaction times could not be compared. Since integrated absorbance is proportional to ligand surface concentration, Morris and Wogelius (2008) set up an IR study in which they were able to monitor the change in phthalate concentration on forsteritic glass as a function of time. In their study decreased phthalate surface concentration was attributed

to the stripping of magnesium surface sites by a surface chelate effect. Unfortunately, the relatively low stability of the mineral coating in the present study did not allow the extraction of adequate information to constrain how the adsorbate concentrations change over time.

(2) The binding and coordination modes of oxalic acid on an important phyllosilicate mineral, kaolinite, could be determined by IR spectroscopy. At low pH (3.5) and an initial oxalate concentration of 5×10^{-4} M, oxalate predominately forms a mononuclear bidentate inner sphere surface complex (chelate complex), involving one oxygen atom from each carboxyl group. At a higher pH (6) and/or higher initial oxalate concentration (5×10^{-4} M), spectroscopic results indicate the existence of an additional outer sphere surface complex. Kaolinite surface sites participating in surface coordination are presumably the more reactive aluminol edge sites.

(3) The coordination mode inferred for the inner sphere complex is consistent with the coordination mode of oxalic acid on other simpler (hydr)oxides of iron, aluminium and titanium.

(4) Enhanced kaolinite dissolution rates in the presence of oxalate have been previously reported and the formation of chelate ring structures, identified here, supports the idea of a direct ligand promoted dissolution mechanism. These findings have important implications for the understanding of the mineral dissolution mechanisms of kaolinite in the presence of organic ligands. For example in their study on the oxalate promoted dissolution of kaolinite, Cama and Ganor (2006) found that there is a threshold oxalate surface concentration, below which the oxalate promoted dissolution rate reduces to zero. The authors suggested that at low concentrations oxalate forms outer sphere complexes that have no effect on the dissolution rates, thus explaining the existence of a threshold concentration value. The authors however did recognise that their theory needs to be confirmed by spectroscopic evidence regarding the effect of oxalate concentration on the type of surface complexes formed on kaolinite. In the present study it has been shown that at low concentrations oxalate coordinates to the surface of kaolinite through an inner sphere binding mode. Therefore the explanation proposed by Cama and Ganor (2006) does not hold true and a different ligand promoted dissolution mechanism must be considered.

An alternative explanation proposed in the study of Cama and Ganor (2006), which appears to be more plausible in light of the results from the present study, is that oxalate can catalyse the hydrolysis of metal oxygen bonds only when oxalate surface complexes are formed on two neighbouring aluminol edge sites.

In addition to this explanation, we propose a third possibility which is also consistent with our observations. The existence of a threshold value for the oxalate proton promoted dissolution mechanism may also be the result of a second parallel indirect mechanism involving proton promoted dissolution caused by the dissociation of the ligand in the vicinity of the surface and that could be operative in addition to the direct oxalate ligand promoted dissolution mechanism. The observations of Cama and Ganor (2006) were made at a pH of about 3 where the speciation of oxalic acid in solution is dominated by the singly protonated hydrogen oxalate species (HOx^{1-}). Our results show that the inner sphere complexed surface species are fully deprotonated, which suggests that upon adsorption, each oxalate molecule releases a hydrogen ion in the vicinity of the kaolinite surface. As a result, as the surface concentration of oxalate species increases, there will be a higher concentration of protons at the interface that can coordinate to available surface sites. Above a certain surface concentration two or more protons may be transferred to a single surface site and thus significantly enhance the rates of dissolution.

From the spectroscopic results it is also possible to estimate the oxalate surface concentration above which the surface of kaolinite becomes saturated with inner sphere complexes. At pH 3.5 and an initial oxalate concentration of 5×10^{-4} M, the IR spectra revealed the existence of only inner sphere complexes whereas at an oxalate concentration of 5×10^{-3} M both inner and outer sphere complexes coexist on the surface. It therefore seems that for the given experimental conditions at a certain concentration above 5×10^{-4} M and below 5×10^{-3} M the surface sites of kaolinite become saturated.

Given that the total surface area of kaolinite deposited initially on the ZnSe crystal is $9.45 \times 10^{-3} \text{ m}^2$ and this amount is exposed to a volume of 0.9 mL (volume of the flow cell's solution cavity) of oxalate solution of 5×10^{-4} M and 5×10^{-3} M at any given time, then the number of moles available to the adsorbent surface area is $4.76 \times 10^{-5} \text{ mol/m}^2$ and $4.76 \times 10^{-4} \text{ mol/m}^2$ respectively. It should be noted that these values are approximations and they just provide an indication of the experimental conditions in which the saturation for inner sphere surface complexation is expected. Moreover these values do not represent surface concentrations. Hence corresponding oxalate surface concentrations need to be estimated in order to investigate whether a relation exists between maximum inner sphere complexed oxalate concentration and the threshold oxalate surface concentration for oxalate promoted dissolution estimated by Cama and Ganor (2006) (0.1 and $0.2 \text{ } \mu\text{mol/m}^2$).

In conclusion the ability of IR spectroscopy to probe the relative concentrations of inner and outer sphere complexes provides an exciting prospect for identifying the dissolution mechanisms by which organic ligands can enhance mineral dissolution rates. The development of experimental methods that can investigate the adsorption of organic ligands at both the macroscopic and microscopic level at the same experimental conditions (same adsorbent to adsorbate ratios) should be the next step in future research. Such methods will allow us to determine accurately the conditions under which inner sphere complexation is the dominant coordination mode and hence the conditions that ligand promoted dissolution could be the dominant dissolution pathway.

Turning back to Cama and Ganor's (2006) study, such an experimental method combining dissolution, adsorption and spectroscopic measurements at the same experimental conditions could provide valuable information regarding the oxalate dissolution mechanism of kaolinite. If outer sphere surface complexed species were found to start forming at oxalate concentrations below the threshold value of oxalate promoted dissolution it would suggest that an indirect proton promoted dissolution mechanism is operative.

In **Chapter 3** the interactions of salicylic and phthalic acid on kaolinite were investigated by both *in situ* IR spectroscopy and macroscopic adsorption experiments. The macroscopic adsorption data were then described by surface complexation modelling using constraints from the IR spectroscopic results such as the number of surface species and their binding mode. The main conclusions derived from chapter 3 are:

(1) IR data strongly suggests a dominant outer sphere mode of adsorbed phthalate on kaolinite over the entire pH range examined (3-6). A minor inner sphere complexed phthalate species, which is favoured by acidic conditions, could also be observed. Similar phthalate adsorption behaviour has been reported for iron and aluminium (hydr)oxides (i.e. a major outer sphere complexed phthalate species coexisting with a minor inner sphere complexed species)

(2) The IR features of the inner sphere surface complex, and thus the coordination mode inferred, are consistent with previous studies that have investigated the adsorption of phthalic acid on aluminium and iron (hydr)oxides. The spectroscopic evidence suggests that the inner sphere complexed species is a mononuclear chelate complex, where one oxygen atom from each carboxyl group is directly coordinated to a single surface cation. However, the identity of this surface complex can not be unambiguously determined from IR spectroscopy and the possibility for the existence of a binuclear bridging complex cannot be excluded.

A chelate complex is in agreement with the effect of phthalic acid on enhancing the dissolution rates of kaolinite through a ligand promoted dissolution mechanism. The low surface concentration of inner sphere complexed phthalate species can also explain the lower effect of phthalate on the dissolution rates of kaolinite when compared to the effect of oxalate and salicylate (Chin and Mills, 1991). Conversely a binuclear complex is expected to inhibit dissolution rates and hence it is difficult to understand how such a complex could promote the dissolution of kaolinite. It must be noted however that Chin and Mills (1991) suggested that phthalate increases the rates of kaolinite dissolution by reducing the activity of aluminium ions in solution due to aqueous aluminium-phthalate complex formation.

If the increased dissolution rates of kaolinite in the presence of phthalate are in fact due to a ligand promoted dissolution mechanism then the findings of the present study signify the importance of outer sphere complexes in the ligand promoted dissolution mechanism. One would expect that a dominant inner sphere binding mode is required for an organic ligand to enhance the dissolution rates of minerals. However, IR data and surface complexation calculations indicate a low surface concentration of inner sphere complexed species (at most 40% of the total phthalate surface concentration). Furthermore, under the most favourable conditions of inner sphere complexation, only about 5% of total surface sites of kaolinite are occupied by inner sphere complexed species. It therefore seems that even a low concentration of inner sphere complexes can still promote the dissolution of minerals.

A possible explanation for this effect could be that outer sphere complexed species act as a reservoir of phthalate molecules near the surface. After the removal of an aluminium-phthalate species from the surface, another phthalate is immediately available for surface coordination. The presence of these outer sphere complexed phthalate molecules, therefore, ensures that dissolution active surface sites on kaolinite are always saturated with phthalate molecules and as a result even a low concentration of inner sphere complexes is sufficient to promote dissolution.

(3) In common with phthalic acid, salicylic acid forms two types of surface complexes in acidic conditions, one inner and one outer sphere complex. Nonetheless, the adsorption behaviour of salicylic acid shows two main differences from that of phthalic acid. First, the importance of inner sphere complexation is much more pronounced in the salicylic acid-kaolinite systems than in the phthalic acid-kaolinite systems. Second, the relative importance of outer sphere complexed salicylate species increases at lower pH values and the relative importance of inner sphere complexed species increases at higher pH. IR data and surface complexation modelling indicate

that at pH 6 the inner sphere complex is the major surface species whereas at pH 4 inner and outer sphere complexes have similar surface concentrations. Similar spectroscopic results were obtained for adsorbed salicylic acid on gibbsite (see Appendix), suggesting that salicylate behaves similarly on kaolinite and gibbsite surfaces.

Decreased surface concentration of outer sphere complexed species at higher pH is in contrast to the behaviour observed for phthalic and oxalic acid. According to the surface complexation modelling results this reverse trend can be explained by the involvement of a protonated surface hydroxyl group in the formation of the outer sphere complexed salicylate species. At higher pH values the concentration of positively charged surface sites decreases, and as a result less surface sites are available for outer sphere surface complex formation. Consequently, the concentration of positively charged surface sites governs the importance of outer sphere complexation rather than a direct pH effect on the adsorptive properties of the salicylate ions.

(4) The importance of inner sphere surface complexation is in agreement with the effect of salicylic acid in enhancing the dissolution rates of kaolinite through a ligand promoted dissolution mechanism.

(5) The salicylate inner sphere complex is most probably a mononuclear monodentate complex where a single carboxyl oxygen is directly bonded to a surface cation and the phenolic group is hydrogen bonded to a neighbouring surface site. This type of coordination mode is consistent with that inferred for aluminium oxides and different from that inferred for iron oxides (Biber and Stumm, 1994). The ability of salicylic acid to form different coordination modes with different types of metal cations is of significance in predicting the adsorption behaviour of salicylic acid in natural soils. Because the mononuclear bidentate complex is more stable than the mononuclear monodentate complex it is expected that salicylate will preferentially bind to iron substrates rather than aluminium substrates.

(6) IR spectroscopy can be extremely helpful in constraining surface complexation model parameters required to fit adsorption data such as the number and type of surface complexes formed. In addition, spectroscopic data can also provide an independent method for obtaining input parameters that may not be readily available from other experimental techniques such as interfacial capacitance. This can be done by choosing model parameters that not only provide satisfactory fits to the macroscopic adsorption data but also can predict surface speciation that is in agreement with spectroscopic data. Therefore it is essential to perform spectroscopic and macroscopic measurements under the same experimental conditions so that we can directly relate model calculations to spectroscopic results.

In chapter 2 and 3 the binding and coordination modes of some LMW organic acids were investigated in order to obtain insights regarding the interactions between organic ligand functional groups and surface sites of kaolinite. In order to investigate whether such interactions are relevant for the same functional groups found in complex organic macromolecules, **Chapter 4** examines the macroscopic and microscopic adsorption properties of a commercial humic acid on kaolinite and gibbsite. The most important findings from this work are as follows:

(1) The macroscopic adsorption behaviour of humic acid on kaolinite and gibbsite is very similar. Spectroscopic results also indicated that humic acid interacts with both mineral substrates through a similar binding mode. As mentioned previously, the binding and coordination modes inferred for surface bound LMW organic ligands on kaolinite are similar to those proposed in the literature for other simpler aluminium (hydr)oxides. Therefore in that respect humic acid behaves similarly to LMW organic acid acids.

(2) The protonation state of humic acid is affected by adsorption, with surface coordination promoting the deprotonation of humic acid. Increased deprotonation upon adsorption has also been observed for some LMW organic acids. This effect will have an impact on the chemical properties of both the mineral surface and the adsorbed humic acid molecules. A practical implication of this observation concerns the prediction of heavy metal mobility in the environment. Humic acids and mineral surfaces are the major adsorbent phases for heavy metals and as a result many studies have investigated the adsorption capacity of humic acids and of mineral surfaces for heavy metals. However the results obtained here suggest that the interactions between humic acids and mineral surfaces can affect the charging properties of the two individual components and hence their binding capacity for solute ions. Thus the use of results obtained from simple systems (e.g. humic acid-metal and mineral-metal systems) in predictive adsorption and transport models may not provide an accurate representation of the behaviour of heavy metals in the presence of humic acid coated mineral surfaces.

(3) The adsorption mechanisms inferred for the adsorption of humic acid on kaolinite and gibbsite are different than any of those inferred for the adsorption of LMW organic acids. Spectroscopic evidence for the existence of direct chemical bonding between humic acids and these two mineral substrates could not be obtained. Cation bridging (i.e. ternary complexation) and van der Waals interactions are probably the dominant types of humic acid adsorption. Conversely for LMW organic acids ligand exchange and anion exchange were the main adsorption mechanisms identified. As a

result doubts are raised concerning the applicability of LMW organic acids as analogs to humic acids. Such a finding is significant for studies investigating the role of organic ligands in the environment since the adsorption properties of LMW organic acids are not comparable to those of humic acids. Because most mineral surfaces in the environment are coated by humic substances more effort must be given to better understand the interactions of humic substances with mineral surfaces rather than those between LMW organic acids with mineral surfaces.

(4) The different types of interactions postulated between mineral surfaces and the functional groups of LMW organic acids vs. humic acids is an unexpected, albeit interesting, finding. One would expect similar binding modes since the chemical properties of humic acids are thought to be governed by the same type of functional groups found in LMW organic acids (i.e. carboxyl and phenolic moieties).

Such a phenomenon could be related to the macromolecular character of humic acid molecules. It is generally assumed that the interactions between LMW organic acids and mineral surfaces are driven by enthalpy changes. However for humic acids, adsorption may be driven by entropy changes. Adsorption via ligand exchange or anion exchange may lead to a greater loss of configurational entropy and as a result cation bridging and van der Waals interactions may present a more energetically favourable mechanism for the binding of humic acids. It must be emphasised that this theory is only speculative and is not derived from the experimental results of the present study. This theory is based on recent studies which investigated the thermodynamic aspects of polyelectrolyte adsorption on charged surfaces. These studies suggested that entropic contribution is the main driving force for the adsorption of polyelectrolytes (Narambuena et al., 2007; Ou and Muthukumar, 2006). Interestingly, entropy driven adsorption has also been suggested for the adsorption of humic acid on bentonite and kaolinite (Salman et al., 2007). Molecular-scale structural observations combined with computational work may be the best way to determine whether a configurational entropy change upon adsorption is the key to understanding humic acid complexation.

References

- Abate, G. and Masini, J. C., 2003. Influence of pH and ionic strength on removal processes of a sedimentary humic acid in a suspension of vermiculite. *Colloids and surfaces. A: Physicochemical and engineering aspects* **226**, 25-34.
- Ali, M. A. and Dzombak, D. A., 1996. Competitive sorption of simple organic acids and sulfate on goethite. *Environmental science and technology* **30**, 1061-1071.
- Angove, M. J., Fernandes, M. B., and Ikhsan, J., 2002. The sorption of anthracene onto goethite and kaolinite in the presence of some benzene carboxylic acids. *Journal of colloid and interface science* **247**, 282-289.
- Angove, M. J., Johnson, B. B., and Wells, J. D., 1997. Adsorption of cadmium(II) on kaolinite. *Colloids and surfaces A: Physicochemical and engineering aspects* **126**, 137-147.
- Angove, M. J., Johnson, B. B., and Wells, J. D., 1998. The influence of temperature on the adsorption of cadmium (II) and cobalt (II) on kaolinite. *Journal of colloid and interface science* **204**, 93-103.
- Angove, M. J., Wells, J. D., and Johnson, B. B., 1999. Adsorption of cadmium(II) onto goethite and kaolinite in the presence of benzene carboxylic acids. *Colloids and surfaces A: Physicochemical and engineering aspects* **146**, 243-251.
- Angove, M. J., Wells, J. D., and Johnson, B. B., 2006. Influence of temperature on the adsorption of mellitic acid onto kaolinite. *Langmuir* **22**, 4208-4214.
- Arnarson, T. S. and Keil, R. G., 2000. Mechanisms of pore water organic matter adsorption to montmorillonite. *Marine chemistry* **71**, 309-320.
- Arnarson, T. S. and Keil, R. G., 2005. Influence of organic-mineral aggregates on microbial degradation of the dinoflagellate *Scrippsiella trochoidea*. *Geochimica et cosmochimica acta* **69**, 2111-2117.
- Au, K.-K., Penisson, A. C., Yang, S., and O'Melia, C. R., 1999. Natural organic matter at oxide/water interfaces: Complexation and conformation. *Geochimica et cosmochimica acta* **63**, 2903-2917.
- Avena, M. J., Koopal, L. K., and Van Riemsdijk, W. H., 1999. Proton binding to humic acids: electrostatic and intrinsic interactions. *Journal of colloid and interface science* **217**, 37-48.
- Axe, K. and Persson, P., 2001. Time-dependent surface speciation of oxalate at the water-boehmite (γ -AlOOH) interface: implications for dissolution. *Geochimica et cosmochimica acta* **65**, 4481-4492.
- Axe, K., Vejgård, M., and Persson, P., 2006. An ATR-FTIR spectroscopic study of the competitive adsorption between oxalate and malonate at the water-goethite interface. *Journal of colloid and interface science* **294**, 31-37.
- Bargar, J. R., Kubicki, J. D., Reitmeyer, R., and Davis, J. A., 2005. ATR-FTIR spectroscopic characterization of coexisting carbonate surface complexes on hematite. *Geochimica et cosmochimica acta* **69**, 1527-1542.
- Bennett, P. C., Melcer, M. E., Siegel, D. I., and Hassett, J. P., 1988. The dissolution of quartz in dilute aqueous solutions of organic acids at 25°C. *Geochimica et cosmochimica acta* **52**, 1521-1530.
- Benyahya, L. and Garnier, J.-M., 1999. Effect of salicylic acid upon trace-metal sorption (Cd^{II} , Zn^{II} , Co^{II} , and Mn^{II}) onto alumina, silica, and kaolinite as a function of pH. *Environmental science and technology* **33**, 1398-1407.
- Bhattacharyya, K. G. and Gupta, S. S., 2008. Adsorption of a few heavy metals on natural and modified kaolinite and montmorillonite: A review. *Advances in colloid and interface science* **140**, 114-131.

- Biber, M. V., Afonso, M. D. S., and Stumm, W., 1994. The coordination chemistry of weathering: IV. Inhibition of the dissolution of oxide minerals. *Geochimica et cosmochimica acta* **58**, 1999-2010.
- Biber, M. V. and Stumm, W., 1994. An *In-Situ* ATR-FTIR Study: The surface coordination of salicylic acid on aluminum and iron(III) oxides. *Environmental science and technology* **28**, 763-768.
- Blake, R. E. and Walter, L. M., 1999. Kinetics of feldspar and quartz dissolution at 70–80°C and near-neutral pH: effects of organic acids and NaCl. *Geochimica et cosmochimica acta* **63**, 2043-2059.
- Boily, J. F. and Fein, J. B., 2000. Proton binding to humic acids and sorption of Pb (II) and humic acid to the corundum surface. *Chemical geology* **168**, 239-253.
- Boily, J. F., Nilsson, N., Persson, P., and Sjöberg, S., 2000a. Benzenecarboxylate surface complexation at the goethite (α -FeOOH)/water interface: I. A mechanistic description of pyromellitate surface complexes from the combined evidence of infrared spectroscopy, potentiometry, adsorption data, and surface complexation modeling. *Langmuir* **16**, 5719-5729.
- Boily, J. F., Persson, P., and Sjöberg, S., 2000b. Benzenecarboxylate surface complexation at the goethite (α -FeOOH)/water interface: II. Linking IR spectroscopic observations to mechanistic surface complexation models for phthalate, trimellitate, and pyromellitate. *Geochimica et cosmochimica acta* **64**, 3453-3470.
- Bradl, H. B., 2004. Adsorption of heavy metal ions on soils and soils constituents. *Journal of colloid and interface science* **227**, 1-18.
- Brady, P. V., Cygan, R. T., and Nagy, K. L., 1996. Molecular controls on kaolinite surface charge. *Journal of colloid and interface science* **183**, 356-364.
- Brady, P. V. and Walther, J. V., 1989. Controls on silicate dissolution rates in neutral and basic pH solutions at 25°C. *Geochimica et cosmochimica acta* **53**, 2823-2830.
- Brown, G. E. J., Parks, G. A., and O'Day, P. A., 1995. Sorption at mineral-water interfaces: macroscopic and microscopic perspectives. In: Vaughan, D. J. and Patrick, R. A. D. (Eds.), *Mineral surfaces*. Chapman & Hall.
- Burdon, J., 2001. Are the traditional concepts of the structures of humic substances realistic? *Soil science* **166**, 752-769.
- Cabaniss, S. E., Leenheer, J. A., and McVey, I. F., 1998. Aqueous infrared carboxylate absorbances: aliphatic di-acids. *Spectrochimica acta Part A* **54**, 449-458.
- Cama, J. and Ganor, J., 2006. The effects of organic acids on the dissolution of silicate minerals: A case study of oxalate catalysis of kaolinite dissolution. *Geochimica et cosmochimica acta* **70**, 2191-2209.
- Cama, J., Metz, V., and Ganor, J., 2002. The effect of pH and temperature on kaolinite dissolution rate under acidic conditions. *Geochimica et cosmochimica acta* **66**, 3913-3926.
- Carroll-Webb, S. A. and Walther, J. V., 1988. A surface complex reaction model for the pH-dependence of corundum and kaolinite dissolution rates. *Geochimica et cosmochimica acta* **52**, 2609-2623.
- Carroll, S. A. and Walther, J. V., 1990. Kaolinite dissolution at 25°, 60°, and, 80°C. *American Journal of Science* **290**, 797-810.
- Casey, W. H., 1995. Surface chemistry during the dissolution of oxide and silicate materials. In: Vaughan, D. J. and Patrick, R. A. D. (Eds.), *Mineral surfaces*. Chapman & Hall, London.
- Chin, P. F. and Mills, G. L., 1991. Kinetics and mechanisms of kaolinite dissolution: effects of organic ligands. *Chemical geology* **90**, 307-317.

- Chorover, J. and Amistadi, M. K., 2001. Reaction of forest floor organic matter at goethite, birnessite and smectite surfaces. *Geochimica et cosmochimica acta* **65**, 95-109.
- Christensen, J. B., Tipping, E., Kinniburgh, D. G., Gron, C., and Christensen, T. H., 1998. Proton binding by groundwater fulvic acids of different age, origins, and structure modeled with the Model V and NICA–Donnan Model. *Environmental science and technology* **32**, 3346-3355.
- Clausen, M., Ohman, L.-O., Axe, K., and Persson, P., 2003. Spectroscopic studies of aluminum and gallium complexes with oxalate and malonate in aqueous solution. *Journal of Molecular Structure* **648**, 225-235.
- Cohen Stuart, M. A., Fleer, G. J., Lyklema, J., Norde, W., and Scheutjens, J. M. H. M., 1991. Adsorption of ions, polyelectrolytes and proteins. *Advances in colloid and interface science* **34**, 477-535.
- Colthup, N. B., Daly, L. H., and Wiberley, S. E., 1990. *Introduction to infrared and raman spectroscopy*. Academic Press, London.
- Cooper, E. M. and Vasudevan, D., 2009. Hydroxynaphthoic acid isomer sorption onto goethite. *Journal of colloid and interface science* **333**, 85-96.
- Cotter-Howells, J. D. and Paterson, E., 2000. Minerals and soil development In: Vaughan, D. J. and Wogelius, R. A. (Eds.), *Environmental Mineralogy*. Eotvos University Press, Budapest.
- Das, M. R. and Mahiuddin, S., 2007. The influence of functionality on the adsorption of p-hydroxy benzoate and phthalate at the hematite-electrolyte interface. *Journal of colloid and interface science* **306**, 205-215.
- Davis, J. A., 1982. Adsorption of natural dissolved organic matter at the oxide/water interface. *Geochimica et cosmochimica acta* **46**, 2381-2393.
- Davis, J. A. and Kent, D. B., 1990. Surface complexation modeling in aqueous geochemistry. *Reviews in mineralogy* **23**, 177-260.
- Day, G. M., Hart, B. T., McKelvie, I. D., and Beckett, R., 1994. Adsorption of natural organic matter onto goethite. *Colloids and surfaces A: Physicochemical and engineering aspects* **89**, 1-13.
- De Wit, J. C. M., Van Riemsdijk, W. H., and Koopal, L. K., 1993a. Proton binding to humic substances. 1. Electrostatic effects. *Environmental science and technology* **27**, 2005-2014.
- De Wit, J. C. M., Van Riemsdijk, W. H., and Koopal, L. K., 1993b. Proton binding to humic substances. 2. Chemical heterogeneity and adsorption models. *Environmental science and technology* **27**, 2015-2022.
- Deacon, G. B. and Phillips, R. J., 1980. Relationships between the carbon-oxygen stretching frequencies of carboxylate complexes and the type of carboxylate coordination. *Coordination chemistry reviews* **33**, 227-250.
- Degenhardt, J. and McQuillan, A. J., 1999. Mechanism of oxalate ion adsorption on chromium oxide-hydroxide from pH dependence and time evolution of ATR-IR spectra. *Chemical Physics Letters* **311**, 179-184.
- Dobson, K. D., Connor, P. A., and McQuillan, A. J., 1997. Monitoring hydrous metal oxide surface charge and adsorption by STIRS. *Langmuir* **13**, 2614-2616.
- Dobson, K. D. and McQuillan, A. J., 1999. In situ infrared spectroscopic analysis of the adsorption of aliphatic carboxylic acids to TiO₂, ZrO₂, Al₂O₃, and Ta₂O₅ from aqueous solutions. *Spectrochimica acta Part A* **55**.
- Dobson, K. D. and McQuillan, A. J., 2000. In situ infrared spectroscopic analysis of the adsorption of aromatic carboxylic acids to TiO₂, ZrO₂, Al₂O₃, and Ta₂O₅ from aqueous solutions. *Spectrochimica acta. Part A, Molecular and biomolecular spectroscopy* **56**, 557-565.
- Drelich, J., Lu, Y., Chen, L., Miller, J. D., and Guruswamy, S., 1988. FTIR internal reflection spectroscopy studies of the effect of pH on adsorption of oleate/oleic

- acid at the surface of a TiO₂ thin film deposited on a Ge single crystal. *Applied Surface Science* **125**, 236-244.
- Drever, J. I., 1988. *The geochemistry of natural waters*. Prentice Hall.
- Drever, J. I., 1994. The effect of land plants on weathering rates of silicate minerals. *Geochimica et cosmochimica acta* **58**, 2325-2332.
- Drever, J. I. and Stillings, L. L., 1997. The role of organic acids in mineral weathering. *Colloids and surfaces. A, Physicochemical and engineering aspects* **120**, 167-181.
- Du, Q., Sun, Z., Forsling, W., and Tang, H., 1997. Acid-Base Properties of Aqueous Illite Surfaces. *Journal of colloid and interface science* **187**, 221-231.
- Duckworth, O. W. and Martin, S. T., 2001. Surface complexation and dissolution of hematite by C₁-C₆ dicarboxylic acids at pH = 5.0. *Geochimica et cosmochimica acta* **65**, 4289-4301.
- Dzombak, D. A. and Morel, F. M. M., 1990. *Surface Complexation Modeling. Hydrous Ferric Oxide*. John Wiley & Sons, New York.
- Eick, M. J., Peak, J. D., and Brady, W. D., 1999. The effect of oxyanions on the oxalate-promoted dissolution of goethite. *Soil Science Society of America journal* **63**, 1133-1141.
- Elfarissi, F. and Pefferkorn, E., 2000. Kaolinite/humic acid interaction in the presence of aluminium ion. *Colloids and surfaces. A, Physicochemical and engineering aspects* **168**, 1-12.
- Evanko, C. R. and Dzombak, D. A., 1998. Influence of structural features on sorption of NOM-analogue organic acids to goethite. *Environmental science & technology* **32**, 2846-2855.
- Evanko, C. R. and Dzombak, D. A., 1999. Surface complexation modeling of organic acid sorption to goethite. *Journal of colloid and interface science* **214**, 189-206.
- Fairhurst, A. J. and Warwick, P., 1998. The influence of humic acid on europium-mineral interactions. *Colloids and surfaces. A, Physicochemical and engineering aspects* **145**, 229-234.
- Feng, X., Simpson, A. J., and Simpson, M. J., 2005. Chemical and mineralogical controls on humic acid sorption to clay mineral surfaces. *Organic Geochemistry* **36**, 1553-1566.
- Filius, J. D., Hiemstra, T., and Riemsdijk, V., 1997. Adsorption of small weak organic acids on goethite: modeling of mechanisms. *Journal of colloid and interface science* **195**, 368-380.
- Filius, J. D., Lumsdon, D. G., Meeussen, J. C. L., Hiemstra, T., and Riemsduk, W. H. V., 2000. Adsorption of fulvic acid on goethite. *Geochimica et cosmochimica acta* **64**, 51-60.
- Franklin, S. P., Hajash Jr, A., Dewers, T. A., and Tieh, T. T., 1994. The role of carboxylic acids in albite and quartz dissolution: An experimental study under diagenetic conditions. *Geochimica et cosmochimica acta* **58**, 4259-4279.
- Furrer, G. and Stumm, W., 1986. The coordination chemistry of weathering: I. Dissolution kinetics of δ-Al₂O₃ and BeO. *Geochimica et cosmochimica acta* **50**, 1847-1860.
- Ganor, J., Cama, J., and Metz, V., 2003. Surface protonation data of kaolinite-reevaluation based on dissolution experiments. *Journal of colloid and interface science* **264**, 67-75.
- Ganor, J., Reznik, I. J., and Rosenberg, Y. O., 2009. Organics in water-rock interactions. *Reviews in Mineralogy and Geochemistry* **70**, 259-369.
- Ganor, J. J., Mogollon, J. L., and Lasaga, A. C., 1995. The effect of pH on kaolinite dissolution rates and on activation energy. *Geochimica et cosmochimica acta* **59**, 1037-1052.

- Geelhoed, J. S., Hiemstra, T., and Van Riemsdijk, W. H., 1997. Phosphate and sulfate adsorption on goethite: Single anion and competitive adsorption. *Geochimica et cosmochimica acta* **61**, 2389-2396.
- Goldberg, S. and Johnston, C. T., 2001. Mechanisms of arsenic adsorption on amorphous oxides evaluated using macroscopic measurements, vibrational spectroscopy, and surface complexation modeling. *Journal of colloid and interface science* **234**, 204-216.
- Groff, R. P., 1983. Adsorption and orientation of benzoic acid on aluminum oxide: An infrared study. *Journal of catalysis* **79**, 259-263.
- Gu, B., Mehlhorn, T. L., Liang, L., and McCarthy, J. F., 1996. Competitive adsorption, displacement, and transport of organic matter on iron oxide: I. Competitive adsorption. *Geochimica et cosmochimica acta* **60**, 1943-1950.
- Gu, B., Schmitt, J., Chen, Z., Liang, L., and McCarthy, J. F., 1994. Adsorption and desorption of natural organic matter on iron oxide: mechanisms and models. *Environmental science and technology* **28**, 38-46.
- Gu, B., Schmitt, J., Chen, Z., Liang, L., and McCarthy, J. F., 1995. Adsorption and desorption of different organic matter fractions on iron oxide. *Geochimica et cosmochimica acta* **59**, 219-229.
- Gustafsson, J. P., 2001. Modeling the acid-base properties and metal complexation of humic substances with the Stockholm Humic Model. *Journal of colloid and interface science* **244**, 102-112.
- Harley, A. D. and Gilkes, R. J., 2000. Factors influencing the release of plant nutrient elements from silicate rock powders: a geochemical overview. *Nutrient Cycling in Agroecosystems* **56**, 11-36.
- Hay, M. B. and Myneni, S. C. B., 2007. Structural environments of carboxyl groups in natural organic molecules from terrestrial systems. Part 1: Infrared spectroscopy. *Geochimica et cosmochimica acta* **71**, 3518-3532.
- Hayes, K., Redden, G., Ela, W., and Leckie, J., 1991. Surface Complexation Models: An evaluation of model parameter estimation using FITEQL and oxide mineral titration data. *Journal of colloid and interface science* **142**, 448-469.
- Hedges, J. I. and Keil, R. G., 1999. Organic geochemical perspectives on estuarine processes: sorption reactions and consequences. *Marine chemistry* **65**, 55-65.
- Heidmann, I., Christl, I., Leu, C., and Kretzschmar, R., 2005. Competitive sorption of protons and metal cations onto kaolinite: experiments and modeling. *Journal of colloid and interface science* **282**, 270-282.
- Herbelin, A. and Westall, J., 1999. FITEQL: A computer program for determination of chemical equilibrium constants from experimental data; Version 4.0. Department of Chemistry, Oregon State University, Oregon.
- Hind, A. R., Bhargava, S. K., and McKinnon, A., 2001. At the solid/liquid interface: FTIR/ATR-the tool of choice. *Advances in colloid and interface science* **93**, 91-114.
- Huertas, F. J., Chou, L., and Wollast, R., 1998. Mechanism of kaolinite dissolution at room temperature and pressure: Part 1. Surface speciation. *Geochimica et cosmochimica acta* **62**, 417-431.
- Huertas, F. J., Chou, L., and Wollast, R., 1999. Mechanism of kaolinite dissolution at room temperature and pressure Part II: Kinetic study. *Geochimica et cosmochimica acta* **63**, 3261-3275.
- Hug, S. J. and Bahnemann, D., 2006. Infrared spectra of oxalate, malonate and succinate adsorbed on the aqueous surface of rutile, anatase and lepidocrocite measured with in situ ATR-FTIR. *Journal of Electron Spectroscopy and Related Phenomena* **150**, 208-219.

- Humbert, B., Alnot, M., and Quiles, F., 1998. Infrared and Raman spectroscopical studies of salicylic and salicylate derivatives in aqueous solution. *Spectrochimica acta Part A* **54**, 465-476.
- Hur, J. and Schlautman, 2003. Molecular weight fractionation of humic substances by adsorption onto minerals. *Journal of colloid and interface science* **264**, 313-321.
- Hwang, Y. S. and Lenhart, J. J., 2009. Surface complexation modeling of dual-mode adsorption of organic acids: Phthalic acid adsorption onto hematite. *Journal of colloid and interface science* **336**, 200-207.
- Hwang, Y. S., Liu, J., Lenhart, J. J., and Hadad, C. M., 2007. Surface complexes of phthalic acid at the hematite/water interface. *Journal of colloid and interface science* **307**, 124-134.
- Ikhsan, J., Johnson, B. B., and Wells, J. D., 1999. A Comparative Study of the Adsorption of Transition Metals on Kaolinite. *Journal of colloid and interface science* **217**, 403-410.
- Ikhsan, J., Wells, J. D., Johnson, B. B., and Angove, M. J., 2004a. The effect of aspartic acid on the binding of transition metals to kaolinite. *Journal of colloid and interface science* **273**, 6-13.
- Ikhsan, J. J., Johnson, B. B., Wells, J. D., and Angove, M. J., 2004b. Adsorption of aspartic acid on kaolinite. *Journal of colloid and interface science* **273**, 1-5.
- Illés, E. and Tombacz, E., 2003. The role of variable surface charge and surface complexation in the adsorption of humic acid on magnetite. *Colloids and surfaces. A: Physicochemical and engineering aspects* **230**, 99-109.
- Janos, P., Krizenecka, S., and Madronova, L., 2008. Acid–base titration curves of solid humic acids. *Reactive & functional polymers* **68**, 242-247.
- Johnson, S. B., Yoon, T. H., and Brown, G. E., 2005. Adsorption of organic matter at mineral/water interfaces: 5. Effects of adsorbed natural organic matter analogues on mineral dissolution. *Langmuir* **21**, 2811-2821.
- Johnson, S. B., Yoon, T. H., Kocar, B. D., and Brown, G. E., 2004a. Adsorption of organic matter at mineral/water interfaces. 2. Outer-sphere adsorption of maleate and implications for dissolution processes. *Langmuir* **20**, 4996-5006.
- Johnson, S. B., Yoon, T. H., Slowey, A. J., and Brown, G. E., 2004b. Adsorption of organic matter at mineral/water interfaces: 3. Implications of surface dissolution for adsorption of oxalate. *Langmuir* **20**, 11480-92.
- Johnson, S. E. and Loeppert, R. H., 2006. Role of organic acids in phosphate mobilization from iron oxide. *Soil Science Society of America Journal* **70**, 222-234.
- Jones, D. L., 1998. Organic acids in the rhizosphere – a critical review. *Plant and Soil* **205**, 25-44.
- Jones, K. D. and Tiller, C. L., 1999. Effect of solution chemistry on the extend of binding of phenanthrene by a soil humic acid: A comparison of dissolved and clay bound humic. *Environmental science and technology* **33**, 580-587.
- Kaiser, K. and Guggenberger, G., 2000. The role of DOM sorption to mineral surfaces in the preservation of organic matter in soils. *Organic Geochemistry* **31**, 711-725.
- Kaiser, K., Guggenberger, G., Haumaier, L., and Zech, W., 1997. Dissolved organic matter sorption on subsoils and minerals studied by ¹³C-NMR and DRIFT spectroscopy. *European journal of soil science* **48**, 301-310.
- Kang, S. and Xing, B., 2007. Adsorption of dicarboxylic acids by clay minerals as examined by in situ ATR-FTIR and ex situ DRIFT. *Langmuir* **23**, 7024-7031.
- Kirwan, L. J., Fawell, P. D., and Bronswijk, W., 2003. In Situ FTIR-ATR examination of poly (acrylic acid) adsorbed onto hematite at low pH. *Langmuir* **19**, 5802-5807.

- Klug, O. and Forsling, W., 1999. A spectroscopic study of phthalate adsorption on γ -aluminum oxide. *Langmuir* **15**, 6961-6968.
- Koopal, L. K., Van Riemsdijk, W. H., and Kinniburgh, D. G., 2001. Humic matter and contaminants. General aspects and modeling metal ion binding. *Pure and Applied Chemistry* **73**, 2005-2016.
- Koretsky, C., 2000. The significance of surface complexation reactions in hydrologic systems: a geochemist's perspective. *Journal of hydrology* **230**, 127-171.
- Kraepiel, A. M. L., Keller, K., and Morel, F. M. M., 1998. On the acid-base chemistry of permanently charged minerals. *Environmental science and technology* **32**, 2829-2838.
- Krishnamurti, G. S. R., Cieslinsky, G., Huang, P. M., and Rees, K. C. J., 1997. Kinetics of cadmium release from soils as influenced by organic acids: implication in cadmium availability. *Journal of environmental quality* **26**, 271-277.
- Kubicki, J. D., Itoh, M. J., Schroeter, L. M., and Apitz, S. E., 1997. Bonding mechanisms of salicylic acid adsorbed onto illite clay: an ATR-FTIR and molecular orbital study. *Environmental science and technology* **31**, 1151-1156.
- Kubicki, J. D., Schroeter, L. M., Itoh, M. J., Nguyen, B. N., and Apitz, S. E., 1999. Attenuated total reflectance Fourier-transform infrared spectroscopy of carboxylic acids adsorbed onto mineral surfaces-II. *Geochimica et cosmochimica acta* **63**, 2709-2725.
- Kummert, R. and Stumm, W., 1980. The surface complexation of organic acids on hydrous γ -Al₂O₃. *Journal of colloid and interface science* **75**, 373-385.
- Lackovic, K., Angove, M. J., Wells, J. D., and Johnson, B. B., 2003a. Modeling the adsorption of Cd(II) onto Mulloorina illite and related clay minerals. *Journal of colloid and interface science* **257**, 31-40.
- Lackovic, K., Johnson, B. B., Angove, M. J., and Wells, J. D., 2003b. Modeling the adsorption of citric acid onto Mulloorina illite and related clay minerals. *Journal of colloid and interface science* **267**, 49-59.
- Langmuir, D., 1997. *Aqueous environmental geochemistry*. Prentice-Hall, New Jersey.
- Lee, J.-F., Crum, J. R., and Boyd, S. A., 1989. Enhanced retention of organic contaminants by soils exchanged with organic cations. *Environmental science and technology* **23**, 1365-1372.
- Loring, J. S., Karlsson, M., Fawcett, W. R., and Casey, W. H., 2001. Infrared spectra of phthalic acid, the hydrogen phthalate ion, and the phthalate ion in aqueous solution. *Spectrochimica acta. Part A, Molecular and biomolecular spectroscopy* **57**, 1635-1642.
- Lützenkirchen, J., 1999. Parameter estimation for the Constant Capacitance Surface Complexation Model: Analysis of parameter interdependencies. *Journal of colloid and interface science* **210**, 384-390.
- Lumsdon, D. G. and Fraser, A. R., 2005. Infrared spectroscopic evidence supporting heterogeneous site binding models for humic substances. *Environmental science and technology* **39**, 6624-6631.
- Lützenkirchen, J., 1998. Comparison of 1-pK and 2-pK versions of surface complexation theory by the goodness of fit in describing surface charge data of (hydr)oxides. *Environmental science and technology* **32**, 3149-3154.
- Lützenkirchen, J., 1999. Parameter Estimation for the Constant Capacitance Surface Complexation Model: Analysis of Parameter Interdependencies. *Journal of colloid and interface science* **210**, 384-390.
- Majzik, A. and Tombacz, E., 2007. Interaction between humic acid and montmorillonite in the presence of calcium ions I. Interfacial and aqueous phase equilibria: Adsorption and complexation. *Organic Geochemistry* **38**, 1319-1329.

- Marshall, S. J., Young, S. D., and Gregson, K., 1995. Humic acid-proton equilibria: A comparison of two models and assessment of titration error. *European journal of soil science* **46**, 471-480.
- Masini, J. C., Abate, G., Lima, E. C., Hahn, L. C., Nakamura, M. S., Lichtig, J., and Nagatomy, H. R., 1998. Comparison of methodologies for determination of carboxylic and phenolic groups in humic acids. *Analytica Chimica Acta* **364**, 223-233.
- Mayer, L. M., 1994. Relationships between mineral surfaces and organic carbon concentrations in soils and sediments. *Chemical geology* **114**, 347-363.
- Mayer, L. M. and Xing, B., 2001. Organic matter-surface area relationships in acid soils. *Soil Science Society of America Journal* **65**, 250-258.
- Meadows, J., Williams, P. A., Garvey, M. J., Harrop, R. A., and Phillips, G. O., 1988. Enhanced polyelectrolyte adsorption. *Colloids and surfaces* **32**, 275-288.
- Mendive, C. B., Bredow, T., Blesa, M. A., and Bahnemann, D. W., 2006. ATR-FTIR measurements and quantum chemical calculations concerning the adsorption and photoreaction of oxalic acid on TiO₂. *Physical chemistry chemical physics* **8**, 3232-3247.
- Milne, C. J., Kinniburgh, D. G., De Wit, J. C. M., Van Riemsdijk, W. H., and Koopal, L. K., 1995. Analysis of proton binding by a peat humic acid using a simple electrostatic model. *Geochimica et cosmochimica acta* **59**, 1101-1112.
- Milne, C. J., Kinniburgh, D. G., and Tipping, E., 2001. Generic NICA-Donnan model parameters for proton binding by humic substances. *Environmental science and technology* **35**, 2049-2059.
- Molis, E., Barres, O., Marchand, H., Sauzeat, E., Humbert, B., and Thomas, F., 2000. Initial steps of ligand-promoted dissolution of gibbsite. *Colloids and surfaces. A, Physicochemical and engineering aspects* **163**, 283-292.
- Morris, P. M. and Wogelius, R. A., 2008. Phthalic acid complexation and the dissolution of forsteritic glass studied via *in situ* FTIR and X-ray scattering. *Geochimica et cosmochimica acta* **72**, 1970-1985.
- Murphy, E. M., Zachara, J. M., Smith, S. C., and Phillips, J. L., 1992. The sorption of humic acids to mineral surfaces and their role in contaminant binding. *The Science of the Total Environment*, **117/118**, 413-423.
- Murphy, E. M., Zachara, J. M., Smith, S. C., Phillips, J. L., and Wietsma, T. W., 1994. Interaction of hydrophobic organic compounds with mineral-bound humic substances. *Environmental science and technology* **28**, 1291-1299.
- Nagayasu, T., Imamura, K., and Nakanishi, K., 2005. Adsorption characteristics of various organic substances on the surfaces of tantalum, titanium, and zirconium. *Journal of colloid and interface science* **286**, 462-470.
- Namjesnik-Dejanovic, K., Maurice, P. A., Aiken, G. R., Cabaniss, S., Chin, Y.-P., and Pullin, M. J., 2000. Adsorption and fractionation of a muck fulvic acid on kaolinite and goethite at pH 3.7, 6, and 8 *Soil science* **165**, 545-559.
- Nara, M., Torii, H., and Tasumi, M., 1996. Correlation between the vibrational frequencies of the carboxylate group and the types of its coordination to a metal ion: an ab initio molecular orbital study. *Journal of physical chemistry* **100**, 19812-19817.
- Narambuena, C. F., Beltramo, D. M., and Leiva, E. P. M., 2007. Polyelectrolyte adsorption on a charged surface. A Study by Monte Carlo simulations. *Macromolecules* **40**, 7336-7342.
- Nilsson, N., Persson, P., Lovgren, L., and Sjoberg, S., 1996. Competitive surface complexation of o-phthalate and phosphate on goethite (α -FeOOH) particles. *Geochimica et cosmochimica acta* **60**, 4385-4395.

- Nordin, J., Persson, P., Laiti, E., and Sjöberg, S., 1997. Adsorption of o-phthalate at the water-boehmite (γ -AlOOH) interface: Evidence for two coordination modes. *Langmuir* **13**, 4085-4093.
- Nordin, J., Persson, P., Nordin, A., and Sjöberg, S., 1998. Inner-sphere and outer-sphere complexation of a polycarboxylic acid at the water-boehmite (γ -AlOOH) interface: A combined potentiometric and IR spectroscopic study. *Langmuir* **14**, 3655-3662.
- Noren, K. and Persson, P., 2007. Adsorption of monocarboxylates at the water/goethite interface: The importance of hydrogen bonding. *Geochimica et cosmochimica acta* **71**, 5717-5730.
- O'Melia, C. R., 1989. Particle-particle interactions in aquatic systems. *Colloids and surfaces* **39**, 255-271.
- Onyatta, J. O. and Huang, P. M., 2003. Kinetics of cadmium release from selected tropical soils from Kenya by low-molecular-weight organic acids. *Soil science* **168**, 234-252.
- Ou, Z. and Muthukumar, M., 2006. Entropy and enthalpy of polyelectrolyte complexation: Langevin dynamics simulations. *The Journal of Chemical Physics* **124**, 154902.
- Parfitt, R. L., Farmer, V. C., and Russell, J. D., 1977a. Adsorption on hydrous oxides I. Oxalate and benzoate on goethite. *Journal of soil science* **28**, 29-39.
- Parfitt, R. L., Fraser, A. R., and Farmer, V. C., 1977b. Adsorption on hydrous oxides. III. Fulvic acid and humic acid on goethite, gibbsite and imogolite. *European journal of soil science* **28**, 289-296.
- Parks, G. A., 1990. Surface energy and adsorption at mineral-water interfaces: An introduction. *Reviews in mineralogy* **23**, 133-175.
- Peacock, C. L. and Sherman, D. M., 2005. Surface complexation model for multisite adsorption of copper(II) onto kaolinite. *Geochimica et cosmochimica acta* **69**, 3733-3745.
- Peak, D., Ford, R. G., and Sparks, D. L., 1999. An in situ ATR-FTIR investigation of sulfate bonding mechanisms on goethite. *Journal of colloid and interface science* **218**, 289-299.
- Persson, P. and Axe, K., 2005. Adsorption of oxalate and malonate at the water-goethite interface: molecular surface speciation from IR spectroscopy. *Geochimica et cosmochimica acta* **69**, 541-552.
- Persson, P. and Lövgren, L., 1996. Potentiometric and spectroscopic studies of sulfate complexation at the goethite-water interface. *Geochimica et cosmochimica acta* **60**, 2789-2799.
- Persson, P., Nordin, J., Rosenqvist, J., Lovgren, L., Ohman, L.-O., and Sjöberg, S., 1998. Comparison of the adsorption of o-phthalate on boehmite (γ -AlOOH), aged γ -Al₂O₃, and goethite (α -FeOOH). *Journal of colloid and interface science* **206**, 252-266.
- Piccolo, A., 2001. The supramolecular structure of humic substances *Soil science* **166**, 810-832.
- Pommerenk, P. and Schafran, G. C., 2005. Adsorption of inorganic and organic ligands onto hydrous aluminum oxide: Evaluation of surface charge and the impacts on particle and NOM removal during water treatment. *Environmental science and technology* **39**, 6429-6434.
- Redman, A. D., Macalady, D. L., and Ahmann, D., 2002. Natural organic matter affects arsenic speciation and sorption onto hematite. *Environmental science and technology* **36**, 2889-2896.
- Ritchie, J. D. and Perdue, E. M., 2003. Proton-binding study of standard and reference fulvic acids, humic acids, and natural organic matter. *Geochimica et cosmochimica acta* **67**, 85-96.

- Robards, K., McKelvie, I. D., Benson, R. L., Worsfold, P. J., Blundell, N. J., and Casey, H., 1994. Determination of carbon, phosphorus, nitrogen and silicon species in waters. *Analytica Chimica Acta* **287**, 147-190.
- Robert, D., Parra, S., Pulgarin, C., Krzton, A., and Weber, J. V., 2000. Chemisorption of phenols and acids on TiO₂ surface. *Applied Surface Science* **167**, 51-58.
- Roddick-Lanzilotta, A. D. and McQuillan, A. J., 2000. An *in situ* infrared spectroscopic study of glutamic acid and of aspartic acid adsorbed on TiO₂: Implications for the biocompatibility of titanium. *Journal of colloid and interface science* **227**, 48-54.
- Rosenqvist, J., Axe, K., Sjoberg, S., and Persson, P., 2003. Adsorption of dicarboxylates on nano-sized gibbsite particles: effects of ligand structure on bonding mechanisms. *Colloids and surfaces. A, Physicochemical and engineering aspects* **220**, 91-104.
- Rotzinger, F. P., Kesselman-Truttman, J. M., Hug, S. J., Shklover, V., and Gratzel, M., 2004. Structure and vibrational spectrum of formate and acetate adsorbed from aqueous solution onto the TiO₂ rutile (110) surface. *The Journal of physical chemistry* **108**, 5004-5017.
- Saada, A., Breeze, D., Crouzet, C., Cornu, S., and Baranger, P., 2003a. Adsorption of arsenic (V) on kaolinite and on kaolinite-humic acid complexes. Role of humic acid nitrogen groups. *Chemosphere* **51**, 757-763.
- Saada, A., Gaboriau, H., Cornu, S., Bardot, F., Villieras, F., and Croue, J. P., 2003b. Adsorption of humic acid onto a kaolinitic clay studied by high-resolution argon adsorption volumetry. *Clay Minerals* **38**, 433-443.
- Sahai, N. and Sverjensky, D. A., 1997. Evaluation of internally consistent parameters for the triple-layer model by the systematic analysis of oxide surface titration data. *Geochimica et cosmochimica acta* **61**, 2801-2826.
- Saito, T., Koopal, L. K., Van Riemsdijk, W. H., Nagasaki, S., and Tanaka, S., 2004. Adsorption of humic acid on goethite: Isotherms, charge adjustments, and potential profiles. *Langmuir* **20**, 689-700.
- Salman, M., El-Eswed, B., and Khalili, F., 2007. Adsorption of humic acid on bentonite. *Applied Clay Science* **38**, 51-56.
- Santos, E. B. H., Esteves, V. I., Rodrigues, J. P. C., and Duarte, A. C., 1999. Humic substances' proton-binding equilibria: assessment of errors and limitations of potentiometric data. *Analytica Chimica Acta* **392**, 333-341.
- Schlautman, M. A. and Morgan, J. J., 1994. Adsorption of aquatic humic substances on colloidal-size aluminum oxide particles: Influence of solution chemistry. *Geochimica et cosmochimica acta* **58**, 4293-4303.
- Schnitzer, M., 1989. Humic substances: chemistry and reactions. In: Schnitzer, M. and Khan, S. U. (Eds.), *Soil organic matter*. Elsevier Science Publishers B. V., Amsterdam.
- Schnitzer, M., 1991. Soil organic matter-the next 75 years. *Soil science* **151**, 41-58.
- Schroth, B. K. and Sposito, G., 1997. Surface charge properties of kaolinite. *Clays and Clay minerals* **45**, 85-91.
- Schroth, B. K. and Sposito, G., 1998. Effect of landfill leachate organic acids on trace metal adsorption by kaolinite. *Environmental science and technology* **32**, 1404-1408.
- Shen, Y.-H., 1999. Sorption of natural dissolved organic matter on soil. *Chemosphere* **38**, 1505-1515.
- Spark, K. M., Wells, J. D., and Johnson, B. B., 1997. Sorption of heavy metals by mineral-humic acid substances. *Australian Journal of Soil Research* **35**, 113-122.
- Sparks, D. L., 2003. *Environmental Soil Chemistry*. Academic Press.

- Specht, C. H., Kumke, M. U., and Frimmel, F. H., 2000. Characterization of NOM adsorption to clay minerals by size exclusion chromatography. *Water Research* **34**, 4063-4069.
- Specht, H. C. and Frimmel, H. F., 2001. An in situ ATR-FTIR study on the adsorption of dicarboxylic acids onto kaolinite in aqueous suspensions. *Phys. Chem. Chem. Phys.* **3**, 5444-5449.
- Stillings, L. L., Drever, J. I., Brantley, S. L., Sun, Y., and Oxburg, R., 1996. Rates of feldspar dissolution at pH 3–7 with 0–8 mM oxalic acid. *Chemical geology* **132**, 79-89.
- Stillings, L. L., Drever, J. I., and Poulson, S. I., 1998. Oxalate adsorption at a plagioclase (An₄₇) surface and models for ligand-promoted dissolution. *Environmental science and technology* **32**, 2856-1864.
- Strobel, B. W., 2001. Influence of vegetation on low-molecular-weight carboxylic acids in soil solution—a review. *Geoderma* **99**, 169-198.
- Stumm, W., 1986. Coordinative interactions between soil solids and water- an aquatic chemist's point of view. *Geoderma* **38**, 19-30.
- Stumm, W., 1992. *Chemistry of the solid-water interface : processes at the mineral-water and particle-water interface in natural systems*. John Wiley & Sons New York.
- Stumm, W., 1993. Aquatic colloids as chemical reactants: surface structure and reactivity. *Colloids and surfaces A: Physicochemical and engineering aspects* **73**, 1-18.
- Stumm, W., 1995. The inner-sphere surface complex. In: Huang, C. P., O'Melia, C. R., and Morgan, J. J. (Eds.), *Aquatic Chemistry*. American Chemical Society, Washington, DC.
- Stumm, W., 1997. Reactivity at the mineral-water interface: dissolution and inhibition. *Colloids and surfaces. A, Physicochemical and engineering aspects* **120**, 143-166.
- Stumm, W. and Wollast, R., 1990. Coordination chemistry of weathering: Kinetics of the surface-controlled dissolution of oxide minerals. *Reviews of Geophysics* **28**, 53-69.
- Sutheimer, S. H., Maurice, P. A., and Zhou, Q., 1999. Dissolution of well and poorly crystallized kaolinites: Al speciation and effects of surface characteristics. *American Mineralogist* **84**, 620-628.
- Sutton, R. and Sposito, G., 2005. Molecular structure in soil humic substances: The new view. *Environmental science and technology* **39**, 9009-9015.
- Sverjensky, D. A. and Sahai, N., 1996. Theoretical prediction of single-site surface-protonation equilibrium constants for oxides and silicates in water. *Geochimica et cosmochimica acta* **60**, 3773-3797.
- Tejedor-Tejedor, I. M., Yost, E. C., and Anderson, M. A., 1992. Characterization of benzoic and phenolic complexes at the goethite/aqueous solution interface using cylindrical internal reflection Fourier transform infrared spectroscopy. 2. Bonding structures. *Langmuir* **8**, 525-533.
- Tertre, E., Castet, S., Berger, G., Loubet, M., and Giffaut, E., 2006. Surface chemistry of kaolinite and Na-montmorillonite in aqueous electrolyte solutions at 25 and 60 °C: Experimental and modeling study. *Geochimica et cosmochimica acta* **70**, 4579-4599.
- Tipping, E., 1981. The adsorption of aquatic humic substances by iron oxides. *Geochimica et cosmochimica acta* **45**, 191-199.
- Tipping, E., 2002. *Cation binding by humic substances*. Cambridge University Press, Cambridge.

- Tipping, E. and Cooke, D., 1982. The effects of adsorbed humic substances on the surface charge of goethite (α -FeOOH) in freshwaters. *Geochimica et cosmochimica acta* **46**, 75-80.
- Tipping, E., Rey-Castro, C., Bryan, S. E., and Hamilton-Taylor, J., 2002. Al (III) and Fe (III) binding by humic substances in freshwaters, and implications for trace metal speciation. *Geochimica et cosmochimica acta* **66**, 3211-3224.
- Tombacz, E., 2002. Adsorption from electrolyte solutions. In: Toth, J. (Ed.), *Adsorption. Theory, modeling, and analysis*. Marcel Dekker, New York.
- Tombacz, E., Dobos, A., Szekeres, M., Narres, H. D., Klumpp, E., and Dekany, I., 2000. Effect of pH and ionic strength on the interaction of humic acid with aluminium oxide. *Colloid & polymer science* **278**, 337-345.
- Tombacz, E., Filipcsei, G., Szekeres, M., and Gingl, Z., 1999. Particle aggregation in complex aquatic systems. *Colloids and surfaces A: Physicochemical and engineering aspects* **151**, 233-244.
- Tombác, E., Libor, Z., Illés, E., Majzik, A., and Klumpp, E., 2004. The role of reactive surface sites and complexation by humic acids in the interaction of clay mineral and iron oxide particles. *Organic Geochemistry* **35**, 257-267.
- Tunesi, S. and Anderson, M. A., 1992. Surface effects in photochemistry: an in situ cylindrical internal reflection-Fourier transform infrared investigation of the effect of ring substituents on chemisorption onto TiO₂ ceramic membranes. *Langmuir* **8**, 487-495.
- Van de Steeg, H. G. M., Cohen Stuart, M. A., De Keizer, A., and Bijsterbosch, B. H., 1992. Polyelectrolyte adsorption: A Subtle balance of forces. *Langmuir* **8**, 2538-2546.
- Van den Brand, J., Blajiev, O., Beentjes, P. C. J., Terryn, H., and de Wit, J. H. W., 2004. Interaction of anhydride and carboxylic acid compounds with aluminum oxide surfaces studied using infrared reflection absorption spectroscopy. *Langmuir* **20**, 6308-6317.
- Van Hees, P. A. W., Jones, D. L., Finlay, R., Godbold, D. L., and Lundstrom, U. S., 2005. The carbon we do not see-the impact of low molecular weight compounds on carbon dynamics and respiration in forest soils: a review. *Soil biology & Biochemistry* **37**, 1-13.
- Van Hees, P. A. W., Lundstrom, U. S., and Giesler, R., 2000. Low molecular weight organic acids and their Al-complexes in soil solution-composition, distribution and seasonal variation in three podzolized soils *Geoderma* **94**, 173-200.
- Vermeer, A. W. P., Leermakers, F. A. M., and Koopal, L. K., 1997. Adsorption of weak polyelectrolytes on surfaces with a variable charge. Self-consistent-field calculations. *Langmuir* **13**, 4413-4421.
- Vermeer, A. W. P., Van Riemsdijk, W. H., and Koopal, L. K., 1998. Adsorption of humic acid to mineral particles. 1. Specific and electrostatic interactions. *Langmuir* **14**, 2810-2819.
- Vermohlen, K., Lewandowski, H., Narres, H. D., and Schwuger, M. J., 2000. Adsorption of polyelectrolytes onto oxides - the influence of ionic strength, molar mass, and Ca²⁺ ions. *Colloids and surfaces. A: Physicochemical and engineering aspects* **163**, 45-53.
- Villalobos, M. and Leckie, J. O., 2001. Surface Complexation Modeling and FTIR Study of Carbonate Adsorption to Goethite. *Journal of colloid and interface science* **235**, 15-32.
- Vreysen, S. and Maes, A., 2006. Adsorption mechanism of fulvic acid onto freeze dried poly(hydroxo aluminum) intercalated bentonites. *Applied Clay Science* **32**, 190-196.
- Wang, K. and Xing, B., 2005. Structural and sorption characteristics of adsorbed humic acid on clay minerals. *Journal of Environmental Quality* **34**, 342-349.

- Wang, L., Chin, Y.-P., and Traina, S. J., 1997. Adsorption of (poly)maleic acid and an aquatic fulvic acid by goethite. *Geochimica et cosmochimica acta* **61**, 5313-5324.
- Wang, X., Li, Q., Hu, H., Zhang, T., and Zhou, Y., 2005. Dissolution of kaolinite induced by citric, oxalic, and malic acids. *Journal of colloid and interface science* **290**, 481-488.
- Warne, M. R., Allan, N. L., and Cosgrove, T., 2000. Computer simulation of water molecules at kaolinite and silica surfaces. *Phys. Chem. Chem. Phys.* **2**, 3363-3668.
- Weisz, A. D., Garcia Rodenas, L., Morando, P. J., Regazzoni, A. E., and Blesa, M. A., 2002. FTIR study of the adsorption of single pollutants and mixtures of pollutants onto titanium dioxide in water: oxalic and salicylic acids. *Catalysis today* **76**, 103-112.
- Welch, S. A. and Ullman, W. J., 1993. The effect of organic acids on plagioclase dissolution rates and stoichiometry. *Geochimica et cosmochimica acta* **57**, 2725-2736.
- Weng, L. P., Koopal, L. K., Hiemstra, T., Meeussen, J. C. L., and Van Riemsdijk, W. H., 2005. Interactions of calcium and fulvic acid at the goethite-water interface. *Geochimica et cosmochimica acta* **69**, 325-339.
- Westall, J. and Hohl, H., 1980. A comparison of electrostatic models for the oxide/solution interface. *Advances in colloid and interface science* **12**, 265-294.
- Westall, J. C., Jones, J. D., Turner, G. D., and Zachara, J. M., 1995. Models for Association of Metal Ions with Heterogeneous Environmental Sorbents. 1. Complexation of Co (II) by Leonardite Humic Acid as a Function of pH and NaClO₄ Concentration. *Environmental science and technology* **29**, 951-959.
- Wieland, E. and Stumm, W., 1992. Dissolution kinetics of kaolinite in acidic aqueous solutions at 25°C. *Geochimica et cosmochimica acta* **56**, 3339-3355.
- Wieland, E., Wehrli, B., and Stumm, W., 1988. The coordination chemistry of weathering: III. A generalization on the dissolution rates of minerals. *Geochimica et cosmochimica acta* **52**, 1969-1981.
- Wogelius, R. A. and Walther, J. V., 1991. Olivine dissolution at 25°C: Effects of pH, CO₂, and organic acids. *Geochimica et cosmochimica acta* **55**, 943-954.
- Xiao, Y. and Lasaga, A. C., 1994. Ab initio quantum mechanical studies of the kinetics and mechanisms of silicate dissolution: H⁺ (H₃O⁺) catalysis. *Geochimica et cosmochimica acta* **58**, 5379-5400.
- Xie, Z. and Walther, J. V., 1992. Incongruent dissolution and surface area of kaolinite. *Geochimica et cosmochimica acta* **56**, 3357-3363.
- Xing, B., McGill, W. B., and Dudas, M. J., 1994. Sorption of phenol by selected biopolymers: isotherms, energetics, and polarity. *Environmental science and technology* **28**, 466-473.
- Xu, R.-K. and Ji, G.-L., 2003. Effect of anions of low molecular weight organic acids on adsorption and desorption of aluminum by and from a kaolinite at different pH. *Soil science* **168**, 39-44.
- Yoon, T. H., Johnson, S. B., and Brown, G. E., 2004a. Adsorption of Suwannee river fulvic acid on aluminum oxyhydroxide surfaces: an in situ ATR-FTIR study. *Langmuir* **20**, 5655-5658.
- Yoon, T. H., Johnson, S. B., and Brown, G. E., 2005. Adsorption of organic matter at mineral/water interfaces. IV. Adsorption of humic substances at boehmite/water interfaces and impact on boehmite dissolution. *Langmuir* **21**, 5002-5012.
- Yoon, T. H., Johnson, S. B., Musgrave, C. B., and Brown, G. E., 2004b. Adsorption of organic matter at mineral/water interfaces: I. ATR-FTIR spectroscopic and quantum chemical study of oxalate adsorbed at boehmite/water and corundum/water interfaces. *Geochimica et cosmochimica acta* **68**, 4505-4518.

- Yost, E. C., Tejedor-Tejedor, M. I., and Anderson, M. A., 1990. In situ CIR-FTIR characterization of salicylate complexes at the goethite/aqueous solution interface. *Environmental science and technology* **24**, 822-828.
- Zelenak, V., Vargova, Z., and Gyoryova, K., 2007. Correlation of infrared spectra of zinc(II) carboxylates with their structures. *Spectrochimica Acta. Part A* **66**, 262-272.
- Zhou, J. L., Rowland, S., Mantoura, R. F. C., and Braven, J., 1994. The formation of humic coatings on mineral particles under simulated estuarine conditions - A mechanistic study. *Water Research* **28**, 571-579.
- Zhou, P., Yan, H., and Gu, B., 2005. Competitive complexation of metal ions with humic substances. *Chemosphere* **58**, 1327-1337.
- Zinder, B., Furrer, G., and Stumm, W., 1986. The coordination chemistry of weathering: II. Dissolution of Fe (III) oxides. *Geochimica et cosmochimica acta* **50**, 1861-1869.
- Zuyi, T., Taiwei, C., and Weijuan, L., 2000. On the application of surface complexation models to ionic adsorption. *Journal of colloid and interface science* **232**, 174-177.

Appendix

The *in situ* IR spectra of salicylic acid on gibbsite were also collected but for continuity of presentation, it was preferred to report these results in an appendix. The IR spectra of adsorbed salicylic acid on kaolinite, presented in chapter 3, show remarkable similarities with the IR spectra obtained for adsorbed salicylic acid on gibbsite. This suggests that the binding mode of salicylic acid is similar for both minerals. In addition, for both substrates the same trend of relative importance between inner and outer sphere complexation was found at different solution conditions. More specifically for both minerals an increase in dominance of inner sphere complexation over outer sphere complexation is observed at higher pH values, higher ionic strengths and lower initial salicylic acid concentrations. However at the same solution conditions the relative importance of inner sphere complexation is always higher for gibbsite.

Figures A-1 to A-5 show representative IR spectra of adsorbed salicylic acid on gibbsite. Due to the strong similarities found in the band frequency positions of the spectra of adsorbed salicylic acid on kaolinite and on gibbsite, band assignments and structural interpretation for the gibbsite systems remain the same as those for the kaolinite systems discussed in chapter 3. Table A-1 summarises the assignment of the absorption bands obtained for the adsorption of salicylic acid on gibbsite at different experimental conditions.

Table A- 1 Absorption peak frequencies for the adsorbed salicylate complexes on gibbsite obtained in this study.

Wavenumber (cm ⁻¹)						
Aqueous HSal ¹⁻	Adsorbed				Vibrational Mode	Assignment*
	5 x 10 ⁻⁴ M		1 x 10 ⁻³ M			
	pH 3	pH 5	pH 3	pH 5		
1620	~1623		~1622		ν_{C-C} (ring)	OSC
	1611	1610	1612	1610	ν_{C-C} (ring)	ISC
1593	1590		1591		ν_{C-C} (ring)	OSC
	1574	1575	1574	1576	ν_{C-C} (ring)	ISC
1577	1545	1541	1545	1543	$\nu^a_{COO^-}$	ISC
1486	1486		1486		ν_{C-C} (ring)	OSC
	1476	1475	1477	1475	ν_{C-C} (ring)	ISC
1459	1461	1462	1461	1462	ν_{C-C} (ring)	ISC
1387	1388		1388		$\nu^s_{COO^-} + \delta_{C-OH}$ (phenol)	OSC
		1391		1389	$\nu^s_{COO^-}$	ISC
1344	1342		1341		$\nu^s_{COO^-} + \delta_{C-OH}$ (phenol)	OSC
1303	1307		1307		ν_{C-H} (ring) + ν_{C-OH} (phenol)	OSC
	~1265	1265	~1265	1265	ν_{C-OH} (phenol)	ISC
1252	1253		1253		ν_{C-OH} (phenol)	OSC

*ISC- Inner sphere complex; OSC- Outer sphere complex

Briefly, the IR spectra of adsorbed salicylic acid on gibbsite reveal that two types of surface complexes coexist on the surface of gibbsite, one inner sphere and one outer sphere complex. At pH 5, the IR spectrum of adsorbed salicylic acid contains IR bands associated only with an inner sphere surface complex (Figure A-1). In accordance to the assignment of adsorbed salicylic acid on kaolinite the most probable structure of this surface complex is a six-membered pseudo-chelate ring in which one C-O bond from the carboxylate group is directly bonded on a surface metal centre and the phenolic group is hydrogen bonded to the same metal centre. At lower pH values new absorption bands emerge in the IR spectrum indicating the existence of an outer sphere complexed HSal^{-1} species (Figure A-2).

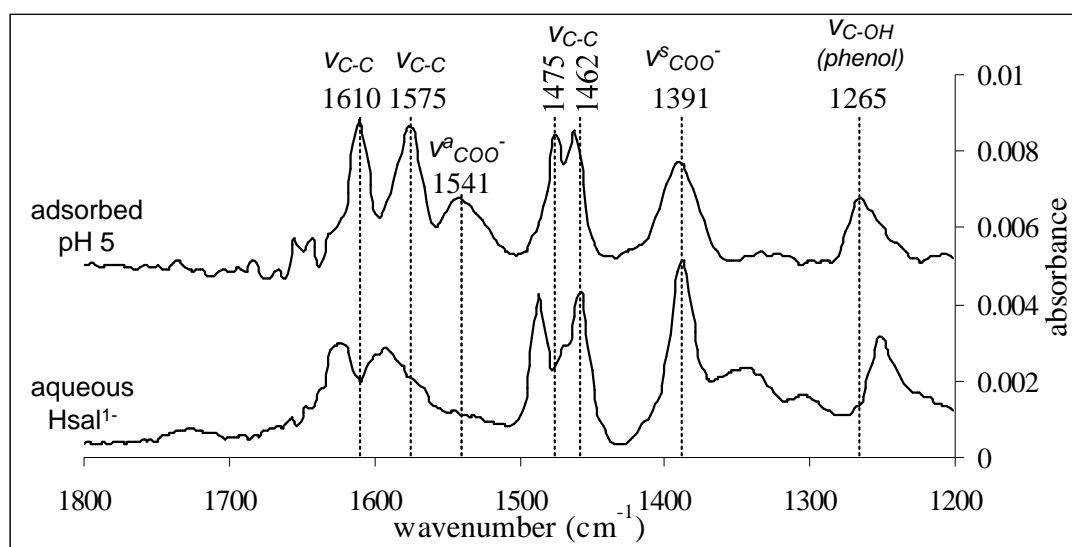


Figure A- 1 Differences in the spectroscopic features of salicylic acid observed following adsorption on gibbsite at pH 5 from a 5×10^{-4} M salicylic acid solution. Peak positions and assignments correspond to the adsorbed species.

Figure A-3 shows that the intensities of the additional bands observed at pH 3 decrease in the presence of 0.01 M NaCl. Such behaviour is consistent with an outer sphere mechanism and therefore the ionic strength dependence of these new bands, emerging at pH 3, supports the assumption that they originate from the presence of an additional outer sphere surface complex.

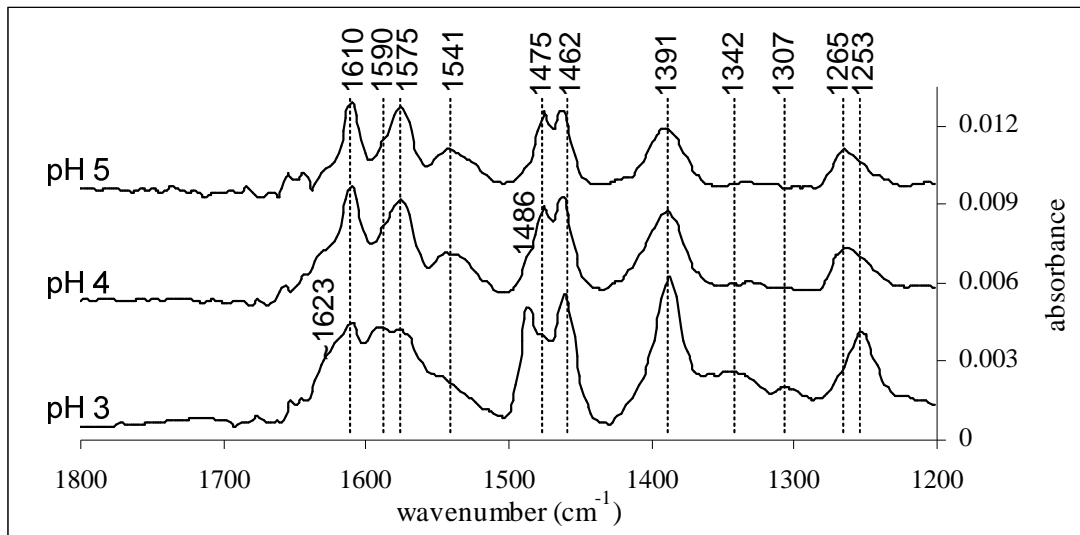


Figure A- 2 IR spectra obtained for adsorbed salicylic acid onto gibbsite at three different pH values, from a 5×10^{-4} M salicylic acid solution. The spectra have been offset for clarity.

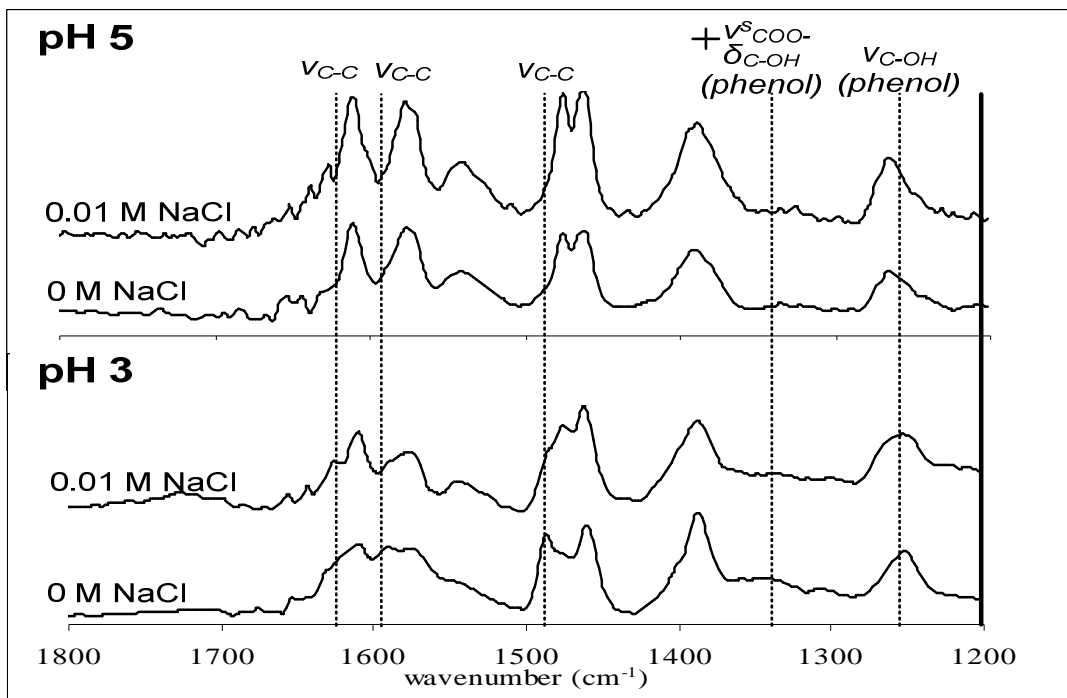


Figure A- 3 IR spectra obtained for adsorbed salicylic acid onto gibbsite from a 5×10^{-4} M salicylic acid solution, in the presence of 0.01 M NaCl and with no added electrolyte, at pH 3 and pH 5.

The effect of ligand concentration on the IR spectra of interfacial salicylic acid, at pH 3 and 5, is shown in figure A-4. At pH 3, increasing salicylic concentration leads to an increase in the intensity of the bands assigned to the outer sphere complex. At pH 5, however, this ligand concentration effect is not evident even at the highest

concentration examined. This suggests that under these conditions the sites available for inner sphere complexation are not saturated.

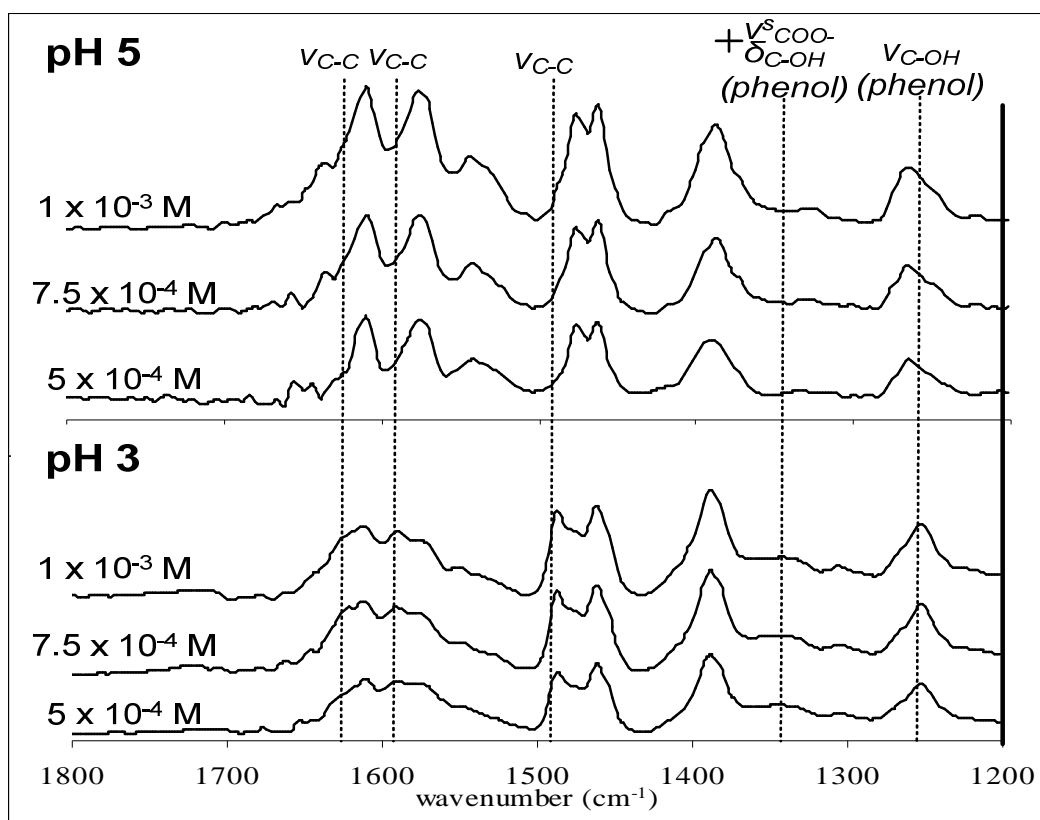


Figure A- 4 IR Spectra of adsorbed salicylic acid onto gibbsite at pH 3 and 5 as a function of salicylic acid concentration. Spectra have been offset for clarity.

Figure A-5 shows the development of inner and outer sphere complexes as a function of time. It can be seen that the IR features assigned to the outer sphere complex grow in importance, with increasing time, relative to those assigned to the inner sphere complex. This trend of increased concentration of outer sphere complexes with time indicates that salicylic acid initially coordinates to the surface in an inner sphere mode and presumably as the surface sites available for direct bonding become saturated, coordination through outer sphere complexation becomes the dominant adsorption mechanism. A similar finding was also observed for the adsorption of salicylic acid on kaolinite.

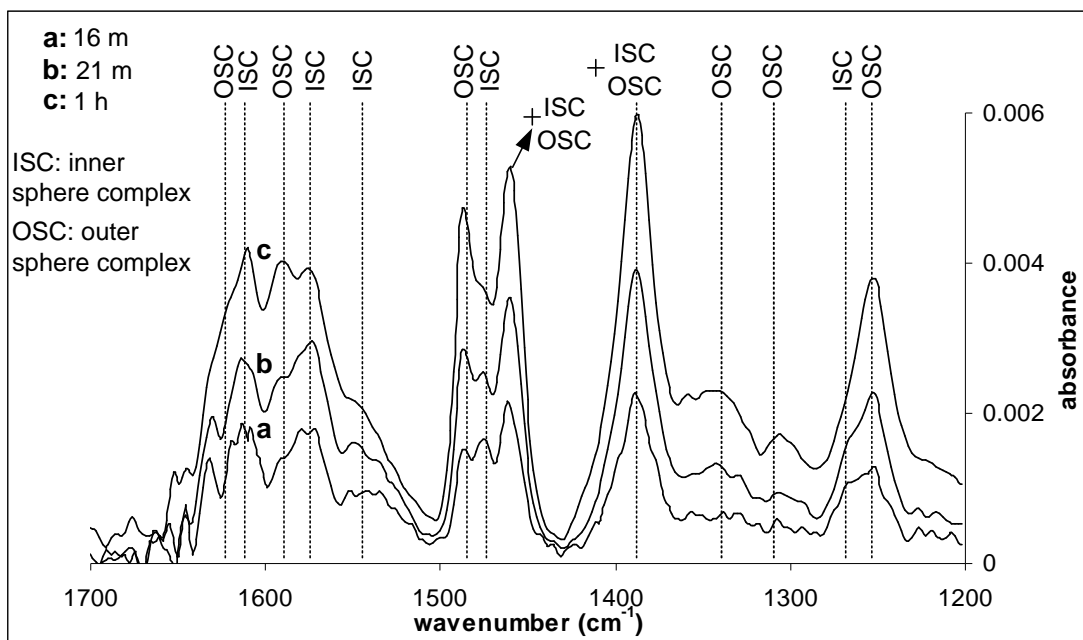


Figure A- 5 The development of surface species during the adsorption of salicylic over time from a 5×10^{-4} M salicylic acid solution at pH 3.